

DISSERTATION

MESENCHYMAL STEM CELL RESCUE FOR BONE FORMATION  
FOLLOWING STEREOTACTIC RADIOTHERAPY OF OSTEOSARCOMA

Submitted by

Anthony L. Schwartz

Graduate Degree Program in Bioengineering

In partial fulfillment of the requirements

For the Degree of Doctor of Philosophy

Colorado State University

Fort Collins, Colorado

Spring 2013

Doctoral Committee:

Advisor: Nicole Ehrhart

Stewart Ryan

Jamie Custis

Susan James

Laurie Goodrich

## ABSTRACT

### MESENCHYMAL STEM CELL RESCUE FOR BONE FORMATION FOLLOWING STEREOTACTIC RADIOTHERAPY OF OSTEOSARCOMA

**Background:** Osteosarcoma (OSA) is the most common form of primary bone cancer in dogs and humans. Curative-intent treatment options include amputation, radiation therapy or surgical limb salvage for local tumor control combined with adjuvant chemotherapy for prevention or delay of metastatic disease. Stereotactic radiotherapy (SRT) delivers high dose per fraction radiation to a defined tumor volume with relative sparing of surrounding normal tissues. It has been successfully used as a non-surgical limb salvage procedure to achieve local tumor control of spontaneous OSA in dogs. The most common complication observed with this treatment is pathologic fracture of the irradiated bone. Mesenchymal stem cells (MSCs) are multipotent stem cells that have the capability to differentiate into many cell types including bone. The ability of MSCs to differentiate into bone suggests that they should be investigated as a potential therapy to regenerate bone in SRT treated bone.

**Methods:** In experiments described herein, we developed an orthotopic model of canine osteosarcoma in athymic rats and evaluated the ability of SRT to achieve local tumor control. We then evaluated the ability of MSCs to regenerate bone after SRT treatment of OSA.

**Results:** We demonstrated that the canine OSA cell line reliably engrafted in the rat femur. We characterized progression in order to create a reproducible model in which to

replicate a clinical scenario to test MSC behavior following SRT of OSA. Two weeks after OSA cell inoculation was identified as the time period when the same clinical characteristics were observed as in canine OSA cases and was chosen to be an appropriate time for SRT treatment. The optimal SRT protocol to achieve local tumor control while minimizing acute radiation effects was determined to be 3 fractions of 12 Gy delivered on consecutive days. MSCs administered either intravenously or intraosseously 2 weeks after SRT revealed no new bone formation; however, decreased tumor necrosis was observed after MSC treatment.

**Conclusion:** The results herein describe the characterization of an orthotopic rat model of canine OSA. This model was useful for the evaluation of different dose and fractionation SRT protocols along with combination adjuvant therapies that may be clinically relevant for canine or human OSA. The administration of MSCs following SRT did not induce new bone growth. The lack of efficacy is most likely due to the radiation-induced alterations to the bone microenvironment that resulted in conditions poorly suited to MSC survival and/or differentiation.

## ACKNOWLEDGEMENTS

I would like to thank my advisor, Dr. Stewart Ryan, for allowing me the opportunity to conduct research in his laboratory. He provided priceless guidance, support and enthusiasm throughout my time at Colorado State University. He involved me in wide range of research projects that has shaped my ability to conduct high quality research and vastly expanded my knowledge in the scientific world.

I would also thank my committee members: Drs. Ehrhart, Custis, James and Goodrich. They were instrumental in providing me with the expertise to solve the complex problems that arose throughout the many projects discussed in this document.

A special thanks goes out to Laura Chubb. She was involved in every aspect of the experiments and provided a great deal of help and expertise. I would not have been able to complete these projects without her. Additionally, Dana Ruehlman, Lily Alanna Baker Parkinson, Kaitlyn McNamara, and Morgan Woodard were always willing to help and key to the success of various aspects of the projects discussed herein.

## DEDICATION

This work is dedicated to the individuals who stand as my platform in life: Frank Schwartz, Lynne Schwartz, Scott Schwartz, Christopher Schwartz and Leonard Kohn.

In memory of Dr. Leonard David Kohn, MD.

## TABLE OF CONTENTS

ABSTRACT.....	ii
ACKNOWLEDGEMENTS.....	iv
Chapter 1: Literature Review.....	1
1.1 Osteosarcoma.....	1
1.2 Stereotactic Radiation Therapy.....	13
1.3 Mesenchymal Stem Cells.....	20
1.4 Specific Aims.....	25
Chapter 2: Development of an Orthotopic Osteosarcoma Model in a Rat.....	30
2.1 Introduction.....	30
2.2 Materials and Methods.....	34
2.3 Results.....	39
2.4 Discussion.....	43
2.5 Figures.....	48
Chapter 3: Optimization of SRT Fraction and Dose Schema.....	54
3.1 Introduction.....	54
3.2 Materials and Methods.....	58
3.3 Results.....	65
3.4 Figures.....	70
3.5 Discussion.....	83
Chapter 4: Mesenchymal Stem Cell Collection & Characterization.....	90
4.1 Introduction.....	90

4.2 Materials and Methods.....	94
4.3 Results.....	98
4.4 Figures.....	101
4.5 Discussion.....	105
Chapter 5: MSC mediated bone growth following SRT for the treatment of OSA.....	108
5.1 Introduction.....	108
5.2 Materials and Methods.....	110
5.3 Results.....	117
5.4 Figures.....	122
5.4 Discussion.....	132
Chapter 6: Summary of Findings and Future Directions .....	139
References.....	142
Appendix A: Specific Aim 1 Detailed Protocols and Data.....	159
7.1 Cell culture of Abram’s OSA CELLS .....	159
7.2 Osteosarcoma Cell Injections into nude rats.....	161
7.3 PYD ELISA .....	163
7.4 Orthotopic Radiographs Supplementary Data .....	165
7.5 Orthotopic Supplemental Histology .....	170
Appendix B: Specific Aim 2 Protocols and Data .....	173
8.1 SRT Supplementary Radiographs.....	173
8.2 SRT Supplementary Histology .....	196
Appendix C: Specific Aim 3 Detailed Protocols and Data.....	217

9.1 Isolation of bone marrow rat mesenchymal stem cells that express GFP.....	217
9.2 Isolation of adipose rat mesenchymal stem cells that express GFP.....	219
9.3 Cell culture of bone and adipose rat mesenchymal Stem cells.....	221
Appendix D: Specific Aim 4 Supplementary Protocols and Data.....	223
10.1 Calculation of Bone Volume via microCT .....	223
10.2 Osteocalcin ELISA .....	224
10.3 Radiographs .....	226
10.4 Histology.....	248
10.5 Supplemental Power Analysis .....	277
List of Abbreviations .....	310

## **Chapter 1: Literature Review**

### **1.1 Osteosarcoma**

#### **Incidence**

Osteosarcoma (OSA) is the most common primary bone tumor in dogs accounting for 85% of all canine bone cancers (1, 2). It is estimated that more than 8000 dogs are diagnosed with OSA each year in the United States (2). Osteosarcoma has been described as one of the most aggressive tumors in canines as it is both locally destructive and has a high metastatic rate. The onset of OSA (middle aged dogs) peaks at age 7 and older, with a secondary peak between 18 and 24 months of age indicating a bimodal age distribution (3). Osteosarcoma occurs predominantly in giant and large breeds such as Saint Bernards, Golden Retrievers, Greyhounds, German Shepherds, Dobermans and Great Danes. Large and giant breed dogs have a sixty-fold greater risk of developing OSA than smaller breeds (4). Less than 5% of all OSA cases are diagnosed in dogs weighing less than 15 kilograms (2). It is also more prevalent in males than females with increased prominence in neutered males (1).

#### **Etiology**

The etiology of spontaneous canine OSA is not completely understood. Several studies suggest that canine OSA may be caused by large breed predisposition, trauma or gene mutations. Canine OSA is most commonly seen in the metaphyseal regions of weight-bearing bones of the appendicular skeleton (5). Excessive load on these bones has been theorized to cause repetitive

trauma to the physal regions resulting in mutagenic signals (5). Genetic mutations have been widely reported as contributors to various canine tumors including OSA. For example, mutations of p53, a critical regulator of cell proliferation, are thought to play an active role in the progression of OSA (6, 7). Other reported initiating environmental events associated with the development of OSA in dogs include fracture, metallic implants, chronic osteomyelitis, and ionizing radiation (2, 5, 8-10).

### **Presentation, Diagnosis & Prognosis**

Osteosarcoma can occur in any bone; however, about 75 % cases occur in the appendicular skeleton with the remaining 25% in the axial skeleton (5). Osteosarcoma occurs in the forelimbs twice as often as the hind limbs (5). This is because the forelimbs bear approximately 60% of the animal's body weight and weight-bearing bones have been shown to be preferentially affected by OSA over non-weight-bearing bones (5). The metaphyseal regions of the distal radius and proximal humerus are the most commonly affected sites in the forelimbs. OSA is comprised of spindle shaped mesenchymal cells that produce osteoid resulting in erratic and aggressive bone formation (11). The clinical characteristics observed in dogs with OSA include chronic lameness, local lysis of the affected bone, abnormal proliferation of bone and pathologic fracture. The radiographic characteristics of the OSA lesion are a mixed lytic-productive pattern. Histology of a biopsy of the affected bone or resected surgical specimen is required to make a definitive diagnosis (2). The biopsy is comprised of disorganized spindle shaped cells with excess production of osteoid (2). Microscopic tumor metastases are presented in greater than 90% of dogs with OSA at the time of initial diagnosis. Osteosarcoma metastasizes

via hematogenous metastatic routes (11). The most common sites of metastasis are the lungs and other bones. Macroscopic evidence of pulmonary metastasis is observed in approximately 10% of dogs at the time of diagnosis; yet lung metastases cause approximately 90% of all OSA deaths in dogs (5, 12). The presence of visible lung metastasis at the time of diagnosis is a poor prognostic indicator; with a reported median survival of 100 to 130 days (13, 14). Bone metastases are observed in ~7% of dogs at the time of diagnosis (15). Metastases to regional lymph nodes have been observed in about 4% of dogs at the time of diagnosis and are also associated with a poor prognosis (16).

### **Relevant Translational Model**

Osteosarcoma is also the most common form of primary bone cancer in humans accounting for approximately 35% of all bone tumors (17). More than 900 new cases are diagnosed each year in the United States (18). It is most prevalent in children during the second decade of life and in individuals greater than 60 years of age (17, 19). Human and canine OSA have several distinct similarities making canine spontaneous OSA models ideal for evaluating novel treatments for primary and metastatic tumor control in humans. Tumor biology and size at presentation histology are almost indistinguishable between human and canine OSA (2, 20). Tumors occur in weight-bearing bones in both species with similar bimodal susceptible age distribution; however, OSA is more prevalent in adolescents whereas in canines it is observed most commonly in middle-aged to older dogs (2, 3). Both are exposed to similar environmental risk factors as they inhabit similar environments (2). Human and canine OSA has been reported to share similar genetic mutations such as the tumor suppressor gene p53 (7, 19). Unlike induced

tumors in rodent models, canine OSA is spontaneous and behaves biologically similar to that in humans with the most common sites of metastases to bones and the lungs. The similarities described herein make spontaneous OSA in dogs an excellent large animal translational model for bone sarcomas in humans (20).

## **Treatment**

Treatment regimens for canine OSA can be broadly divided into palliative and curative-intent options (1).

### *Palliative-intent Treatment*

The aim of palliative management is to decrease pain and lameness. Palliative treatment is indicated for dogs that present with metastatic disease or when the owners do not want to pursue curative-intent treatment options. The goal of this type of treatment is to improve the quality of life for the dog but will not provide increased survival time nor provide long-term local tumor control. Palliative therapy options include oral analgesics, external beam radiation therapy, bisphosphonates, and limb amputation.

Palliative radiotherapy (XRT) of canine OSA decreases pain by reducing local tumor site inflammation and delaying local disease progression, thus improving the animal's quality of life (5). Treatment involves administration of coarsely fractionated doses of ionizing radiation, such as three or four fractions of 8 Gy delivered at 0, 7, 14 and 21 days or two fractions of 8 Gy

delivered on two consecutive days to the primary tumor (21, 22). At these radiation doses, adjacent normal tissue will recover from sub-lethal doses of radiation whereas the tumor will have more severe inhibitory effects due to its relative radiosensitivity (23). Side effects to normal tissues are typically minimal with palliative XRT. However, at these dosages, desirable long-term tumor control is not achieved resulting in eventual tumor progression. Increasing total radiation dosage along with the combination of anti-inflammatory analgesics can improve the response duration. Bisphosphonates, which inhibit tumor-associated bone resorption by inducing osteoclast apoptosis, can be administered alone or in conjunction with other palliative modalities to decrease pain and incidence of pathologic fracture (24-26). Acute radiation side effects are minimal and a median survival time ranging of 122 to 313 days has been reported with palliative treatments that include radiation alone or in combination with bisphosphonates (21, 27).

Dogs that are unresponsive to palliative radiation therapy or that have pathologic fracture are potential candidates for palliative amputation. Amputation, when used for palliative therapy, removes the source of tumor-associated bone pain and the majority of dogs function well on three legs. After amputation surgery alone, the median survival time is between 103 and 175 days (28, 29).

### *Curative-intent Treatment*

Curative-intent treatment of osteosarcoma is directed at achieving complete tumor control of the primary bone lesion and delaying or preventing the onset of metastatic disease. Even though these treatments are pursued with curative-intent, long-term cure is rarely achieved with

this disease. Approximately 90% of dogs still die within 3 years of diagnosis due to the highly metastatic nature of OSA (5). Treatment options with curative-intent include amputation or limb sparing surgery for local tumor control followed by adjuvant chemotherapy for systemic disease. Other treatment options include the use of immunomodulators and high dose radiation therapy (5).

Amputation followed by chemotherapy is the most common procedure used for curative intent treatment of OSA (30). This option removes the primary tumor with radical margins, while eliminating the risk of pathologic fracture and tumor associated bone pain. The surgical procedure is well tolerated, has a low complication rate and most dogs function very well after amputation (5, 30). Limb sparing surgery is a treatment option for animals that are poor candidates for amputation due to concurrent severe osteoarthritis, neurological diseases or owner unwillingness for amputation (5). This procedure involves surgical resection of the tumor and reconstruction of the resultant bone defect with an allograft bone or metallic endoprosthetic spacer that is fixed to the host bone (31-33). The distal radius has been shown to be the most ideal and reliable site for limb salvage (34). Complications associated with surgical limb salvage are high and include implant loosening, infection and local tumor recurrence (31, 32). These common complications may result in revision surgeries or amputation (1, 32, 34, 35). About 20% of dogs experience local tumor recurrence which can be treated by further surgery or amputation without decreasing median survival time (32). Nearly 40% of all limb sparing surgeries become infected; however, it is interesting to note that these dogs tend to have longer survival times than animals that do not develop infections (32, 36). Similar observations have also been reported in human OSA patients with post-operative infections (37). This suggests that

increased immune surveillance triggered by the acute infection may be suppressing metastatic growth leading to prolonged survival time.

Adjuvant chemotherapy must be administered following both amputation and limb sparing surgery to improve survival times (35). The primary reason for chemotherapy is to prevent or delay the development of distant metastases (35). The most commonly used chemotherapeutics for bone sarcomas are cisplatin, carboplatin and doxorubicin (35, 38). Cisplatin is a heavy metal platinum compound that has been shown to have adverse effects on the renal system. Carboplatin is a second-generation platinum drug that has less severe effects on the kidneys and other organs. Doxorubicin is an anthracycline chemotherapeutic with the potential to cause dose related cardiomyopathy. These drugs damage cellular DNA and inhibit DNA repair mechanisms; therefore, interfering with cellular division and causing apoptosis of the cancerous cells (39). The median survival time for dogs treated with amputation or limb salvage surgery followed by adjuvant single agent or combination chemotherapy is approximately 1 year (5).

Despite increased survival observed with the addition of adjuvant chemotherapy over amputation alone; only about 50% of these dogs survive 12 months and 25% two years (20, 40). This relatively short time is due to OSA resistance to chemotherapeutics (20). However, there is evidence that activation of the immune system can kill chemoresistant cancer cells by activating tumoricidal macrophages and monocytes targeting the cancerous cells (41). Several immune modulators have been developed to help stimulate the immune system to attack the tumor. One such modulator, Liposome-Encapsulated Muramyl Tripeptide (LMTPE), has been shown to

increase median survival in dogs with OSA from 77 to 222 days; thus, the use of these modulators may provide a therapeutic advantage in the future (42).

### **Radiotherapy for Osteosarcoma**

Osteosarcoma has been reported to be relatively radioresistant (43). Curative-intent fractionated XRT of OSA has been shown to be ineffective for long-term local tumor control unless very high doses of radiation are administered (43-45). At these higher total doses, the complication rate from acute and late radiation effects to normal tissue are unacceptably high. Because of this, curative-intent XRT of OSA has not been widely utilized in the curative-intent treatment of OSA. Total radiation dose delivered with XRT is limited by the radiation tolerance of adjacent normal tissues. Human studies have found similar results using XRT for the treatment of OSA. Total doses of 30 Gy (1.5–3 Gy daily fractions) don't result in tumor control of OSA, whereas higher total doses exceeding 55 Gy (1.5–3 daily Gy fractions) were successful (8, 46). Unfortunately, high doses have historically resulted in adverse effects to normal tissues and organs in the radiation field when fractionated XRT is used (43).

In a study by Walters *et al*, 14 dogs diagnosed with OSA were treated with full course XRT and adjunct chemotherapy as a curative-intent therapy (47). Dogs received total radiation dosages between 48 and 59.6 Gy over approximately 19 fractions (2.9 Gy/Fx) delivered daily (Monday – Friday). Local tumor control was achieved in approximately 4 of 6 tumors analyzed (14 total) (47). It was also reported that the majority of dogs experienced acute radiation related side-effects. Reported median survival time was 209 days which was not significantly increased

survival when compared with palliative XRT. This study was limited by small number of cases, had varied sites of primary tumor location and lacked complete histological analyses after euthanization (47). However, it demonstrates known limitations of utilizing finely fractionated XRT for curative intent treatment.

Intraoperative irradiation therapy (IORT) is an alternative strategy that has been used to deliver a high biologically effective dose to the tumor while sparing normal tissues (14, 48). This technique involves a surgical procedure where the skin, tendons, muscles and nerves are retracted from the tumor-bearing bone. The patient is then treated with high doses of radiation in a single treatment in which normal tissues are refracted outside the treatment field. In a study by Liptak, et al., thirteen dogs diagnosed with primary bone sarcoma underwent IORT with a single fraction of 70 Gy followed by chemotherapy. Local tumor control was achieved in 10 dogs while the remaining three experienced local tumor recurrence (48). Complications included pathologic fracture, which was observed in 7 dogs, and infection in 3 dogs (48). The median survival of the animals was 298 days. In a separate study, five dogs with osteosarcoma (n=4) or anaplastic sarcoma (n=1) of the distal radius were treated with IORT with the aim of preservation of function of the radiocarpal joint. A single fraction of radiation between 45 and 100 Gy was delivered to the lesion (14). Chemotherapy was also locally delivered to the tumor site (14). The dog with anaplastic sarcoma experienced local tumor recurrence and was euthanized. One of the dogs with osteosarcoma experienced implant failure and the other three developed pathologic fracture. Survival, although in a small population dogs, was encouraging and ranged from 15 to 24 months (14). The use of IORT when combined with adjuvant chemotherapy, exhibits survival times similar to that of other limb-sparing surgeries. In addition to dogs, IORT has been

successfully used for the treatment of advanced pelvic, head and neck cancers in humans (49). This approach suggests that local tumor control and extended survival times may be achieved with high dose radiation therapy.

### *Fractionated curative intent Radiation Therapy in Humans*

In humans, standard of care therapy for OSA involves limb-sparing surgery in combination with neoadjuvant chemotherapy (50). Amputation provides excellent tumor control; however, it is considered less ideal due to the resulting physical limitations. Limb sparing surgery may be associated with local tumor recurrence due to the inability to achieve wide margins during resection especially in difficult areas such as the pelvis and axial skeleton (46). Using radiation therapy alone has not traditionally been successful as it does not treat metastatic disease (51). A combination of chemotherapy and radiation, limb-sparing, pre-operative radiation therapy and chemotherapy have shown to be most effective (46, 52).

In a study by Caceres, et al., 15 human patients were treated with radiation in combination with chemotherapy. Tumor control was observed in 80% of the patients compared with a previous study using radiation alone resulting in 20% tumor control (51, 53). However, pathological fracture frequently occurred and pulmonary metastases were present in 71% of the patients indicating the chemotherapy treatment was aiding in local tumor control but not for the prevention of metastatic disease (53). A limitation of this study was the lack of long-term follow-up due to deaths from metastatic disease. The use of chemotherapeutics to prevent metastasis and increase survival has greatly improved in the past several years. Recent studies have shown local

tumor control at 5 years of approximately 56 percent (52). These patients were treated with 2.5 to 3 Gy daily fractions for a median total dose of 60 Gy along with chemotherapy (52). In a similar study, the combined 5 year survival was 68 percent when patients were treated with a median dose of 66 Gy in 1.5 to 3 Gy daily treatments with chemotherapy (46). Interestingly, this study also included patients with previous gross or subtotal tumor resection which yielded a 78% median survival at 5 years (46). Other studies have shown that a combination of limb-sparing, chemotherapy and radiation therapy offers promise in the treatment of OSA. Dincbas et al. showed that pre-operative radiation combined with chemotherapy showed a 5-year local tumor control rate of 97 percent and survival of 48 percent (50). The satisfactory local tumor control achieved with pre-operative radiation and limb sparing may be due to the further killing of OSA tumor cells at the resected margins which were not the previously removed due to narrow resection margins.

### *Radiation Tissue Tolerance*

To better predict the radiation tolerance of tumors and normal tissues, a linear-quadratic model based on cell survival of many cell types (normal and cancerous) has been developed (Figure 1) (54).

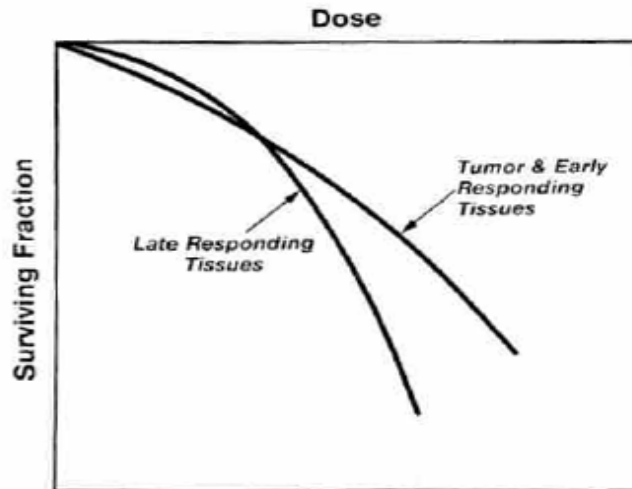


**Figure 1: Late responding tissues have a lower alpha:beta ratio while most tumors and early responding tissues have a higher alpha:beta ratio (55).**

The alpha (linear) and beta (quadratic) ratio describes the curvature of the cellular survival curve in the model (54). Most tumors have a high  $a/b$  ratio ( $>7$ ) and are considered to be radiosensitive to XRT (54). Normal tissues such as kidney, skin, gastrointestinal tract and bone marrow undergo regular cellular proliferation and as such are also very sensitive to the effects of radiation. These tissues are known as acute responding tissues. However, normal tissues are better able to repair DNA damage between fractionated radiation doses compared to tumor tissue treated with XRT. Other normal tissues such as nervous tissue, lung, muscle and bone undergo cell division less frequently and are considered late-responding tissues. Tumors with a low alpha:beta ratio behave more like late responding tissues and are difficult to control with traditional fractionated radiation protocols. Fractionated radiation therapy can be successfully used to treat acute responding tumors (high  $a/b$  ratio) because the biologically effective dose to achieve tumor control is smaller, thus allowing for normal tissue recovery (54). In radio-resistant

tumors (low alpha:beta ratio); however, a higher total dose of radiation or a high dose per fraction is needed to obtain efficacy. Unfortunately, the high doses required to achieve tumor control results in unacceptable toxicity to the surrounding normal tissues when delivered via conventional XRT protocols.

## **1.2 Stereotactic Radiation Therapy**

Stereotactic radiotherapy (SRT) is a newer radiation treatment modality that precisely delivers high doses of radiation to well-defined tumor volumes with rapid dose fall off in surrounding normal tissues, thereby minimizing radiation exposure to these tissues. SRT has been successfully used for solid tumor ablation in tissues such as; lung, liver, brain, prostate, head, neck and spine. SRT has the unique ability to accurately deliver high dose per fraction radiation using image guidance, multiple radiation beams and intensity modulation directly to the isocenter of a tumor. This ability, along with the ability to sculpt dose centered geometrically around to tumor allows for the preferential sparing of normal tissue (56). Because adjacent normal tissue is protected by this steep dose gradient, it allows for a smaller normal tissue volume to be affected by the radiation thus a higher biologically effective radiation doses may be administered to the tumor. This strategy is advantageous for treating relatively radio-resistant tumors (low alpha:beta ratio). Reports have indicated that OSA is relatively radiosensitive with a mean alpha:beta ratio of 3.5 and suggests SRT may be an advantageous therapy (57).

Stereotactic radiotherapy has been successfully used for local tumor control of primary and metastatic vertebral tumors in humans (58). It is well recognized that dosages exceeding 65

Gy of conventional XRT dosages are needed to achieve local tumor control in metastatic vertebral tumors (59). These higher radiation dosages are feasible with XRT, but the fraction sizes must be smaller due to the close proximity to the spinal cord (58). Smaller fractions make it difficult to achieve tumor control of OSA with XRT in this setting. Stereotactic radiotherapy is better suited for locations such as the spine because it reduces the volume of normal tissue exposed to radiation. In a recent study consisting of 24 patients, SRT was delivered in 3 daily fractions of 30 Gy to patients with primary and metastatic vertebral tumors (58). Patients with primary tumors (n=7) exhibited significantly greater pain relief and survival (Range: 29-49 months) at a 33-month follow-up compared to those who received XRT. The remaining seven patients with metastatic tumor reported decreased pain and a mean survival of 11 months compared to five months with traditionally delivered XRT. Complications related to SRT were minimal and no incidence of radiation myelopathy was reported (58). These results suggest that SRT may have a role in the treatment of primary vertebral tumors and palliative treatment of metastatic disease.

In the past several years, SRT has become a new treatment paradigm for non-surgical limb salvage of canine OSA. In a study by Farese, et al, 11 dogs that presented with OSA in the appendicular regions were treated with SRT. The radiation treatment protocol consisted of one large fraction of radiation (20-30 GY) with the intent to achieve local tumor control (60). Additionally, six of these animals were given carboplatin chemotherapy prior to SRT and then adjuvantly (60). Carboplatin acts as a radiosensitizer when given in combination with radiation therapy by enhancing single and double strand DNA breaks (27, 52, 61). It can also inhibit the repair of radiation induced single-strand breaks (62). Follow-up radiographs of the primary

tumors revealed decreases in tumor-associated swelling and calcification of the lesions at three months post SRT. Lameness decreased in all animals for up to three months post-treatment. At four months, dogs that were treated with SRT alone experienced pathologic fracture or tumor recurrence. Those that received chemotherapy combined with SRT had a median survival time greater than 365 days (n=6) (60). Similarly, we have observed excellent local tumor control in a prospective study with 50 dogs with appendicular OSA treated with SRT at Colorado State University. A Varian Trilogy linear accelerator with image guidance was used to deliver 3 fractions of 12 Gy (36 Gy total) to the tumor lesion on consecutive days. Carboplatin was administered at the time of the first or second fraction of SRT and then continued every three weeks for a total of 6 treatments. Tumor control was assessed by percent tumor necrosis. The most common complication was pathological fracture, which occurred in 40% of dogs at a mean time of 5.8 months after SRT. The median survival time for the dogs treated with this protocol was 275 days (Range: 66 to 723 days) (63). Taken together, these studies suggest that the combination of SRT and adjuvant chemotherapy is efficacious for tumor control in the treatment of appendicular canine OSA. However, pathologic fracture as a late-term complication continues to be a challenge.

#### *Normal Bone Healing and effects of Radiation on bone formation and healing*

Normal bone remodeling involves a dynamic equilibrium in which osteoclasts and osteoblasts are continually renewing bone to achieve homeostasis with no net gain or loss of bone. In normal bone, osteoclasts resorb calcified bone and then osteoblasts induce new bone growth in a process called osteogenesis. Osteogenesis occurs via two distinct pathways known as

intramembranous and endochondral ossification. Intramembranous ossification is important for the development of flat bones such as the skull and clavicles. In these bones, bone is formed from mesenchymal progenitor cells that differentiate directly into bone forming osteoblasts (64, 65). These osteoblasts secrete osteoid (bone matrix) and cells within this matrix become osteocytes (66). The accumulating osteoid with the formation of blood vessels and nerves become the trabeculae. Finally, the external face of the matrix condenses to form the outer surface of the bone called the periosteum (66). Endochondral ossification is important for the development and growth of the long bones as well as for fracture healing (67). This process differs from intramembranous ossification. In this process, mesenchymal cells differentiate to form a collagen template (66). This template then recruits osteoblasts to form a primary site of ossification in the center of the diaphysis (64). Next, osteoblasts begin to produce osteoid to form the bone matrix and results in the formation of the bone collar around the shaft of the collagen templates. This matrix then begins calcification and results in the formation of cavities within the bone as well as two new centers of ossification in the epiphyses (66). Finally, ossification of the epiphyses occurs and cartilage remains in the growth plates and articular regions (66).

Fracture healing is a complex and highly regulated process that involves a cascade of biological events involving progenitor cells, osteoclasts, vascular and inflammatory cells as well as proinflammatory cytokines, growth factors and pro-osteogenic and angiogenic proteins. It has been described as a four stage process (68). A fracture results in disruption to the bone, marrow, and vasculature integrity. The first stage results in a response to the injury where macrophages, platelets and other inflammatory cells are recruited by the secretion of a plethora of cytokines (e.g. transforming growth factor- $\beta$ , platelet-derived growth factor, vascular endothelial growth

factor, interleukin 6, etc.). These immune cells participate in the debridement of damaged cells and other debris. (68, 69). The second stage involves the development of the soft callus. Mesenchymal progenitor cells migrate to the affected area and begin to differentiate into chondrocytes, forming a soft callus (cartilaginous matrix) that provides mechanical support as well as a template for new bone formation to occur (68). This callus grows to fill the void between the injury and normal bone. The chondrocytes then begin to mineralize the matrix by recruiting osteoblasts (68). Vascular endothelial cells also begin to infiltrate the matrix in this stage. The third stage involves the formation of the hard callus and where primary bone is formed. The soft callus is slowly removed by osteoclasts and osteoblasts begin synthesizing the mineralized bone matrix (unremodeled) (68). The final stage consists of remodeling the immature hard callus into mature bone (Cortical/trabecular bone). This occurs through the dynamic process of remodeling with osteoblasts and osteoclasts which converts the woven bone into normal cortical bone (68).

Radiotherapy has been shown to have detrimental effects on bone structure, remodeling and healing. It can decrease bone mineral density otherwise known as osteopenia. Studies have shown that irradiation with greater than 20 Gy can result in a 23% decrease in mineral density resulting in decreased bone strength and increasing the risk of fracture (70). Radiation also affects the nonmineralized bone components such as vasculature, marrow, osteoprogenitor cells, osteoclasts and bone forming osteoblasts (71). Whole body radiation doses as low as 10-12 Gy, a dose often used for the treatment of leukemia, will completely ablate the bone marrow (72). Bone forming osteoblasts and osteocytes as well as bone resorbing osteoclasts are also radiosensitive. Osteoblasts are most sensitive to radiation. Osteoclasts, which are less sensitive,

survive longer than osteoblasts post-radiation and continue to resorb bone and degrade the bone matrix (73). Uncoupling of the normal remodeling process can result in pathologic fracture, bone fragmentation, and impaired healing (73-75). Inflammation induced by irradiation can also be detrimental to bone healing by causing bone to release cytokines that attract immune cells that can destroy endothelial cells, induce thrombosis, and necrosis. In normal wound healing, the duration of cytokine release is relatively short; however, in radiation injury the inflammatory process can linger for much greater lengths of time. The length of the inflammatory processes after radiation has been shown to linger from 2 to 26 weeks depending on the total dose, fraction size and the time in which treatment was delivered (76). Larger fraction sizes over longer periods of time resulted in markedly increased production of inflammatory mediators (76). Clearly, radiation injury to bone involves many complex and detrimental processes affecting the bone structure, cellular components and recruitment of inflammatory cells that can inhibit the ability of bone to recover after radiotherapy. These effects persist longer with increasing dose and fractionation. Therefore, therapies designed to improve bone health following radiation injury must address these issues.

As previously discussed, the most common complication associated with SRT or any high dose radiation therapy of OSA-affected bone is pathologic fracture. This occurs due to pre-existing tumor-associated osteolysis which causes biomechanical and structural weakening of the bone as well as the cytotoxic effects of radiation on the surrounding normal bone impairing the ability of bone to remodel and heal (14, 47, 60, 63). Pathologic fracture is a serious, limb threatening complication of SRT for the curative-intent treatment of OSA often resulting in limb amputation (14, 77, 78).

New therapies that diminish the risk of fracture through radioprotection or bone regeneration strategies are needed in order to advance the use of SRT as a viable non-surgical limb salvage procedure for OSA. In humans, bisphosphonates such as pamidronate and zoledronic acid have been successfully used to decrease the frequency of fracture in osteoporosis and metastatic bone cancer by inducing apoptotic cell death of osteoclasts; therefore, inhibiting their ability to resorb bone a component of tumor associated osteolysis (79). The use of growth factors such as Transforming Growth Factor beta (TGF- $\beta$ ), have been used because of their ability to stimulate the proliferation and differentiation of osteoblasts (80). Ehrhart et al. showed that administration of TGF- $\beta$  to rabbits after radiotherapy enhanced bone formation (81). Other important growth factors such as Basic fibroblast growth factor (bFGF) and Bone Morphogenetic Protein-2 (BMP-2) have also shown regenerative properties in irradiated bone (82). These growth factors administered alone, or in combination show promise for decreasing the risk of fracture in irradiated bone and are being investigated.

The late effects of radiation therapy on bone and other tissues have been well documented and include secondary tumor induction, fibrosis, endocrine disorders and neural damage (83-85). These effects usually occur within 5 to 10 years after radiation treatment and can be irreversible or progressively more severe than that of short term effects (84). There is potential concern that SRT may induce similar late term effects due to the large dose per fraction radiation protocol used in late responding tissues such as bone, muscle and nerves. Currently, the long-term effects of SRT on bone are not well understood. Further studies are needed to better understand the long-term risks of SRT (84, 86).

### 1.3 Mesenchymal Stem Cells

Mesenchymal stem cells (MSCs) are multipotent adult stem cells found primarily in the bone marrow, but have also been observed in other tissues including the liver, adipose tissue, lungs, placenta, blood and umbilical cord (87). MSCs have the potential to differentiate into various cell types including chondrocytes, adipocytes and osteocytes (88). Differentiation of MSCs is modulated by a variety of biological factors that are unique for each differentiation lineage. While the complex interactions that are required to promote differentiation are still being investigated, key pathways have been identified. For example, in chondrogenesis, transforming growth factor (TGF- $\beta$ ), bone morphogenetic proteins (BMPs), growth differentiation factors (GDF) and Wnts (early mediators of differentiation) are critical for the differentiation of chondrocytes (87). Nuclear hormone receptor peroxisome proliferator-activated Receptor (PPAR $\gamma$ ) has been shown to be a potent regulator of adipogenesis (87). In osteogenesis, BMPs, specifically BMP-2 and BMP-6, induce a gene called Runx2 which is a master osteogenic gene (87). Interestingly, various factors interact to promote a specific lineage. For example, Runx2 can repress PPAR $\gamma$  thus blocking adipogenesis and promoting osteogenesis. The converse is also possible where coregulators in combination with PPAR $\gamma$  can block Runx2 to induce adipogenesis (87). The ability of MSCs to differentiate into many different cell types holds promising regenerative therapeutic potential.

Because MSC's can differentiate into osteoblasts, the use of MSCs to help generate new bone is of particular relevance to this thesis. MSCs have been shown to promote bone new bone formation in several animal models. These studies have shown that MSCs can home to damaged

tissues, promote angiogenesis, regenerate bone, and accelerate healing (71, 89, 90). One mouse model consisted of an allograft implantation into diabetic mice that incorporated MSCs into the allograft (89). The presence of diabetes was hypothesized to additionally delay the bone repair process. Briefly, a segment of the femur was removed and replaced with a demineralized bone matrix (DBM) allograft containing no cells or MSCs. At just four weeks, significant increases (300%) in bone formation were observed in the mice with MSCs compared with the DBM alone. Furthermore, more mature bone was observed at 8 weeks in the MSC group (89). A larger animal model using rabbits seeded MSC into the medullary canal and periosteal surface of allografts and compared healing to allografts without MSCs (91). Rabbits with MSCs exhibited significantly increased bone formation. Another important aspect of this experiment was the evaluation of allograft incorporation into the host bone. Poor allograft incorporation is the major cause of allograft failure (92). The results further indicated that MSCs enhanced allograft incorporation into the host bone at 12 weeks (91).

A fracture healing study investigated the healing potential of MSCs transplanted into fractured mouse tibias. (90). Tibias were stabilized with a stainless steel pin and then fractured using a bending device. MSCs were injected at the fracture site and evaluated at 7 and 14 weeks. Significant increases in bone callous and mature bone were observed in the MSC treated mice. Tibias were then subjected to biomechanical testing which revealed that MSC treatment increased stiffness and ultimate tensile strength (90). A rat model utilizing a femoral defect showed similar results; however, MSC's in this study were infused through the left ventricle (93). Additionally, MSCs expressed the Green-fluorescent protein, which allowed for ex vivo imaging. As with the murine model previously discussed, this rat model also resulted in

increased bone healing as compared to the control group (no MSCs). Furthermore, fluorescent imaging showed MSCs were present at the site of the fracture which confirmed the ability of MSCs to home to the site of injury (93). These studies indicate that MSCs administered locally or systemically resulted in accelerated fracture healing when compared to animals that did not receive MSCs.

Mechanisms by which MSCs induce new bone growth have been proposed. They have been shown to directly induce bone formation by directly differentiating into osteoblasts (intramembranous ossification). Alternatively, they have been shown to form a collagen template first and then produce new bone via the endochondral pathway (94). Both localized delivery and systemic injection of MSCs have been effective in generating new bone (90). For systemic delivery, it has been shown that the inflammatory response (e.g. cytokines and chemokines) to bone injury creates a chemotactic gradient that allows administered MSCs to migrate to the site of injury (90). Additionally, MSCs can indirectly induce bone formation through osteoinduction. Osteoinduction is the process whereby cells can be stimulated to differentiate into bone forming osteoblasts (95). This means that MSCs have the ability to secrete factors, such as stimulatory cytokines and growth factors, to nearby cells to induce growth (95). These factors then interact with host cells to induce cellular migration of osteoprogenitor cells, promote proliferation, modulate inflammatory responses and promote host angiogenesis (96). Although the indirect actions by which MSCs stimulate other cells to produce bone are poorly understood, it is believed that these indirect actions may be as important if not more than the direct action in forming new osteoblasts (97).

Osteoinduction is often confused with osteoconduction, which is a material that possesses properties that allow bone to grow on its surface (95). Osteoconductive surfaces such as bone grafts or implanted biomaterials can serve as a scaffold conducive for bone formation. Examples of osteoconductive biomaterials can include pure titanium, hydroxyapatite, allografts and xenografts. Some materials can be both osteoconductive and osteoinductive as they can be coated with growth factors (e.g. insulin-like growth factors, TGF- $\beta$ , Fibroblast-growth Factor (FGF) and BMPs) and/or seeded with stem cells that can trigger bone formation in addition to serving as a scaffold. A few examples of these materials include demineralized bone matrix, autografts, and hydroxyapatite coated with growth factors or stem cells (98, 99).

#### *Mesenchymal Stem Cells and Radiation*

Few studies have assessed the ability of MSCs to regenerate bone in irradiated areas, especially following high dose irradiation. Interestingly, a murine study suggests that MSCs can migrate directly to radiation-injured tissues (100). Another experiment showed that MSCs more readily migrate to irradiated tumors (101). Furthermore, MSCs have been shown to revitalize bone that has been previously irradiated (102). Together, these observations suggest MSCs may be targeted towards radiation-injured tissue such as bone and may subsequently result in bone generation or healing. (100-102). Therefore, it is important to investigate the potential of MSC as a novel treatment for radiation induced bone injury since it is one of the leading complications of radiation treatment.

The effects of radiation on the structural integrity and regeneration of bone has been extensively studied. Studies have shown the negative effects of radiation on bone mesenchymal stem cells (71). It is well known that the bone marrow and subsequently bone marrow MSCs are very sensitive to radiation therapy (103). This may help explain the decreased regenerative properties of irradiated bone. In a study by Cao, et al, the distal half of femurs in mice were subject to 4 Gy of ionizing radiation per day for 5 consecutive days while the proximal half were left untreated (71). Initially, all MSCs from the entire bone disappeared; however, MSCs repopulated in the proximal half while MSCs in the direct radiation field were absent. Free radicals induced by radiation have been shown to have detrimental effects to adjacent bone marrow MSCs (104). In the unirradiated half, free radicals increased directly after radiation but returned to basal levels at four weeks; however, in the untreated half, free radical levels remained high. The authors suggested that free radicals induced by radiation treatment caused a temporary dormancy of the MSCs in the non-irradiated half of the femur but the high levels remaining in the distal half led to MSC death. Histological analysis of the treated femurs also revealed decreases in the numbers of osteoclasts, osteoblasts and MSCs in the irradiated area compared to the unirradiated area (71). The authors proposed that destruction of the vasculature in the irradiated area most likely prevented migration of MSCs to the site of radiation injury. Decreasing radiation-mediated MSC death or introducing MSCs into these irradiated regions may be a viable method to restoring radiation damaged bone health.

## *Mesenchymal Stem Cells and Tumor Promotion*

Although MSCs have a number of promising therapeutic applications, there is also concern about their potential to promote oncogenesis (105). The ability to differentiate into multiple lineages poses the possibility that they may also mutate into cancerous cells or migrate to existing cancerous cells and promote abnormal growth and migration (105). A study by Hung et al showed intravenously injected MSCs migrated to existing tumor xenografts and resulted in increased tumor size compared with no MSC injection (105). In a subsequent osteosarcoma model, MSCs were also shown to migrate to the osteosarcoma tumor site and promote local tumor growth and metastasis (106). The tumor promoting properties of MSCs pose a potential risk for local tumor reoccurrence or acceleration of distant metastatic growth if used as therapy to regenerate bone. Given these observations, using MSCs for bone healing of primary OSA may promote the development of undetectable disease in the lungs or bone.

### **1.4 Specific Aims**

Osteosarcoma is the most common form of primary bone cancer in dogs and humans. Curative-intent treatment options include amputation, stereotactic radiation therapy or surgical limb salvage for local tumor control with the use of adjuvant chemotherapeutics for the treatment of micrometastases. Stereotactic radiotherapy (SRT) is an emerging treatment modality for local tumor control of primary osteosarcomas due to its ability to deliver high dose per fraction radiation while sparing surrounding normal tissues. The most common complication observed

with this treatment is pathologic fracture in the irradiated area due to pre-existing tumor associated osteolysis and loss of local remodeling capability of osteocytes secondary to SRT.

Mesenchymal Stem Cells (MSCs) are multipotent stem cells that have the capability to differentiate into many cell types including bone. The capability of MSCs to differentiate into bone suggests that they may have therapeutic benefit in sites of SRT treated bone thereby reducing the risk of pathological fracture. These observations, along with the clinical need for novel treatments for osteosarcoma, have led us to pose and explore the following hypothesis:

***Mesenchymal stem cells will promote new bone formation in osteosarcoma affected irradiated bone treated with ablative stereotactic radiotherapy***

This hypothesis will be evaluated by the following specific aims:

**Specific Aim 1: Developed an orthotopic rodent model of canine osteosarcoma.** Completion of this aim will characterize an athymic rat model of a luciferase expressing osteosarcoma. This model will then be used in subsequent experiments to evaluate SRT as a treatment modality for OSA and the ability of MSCs to enhance bone regeneration post-SRT. Approach: We will characterize the growth and progression of canine osteosarcoma tumor cells injected into athymic rat tibias and femurs with serial radiography, bioluminescent luciferase imaging, micro-computed tomography (microCT) and histological analysis. Additionally, a biomarker for bone resorption, pyridinium (PYD), will also be measured to correlate tumor-associated osteolysis with imaging.

We hypothesized that the canine OSA cell line would engraft and exhibit predictable temporal progression in the tibia and femur. We expected increased radiographic evidence and bioluminescence over time as well as increased PYD levels as a consequence of tumor progression.

**Specific Aim 2: Evaluated the effectiveness of SRT to achieve local tumor control in an orthotopic tumor model.** This aim will test the hypothesis that SRT effectively achieved local tumor control in the orthotopic OSA rat model developed in Specific Aim 1. Approach: Athymic rats were inoculated with a canine OSA cell line in the distal femur and SRT was administered approximately two weeks later when engraftment was established. Different fractionation and total radiation dose protocols were evaluated. Local tumor control after SRT was monitored by serial *in vivo* radiography, luciferase imaging, urine PYD analysis and histology to evaluate the effectiveness of SRT to achieve local tumor control.

We hypothesized that there would be a dose dependent increase in percent tumor necrosis. We further hypothesized that higher doses would be associated with higher necrosis (i.e. %TN > 80%) and smaller doses would be associated with lower necrosis (i.e. %TN < 80%). We also expected the severity of any acute effects to be increased with an increased total dose. The results from this experiment determined the optimal fractionation and total radiation dose protocol needed to achieve desirable local tumor control and was used in Specific Aim 4.

**Specific Aim 3: Isolated Green Fluorescent Protein (GFP) expressing mesenchymal stem cells from transgenic GFP rats and evaluated their ability to differentiate into all three**

**lineages.** This aim involved isolating bone marrow and adipose MSCs from transgenic rats that ubiquitously express GFP. Approach: MSC cell lines were established from bone and adipose tissues and GFP expression was confirmed by fluorescent imaging using a Xenogen camera. Additionally, isolated GFP-expressing MSCs were subject to three different lineage specific differentiation growth media to confirm their ability to differentiate into osteoblasts, chondrocytes and adipocytes.

We hypothesized that MSCs isolated from the bone marrow and adipose tissue from rats would exhibit multipotency when subjected to differentiation media as well as GFP expression. These cells were used in subsequent experiments to evaluate the potential of MSCs to promote bone formation after SRT in the rodent model developed in Specific Aim 2. The GFP expression enabled the identification of the MSCs in histological analysis of the bone as well as differentiated between host and MSC mediated bone formation.

**Specific Aim 4: Evaluated the ability of allogenic MSCs to induce new bone growth after SRT.** This aim tested the hypothesis that adipose MSCs could regenerate bone in SRT-treated bone. Approach: Rats were injected with canine OSA cells and treated with the optimal SRT protocol derived in Specific Aim 2. Two weeks after radiation, allogenic rat GFP expressing MSCs were injected either intravenously (IV) or intraosseously (IO) directly into the previous tumor-bearing site of the femur. New bone formation was determined using histology and the source of new bone formation (host or MSCs) by immunohistochemistry analyses. Animals were also monitored bi-weekly by radiography and luciferase imaging to determine if MSCs used for bone regeneration post-SRT treatment of OSA induced local tumor recurrence or metastatic

lesions. We hypothesized that MSCs would induce new bone growth in both the IV and IO treatment groups and no new bone growth would be observed in the SRT only group.

## **Chapter 2: Development of an Orthotopic Osteosarcoma Model in a Rat**

### **2.1 Introduction**

The goal of these experiments was to develop and characterize an orthotopic model of canine OSA in a rat. This model could serve as a valuable tool to evaluate SRT as well as other adjunctive therapies. It allowed us to determine the appropriate timing of SRT intervention and optimization of SRT treatment protocols (dose and fractionation schemes) to achieve local tumor control that was developed in Chapter 3. Furthermore, it allowed us to investigate the potential therapeutic use of MSCs for bone generation after SRT in a tumor affected bone location as described in Chapter 5.

Animal models of cancer have been developed to help characterize the disease and evaluate the efficacy of new therapeutic treatments. Allogeneic and xenogeneic tumor models have been used for studying the effects of new treatments. Xenogeneic models involve the use of cells from a species different from the host whereas allogenic models use cells from different individuals within the same species. Xenogeneic studies are often performed in immune-compromised animals, so that tumors from different species can grow without rejection from the host. Despite this advantage, it is important to understand that immune-compromised recipients lack a normal immune response. This may alter response to treatment and therefore may not reflect the clinical scenario. Despite this limitation, xenogeneic models allow for the study of specific mechanistic questions and the evaluation of new treatments in large numbers of experimental animals with control of specific variables.

Orthotopic animal models of cancer have been shown to better simulate localized disease than heterotopic models, as they allow the tumor to grow in the typical anatomical site similar to the conditions in which spontaneous tumors occur. As a result, cancerous cells encounter a similar microenvironment to the spontaneously-occurring disease, wherein the cellular microenvironment more closely mimics the biologic and metastatic properties of the native cancers (107). In regards to these studies, the orthotopic model will better simulate the osteolytic processes such as lysis and destruction of the existing bone that are observed in clinical cases of OSA. Heterotopic locations do not expose the tumor to the same environment; therefore, they may behave in a manner less like that of spontaneously occurring disease in an orthotopic location. These locations are often used to simulate metastatic disease. Outcomes of experimental therapeutic interventions in these models may not translate accurately or reliably to the clinical setting. As such, orthotopic models are considered superior as they more readily predict treatment outcome of spontaneous tumors when subjected to different therapies for localized treatment (107).

Orthotopic mouse and rat models of primary osteosarcoma have been previously characterized (108-110). In a study by Nieves, et al, various canine osteosarcoma cell lines were injected into the tibiae of athymic mice (108). OSA successfully developed and progressed in 50 to 88 percent of mice depending on the particular cell lines. An orthotopic rat model of rat osteosarcoma has also been recently developed that showed reliable and repeatable implantation and progression (109). To our knowledge, no orthotopic rat models of canine osteosarcoma have been developed.

The goal of specific aim 1 was to develop a reproducible, temporally predictable orthotopic rat model for canine OSA for the evaluation of SRT in Chapter 3. The rat was preferred over the mouse due to its larger relative size. It would not be feasible to administer SRT to a mouse due to the treatment field limitations of the linear accelerator. We hypothesized that an OSA intraosseously injected into the cancellous bone of the proximal tibiae or distal femurs of nude rats would engraft and exhibit predictable temporal progression. The cell line used for these experiments was established from a spontaneous metastatic bone tumor in a dog. It was also transfected to express a bioluminescent luciferase reporter gene. When the luciferin enzyme interacts with the luciferase promoter on the luciferase gene of the OSA cell, photons are emitted and can be visualized through a bio-luminometer or specialized imaging equipment (111). This permits serial real-time *in vivo* visualization of the OSA cells throughout the experiment without the need to sacrifice additional animals. In addition, radiography, histology and microCT imaging techniques were also used to evaluate tumor engraftment, predictability of temporal progression and consequent production of osteolytic lesions.

Osteosarcoma results in breakdown and release of Type I collagen due to tumor-associated osteolysis. Bone tumors promote bone resorption by secreting growth factors and cytokines that stimulate osteoclastic bone resorption (112). The breakdown products of osteolysis (NTx, PDY, and DPD) can be measured in the serum or urine by various commercial assays (113). Serum and urine NTx levels can differentiate bone resorption associated with OSA compared to other orthopedic diseases such as osteoarthritis in dogs (114). In dogs with spontaneous OSA, NTx levels are elevated compared to healthy animals (114, 115). Treatment by amputation of the affected limb, administration of radiation and bisphosphonates in these animals resulted in a decrease in NTx levels, indicating response to therapy (24, 115).

Commercial assays for the detection of NTx do not exist for rats. However, assays do exist for the measurement of PYD and DPD in rats. To evaluate the degree of tumor-associated osteolysis, we measured the levels of PYD in the urine and compared the mean PYD values between treatment groups.

More than 90% of bone matrix is made up of Type I collagen which is cross-linked with deoxypyridinoline (DPD) and pyridinoline (PYD) providing support rigidity and strength (113). The breakdown of type I collagen by osteoclasts releases collagen fragments (NTx) and the pyridinoline cross-links (PYD and DPD (peptide bound or free)) from bone. These fragments are excreted in the urine. Peptide bound (Type I collagen fragment bound to PYD or DPD) assays include N-telopeptide ( NTx) which measures the N-terminus of the collagen fragment and N-telopeptide (CTx) which measures the C-terminus of the collagen fragment (113). These are a direct measure of Type I collagen breakdown. Unbound PYD and DPD peptides are the end products of the metabolism of Type I collagen have also been shown to indirectly measure Type I collagen breakdown (113). These values have been shown to increase in rat models of metastatic bone cancer thus it should allow for the measurement of the osteolytic processes occurring as a result of the progression of OSA. (116).

## 2.2 Materials and Methods

**2.2.1 Experimental Design:** Two experiments were conducted to develop and characterize the animal model. See Appendix A for complete experimental details of experiments outlined in this Specific Aim.

- a. Twelve rats were inoculated transcortically with a canine OSA cell line into the proximal tibial metaphysis. Tumor engraftment and progression was documented with weekly radiography, bioluminescence imaging and urine PYD measurements. Three randomly-selected rats were euthanized at 2, 3, 4 and 5 weeks after OSA inoculation and the tibias were subject to microCT and histology analysis.
- b. Six rats were inoculated with OSA into the distal femur and followed for 6 weeks. The aim of this experiment was to increase the animal numbers to increase the statistical power of the data and to evaluate a different tumor cell inoculation site. Tumor engraftment and progression was documented with weekly radiography, bioluminescence imaging and urine PYD measurements. All rats were euthanized 6 weeks after tumor cell inoculation and the femurs subject to histological analysis.

**2.2.2 Cells:** Abram's luciferase-expressing canine osteosarcoma cell line was generously provided by the Colorado State University Animal Cancer Center. Canine OSA cell validation was performed by multiplex PCR using mitochondrial DNA to ensure the cell line was from canine origin and free of contamination (117). The cells were grown at 37°C with 5% CO<sub>2</sub> in Minimum Essential Media (MEM) supplemented with 10% fetal

calf serum, 7.5% sodium bicarbonate, MEM essential amino acids, 10mM non-essential amino acids, L-glutamine and antibiotic-antimycotic. Cells were split approximately every 3 days (~90% confluency) by incubating in 0.25% Trypsin for 5 minutes, centrifugation at 1000g for 5 minutes followed by re-suspension and plating in growth media. Luciferase activity was confirmed by exposing luciferase expressing OSA cells for 5 minutes to 75 ug/ml of expression was confirmed using a Xenogen IVIS 100 (Caliper, Hopkinton, MA) at a 30 second exposure with medium binning. An example of the bioluminescence observed is depicted in Figure 2.

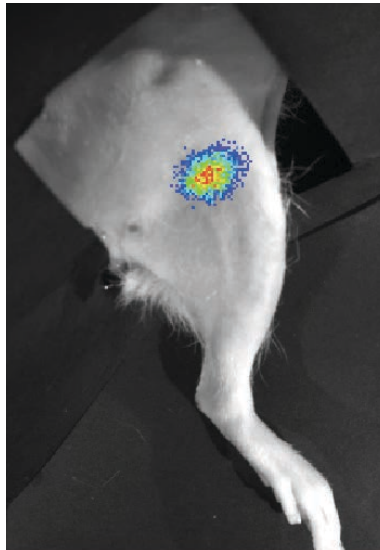


**Figure 2: Representative image of bioluminescence of the luciferase expressing OSA cells**

**2.2.3 Animals:** Immunocompromised athymic nude rats (RH-Foxn1<sup>rnu</sup>) were obtained from the National Institutes of Health and housed by Laboratory Animal Resources. All animal procedures were approved by the CSU IACUC Animal Protocol 10-1959A. A total of 20 rats, six to eight weeks of age, were individually identified with ear tags.

**2.2.4 Tumor Inoculation:** Rats were injected with Abrams luciferase expressing canine osteosarcoma cell line into the proximal left tibia or distal left femur. For the tibia injections, a 22G hypodermic needle was inserted transcortically into the proximal metaphysis and  $1 \times 10^6$  OSA cells in 50  $\mu$ l of PBS were injected. In the femurs, a 22G needle was inserted into the femur at level of the trochanteric fossa (Figure 3), advanced distally within the medullary canal with a rotating motion to the distal metaphysis and then withdrawn. A second needle attached to a 1cc syringe was then advanced to the distal metaphyseal region and  $1 \times 10^6$  OSA cells in 50  $\mu$ l of PBS were injected.



**Figure 3: OSA cell injection technique into the distal femur.**

**2.2.5 Luciferase Imaging:** Rats were imaged weekly using a Xenogen IVIS 100 (Caliper, Hopkinton, MA). Five minutes prior to imaging, rats were anesthetized by chamber induction and maintained by mask (2-4% isofluorane with O<sub>2</sub>) and injected intraperitoneally with 150 mg/kg of luciferin (Caliper, Hopkinton, MA). Rats were positioned in left lateral recumbency in the Xenogen machine and images of the left tibia or femur were taken at 1 and 3 minute time intervals at medium binning. Quantitative analysis of luciferase expression was analyzed using the IVIS quantification software

(Caliper, Hopkinton, MA) by quantifying total photons/sec. The mean of the expression value (photons/sec) was recorded for each animal at each time point. The mean expression value for all animals were plotted to document the weekly change in luciferase expression.

**2.2.6 Radiography:** Under inhalation anesthesia with isoflurane, digital radiographs of the tibias were acquired weekly following OSA cell injection using a MinXray TR90 X-Ray machine (Northbrook, Illinois) to document radiographic onset of tumor associated osteolysis and tumor progression. Rats were positioned in left lateral recumbancy with the affected leg down and the contralateral leg positioned away from the affected leg to obtain lateral and anteroposterior view radiographs of the affected tibia. Images were acquired with settings of 40kV, 3.72 mA at 0.14 seconds of all animals and stored electronically for comparison.

**2.2.7 Pyridinium (PYD) ELISA assay:** Urine (~500 uL) was collected weekly starting immediately prior to tumor cell inoculation from the rats by manual expression, cystocentesis or catheterization while under anesthesia and stored in individually labeled Eppendorf tubes at -20°C until PYD analysis. The MicroVue Pyridinium cross-links kit (Quidel, San Diego, CA) was used to measure PYD in the urine. Samples were diluted 1:20 in PBS and PYD levels measured by analysis per the manufacturer's instructions. Urine creatinine levels were measured using the Cayman Chemical Creatinine Kit (Ann Arbor, MI) to correct for differences in urine creatinine concentration. The corrected PYD values (nmol PYD/nmol creatinine) were calculated by dividing the PYD values by

the creatinine values. The data for each animal were recorded in a Microsoft Excel worksheet. Mean +/- standard deviation corrected PYD values were calculated for each treatment group and plotted at each time point. Statistical comparison of corrected mean PYD values was done between post inoculation time points and the baseline levels.

**2.2.8 Euthanasia:** Three, randomly selected rats were euthanized at 2, 3, 4 and 5 weeks after OSA inoculation in the tibial inoculation experiment, so representative histology samples could be available at these timepoints. Eight rats were euthanized 6 weeks after OSA inoculation in the femur inoculation experiment. The rats were euthanized by deep general anesthesia (isoflurane by induction chamber and mask), followed by exsanguination by intracardiac aspiration and finally by cervical dislocation as a secondary means of ensuring euthanasia. The left hind legs of the rats were disarticulated at the coxofemoral joint. Soft tissues were removed and the legs were placed in 10% formalin.

**2.2.9 microCT:** The tibias were imaged by microCT analysis using a Scanco uCT40 (Brüttisellen, Switzerland) at a 10-micron resolution in 10% formalin. Images were acquired of the entire length of the tumor bearing femurs to document loss of bone.

**2.2.10 Histology:** Tibias or femurs were removed from formalin and decalcified in 10% formic acid for five days. Bones were sectioned (three 10um sections per sample) in the mid-sagittal anterioposterior plane and stained with hematoxylin and eosin (H&E) by the CSU Veterinary Diagnostic Laboratory. Histology slides were read by an ACVP boarded

pathologist experienced with osteosarcoma (Dr. Barbara E. Powers). The slides were examined and validated for the presence or absence of osteosarcoma.

**2.2.11 Statistics:** Luciferase activity and PYD data were validated for normality using the Kolmogorov-Smirnov test. If data was normally distributed, data were expressed as mean +/-SD and were evaluated for statistical significance using a repeated-measures ANOVA. Statistical significance for comparison of means of different groups was calculated using the pair-wise T-test using SPSS statistical analysis software. The differences were considered significant at P values less than 0.05.

## **2.4 Results**

Tumor lesions were observed in 10 out of 12 rats injected in the proximal tibia based on bioluminescence, radiobiology and histology resulting in an engraftment rate of 83 percent.

**Osteosarcoma cell injections.** Insertion of the needle through the proximal tibial cortex was variable and difficult with this injection technique. The needle would slide off the cortical surface due to the shape and density of the proximal tibia bone. In some animals, a limited open approach was used in an effort to visualize and penetrate the cortex. This introduced additional anesthesia time and the possibility of surgical complications such as infection. Since the transcortical hole created was perpendicular to the long axis of the bone, cells could escape into the surrounding soft tissues or could be seeded on needle exit. Soft tissue swelling of the insertion site was observed after OSA cell injection.

Modification of the tumor cell injection technique in the second part of the experiment involved introducing the needle through the cortical bone of the proximal femur at the level of the trochanteric fossa and then into the distal metaphyseal region of the femur. This resulted in a more reliable inoculation technique. The access point was remote to the tumor cell inoculation site; so extraosseous tumor development was not observed. The procedure was very rapid, resulting in less morbidity for the animals. This became our preferred method for tumor cell inoculation through the remainder of the studies with successful tumor engraftment in 8 out of 8 rats (100%).

**Canine osteosarcoma cells successfully engraft and progress in the proximal tibia and distal femur metaphyses.**

***Bioluminescence:*** Tumor cell viability was evaluated during the course of the experiment using bioluminescence imaging as shown in Figure 4. Relative luciferase expression levels were measured in all rats over the course of five weeks using the IVIS quantification software (Figure 5). In the tibia model, luminescence intensity (an indirect measurement of tumor cell viability) of the OSA cells was relatively consistent with no differences over the first 4 weeks (Figure 4 & 5); however, by the 5<sup>th</sup> week no expression was detected (Figure 4 & 5). In the femur model, luciferase activity increased (Figure 4 & 5) and remained consistent with no significant differences until weeks 4 and 5 in which a significant 5-fold increase in luciferase expression was observed ( $p < .001$ ). These results conclude that luciferase levels were unchanged in the tibia and decreased completely after the 4<sup>th</sup> week with a high degree of variability between time

points. The luciferase expression in the femur model; however, significantly increased by weeks 4 and 5 indicating a more reliable indicator of disease progression.

**Radiography:** The tumor-inoculated tibias and femurs of the rats were imaged weekly by digital radiography. Radiographic changes observed in the tibias consisted of a mixed lytic/proliferative change in the proximal tibia, which progressed in animals with successful tumor engraftment (10/12) over five weeks. Representative radiographs shown in Figure 6 A demonstrate the radiographic progression of the tumor lesion throughout the duration of the experiment. By the fifth week, the tumor involved the entire proximal half of the tibia and resulted in impairment of limb function (Figure 6A). In the femur model, tumor engraftment and progression was observed in all rats (6/6) as shown in Figure 6B. By the fifth week, pathologic fracture was observed in the majority of animals and the experiment was terminated. The observed radiographic changes and tumor progression were similar to those observed in spontaneous canine OSA cases.

In both the tibia and femur model experiments, radiographic evidence of tumor was reliably evident by week 2 after tumor cell inoculation and observed radiographic changes at the week 2 timepoint were similar to those seen at presentation in spontaneous osteosarcoma in dogs (Figure 6). No fractures had occurred in any animal at the week 2 time point; therefore, this timepoint was chosen to deliver SRT in the subsequent experiment.

**PYD levels increase after tumor inoculation in the femur model.** To measure the degree of tumor-associated osteolysis, a PYD ELISA and urine creatinine was used to measure bone resorption. Urine samples were collected weekly in each animal. In the tibia model, there were no statistically significant changes in corrected PYD levels over time (Figure 7A). In the femur

model, corrected PYD levels were significantly increased over baseline (Week 0) levels throughout the duration of the experiment ( $p < 0.005$ ) (Figure 7B).

**MicroCT confirms tumor associated bone destruction.** To further confirm the progression of the OSA tumor and to document the degree of bone destruction, tibias and femurs were subject to microCT imaging. As depicted in Figure 9, microCT shows a comparison of a normal tibia and femur and the OSA-affected tumor lesions at 5 weeks. There is evidence of bone loss and possible fracture due to tumor associated osteolysis in week 5.

**Histology:** In the tibia model, histological analysis confirmed the presence of OSA in 10 out of the 12 rats. The femur model showed histological OSA in all distal femurs.

**Results Conclusion:** The tumor engraftment rate was 83% in the tibia model and 100% in the femur model. Two weeks post OSA tumor inoculation was identified as the time point when tumors were detectable radiographically, exhibited elevated PYD activity and exhibited no signs pathological fracture. The femur model was chosen because it exhibited the highest tumor engraftment rate, predictable luciferase activity and PYD levels. This time point was chosen as the best time for treatment interventions in subsequent experiments in Chapters 3 and 5 using this animal model as it most closely resembles the clinical presentation in spontaneous canine OSA cases.

## 2.5 Discussion

The aim of this study was to develop an orthotopic rat model of canine osteosarcoma to determine the engraftment rate and temporal progression of tumor development in the proximal tibia and distal femur. Canine osteosarcomas lesions commonly develop in the metaphyseal regions of long bones of the appendicular skeleton such as the proximal humerus, distal radius, distal femur and proximal tibia (11). To our knowledge, there are no established orthotopic rat models of canine osteosarcoma, thus the development of this model provides a valuable translational tool to evaluate novel local treatments of OSA. Based upon the aforementioned results, the femur model was selected as the most appropriate to be used in subsequent experiments. This animal model will be used in Chapter 3 (Specific Aim 2) to evaluate the effects of SRT on normal and tumor-affected bone and in Chapter 5 (Specific Aim 4) to evaluate potential bone regeneration by MSCs after SRT.

We first injected canine OSA cells into the proximal tibia by inserting a needle through the tibial cortex and injecting the cells into the metaphyseal region. This technique has been previously used in mouse models of OSA; however, a rat proximal tibia is much larger and denser making needle insertion difficult (108). We observed evidence of cell leakage into the muscular tissues resulting in an inadequate representation of the localized disease. We experienced a tumor engraftment rate in tibial injection rats of 83 percent, which is comparable to similar orthotopic studies in mice that resulted in an 88 percent engraftment (108).

Due to the technical difficulty and variability experienced with injecting cells into the proximal tibia, we then injected the OSA cells into the distal femur via a distant access site for the second experiment. Slowly injecting the cells is critical to this technique as we observed in a pilot study that injecting cells quickly could result in an embolism and death. The femur injection technique was much easier to replicate and we believe it minimized the potential for extraosseous cell leakage after injection. Tumor progression was consistently observed with radiography and luciferase imaging. These findings were confirmed in all animals by histology. Engraftment rate in this model was 100 percent as compared to 83 percent in our tibia model. Similarly, a 100% engraftment rate was observed in a previous allogenic orthotopic rat model of rat OSA in which cells were injected into the distal femur (109). This technique allowed for growth of the OSA from the intramedullary tissue and eventual extension through the cortical bone from the endosteal surface, which is most representative of spontaneous tumor development.

To evaluate the tumor cell viability, canine OSA cells were previously transfected to express a luciferase reporter gene. This enabled us to track the cell viability in real-time throughout the duration of the experiment. We showed increasing luciferase expression (Weeks 1-4) by the OSA in the tibia model suggesting the cells are viable and proliferating as the experiment progressed (10/12 animals). Interestingly, by week 5 the cells appear to lose their ability to express luciferase. In the femur model, we observed a consistent increase in luciferase expression in all animals until sacrifice at week 5. It is unclear as to why the tibia model lost luciferase expression at week 5; however, several factors may have contributed to this observation. First, unlike the femur model, there were only the three remaining animals at the 5

week time point for evaluation and may not be an accurate representation of the tumor progression in a larger population. Next, histological analysis revealed viable OSA cells were present at week five despite the loss of luciferase expression; therefore, its possible the cells may have lost their ability to express luciferase (118). In addition to the viable cells observed, OSA has been shown to have a variable innate level of tumor necrosis with an average percent tumor necrosis level of 26.8 percent observed in this study. The large necrotic areas could have prevented the luciferin from reaching the luciferase transfected tumor cells due to lack of blood supply in these regions. It is possible that the tumor cells were still viable and the lack of bioluminescence may be due to inability of the luciferin to physically connect and react with the luciferase containing tumor cells. It has also been shown that small decreases in oxygen levels can affect the ability of cells to express luciferase (118). Osteosarcoma has been traditionally been considered hypoxic due to large necrotic regions, thus, the lack of oxygen could have affected bioluminescence of the cells (118). Signal attenuation is also a potential inhibiting factor, due to the altered absorption of the light through mammalian tissues (119). It is estimated that the signal can be attenuated as much as 10 fold through each centimeter of tissue; therefore, it is possible that the bone and soft tissues could be decreasing or eliminating the signal (119). Although bioluminescence allows for real-time imaging *in vivo*, it requires a complex interaction of many molecules and may not provide a true representation of the biological processes present (118).

We also measured pyridinoline (PYD) levels in order to establish baseline values and compare PYD levels over time after OSA inoculation to this baseline value. Increases in PYD levels have been shown to increase in humans and dogs with osteosarcoma and can be useful in

monitoring response to treatment (115, 120). Similarly, a rat model of metastatic bone cancer showed increased PYD levels associated with tumor progression (116). We needed to characterize PYD changes over time in this model to ascertain the influence of SRT on this parameter in later experiments. In the tibia model, we showed no differences between groups throughout the experiment. In the femur model, we observed significant increases in PYD levels two weeks after tumor inoculation. These increased PYD levels persisted throughout the duration of the experiment and indicate an ongoing osteolytic process induced by the tumor. It is unclear as to why PYD levels did not increase in the tibia model while increases were observed in the femur model. The data may have been confounded by the fact that we experienced difficulty obtaining urine, initially. We were unable to obtain adequate amounts of urine from each animal in the tibia studies for an accurate analysis. Our technique greatly improved in the femur model, which allowed for a more thorough analysis.

A major limitation of this aim is the limited number of animals in the tibial study. The serial sacrifice required to obtain histologic specimens at each week greatly reduced the number of animals that could be used for the PYD analysis in the later weeks of the experiment. It may have yielded a higher engraftment rate as well if all 12 animals were alive at the five-week time point. Increasing the number of animals could help decrease the variability of the PYD data and possibly yield a higher tumor engraftment rate. An additional group of animals of the same age, without OSA, would also help determine better baseline PYD levels during the experiment.

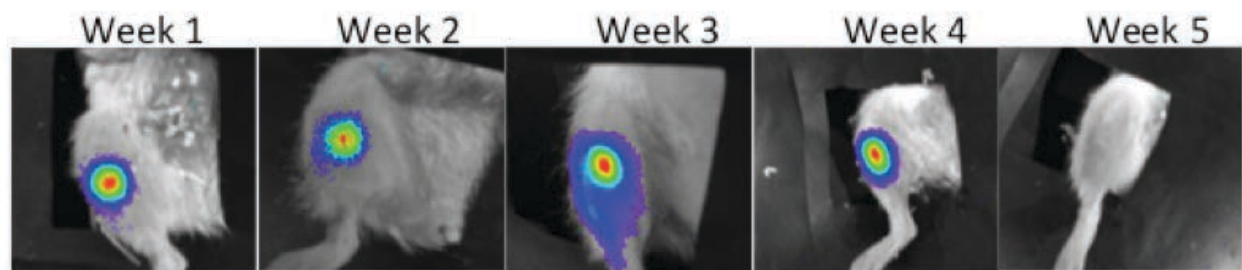
## **Conclusion**

In this study, we developed an orthotopic model of canine osteosarcoma in the proximal tibia and distal femur of athymic rats. This model exhibited similar radiologic and histologic characteristics to spontaneous OSA in dogs. We showed a predictable temporal progression of the tumor lesion with an 83% engraftment rate in the tibial and a 100% engraftment rate in the femur model. Additionally, we showed that radiographic tumor progression is consistent with increased luciferase expression as well as breakdown of collagen by measurement of PYD levels. The increased bone resorption as supported by the increased PYD levels is commonly associated with OSA progression. This series of experiments described a novel orthotopic rat model of canine OSA that was used in subsequent experiments. This model may be advantageous in that it can be used to evaluate new therapies that cannot otherwise be performed in mice due to size constraints or in client-owned dogs due to ethical concerns.

The experiment described in this Chapter has been accepted for publication in the American Journal of Veterinary Research (March 2013).

## 2.6 Figures

### Tibia Luciferase



### Femur Luciferase

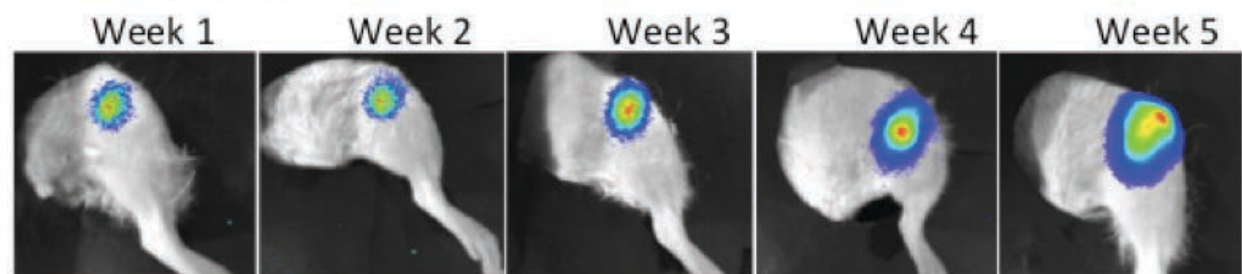
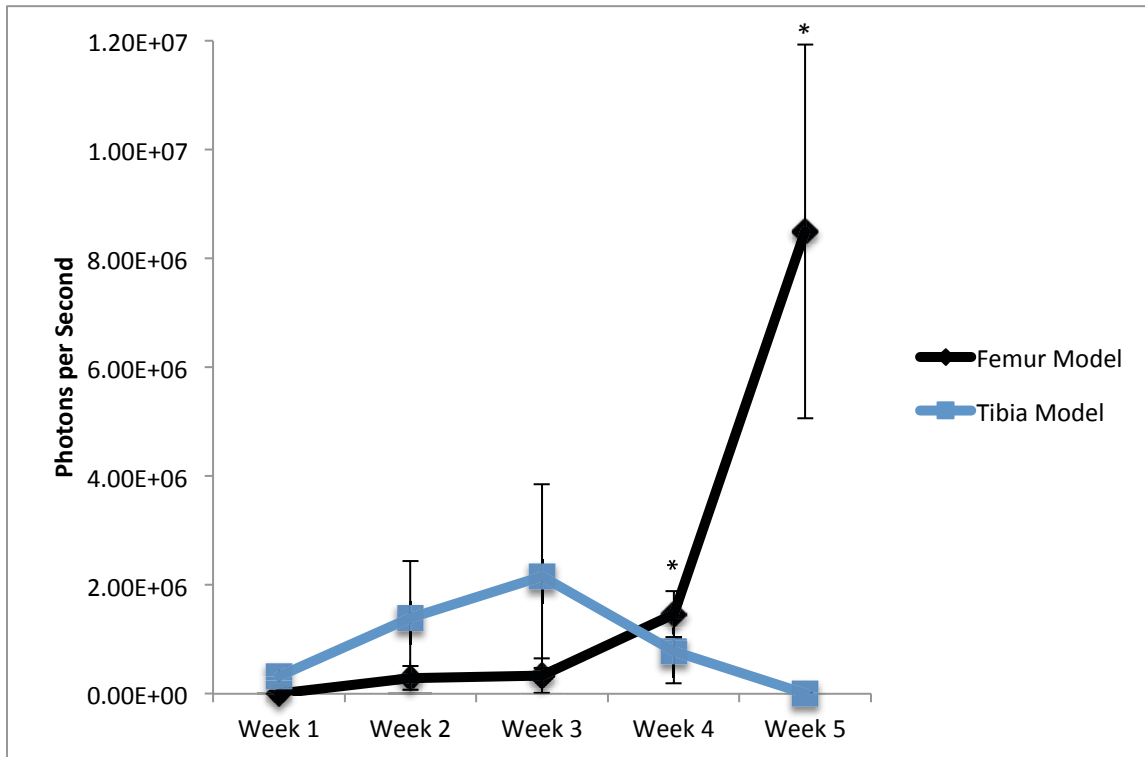
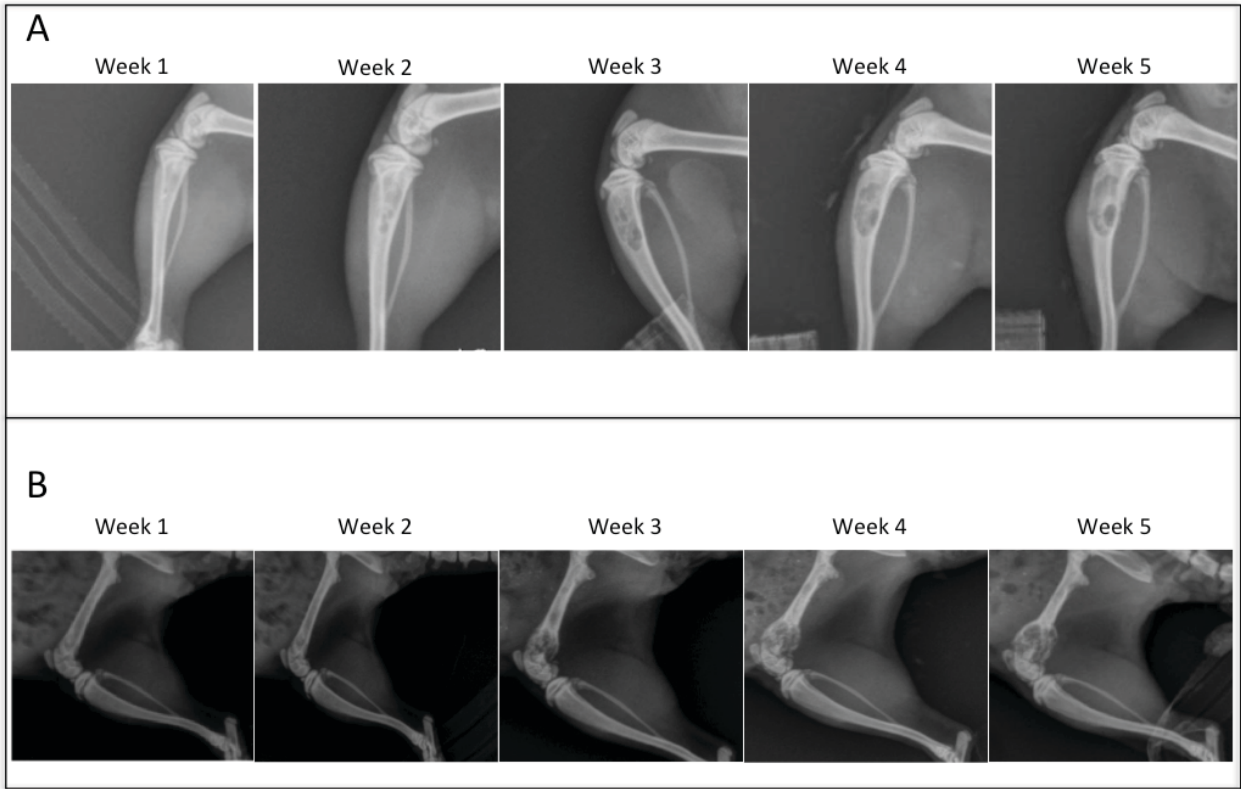


Figure 4: Representative bioluminescence imaging of the luciferase expressing OSA cells in the femur and tibial locations.



**Figure 5: Relative Luciferase expression over 5 weeks in the tibia and femur models. In the tibia model, the number of animals per weeks is as follows: week 1 (n=12), Week 2 (n=12), week 3 (n=9), week 4 (n=6), and week 5 (n=3). There were not statistical differences between weeks. The femur group consisted of 6 animals per group at each time point. Levels significantly increased at weeks 4 and 5 compared to weeks 1, 2 and 3 in the femur group ( $p < 0.010$ ).**



**Figure 6: Representative radiographs of the tumor-inoculated proximal tibias (A) and distal femurs (B). Radiographs demonstrate the radiographic progression of the tumor lesion during the five weeks of the experiment.**

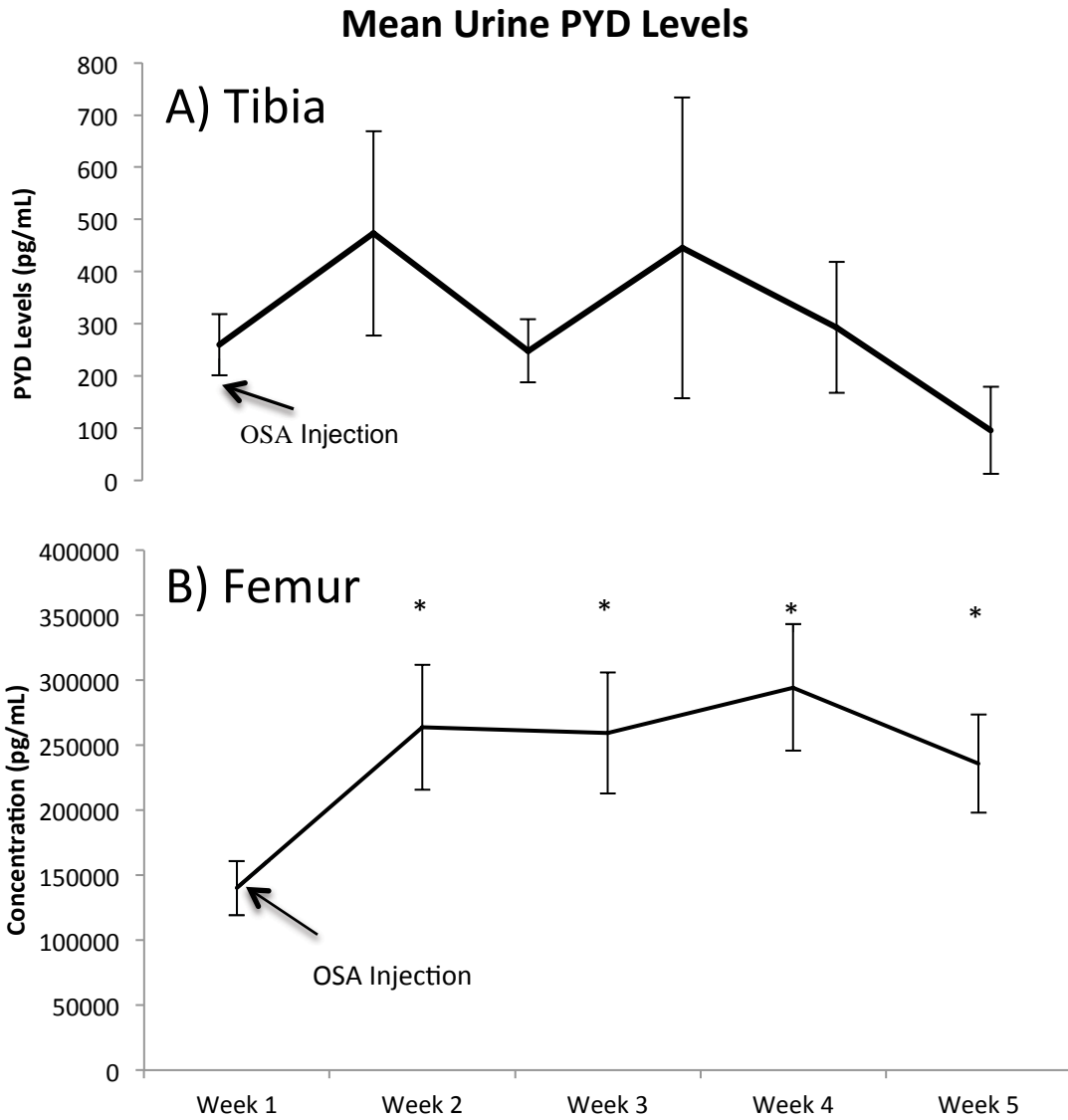


**Figure 7: Weekly PYD levels over 5 weeks in the tibia and femur models. A) PYD levels are unchanged throughout the 5 weeks of the tibia experiment. B) PYD levels significantly increase from baseline (Week 1) at Week 2 and remain increased over baseline at weeks 2, 3, 4 and 5 (\* indicates  $p < 0.005$ ).**

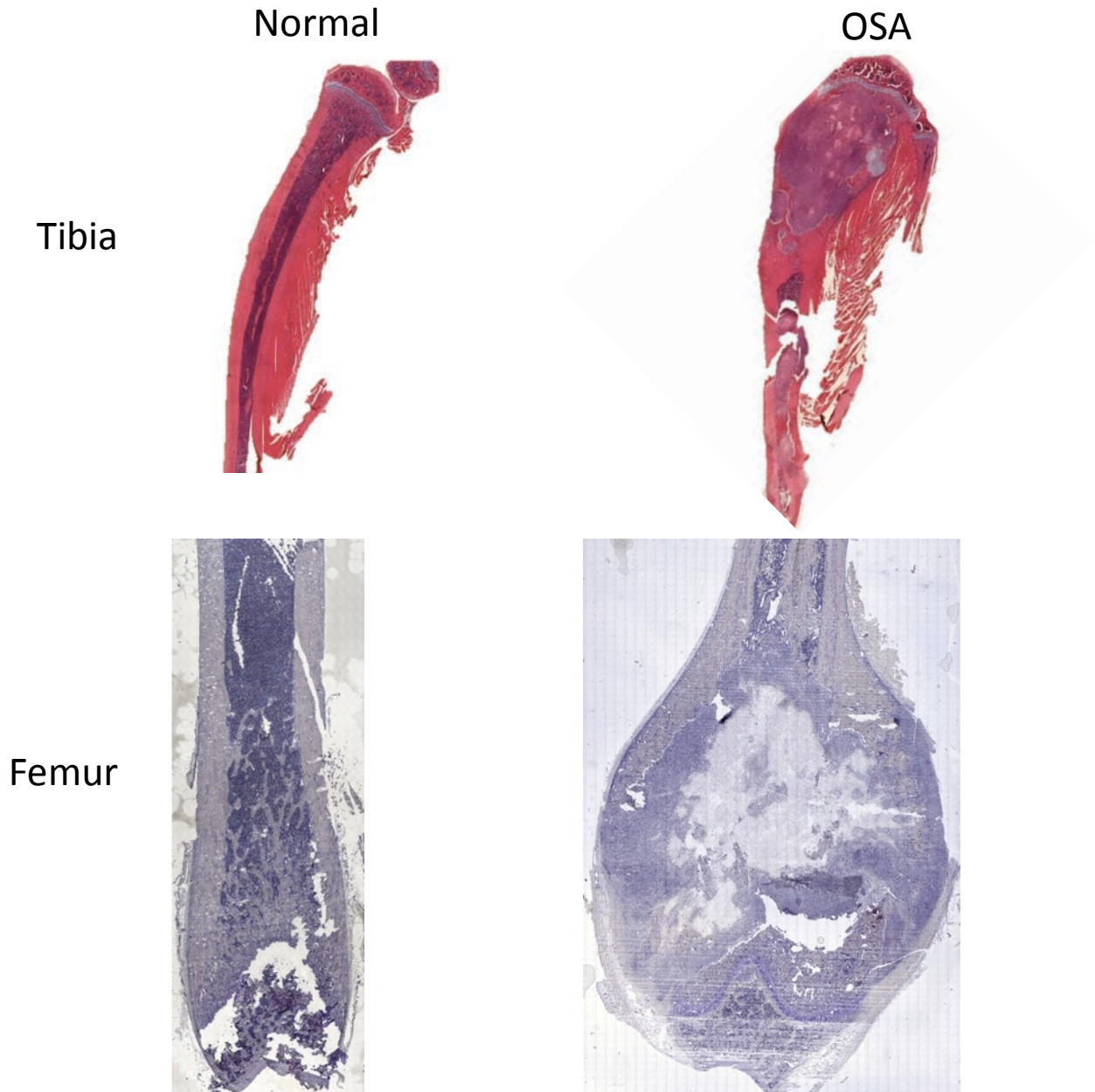


**Figure 8: OSA tumor lesion in the proximal tibia (Top) and distal femur (Bottom) five weeks after inoculation.**



**Figure 9: MicroCT of the tumor lesion in the proximal tibia (Top) and distal femur (Bottom) compared to normal bones. The tibia and femurs with OSA show extreme tumor associated osteolysis and bone destruction.**

## **Chapter 3: Optimization of SRT Fraction and Dose Schema**

### **3.1 Introduction**

Stereotactic radiotherapy is a novel treatment modality for local tumor control of OSA in canines. It has the ability to accurately deliver large dose per fraction radiation precisely to the tumor lesion with relative sparing of the adjacent normal tissues and organs (60, 63). Durable local tumor control has been observed in dogs with spontaneous OSA of the extremity treated by SRT and the radiation side effect toxicity profile is acceptable (60, 63). The most common post-SRT complication observed after treatment of primary OSA in dogs has been pathologic fracture. This is caused by pre-existing tumor-associated osteolysis and the adverse effects of high dose radiation such as decreased bone mineral density and the destruction of vasculature, osteoblasts and osteoclasts. (60). The overall objective of this thesis involved exploring the use of mesenchymal stem cells as a novel technique for regenerating bone after SRT of a primary bone tumor. Before this objective was met, a study was required that evaluated the optimal dosing and fractionation parameters of SRT to achieve local tumor control while sparing adjacent normal tissues in the model developed in Specific Aim 1.

Conventional finely fractionated radiotherapy (XRT) involves delivery of radiation in small dose fractions (typically 2-3Gy per fraction) to achieve a larger total radiation dose to the tumor yet permitting normal tissues to repair. This commonly used technique can result in better tumor control as well as decreased acute and late radiation effects because of the differences in radiosensitivity of the tumor and normal tissues and the ability of these tissues to repair damage. The classic 4 R's of radiotherapy; reoxygenation, redistribution, repair and regeneration, help

describe the benefits of using fractionated schemes for maximizing tumor control while minimizing acute effects of normal tissues (55). One-third of radiation induced DNA damage (direct damage) is caused by direct ionization and damage to the DNA molecules (55). The other two-thirds of DNA damage (indirect damage) is the result of the ionization of water ( $H_2O$ ) to form highly reactive hydroxyl (OH) free radicals (55). A large single dose of radiation to a tumor can deplete the available oxygen for this reaction to occur thus limiting the formation of OH free radicals and decreasing efficacy. The depleted oxygen can also help the tumor cells to better repair DNA damage. Thus, a large single dose decreases the effects of indirect damage and subsequently limits the total overall damage to the DNA (55). Radiation delivered in smaller fractions over a period of many days allows time for intra-tumoral pressure to decrease, opening blood vessels. Oxygen can then return to the tumor thus increasing the effectiveness of the radiation treatment via indirect action. The benefits of reoxygenation are particularly important for hypoxic tumors such as OSA.

The relative radiation sensitivity of cells at different stages of the cell cycle is also important for fractionation. Cells are most sensitive to radiation in early S phase and G2/M phase of the cell cycle (55). Although it is possible to determine the current the proportion of cells within a particular phase of the cell cycle *in vitro*, it is not feasible in the clinical setting (121). However, fractionated radiation therapy provides a greater chance of treating during a radiation sensitive cell cycle relative to a single dose of radiation. This redistribution of cells to a vulnerable phase within the cycle between fractions increases the total number of cells damaged.

Repair and regeneration are important benefits of fractionated radiation therapy for the protection of normal tissues. Normal cells repair themselves from radiation damage differently than tumor cells. Fractionation allows for repair of acute responding normal tissues from sub lethal radiation damage between fractions. The relative difference between normal acute responding tissues and more rapidly dividing tumor cells allows the therapeutic effect of radiation therapy to occur. The repopulation of undamaged cells, both normal and malignant, must also be taken into account in terms of time between fractions. An optimized fractionation and total dose protocol is developed based on the radiosensitivity of the specific tumor type as well as the normal tissues surrounding the tumor.

Osteosarcoma has been traditionally referred to as “radio-resistant” due to the large total dose of radiation needed in order to achieve local tumor control. Conventional fractionated radiation therapy for local control of bone tumors has been generally unsuccessful due to the adverse effects on normal tissues because of the cumulative dose required for tumor control. Studies of human vertebral tumors required total doses exceeding 70 Gy (59). Similarly in canines, more than 90 Gy is needed for local control of osteosarcoma when given in several fractions (122). These higher total doses increase the rate for detrimental and permanent effects to the normal surrounding tissues including bone thus these large doses are not used clinically. Unlike conventional XRT which utilizes small doses of radiation over longer periods of time, SRT uses a larger dose in fewer fractions (56). Delivering a larger dose per fraction in fewer fractions has been shown to be advantageous in killing less radiosensitive tumors with a high alpha:beta ratio such as OSA (60). Although larger fractions can achieve better therapeutic response, the large dose increases the risk for late effects. The use of fractionated SRT over

conventional fractionated radiation therapy allows for a large dose to be administered to the tumor with a rapid dose fall off surrounding normal tissues. This is accomplished by using image guidance where radiation is precisely administered directly to the tumor while sparing surrounding normal tissues (56). The rapid fall off of radiation within short distances from the tumor also results in a smaller volume of normal tissue receiving the high and potentially deleterious dose. SRT also takes advantage of the reoxygenation, regeneration, repair and redistribution. Thus SRT allows for administering a higher biologically effective dose while sparing normal tissues, which cannot be accomplished with conventional fractionated radiation therapy.

In this experiment, our aim was to determine the optimal SRT fractionation scheme and dose protocol to achieve local tumor control while sparing normal tissue in the orthotopic rat model of canine OSA developed in Specific Aim 1. First, we evaluated the feasibility of using SRT in small animals. We then investigated the ability to achieve local tumor control using three different fractionation protocols consisting of either one fraction of 25 Gy (total dose = 25Gy), two fractions of 15 Gy (total dose = 30Gy) or three fractions of 12 Gy (total dose = 36Gy). For the two and three fraction protocols, each treatment was delivered on consecutive days. Acute radiation effects were monitored and compared between groups. Using the results from this experiment, we then assessed 4 different total radiation dose protocols of either 9 Gy (27 Gy total), 10 Gy (30 Gy total) , 11 Gy (33 Gy total) and 12 Gy (36 Gy total), delivered in three fractions, and compared local tumor control and acute radiation effects in each group. We started with 3 fractions of 12 Gy because we have observed excellent tumor control with this protocol in dogs and the acute affects were tolerable and transient. (63). The total dose was then decreased in

an effort to minimize the acute and late radiation effects. We measured percent tumor necrosis as a measure of efficacy and additionally measured PYD levels to measure any decreases in osteolysis to the affected femurs. We hypothesized that percent tumor necrosis would increase as the total dose increased as well as decreases in PYD levels after SRT. We also expected the severity of any acute effects to increase as the total dose was increased. The protocol that resulted in the highest percent necrosis, while minimizing acute effects to normal tissue was used for the remaining studies.

## **3.2 Materials and Methods**

**3.2.1 Experimental Design:** Two experiments were conducted to evaluate the effect of different fractionation schemes and different total dose (uniform fractionation) protocols. See Appendix B for complete experimental details outlined in this Specific Aim.

**1) Fractionation Experiment:** This experiment compared delivery of SRT in one, two or three fractions. Three nude rats were inoculated ( $1 \times 10^6$  canine OSA cells) into the distal femur as described in Specific Aim 1. Two weeks after tumor cell injection, rats were administered SRT in the following fractionation schemes: 1 fraction of 25 Gy (n=1), 2 fractions of 15 Gy (30 Gy total dose, n = 1) or 3 fractions of 12 Gy (36 Gy total dose, n = 1). Local tumor control was assessed after SRT by serial radiography to monitor the progression of the lesion in comparison to OSA tumor progression documented in Specific Aim 1. Bioluminescence levels were used to assess tumor cell viability. Acute radiation side effects were monitored by digital photography of the treated leg and scored

using the VRTOG acute toxicity scoring system for skin. Rats were sacrificed six weeks after OSA cell injection or earlier if pathologic fracture occurred. The treated femurs were collected and analyzed to determine percent tumor necrosis of each sample. The experimental timeline is depicted in Figure 10.

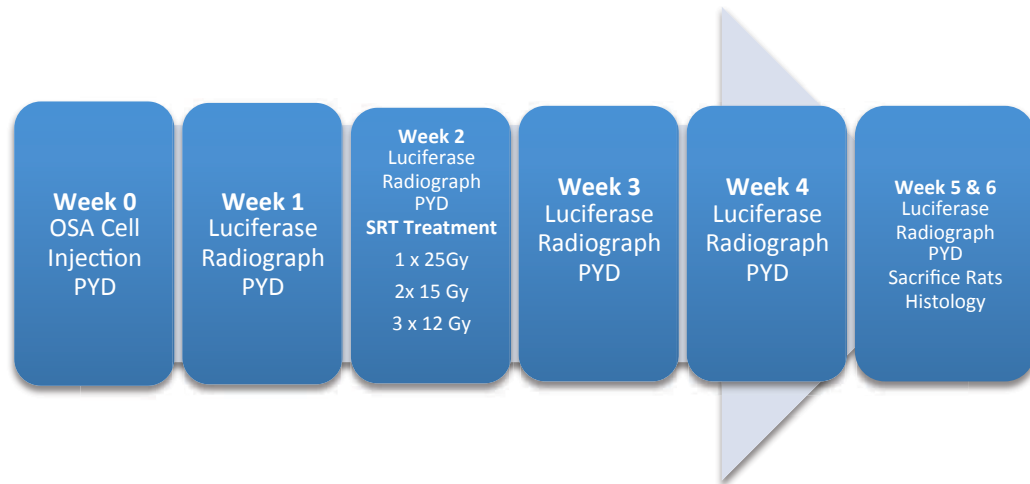


**Figure 10: Fractionation experiment timeline**

- 2) **Total Dose Experiment:** This experiment was designed to assess different total radiation doses delivered with the same fractionation protocol. Twenty-four nude rats were inoculated ( $1 \times 10^6$  canine OSA cells) into the distal femur as described in Specific Aim 1. Two weeks after tumor cell injection, SRT was administered in 3 fractions delivered on consecutive days to the following groups: 9 Gy (27 Gy total,  $n = 6$ ), 10 Gy (30 Gy total,  $n = 6$ ), 11 Gy (33 Gy total,  $n = 6$ ) or 12 Gy (36 Gy total,  $n = 6$ ). Local tumor control was assessed after SRT by weekly radiography to monitor the progression of the lesion in comparison to OSA tumor progression documented in Specific Aim 1. Bioluminescence levels were used to assess tumor cell viability and increasing proliferation and PYD levels were used

to monitor changes in bone resorption after SRT. Acute radiation side effects were monitored by digital photography of the treated leg and scored using the VRTOG acute toxicity scoring system for skin. Rats were sacrificed eight weeks after OSA cell injection. If pathologic fracture occurred, the animals were euthanized immediately. The treated femurs were collected, stained with decalcified hematoxylin and eosin staining (H&E) and percent tumor necrosis was determined by a pathologist. The experimental timeline is depicted in Figure 10.

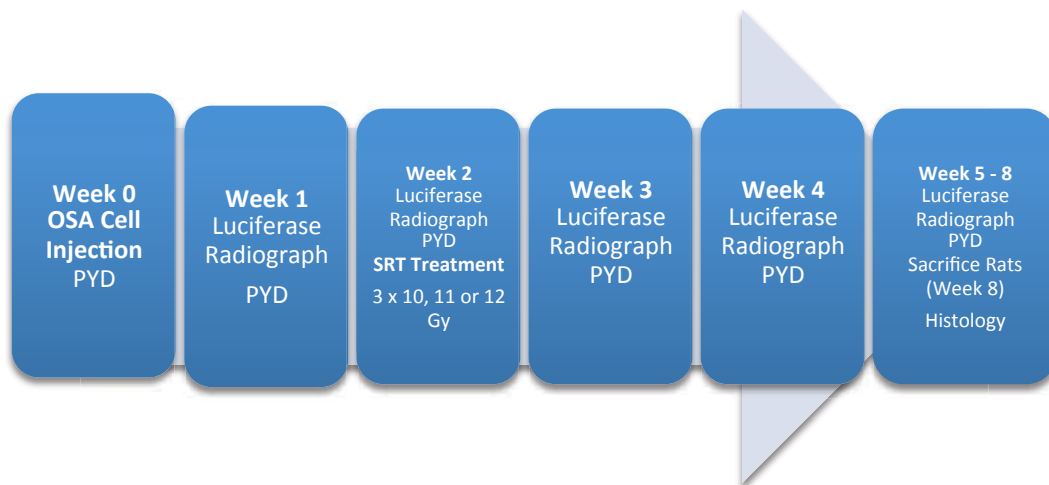


**Figure 11: Different total radiation dose, constant fractionation experiment timeline**

**3.2.1 Stereotactic Radiotherapy Method:** We previously determined that two weeks post-OSA inoculation was the optimal time for SRT administration based on our results from Specific Aim 1. This time frame was sufficient to allow the tumor to engraft and progress such that it was detectable by radiography, bioluminescence imaging and increased PYD levels, yet the risk of fracture due to progression of the tumor remained minimal.

Two weeks following tumor injections, rats were anesthetized as previously described in Specific Aim 1 and cone beam computed tomography (CBCT) imaging of the affected femur was performed for the purpose of radiation therapy planning. Animals were covered in bubble wrap to help maintain normothermia. Breathing was observed by closed circuit video monitors during each treatment episode. Non-invasive immobilization was achieved by positioning each rat in left dorsal recumbency (affected femur down) within an Accuform™ cushion indexed to the couch of the Varian Trilogy™ linear accelerator via a Civco™ baseplate (Figure 1). Transaxial computed tomography images of the affected femur were captured via onboard cone-beam computed tomography (CBCT). CBCT images were imported into the radiation therapy planning software (Varian Eclipse). Contouring of the CT images was performed on each tumor-bearing femurs, thus identifying the gross tumor volume (GTV), planned target volume (PTV), normal bone, and skin. The GTV consisted of contouring of the actual tumor itself and the PTV resulted from a 2 mm symmetrical expansion beyond the GTV. A SRT plan consisting of seven isocentrically placed treatment beams was created. A static multi-leaf collimator (MLC) was utilized to increase the conformality of dose achieved within the tumor volumes, while preferentially sparing surrounding normal tissues. Each plan was normalized to achieve a minimum of 99% of the desired dose within the GTV, and a minimum of 95% of the desired dose within the PTV based upon evaluation of the dose volume histogram (DVH). The total planning time for each subject was approximately two hours. In the fractionation experiment, rats were treated with either a single fraction of 25Gy; two, daily fractions of 15Gy; or three, daily fractions of 12Gy. These animals were anesthetized during the entire planning stage and the delivery of the first fraction. In the total dose experiment, rats were treated with 3 fractions delivered on

consecutive days of either: 9 Gy (27 Gy total), 10 Gy (30 Gy total), 11 Gy (33 Gy total) or 12 Gy (36 Gy total). These animals were anesthetized briefly for the CBCT acquisition, recovered and then anesthetized again the next day for the delivery of the first fraction. Prior to delivery of the second and third SRT fractions, rats were anesthetized and an orthogonal pair of kilovoltage radiographs of the femur were obtained with the Trilogy's on-board imaging (OBI) system. These radiographs were matched to the digitally reconstructed radiographs derived from the original CBCT. Changes in couch position were made based upon the matching process to ensure precision and accuracy of SRT delivery. Each field of the SRT plan was then delivered individually. Once SRT was completed, each rat was recovered from general anesthesia and returned to their cages. Rats were then monitored weekly for response to therapy by radiography, bioluminescence imaging and PYD analysis.



**Figure 12: Rat positioning in the bolus for SRT**

**3.2.2 Imaging to document tumor progression and response to SRT:** Luciferase and radiograph images were acquired once weekly starting before tumor inoculation for eight weeks as described in 2.2.5 and 2.2.6 to document tumor progression and response to SRT.

**3.2.3 Pyridinium (PYD) cross-links ELISA:** Urine levels of pyridinoline cross-links (PYD), a marker of bone breakdown, were measured to document tumor associated osteolysis and response to SRT. Approximately 500ul of urine was obtained weekly from each rat for six weeks in the fractionation experiment and eight weeks in the total dose experiment as described in 2.2.7. The MicroVue PYD ELISA (Quidel, San Diego, CA) was used to evaluate

changes in PYD associated with SRT over time. Each urine sample was diluted 1:20 and analyzed in duplicate using the MicroVue kit per the manufacturers instructions. Samples concentration was then corrected by dividing the PYD level by the creatinine levels in each sample.

**3.2.4 Evaluation of acute radiation skin effects:** Following SRT, digital photographs for each treated leg were taken daily to evaluate acute radiation skin effects until the skin returned to normal pre-SRT appearance. The skin effects of SRT were then scored based on the Veterinary Radiation Therapy Oncology Group scoring system (Score 0 = No Change, Score 1 = mild, Score 2=moderate, Score 3 = severe) (123). The maximum grade skin effect and day of occurrence were recorded for each animal for comparison between treatment groups.

**3.2.5 Histology:** Histological analysis was performed as described in 2.2.10. A single board certified pathologist evaluated percent tumor necrosis of all femurs. Tumor necrosis was calculated by dividing the necrotic tumor area by the sum of the total tumor area plus the necrotic tumor area (necrotic tumor area/(total tumor area + necrotic tumor area)) (124). Animals that exhibited no radiographic evidence of tumor or luciferase expression were omitted from the histology and PYD analysis because they would have skewed the data. Additionally, animals that exhibited radiographic evidence of tumor engraftment, but no luciferase expression at the end of the experiment were considered to have 95% tumor necrosis and included in the PYD analysis. The tumors in these animals were most completely

killed due to successful SRT.

**3.2.6 Statistics:** Data in the PYD ELISA tests were logarithmically transformed and expressed as mean +/-SD. Data were evaluated for statistically significant differences using a repeated measures ANOVA. Statistical significance for comparison of means of different groups was calculated using the pair-wise T-test. Mean percent tumor necrosis for each group is expressed as mean +/-SD and were evaluated for statistical significance using a one-way ANOVA. Statistical significance for comparison of means of each group was calculated using Tukey HSD and Bonferroni post-hoc analysis. The differences were considered significant at P values less than 0.05. IBM SPSS software was used for all statistical analysis <sup>1</sup>.

### 3.3 Results

#### **Stereotactic Radiotherapy results in high percent tumor necrosis of distal femur OSA.**

##### **3.3.1 Fractionation Experiments**

- 1) Response to SRT: One fraction of 25 Gy SRT caused 99% tumor necrosis by 6 weeks.** Radiographs of the tumor lesion (n=1) showed progression and enlargement of the tumor along with increased bioluminescence at 1 and 2 weeks post tumor inoculation consistent with observations from Aim 1. One week after SRT treatment, luciferase imaging revealed a 60 % decrease in detectable bioluminescence suggesting SRT causes some tumor cell death ( Figure 14 & Figure 15). By 2, 3 and 4 weeks after SRT, no bioluminescence was observed and the lesions showed no progression indicated by no

---

<sup>1</sup> IBM SPSS Statistical Analysis Software. <http://www-01.ibm.com/software/analytics/spss/>

change in tumor size when compared to the femurs not treated with SRT at the same time points (weeks 2, 3 and 4) in Specific Aim 1 (Figure 13)., Interestingly, bioluminescence increased slightly at week 5 to 10% of baseline levels ( Figure 14 & Figure 15).

Histological analysis indicated 99 percent tumor necrosis four weeks after treatment (Week 6) (Figure 16).

**2) Response to SRT: Two fractions of 15 Gy achieved 99% tumor necrosis by 6 weeks.**

Radiographs and bioluminescence showed engraftment and progression after OSA cell injection at weeks 1 and 2 (n=1). One week after SRT (week 3 post-tumor injection), luciferase imaging indicated a 57% decrease in detectable bioluminescence suggesting decreased tumor viability ( Figure 14 & Figure 15). By weeks 2 and 3 after SRT, no bioluminescence was observed and radiographs again indicated no tumor progression. Bioluminescence then increased 26% at week 4 and 57% at week 5 when compared to baseline ( Figure 14 & Figure 15). Histological analysis revealed a 99 percent tumor necrosis at week six (Figure 16).

**3) Response to SRT: Three fractions of 12 Gy SRT caused 80% necrosis at 6 weeks.**

As previously observed, tumor engraftment and progression was observed at weeks 1 and 2 after OSA cell injection (n=1). One week after the third fraction of SRT, bioluminescence decreased 80% ( Figure 14 & Figure 15). As shown in Figure 14, bioluminescence was undetectable throughout the remainder of the experiment and OSA lesion was stable radiographically (Figure 14Figure 15). A mean tumor necrosis level of

80 percent was observed in the femurs in this treatment group at week six (Figure 16).

## **Acute Radiation Effects**

**Mild to moderate acute effects were observed after SRT in the fractionation experiment.** Rats in each fractionation scheme were scored for radiation induced skin effects after SRT treatment each week until sacrifice at week six. Moderate acute effects were observed in the 1 x 25 Gy animal with a maximum effect at day 15 (VRTOG Score = 2, Table 1). In the 2 x 15 Gy and 3 x 15 Gy animals, effects were mild with a maximum effect at day 15 (VRTOG Score = 1) (Figure 16, Table 1). Skin recovered in all groups with noticeable healing and virtually no abnormalities by 18 days or for the rest of the experiment (Figure 16).

### **3.3.2 Total Radiation Dose Study**

1. **Tumor Engraftment:** As shown in Figure 18, radiographs of the affected femur indicate the OSA tumor lesions engrafted and progressed as previously observed (Weeks 0-2). Mean PYD levels also increased before SRT treatment (Figure 20)
2. **Local Tumor Control:** After SRT, serial radiographs (Weeks 2-8) of the tumor lesion showed no progression (Figure 18). Mean percent tumor necrosis at the end of the experiment in each group is as follows: 74% in 27 Gy (Range: 38-99%), 63% in 30 Gy (Range: 40-80%), 58% in 3 Gy (Range: 20-99%) and 87% in 36 Gy (Range: 80-99%) (Figure 22). The mean overall percent tumor necrosis was 70% with no statistical

significance between treatment groups. No statistical differences in luciferase activity were observed in this experiment due to the high degree of variability in expression levels. However, there was an upward trend in expression after tumor implantation at weeks 1 and 2 (Figure 19) After SRT, luciferase activity decreased in a downward trend to negligible levels at 5 weeks (Figure 19). Spikes in luciferase activity were observed in limited numbers as follows 1 rat in 30 Gy (Week 6), 3 rats in 33 Gy (Week 6, n= 1, Week 7, n =2) and 1 rat in 36 Gy (Week 7). There were no rats in the 27Gy group that showed recurrence of bioluminescence throughout the 8-week observation period.

- 3. Stereotactic radiation therapy reduces PYD levels:** No statistical differences between dosing groups were observed. In all treatment groups combined, mean PYD levels significantly increased by 2 Weeks post tumor injection from baseline (Week 0) ( $p < .0001$ ) (Figure 20). After SRT treatment, levels significantly decreased 5 weeks (post-injection) ( $p < 0.0001$ ) suggesting that SRT is reducing normal bone resorption as well as tumor induced bone resorption by inhibiting tumor growth. By weeks 6 and 7, PYD levels increased to baseline levels ( $p < 0.004$ ).

## **Acute Radiation Effects**

**Three daily fractions of 9, 10, 11 or 12 Gy per fraction cause mild acute effects to the skin.**

As previously observed with the fractionation study, mild skin lesions occurred predictably at a mean of 11 days (mean) after SRT treatment in all groups. As shown in Figure 23, increased desquamation was visually observed as the total radiation dose

increased; however, no animals were scored above a 1 for the VRTOG scale (Table 2).  
By 18 days, all animals showed little or no skin irritation, had healed and remained that way for the duration of the experiment.

### 3.4 Figures



Figure 13: Radiographs of each fractionation protocol at weeks 1, 2 and 5 (Post-SRT)

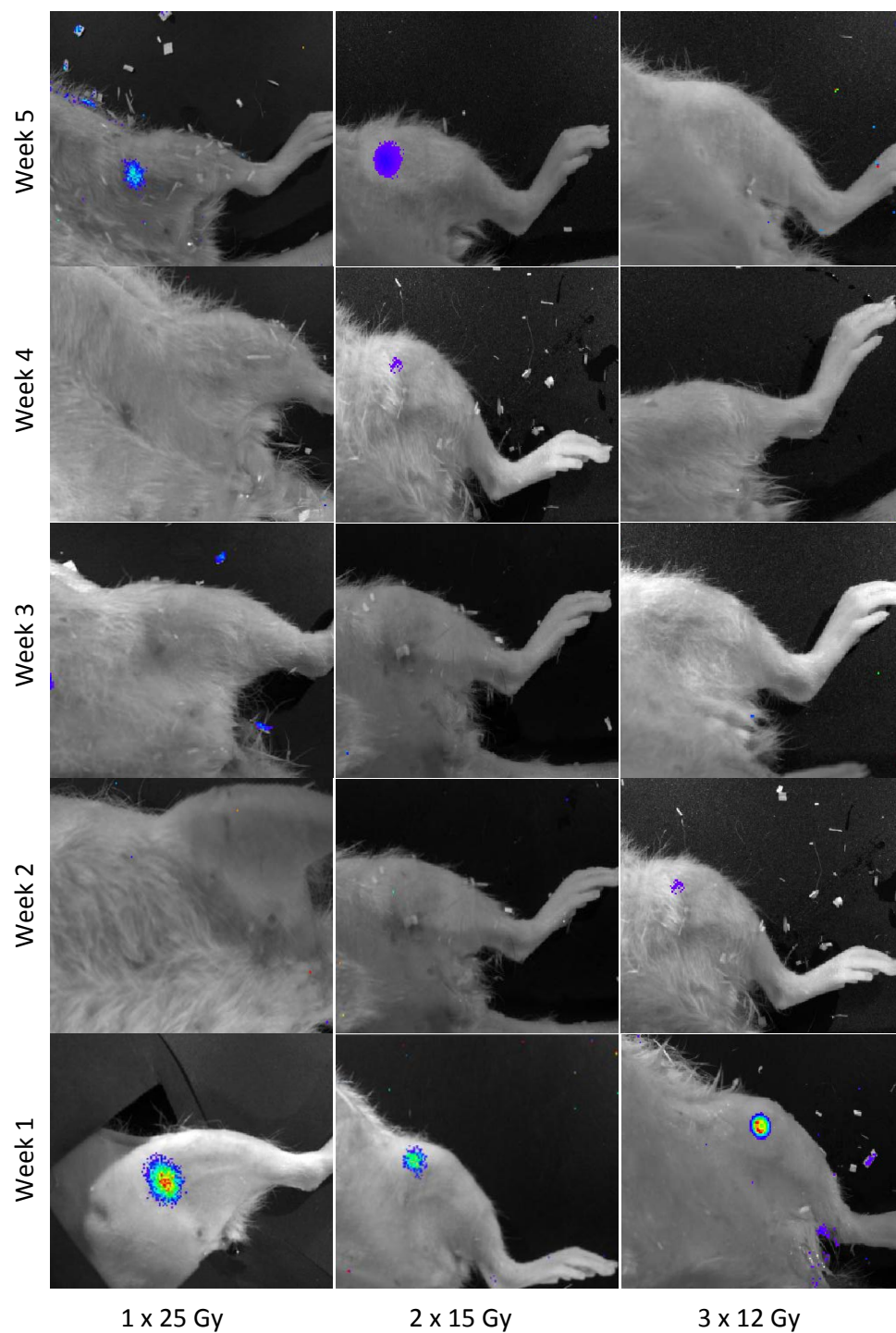


**Figure 14: Luciferase expression before SRT (Weeks 1 and 2) and after SRT (Weeks 3-5) for each fractionation protocol.**

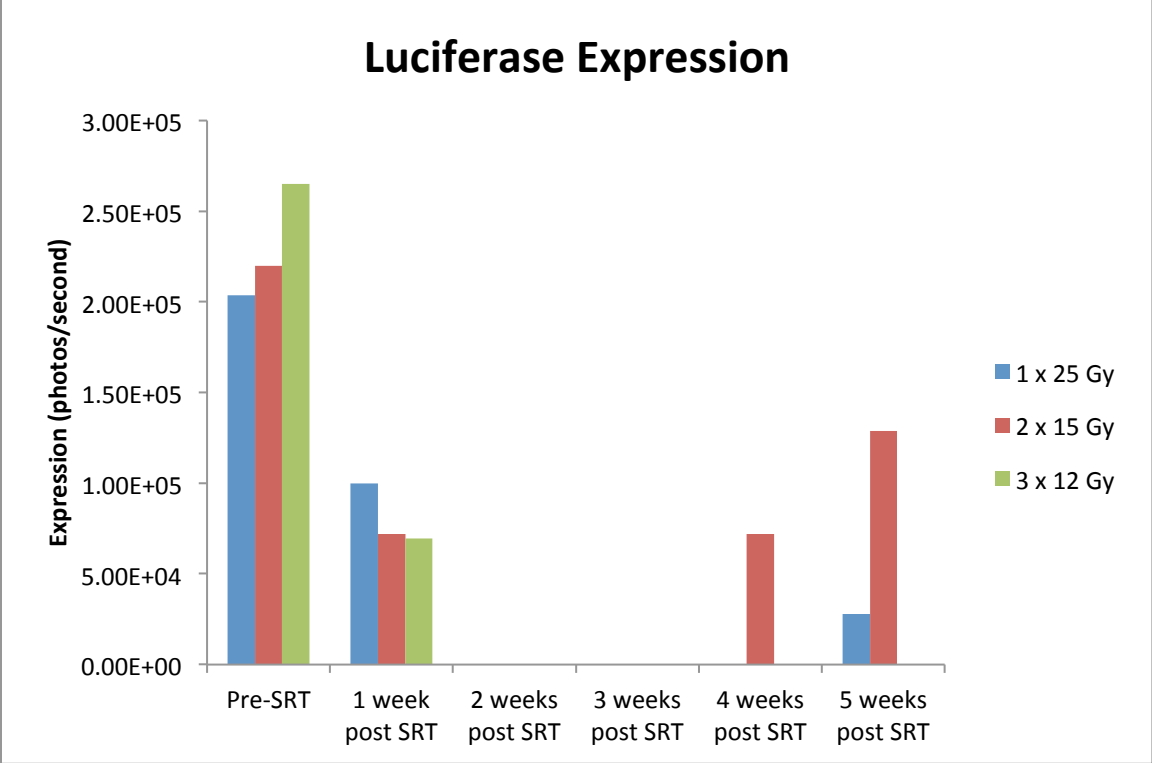
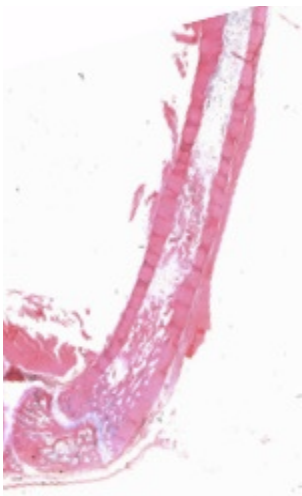
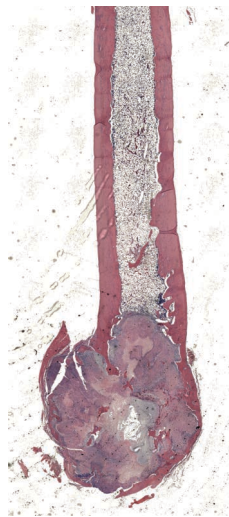


Figure 15: Luciferase expression in the fractionation protocols (n=1 per group)

1 x 25 Gy



2 x 15 Gy



3 x 12 Gy



**Figure 16: Histology (H&E) of each femur at 6 weeks. Histological findings include areas of tumor necrosis, osteosclerosis and necrotic bone marrow.**

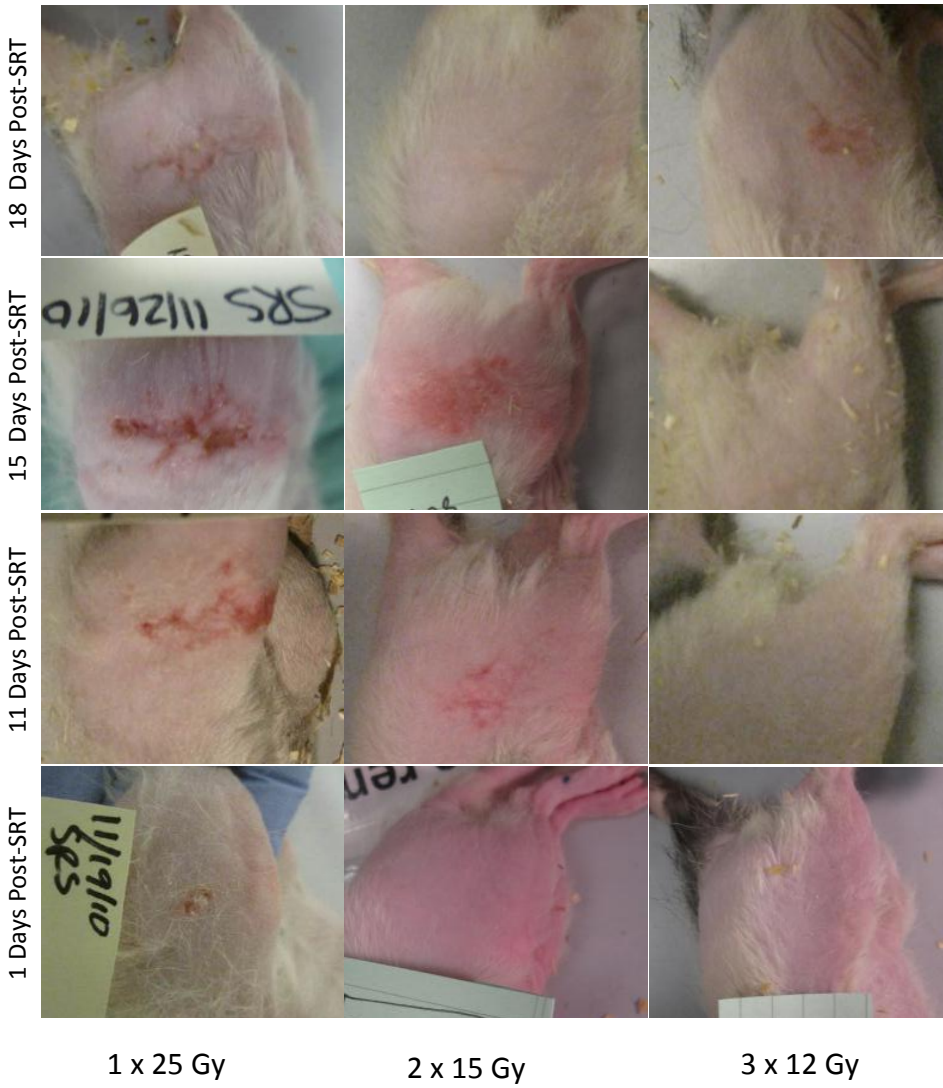


**Figure 17: Acute radiation effects in each fractionation protocol**

**Table 1: VRTOG radiation scoring for each fractionation protocol**

<b>Organ/Tissue</b>	<b>0</b>	<b>1</b>	<b>2</b>	<b>3</b>
<b>Skin</b>	No change over baseline	Erythema, dry desquamation, alopecia/epilation	Patchy moist desquamation without edema	Confluent moist dequamation with edema and/or ulceration, necrosis, hemmorhage
<b>1 x 25 Gy</b>			X	
<b>2 x 15 Gy</b>		X		
<b>3 x 12 Gy</b>		X		

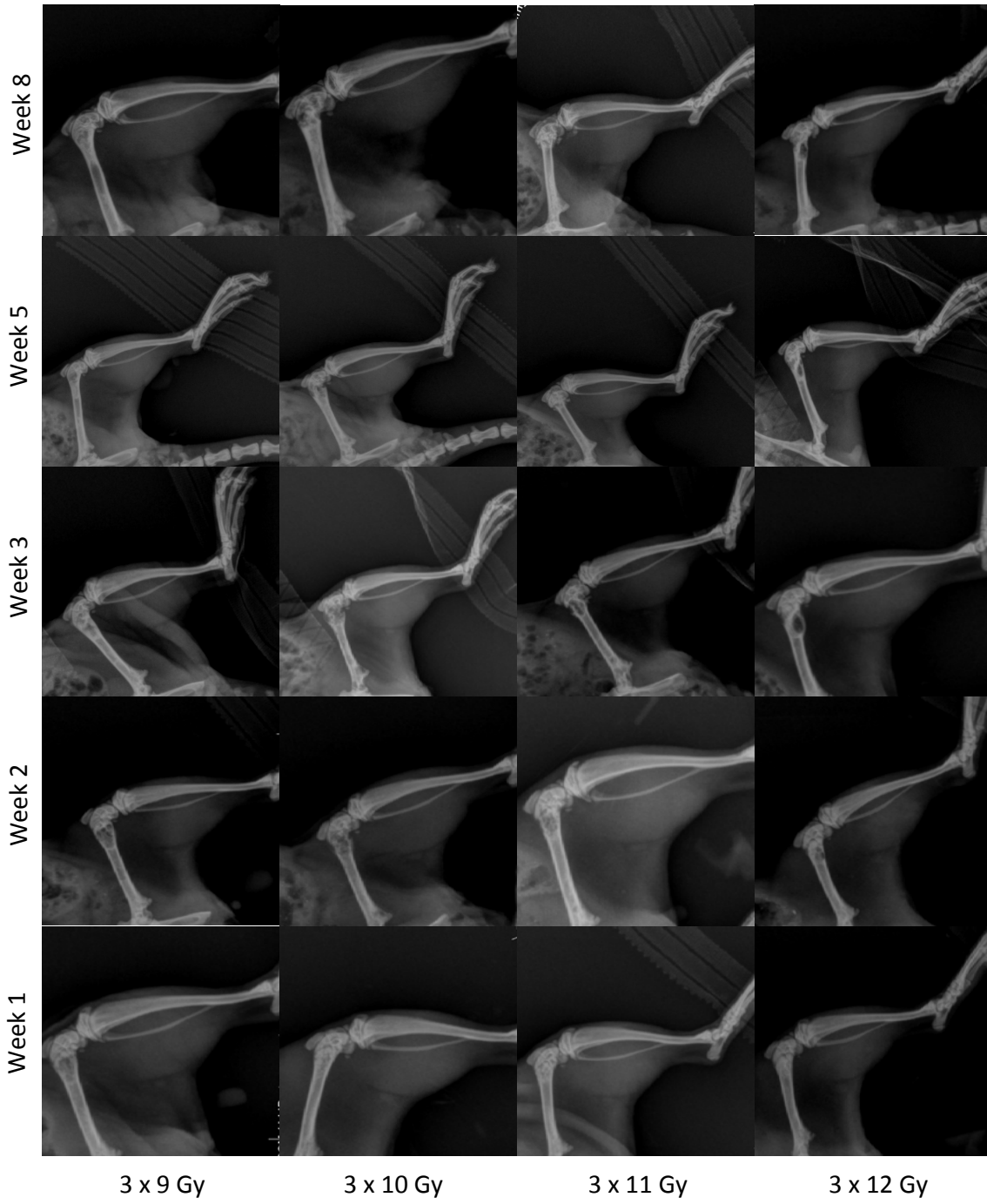


Figure 18: Representative femur radiographs in each total dosing protocol

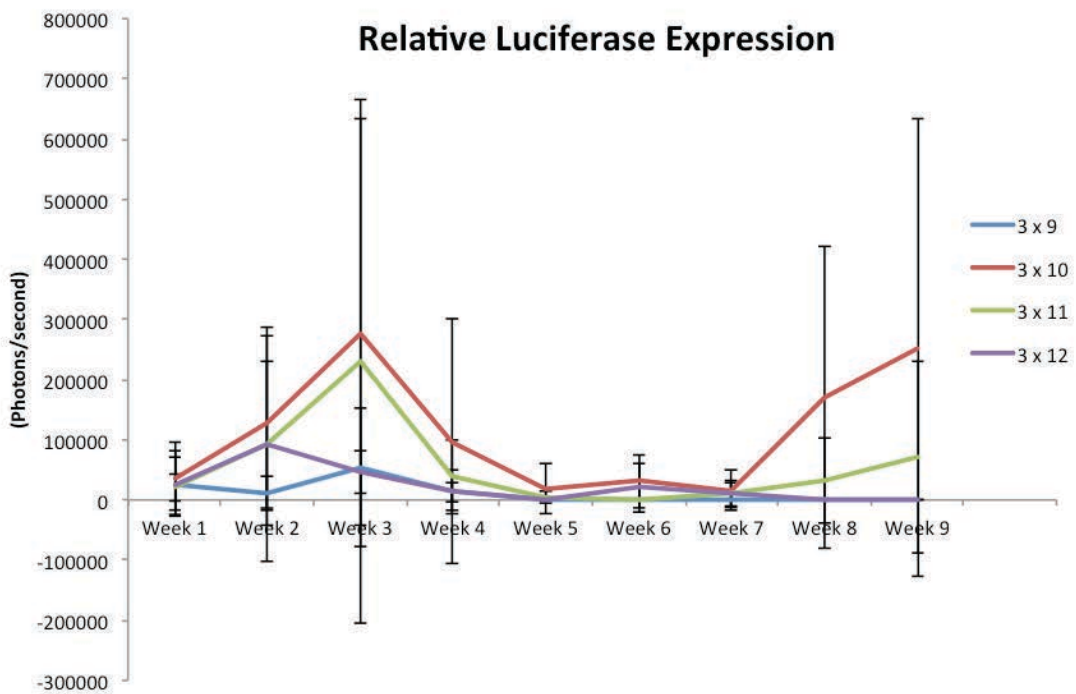


Figure 19: Relative luciferase expression in the total dose experimen

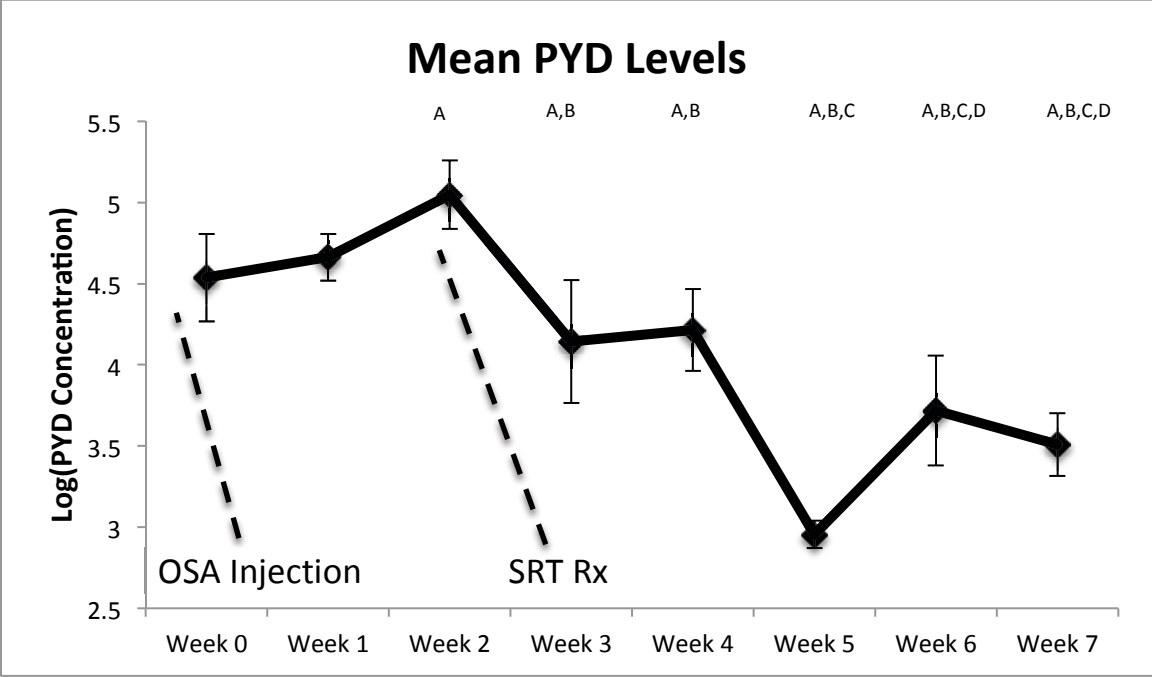
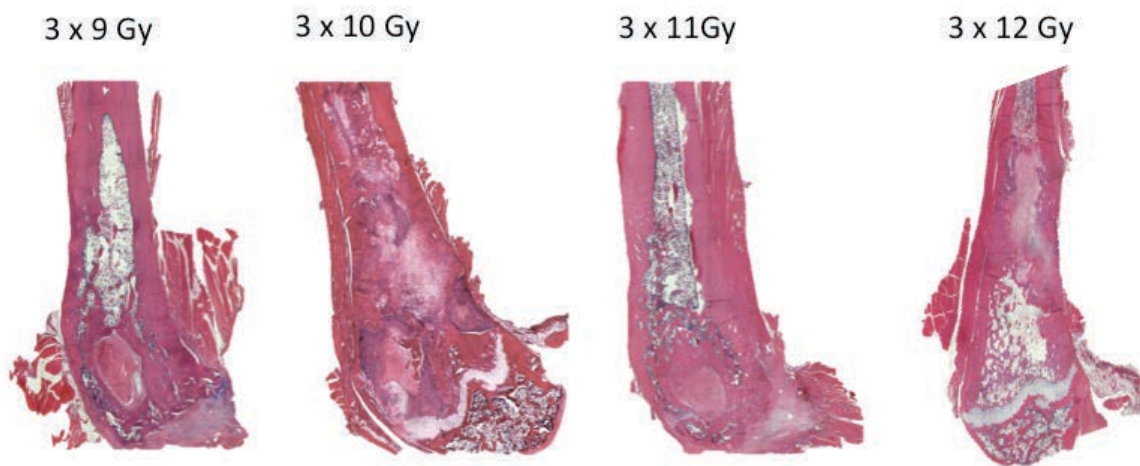


Figure 20: Mean PYD levels increased above baseline levels (week 0) at week 2 ( $p < 0.01$  (A)) after tumor inoculation and then significantly decreased as compared to Week 2 (C) after SRT treatment (Week 3,  $p < 0.0001$ ). At week 5, PYD levels further decreased as compared to Weeks 2, 3, & 4 (C, D) ( $*p < 0.0001$ ). PYD concentrations remained at these levels through weeks 6 and 7.



**Figure 21: Representative histology (H&E) in each total dose protocol at week eight. Histological findings include areas of tumor necrosis, osteosclerosis and necrotic bone marrow.**

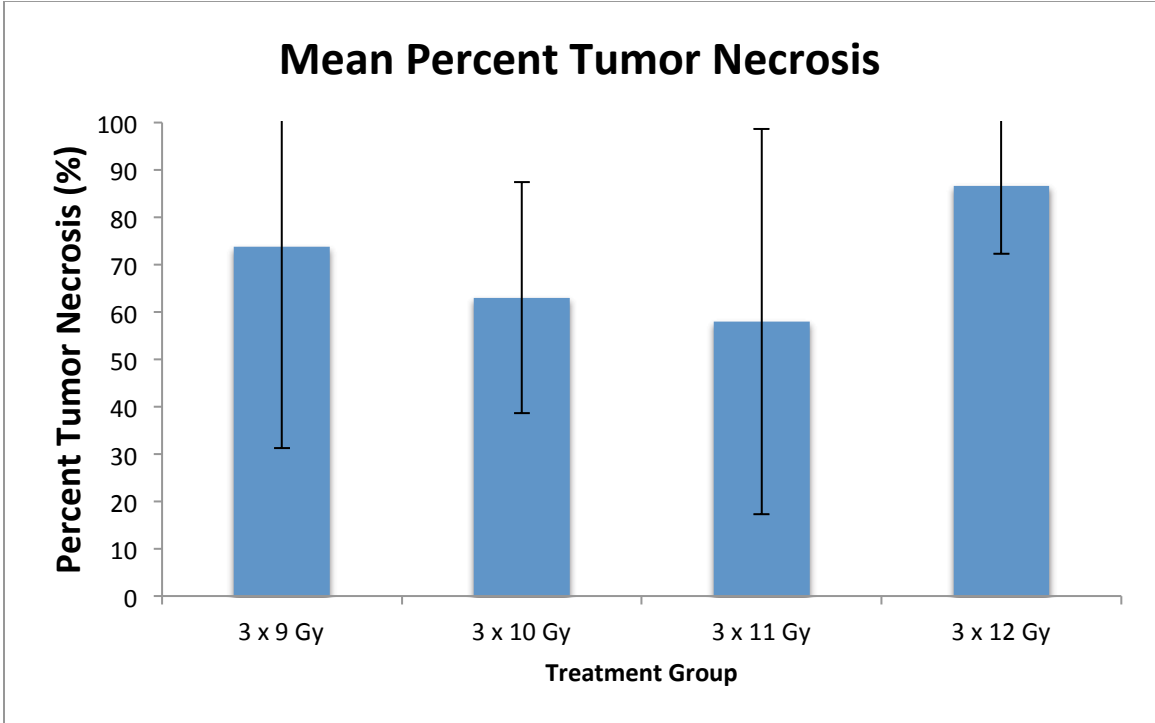


Figure 22: Mean percent tumor necrosis in each dosing protocol with no differences were observed between groups. Large variability was observed between each group as follows: 3 x 9 Gy: (range 10-95%) 3 x 10 Gy: (range 40-95%) 3 x 11 Gy: (range 10-95%) 3 x 12 Gy: (range 70-95%).

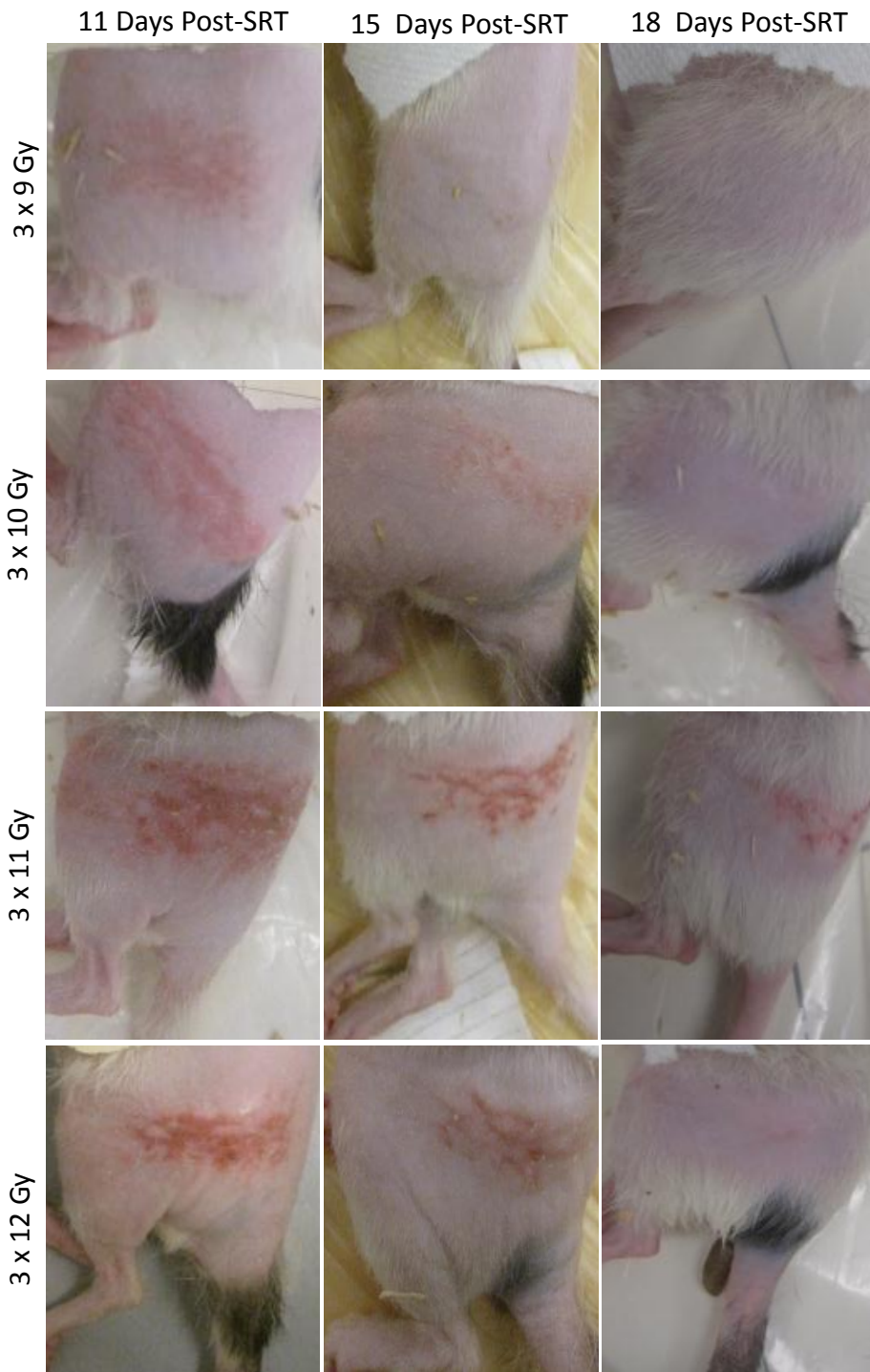


Figure 23: Representative acute radiation affects in each protocol

**Table 2: VORTG scoring in each protocol**

<b>Organ/Tissue</b>	<b>0</b>	<b>1</b>	<b>2</b>	<b>3</b>
<b>Skin</b>	No change over baseline	Erythema, dry desquamation, alopecia/epilation	Patchy moist desquamation without edema	Confluent moist dequamation with edema and/or ulceration, necrosis, hemmorhage
<b>3 x 9 Gy</b>		X		
<b>3 x 10 Gy</b>		X		
<b>3 x 11 Gy</b>		X		
<b>3 x 12 Gy</b>		X		

### 3.5 Discussion

Fractionated radiation therapy is commonly used for the palliative management of OSA in dogs in clinical cases. Previous studies have shown that administration of fractionated doses of ionizing radiation can help delay tumor progression and reduce pain (21, 27, 47). Studies using fractionated protocols such as 8-10 Gy fractions at 0, 7 and 21 days, 8-10 Gy at 0, 7, 21 or 28 days or 2 x 8 Gy on consecutive days showed a positive correlation in pain reduction (21, 27, 125). Although the side effects to normal tissue with palliative XRT were minimal, the total radiation dose and fraction scheme was not intended to achieve long-term local tumor control. Tumor recurrence and the associated clinical signs of pain and lameness occur again in the majority of cases. Another study evaluated curative-intent fractionated radiation therapy, dogs given total doses ranging between 48 and 60 Gy in 19 fractions showed local tumor control; however, the acute effects were excessive and thereby limited its clinical use (47). These studies showed that lower total doses exhibit fewer acute affects, but result in decreased tumor control. In contrast, studies using large doses per fraction with increased dose intensity over three days versus three weeks achieved better tumor control for tumors with low alpha:beta ratios such as OSA (47). The orthotopic model developed in Specific Aim 1 demonstrated a predictable tumor engraftment and progression of OSA that simulated the clinical setting. In this present study, we used this orthotopic rat model to evaluate the ability of SRT to achieve local tumor control with different fractionation and total dose treatment schemes.

## **Fractionation**

First, we conducted a pilot fractionation study that consisted of administering either one fraction of 25 Gy, two fractions of 15 Gy or three fractions of 12 Gy to the tumor-bearing femur. We evaluated the feasibility of administering SRT as well as the ability of these protocols to cause tumor necrosis and the potential acute radiation effects on normal tissues (skin) surrounding the tumor lesion.

Previous studies evaluating radiation treatment of canine osteosarcoma have shown that a tumor necrosis of 80 percent or greater correlates with durable local tumor control and increased survival (124). In this study, we show that all three fractionation protocols result in 80 percent or greater tumor necrosis. Although all three protocols achieved desirable necrosis, the acute skin effects were markedly increased in the one and two fraction protocols. The three-fraction protocol achieved tumor control while minimalizing the acute skin effects. It is interesting to note the recurrence of luciferase expression in the one and two fraction protocols. This is difficult to explain because the mean percent tumor necrosis was higher in these groups than in the three-fraction protocol, which showed no recurrence of luciferase activity. Although luciferase activity has been shown to be a measure of *in vivo* cell viability, it requires a multitude of complex factors in order for adequate expression (118). Decreases in oxygen levels have been shown to decrease luciferase expression *in vivo* (126). These decreased oxygen levels have been observed in osteosarcomas, which are often found to be hypoxic (127). Additionally, the percent tumor necrosis was evaluated from three, 10 um sections of the tumor. It's feasible that the tumor

could be viable in other areas of the femur that were not observed by the pathologist. A major limitation of this pilot experiment was the small number of animals evaluated (n=3). Increasing animal numbers to at least eight per group would provide more statistical power to help better evaluate tumor control. Even though preliminary, this experiment guided our choice of fractionation and doses for the remainder of the experiment. We concluded that SRT administered at 3 fractions of 12 Gy achieved acceptable tumor necrosis and minimized the adverse effects of radiation on normal tissue in this femoral rat model of OSA. We also determined that it was feasible to accurately position the rat for SRT treatment on consecutive days. This fractionation scheme has also been used in clinical cases of canine OSA. Furthermore, this experiment describes the first rat model of OSA using SRT that can serve as a basis of future experiments using SRT.

### **Total Radiation Dose**

The results observed in the fractionation study suggest that a three-fraction treatment protocol was optimal to maximize tumor control and minimize acute radiation affects to normal tissue in this model. We then developed a dosing protocol to determine the minimal total dose needed to achieve tumor control using the three-fraction treatment regime. In this study, we used total dose protocols of 27, 30, 33 or 36 Gy delivered in three fractions over consecutive days. We expected to achieve the best tumor necrosis with 3 fractions of 12 Gy. We also expected decreased tumor necrosis as the total dose decreased. Acute radiation affects were expected to be

minimal as previously observed in the fractionation study; however, we expected to further minimize the effects with reductions in dose per fraction and total dose.

Our results indicated that the mean percent tumor necrosis in all groups to be approximately 70 percent (Range: 10-95% ). Although we expected a difference in tumor necrosis between groups, no statistical significance differences were observed. Interestingly, the 3 x 12 Gy total dose protocol resulted in the highest mean tumor necrosis of 87% (Range: 70-95%) with the smallest variability. Tumor necrosis of 80% or higher after radiotherapy of OSA has been shown to be a valuable indicator of treatment response in both humans and dogs (124, 128). Thus, we chose the 3 x 12 Gy protocol in subsequent experiments since it achieved the highest consistent tumor necrosis (>80%) when compared to the other protocols.

To help compare our SRT protocol to that of previous studies, the concept of a biologically effective dose (BED) has been defined to more accurately describe the total dose delivered to as compared to conventional dose measurements (Equation 1).

**Equation 1: Equation for biologically effective dose where n=number of fractions, d=total dose.**

$$BED = n * d \left[ 1 + \frac{d}{\alpha/\beta} \right]$$

It takes into account the fraction size as well as the alpha:beta ratio of early and late responding tissues (55). Our results indicate that the BED delivered in the 3 x 12 Gy SRT protocol, assuming a reported mean alpha:beta ratio of 3.5 Gy, was 159 Gy (57). Thus, this protocol administered a higher BED and resulted in higher tumor necrosis than that of previous studies in dogs, which used lower BEDs (21, 27, 47, 124). Since canine OSA cells are not as radio-

responsive and have a low alpha:beta ratio, radiation delivered in a larger dose per fraction yielding a higher BED appears to be more effective (127). This observation suggests that the 3 x 12 Gy protocol may be directly applicable to clinical cases in canines and could result in better efficacy than that of traditional radiation protocols with low BEDs. The addition of chemotherapy along with conventional fractionated radiotherapy has also been shown to reduce the total radiation dose required for tumor control in OSA (124). Additional studies using our rat model of SRT in combination with chemotherapy may show that a reduction in total dose is possible whilst achieving the same or greater degree of tumor necrosis.

We also measured pyridinoline cross-links (PYD) levels to document the tumor-associated bone resorption in response to SRT. We expected to observe decreases in PYD levels in the weeks following SRT treatment. We showed increased PYD levels at week two after tumor inoculation and significantly decreased levels after SRT treatment by week three in all groups. These decreased PYD levels suggest that SRT is inhibiting tumor associated bone resorption. Decreased PYD levels observed in this study along with increased tumor necrosis may serve as an indirect indicator of response to treatment. At week five PYD levels decreased further but increased slightly at weeks six and seven but remained below baseline levels. It is important to note PYD is a marker of global bone turnover; therefore, if PYD levels are not increasing it may indicate recurrence of OSA after SRT. Further studies are needed at longer time points to determine whether the increases observed at weeks six and seven continue in an upward trend. If these levels increase it could indicate possible tumor recurrence.

Finally, we monitored for skin effects with different total doses of SRT. As previously shown in our dosing study, minimal effects were observed in the 3 x 12 Gy treatment group. We expected to see similar acute effects as observed in the pilot experiment in the 3 x 12 Gy group. We then expected these effects to decrease as the total dose decreased. In this study, we observed similar effects in the 3 x 12 Gy group as in the pilot experiment. These effects decreased in severity as the total dose was reduced. The 3 x 12 Gy and 3 x 11 Gy group were similar while the 3 x 10 Gy and 3 x 9 Gy groups showed little, if any, adverse effects. Moreover, none of the groups scored greater than a 1 on the VORTG radiation-scoring chart. Longer experiments are needed to evaluate the potential late-term affects of SRT especially on bone, muscle and peripheral nerves.

## **Conclusion**

The studies described herein evaluated the ability of different fractionation and total radiation dose SRT protocols to achieve tumor necrosis and minimize the acute radiation side effects to skin. In the preliminary fractionation study, all fractionation schemes achieved an average percent necrosis of greater than 80 percent. It is important to note the limited number of animals of this pilot study make it difficult to make an accurate conclusion as to differences in tumor necrosis between groups. Acute skin effects were higher in the 1 x 25 and 2 x 15 Gy on the VORTG scoring scheme than the 3 x 12 Gy group. The 3 x 12 Gy group had the lowest VORTG score with minimal acute effects. This led us to use this fractionation protocol to evaluate the minimum total dose using three fractions required to achieve tumor control. In the total dose experiment, we observed a 70% mean tumor necrosis. Although, we did not see a difference between groups, the small standard deviation and higher average percent necrosis (87%) of the 3 x 12 Gy groups suggest that this fractionation and total dose was optimal to utilize

in the remaining experiments. These data are relevant as they show SRT delivered in 3 fractions of 12 Gy is capable of achieving greater than 80% necrosis. It also suggests that this model could be utilized to evaluate novel therapeutics for bone regeneration strategies after the use of SRT. This fractionation and total dose protocol (3 x 12 Gy) was chosen for the final experiment to evaluate the efficacy of mesenchymal stem cells to rescue irradiated bone after the treatment of OSA by SRT in Specific Aim 4.

## Chapter 4: Mesenchymal Stem Cell Collection & Characterization

### 4.1 Introduction

Mesenchymal stem cells (MSC) are multipotent adult stem cells that have the potential to differentiate into various cell types, including chondrocytes, adipocytes and osteoblasts (88, 129). The ability of these cells to differentiate into osteoblasts makes them an attractive candidate as a new therapeutic option for bone regeneration. In cell culture, MSCs will not spontaneously differentiate and need to be driven towards a specific lineage by certain culture conditions (e.g. growth factors) (130). However, *in vivo*, the dynamic microenvironment in which the cells are exposed to have been shown to play an important role in their fate. MSCs exposed to an extra-cellular bone matrix tend to undergo an osteogenic commitment whereas MSCs exposed to cartilaginous tissue are likely to commit to chondrocytes (131, 132).

Methods to distinguish MSCs from other cells such as hemacytoblasts and fibroblasts are controversial as there are no universally accepted methods (130). Morphologically, MSCs exhibit plastic adherence as well as a swirling pattern of spindle-like and stellar shaped cells (133). One method of determining if plastic adherent cells are multipotent MSCs is to prove that they can differentiate into the three main MSC differentiation lineages (chondrocytes, adipocytes and osteocytes) (130, 134). This is accomplished by incubating MSCs with specific growth factors that can drive MSCs into different lineages thus aiding in identifying MSC characteristics. For osteogenic differentiation, the addition of dexamethasone to the growth media has shown to lead to osteoblast differentiation (130). Similarly for adipocytes, dexamethasone with the addition of  $\beta$ -glycerol phosphate leads MSCs to differentiate into

adipocytes. Finally, chondrogenic differentiation can be obtained by adding TGF- $\beta$  to the growth media (130). These differentiated cells can then be visualized under a microscope using the following staining techniques. Alizarin staining binds to osteoblasts actively forming calcium and Oil Red O binds to lipid forming adipocytes (130). Chondrocyte differentiation can be confirmed by H & E staining and exhibits a distinct morphologic difference between undifferentiated MSCs and chondrocytes (130).

Flow cytometric analysis can also be used to differentiate various cell types by analyzing antigen expression patterns on the cellular surface. For example, hematopoietic cells have distinct and well-characterized antigen expression, which include CD34, CD38 and SCA-1 (130, 135). Unfortunately for MSCs, many of the same antigens expressed on hematopoietic cells can also be expressed on MSCs. Furthermore, MSC antigen expression profiles vary greatly by experiment, laboratory and species. Many laboratories are attempting to identify a universal antigen expression profile of MSCs. Currently, some of the most commonly reported positive antigen patterns believed to be specific to MSCs are CD44, CD73, CD29, CD13, CD34, CD56, CD146, CD 106, CD 54, CD90, CD166 and CD105 (130). Negative antigen expression most commonly includes CD34, CD14, CD45, CD11b, CD49d, CD106, CD10 and CD31 (136). In some cases (CD34 and CD106) have both been shown to be negative and/or positive depending on the study. This is thought to occur because the antigen analysis of whole population of MSCs can include cells that may not be MSCs or that have already begun to differentiate into a specific lineage (adipose, osteoblast, etc.) (136, 137). Thus, there is no clear consensus as to a specific antigen expression profile for MSCs at this time (130).

Although there does not appear to be a universally agreed upon antigen expression profile for MSCs, there are individual subpopulations of MSCs that can express specific markers. Some of these subpopulations have been associated with better differentiation down different lineages. For example, a recent report showed that subpopulations of MSCs could express a particular epitope of CD56 called 39D5. Cells positive for both CD56 and 39D5 exhibited greater differentiation potential towards chondrocytes. Cells expressing CD56 but lacking the 39D5 epitope lacked the ability to differentiate into chondrocytes. The authors also noted a novel marker, MSCA-1, that when expressed resulted in better differentiation into adipocytes. Interestingly, when MSCA-1 was co-expressed with CD56, MSCs lost the ability to differentiate into adipocytes. Another study reported that subsets of MSCs expressing CD105 are more capable of differentiating into chondrocytes (138). Thus, the isolation of subsets of MSCs with specific markers known to have better differentiation capabilities may have better regenerative properties than whole populations of MSCs.

MSCs can be found in many locations throughout the body; however, the bone marrow and adipose tissue serve as easily accessible sources of MSCs (139). Both of these locations allow for collection through minimally invasive procedures. Bone marrow and adipose MSCs have been shown to differentiate down multiple lineages and have shown potential therapeutic efficacy (134, 140).

In this study, we isolated bone marrow and adipose derived MSCs from transgenic rats that ubiquitously express Green Fluorescent Protein (GFP) by techniques previously described (see 4.2.2) (133, 141-143). These animals had the GFP gene inserted in the ubiquitin C promoter

region. This promoter region has resulted in excellent expression of inserted genes in all tissues of the animal (144). Ubiquitous expression is of great value to these experiments because it enables all cells in the animal, including MSCs, to express GFP (143). It also allows for the progeny of cells isolated from these rats to also express the GFP protein. The ability of these MSCs to express GFP allows investigators to examine the fate of these cells after implantation into recipient animals by using histological analysis to determine their role in any new bone formation experiments conducted in Chapter 5 (143). The multipotent characteristics of MSCs isolated from adipose and bone marrow aspirates in GFP expressing rats were characterized by three-lineage differentiation. This was accomplished by administering osteogenic, adipogenic and chondrogenic factors to these cells, which have been shown to induce differentiation of MSCs into osteocytes, adipocytes and chondrocytes (130, 145). These experiments evaluated the isolation techniques by yielding cell cultures that exhibited morphologic characteristics similar to MSCs. Additionally, it assessed the ability of these cells to differentiate into the three main differentiation lineages to further confirm and characterize these cells as MSCs. We hypothesized that cells isolated from bone marrow and adipose tissue that exhibited plastic adherence and multipotency were indeed MSCs and would express GFP. These cells were used in Chapter 5 to evaluate whether exogenously administered MSC induce or directly cause new bone formation in irradiated bone.

## 4.2 Materials and Methods

See Appendix C for complete experimental details outlined in this Specific Aim

### *Mesenchymal Stem Cell Isolation*

**4.2.1. Animals:** Four Lewis 344-Tg rats ubiquitously expressing enhanced Green Fluorescent Protein (eGFP) were obtained from the Rat Resource and Research Center (Columbia, MO) and housed by Laboratory Animal Resources under approved IACUC Animal Protocol 11-2537A (143). These transgenic rats express the EGFP transgene under the control of the Ubiquitin C promoter region.

**4.2.2. Bone Marrow Derived MSC Isolation:** Rats were anesthetized and then euthanized by cardiac puncture. Femurs (n=8) were harvested and placed in MSC growth media containing low glucose DMEM + 15% FBS. The distal and proximal ends of the femurs were removed exposing the medullar cavity (133). The cavity was then flushed with MSC growth media using 16, 18 and 20 gauge needles to disperse cells. Cells and media were collected into a conical tube and centrifuged for 5 minutes at 1000 RPM. Supernatant was removed and the cell pellet was re-suspended in MSC growth media and transferred to a 15 mL flask (133). The media was changed every three days until cells were 70% confluent and then maintained by sub culturing into additional flasks. To create frozen cell stocks, cells were trypsinized, washed with HBSS and frozen in freezing medium containing 10% DMSO, 44.5% FBS and 44.5% DMEM.

**4.2.3. Adipose Derived MSC Isolation:** Subcutaneous and visceral fat were removed using a scalpel from the same four rats used for bone marrow MSC isolation (142). Adipose fat

was then minced with a scalpel, placed in PBS and agitated for approximately 1 minute. An equal volume of collagenase was added to the adipose tissue cell suspension and placed at 37°C until the solution became homogenous (142). Cells were then vortexed and then centrifuged at 1,200 RPM for 5 minutes. The supernatant was removed and the remaining cells were then placed in MSC growth media containing low glucose DMEM + 15% FBS. The media was changed every three days until 70% confluency and then maintained by sub culturing into additional flasks. Cells used in these experiments were in the third or fourth passage from initial isolation. Frozen cell stocks were made as previously described.

### ***Mesenchymal Stem Cell Characterization***

**4.2.4. Osteogenic Differentiation:** Rat bone and adipose derived MSCs were seeded separately onto 6 well plates at a density of 200,000 cells/mL and cultured as previously described until ~70-80% confluency. Osteogenic differentiation media was prepared as follows: Low glucose Dulbecco's Modified Eagle Medium (DMEM) supplemented with 10% FBS, 1mM dexamethasone, 01.M ascorbic acid, 1M glycerol-2-phosphate, 100X L-glutamine and 100X antibiotic-antimycotic (130). Media was added to wells and replaced every three days for 21 days. A separate well with only growth media served as a control. Alizarin Red Calcium Stain was used to detect the presence of calcium after differentiation incubation period. Media was removed from plates and cells were fixed with ice cold 70% ethanol for 1 hour at room temperature. Cells were then rinsed twice for 10 minutes with PBS. Alizarin red solution (Invitrogen, Carlsbad, CA) was then

added to cover the plate and incubated for 30 minutes (130). The plate was washed with PBS and then viewed under a microscope and stained osteocytes were visually observed and documented using digital photography under a microscope (4X magnification).

**4.2.5. Adipocyte Differentiation:** Rat bone and adipose derived MSCs were seeded onto 6 well plates at a density of 200,000 cells/mL and cultured as previously described until ~70-80% confluency. Adipocyte differentiation media<sup>2</sup> was obtained from GIBCO (Catalog #A10071-01) and supplemented with 50 ug/ul antibiotic-antimycotic. Media was added to wells and replaced every three days for 21 days (130). A separate well with only growth media served as a control. Oil red-O staining was used to detect the presence of adipocytes after differentiation incubation period. Media was removed from plates and cells were fixed with ice cold 70% ethanol for 1 hour at room temperature. Cells were then rinsed twice for 10 minutes with PBS. Oil red O (Invitrogen, Carlsbad, CA) was then added to cover the plate and incubated for 30 minutes (130). Wells were then rinsed twice and visually observed and documented using digital photography under a microscope (4X magnification). Red coloration indicated that adipocyte cells were present.

**4.2.6. Chondrogenic Differentiation:** Rat bone and adipose derived MSCs were harvested from 75 cm flasks and transferred to a 15 mL conical polypropylene tube at a density of approximately 100,000 cells in 500 ul of chondrogenic differentiation media.

---

<sup>2</sup> STEMPRO® Chondrogenesis Differentiation Kit  
<http://products.invitrogen.com/ivgn/product/A1007101>

Chondrogenic differentiation media<sup>3</sup> was obtained from GIBCO (Catalog #A10070-01) and supplemented with 50 ug/ul antibiotic-antimycotic. Cells were then centrifuged at 450g for 10 minutes and incubated at 37oC with the caps loosened (130). Media was changed every three days for 21 days taking great care to not aspirate the pellet during media changes. A separate well with only growth media served as a control. At 21 days, the cell pellet had increased in size to approximately 1-2 mm. The chondrocyte pellet was carefully removed from the conical tube and placed in Histogel (Thermo Scientific, Waltham, MA). Cells were then sectioned into 5 um sections and placed onto glass slides. Slides were then stained with 1% toluidine blue/1% sodium borate for 5 minutes (130). The slides were then visually observed under a microscope for chondrocytes (positive for blue coloration) and digital photographs were acquired and recorded.

**4.2.7. GFP Imaging:** Cells were washed twice with PBS and then viewed under a fluorescence microscope with the GFP filter and a digital picture was acquired. OSA of cells that did not express GFP were also imaged and served as a control (Figure 27).

---

<sup>3</sup> StemPro® Adipogenesis Differentiation Kit  
<http://products.invitrogen.com/ivgn/product/A1007001>

### 4.3 Results

**Rat bone marrow and adipose derived mesenchymal stem cells exhibit MSC-like morphology and growth characteristics.** We were able to successfully isolate cells from the bone marrow and adipose tissue of rats that were consistent with MSC characteristics. Both bone marrow and adipose derived MSC cell lines exhibited plastic adherence and visually resemble MSCs morphologically by exhibiting spindle-like and stellar shaped cells in an overall swirling pattern as previously described (Control group Figure 24) (133). Bone marrow derived cells grew significantly slower with a doubling time of approximately 3 to 4 days. Adipose derived cells grew much more quickly with a doubling time of approximately 24 hours.

**Rat bone marrow and adipose derived mesenchymal stem cells differentiate into osteoblasts.** Bone marrow and adipose derived mesenchymal stem cells were isolated from rats as described above. To confirm the potential of these cells to differentiate into bone, osteogenic factors (see 4.2.4) were added to the growth medium (differentiation medium) and evaluated for the presence of calcium by the Alizarin Red calcium-staining assay. After a 21day incubation period, no Alizarin Red staining was observed in cells incubated with normal growth medium (Figure 24A & C), which indicates no calcium was produced. In contrast, MSCs incubated with differentiation medium clearly show osteoblastic lineage as shown in Figure 24B & D indicated by the red staining. These results demonstrate and confirm the ability of the isolated rat MSCs to differentiate into osteoblasts.

**Rat bone marrow and adipose derived mesenchymal stem cells are capable of differentiating into adipocytes.** To confirm the potential of these cells to differentiate into adipocytes, adipogenic factors were added to the growth medium (differentiation medium) and evaluated for the presence of fat globules by the Oil O Red staining assay. After the 21-day incubation period, no Oil O red staining was observed in cells incubated with normal growth medium (Figure 25A & C), which indicates cells were not differentiation into adipocytes. However, cells incubated with adipogenic differentiation medium clearly show adipogenic lineage as shown in Figure 25B & D indicated by the red staining of fat globules. These results demonstrate the ability of rat MSCs to differentiate into adipocytes.

**Rat bone and adipose derived mesenchymal stem cells are capable of differentiating into chondrocytes.** To confirm the potential of these cells to differentiate into chondrocytes, chondrogenic factors were added to the growth medium (differentiation medium) and evaluated for the presence of chondrocytes by the Toluidine Blue staining after a 21-day incubation period. As shown in Figure 26, cells stained purple are indicative chondrocytes while cells stained blue are undifferentiated MSCs (130). These results demonstrate the ability of rat MSCs to differentiate into chondrocytes.

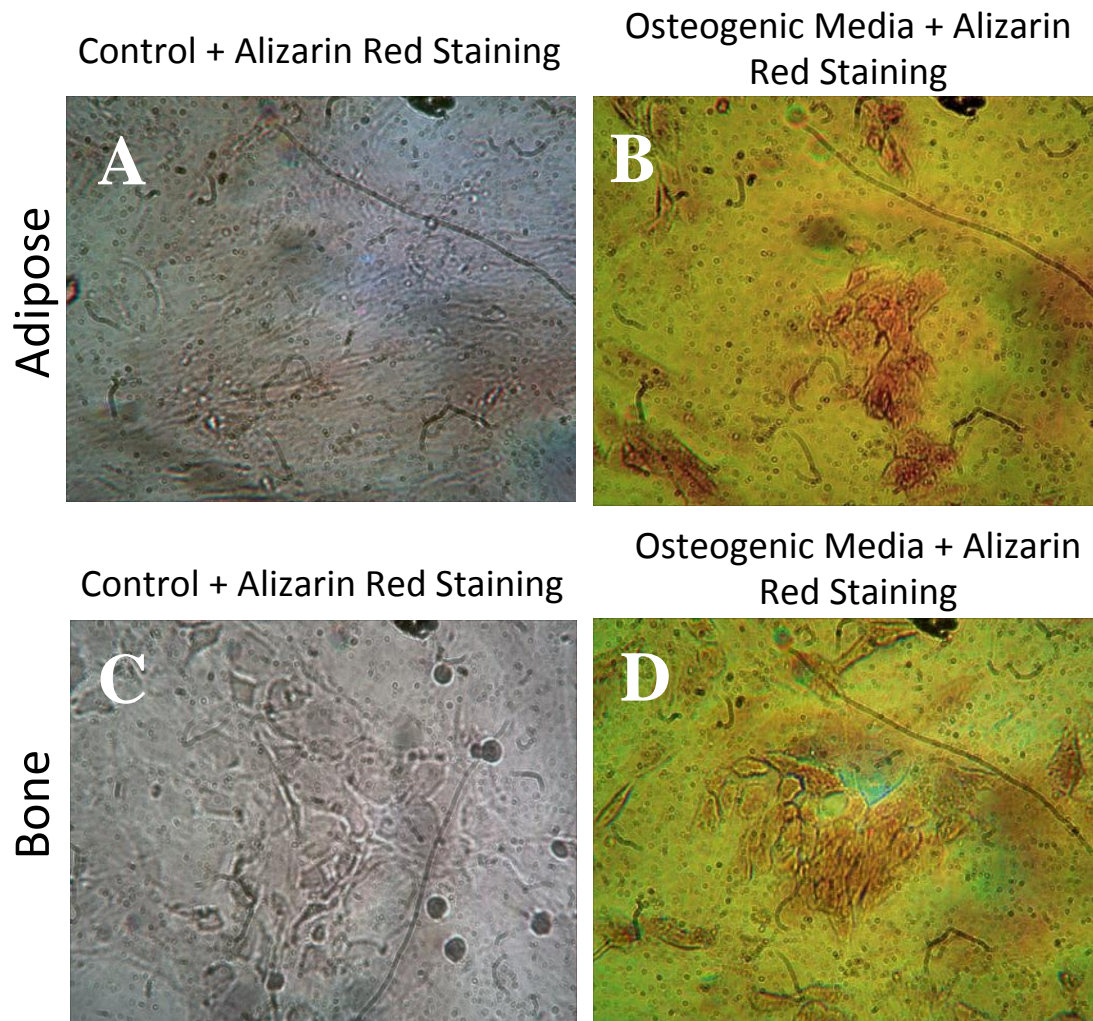
**Rat bone and adipose derived mesenchymal stem cells express GFP.** GFP expressing bone marrow adipose derived mesenchymal stem cells were viewed under a fluorescent microscope (GFP Filter). As shown in

Figure 27, both adipose (A) and bone marrow (B) derived MSCs expressed GFP. This confirms that the isolated MSCs express the green fluorescent protein. The control groups (C & D) did not express GFP.

**Conclusions:**

The bone marrow adipose derived cells isolated from the GFP transgenic rats were determined to be multipotent mesenchymal stem cells based on characteristic morphology, plastic adherence and successful differentiation into osteogenic, adipogenic and chondrogenic lineages and GFP expression.

#### 4.4 Figures



**Figure 24:** Adipose and bone marrow derived mesenchymal stem cell differentiation into osteoblasts as indicated by Alizarin red staining. A) Adipose derived MSCs incubated with control media and B) adipose derived MSCs incubated with osteogenic media. C) Bone marrow derived MSCs incubated with control media and D) bone marrow derived MSCs incubated with osteogenic media.

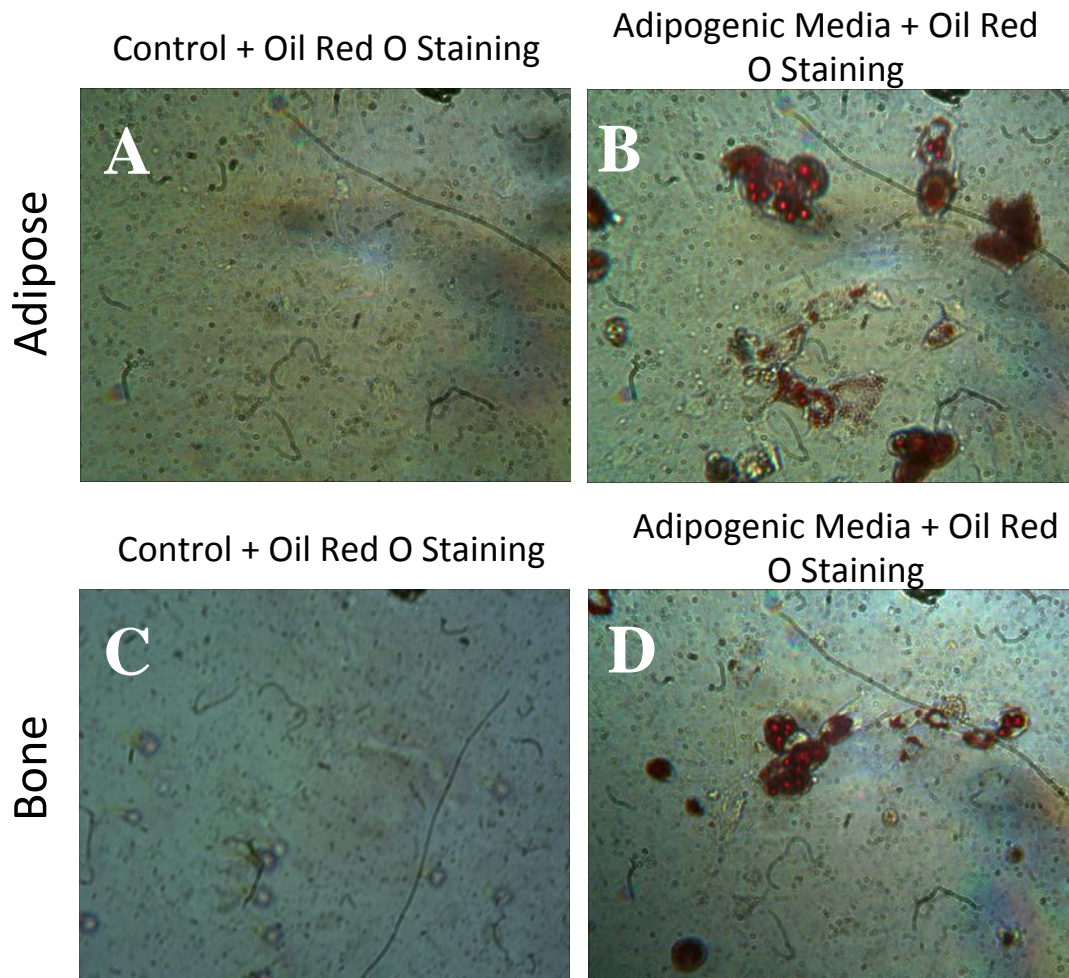


**Figure 25: Adipose and bone marrow derived mesenchymal stem cell differentiation into adipocytes as indicated by oil red O staining. A) Adipose derived MSCs incubated with control media and B) adipose derived MSCs incubated with adipogenic media. C) Bone marrow derived MSCs incubated with control media and D) bone marrow derived MSCs incubated with adipogenic media**

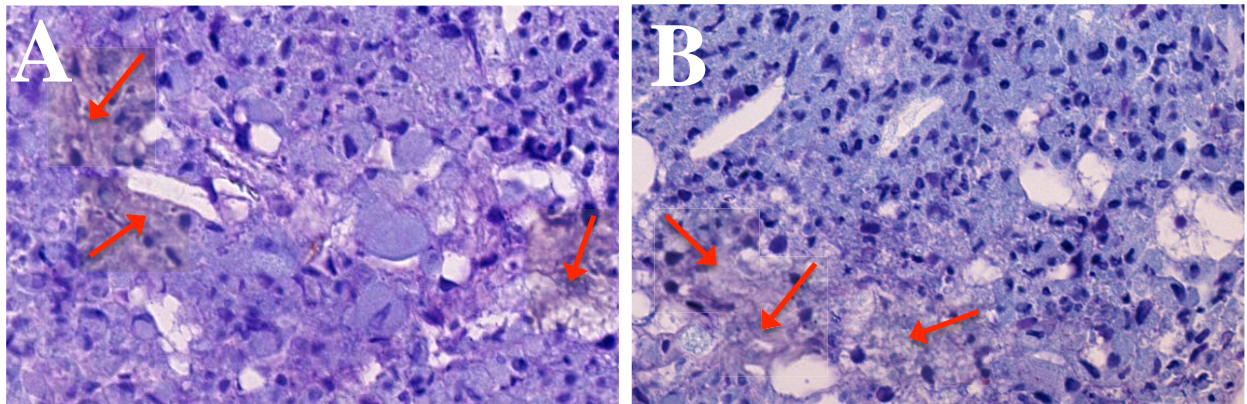


**Figure 26: Chondrogenic differentiation of MSCs. A) Adipose derived MSCs differentiated into chondrocytes. B) Bone marrow derived MSCs differentiated into chondrocytes. Purple staining is indicative of chondrocytes and the blue staining is undifferentiated MSCs.**

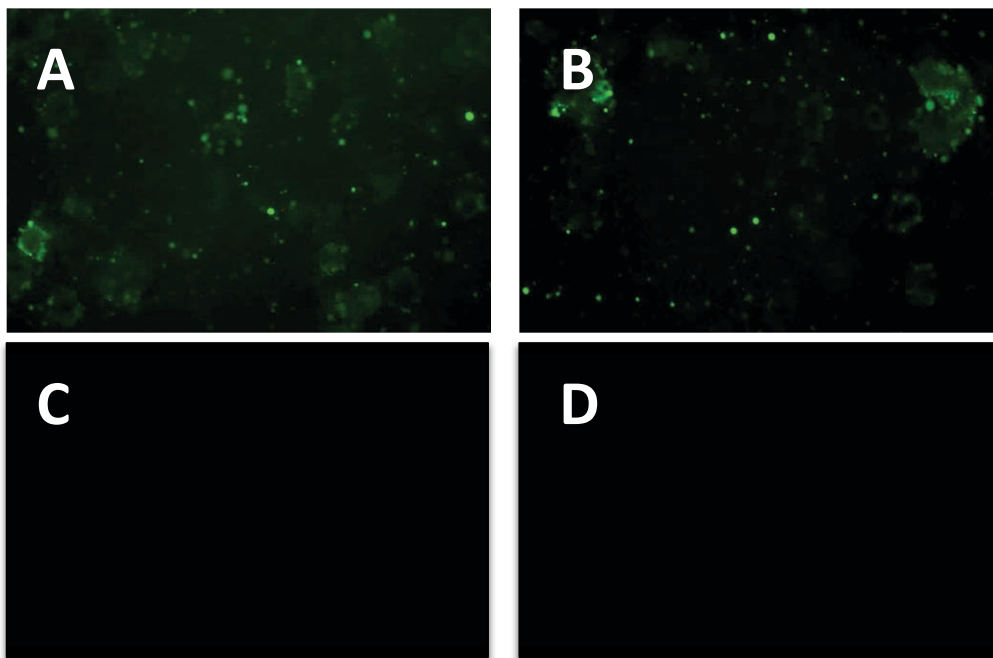


**Figure 27: GFP expression in Adipose derived (A) and bone marrow derived (B) MSCs. GFP expression was not observed in (C) and (D) as they were GFP negative and served as controls.**

## 4.5 Discussion

Mesenchymal stem cells have the ability to differentiate into osteoblasts, chondrocytes and adipocytes. The osteogenic potential of these cells offers new opportunities to develop therapies to regenerate bone in many different diseases. In this study, we evaluated the feasibility of isolating MSCs from bone marrow and adipose tissue from rats that ubiquitously express GFP. We also evaluated the ability of these cells to differentiate into osteoblasts, adipocytes and chondrocytes and confirmed GFP expression.

Initially, we were able to successfully isolate cells purported to be MSCs from the bone marrow and adipose tissue of rats. Both MSC cell lines exhibited plastic adherence and visually resembled MSCs morphologically by exhibiting spindle-like and stellar shaped cells in an overall swirling pattern as previously described (133).

Although these findings suggested that the cells isolated are MSCs, more confirmation is needed to further confirm the ability to differentiate into the three main lineages. Flow cytometry has been previously used in an attempt to identify cell specific markers for MSCs. These studies have been inconclusive as there is no consensus in the scientific community as to specific MSC markers. Additionally, the large number of anti-bodies needed is extremely costly and also requires a large number of cells (130). For the characterization studies described herein, we chose to characterize our MSCs by differentiating them into osteoblasts, adipocytes and chondrocytes, which has been described by several previous studies (130, 146, 147). In this study, we exposed our isolated MSCs to specific differentiation factors for osteogenic, chondrogenic and adipogenic differentiation and showed that the isolated cells can

differentiate into each of these cell types. These observations described herein suggest that the cells isolated from the bone marrow and adipose tissue are multipotent and meet the criteria of MSCs. Confirmation that the cells isolated in these rats are indeed MSCs is of particular importance because we intended to use these MSCs to regenerate irradiated bone in Chapter 5. Using cells that do not exhibit osteogenic potential would be detrimental to bone regeneration experiments.

Both bone marrow and adipose derived MSCs were isolated in these experiments because they both have the potential to generate bone. Bone marrow MSCs; however, are scarcer, proliferate much slower and are more difficult to isolate than adipose MSCs (148). The abundance of adipose tissue in rats as well as in other animal models potentially makes adipose MSCs more ideal for tissue regeneration. Adipose MSCs are similar to bone marrow MSCs as they exhibit multipotent potential as well as similar phenotype and surface antigen expression (139, 149). It is thought that adipose MSCs are derived from bone MSCs that have circulated through the vascular system and deposited into the adipose tissue (149). As with bone MSCs, adipose MSCs have also shown to aid in bone healing and regeneration. Adipose MSCs have been shown to repair bone in rat and rabbit critical defect models (150, 151). These MSCs can also recruit host osteoprogenitor factors and induce osteogenesis (148).

A potential drawback of using MSCs to regenerate bone is that the difference between host induced and MSC induced osteogenesis cannot readily be distinguished. Our cells, as previously discussed, were isolated from rats that ubiquitously expressed GFP. We were optimistic that GFP expression would allow us to distinguish between host-induced new bone

formation versus MSC induced new bone formation through GFP histological analysis. New bone formed by implanted MSCs would express GFP while host cells would not express GFP. Additionally, using alizarin staining which binds to calcium, GFP expressing cells that stain positive for alizarin would indicate active bone formation from implanted MSCs. These histological techniques make it possible to distinguish between host and MSC mediated bone formation.

The data described herein show the successful isolation, differentiation and establishment of a MSC cell line from the bone marrow and adipose tissue from GFP expressing rats. Differentiation into the three main lineages of the cells characterizes these cells as MSCs and confirms their potential to differentiate into bone in an animal model. Furthermore, GFP expression may aid in evaluating host and MSC mediated bone growth. Due to the abundance of adipose MSCs as well as their demonstrated osteogenic potential, we chose to use adipose derived MSCs for all subsequent experiments in Chapter 5 (Specific Aim 4).

## **Chapter 5: Evaluation of MSC mediated bone growth following SRT for the treatment of OSA**

### **5.1 Introduction**

Mesenchymal stem cells (MSCs) are multipotent adult stem cells found in the bone marrow and adipose tissues. They are capable of differentiation into various cell types including osteoblasts, chondrocytes and adipocytes (88). The ability of MSC's to differentiate into osteoblasts is of particular relevance to our studies as they could potentially generate new bone in osteosarcoma-affected bone irradiated with SRT. Several studies have shown that MSCs can home to damaged tissues, promote angiogenesis and regenerate bone (71, 89, 90). The observation that MSC's migrate directly to radiation-injured bone suggests they could potentially be used to regenerate bone after irradiation. (100-102).

Although MSCs have a number of promising therapeutic applications, there is concern about their potential to promote tumor growth, especially when used as part of therapy in a cancer setting (105). They have been shown to migrate to existing tumors and there is concern that their presence may promote or accelerate tumor growth or metastasis (105). A recent study of OSA implanted into the proximal tibia of mice showed that systematically injected MSCs targeted local OSA, promoted growth of the existing tumors and resulted in pulmonary metastasis (152). Migration to the tumor by MSCs is likely mediated by various cytokines, chemokines and other growth factors secreted by tumors (152). MSCs also produce these same mediators and can directly contribute to the growth and migration of tumors (153). The tumor

promoting properties of MSCs may pose a risk for local tumor recurrence or acceleration of distant metastatic growth if used as therapy to regenerate bone after irradiation of local OSA lesions. Thus, it is essential to examine the potential for tumor recurrence or progression when evaluating the therapeutic use of MSCs. Future studies are needed to evaluate safety, in addition to efficacy, before MSCs can be used in the clinical setting.

The primary aim of these experiments was to determine if MSCs, administered by either the intraosseous (IO) or intravenous (IV) route, have efficacy in forming new bone within the irradiated site following SRT of osteosarcoma. Our secondary aim was to observe animals treated for signs of potential for local or distant tumor progression. We hypothesized that MSCs would induce new bone growth in both the IV and IO treatment groups and no new bone growth would be observed in the SRT only group.

To test this hypothesis, we used the rat orthotopic canine OSA model developed in specific aim 1 and SRT treatment protocols as described in specific aims two and three. SRT was administered to the tumor-bearing limb two weeks after OSA cell inoculation using 3 x 12 Gy fractions delivered on consecutive days as previously described. Two weeks after the delivery of SRT, GFP-expressing MSCs were injected either intravenously through the tail vein (IV MSCs) or intraosseously into the left distal femur (IO MSCs). Control animals had their OSA lesions treated with SRT alone but did not receive any MSCs (SRT Only). Based on the acceptable local tumor control (87% tumor necrosis and 5 of 6 rats with no recurrence of luciferase expression 6 weeks after SRT) achieved using the 3 x 12 Gy SRT treatment protocol described in Chapter 3, we do not expect spontaneous local tumor recurrence in animals treated with this SRT protocol.

Any local tumor recurrence observed would thus be due to the direct or indirect effect of the administered MSCs. Serum Osteocalcin (OC) and urine PYD bone biomarker levels were measured throughout the experiment to monitor for evidence of bone generation and resorption respectively. Two days before sacrifice (Week 10), animals were injected with Alizarin red which binds to newly formed calcium in bone and has been shown to be indicative of new bone formation (154). After sacrifice, the femurs were imaged with microCT imaging to evaluate for differences in bone volume between treatment groups. A novel fluorescent histology technique was used to visualize and quantify alizarin staining, alkaline phosphatase for osteoblast activity and Tartrate resistant acid phosphatase (TRAP) staining for osteoclast activity and identification of any GFP expressing cells (155, 156). This novel technique involves overlaying each histological image (Alizarin, alkaline phosphatase and GFP) into one combined image that allows for distinction between host and donor mediated bone formation. Non-decalcified hematoxylin histological staining was also used to document percentage tumor necrosis, new bone growth and possible tumor recurrence.

## **5.2 Materials and Methods**

### **Experimental Design:**

Twenty-four rats were injected with  $1 \times 10^6$  canine osteosarcoma cells into the left distal femur using the technique described in Specific Aim 1. Rats were randomly placed into one of three treatment groups (Table 1). All rats were treated with 3 x 12 Gy (36 Gy total) SRT two weeks after tumor cell inoculation. Two weeks after SRT, GFP-expressing adipose-derived MSCs (previously isolated as described in Chapter 4) were injected either intraosseously into the femur

( $4 \times 10^6$  MSCs) (IO MSC Group, n=8) or intravenously into the tail vein ( $2 \times 10^6$  MSCs) (IV MSC Group, n=8). The remaining 8 rats received identical treatment but without MSCs (SRT only Group, n=8). Rats were followed after MSC injection by weekly radiography, bioluminescence imaging, PYD and osteocalcin markers for six weeks. Rats were sacrificed at week 10 and the femurs were subject to microCT imaging and fluorescent and histological analysis to determine total bone volume, GFP expression, osteoblast and osteoclast counts and percent tumor necrosis. See Appendix D for complete experimental details outlined in this Specific Aim.

**Table 3: Treatment Groups**

<b>Treatment Group</b>	<b>Description</b>
SRT only Group: (n=8)	OSA + SRT
IO MSC Group: (n=8)	OSA + SRT + IO MSC
IV MSC Group: (n=8)	OSA + SRT + IV MSC



**Figure 28: Experimental Timeline**

**5.2.1 Tumor Cell Inoculation:** One million ( $1 \times 10^6$ ) canine OSA cells were injected into the left distal femur of 24 rats using the luciferase-expressing Abram's OSA cell line and inoculation technique as described in Chapter 2.2.4.

**5.2.2 SRT Treatment:** Stereotactic radiotherapy was administered to all rats with 3 fractions of 12Gy (36Gy total) delivered on consecutive days. The same animal positioning, CBCT imaging, radiation treatment planning and SRT delivery was used in this experiment as previously described in Chapter 3.2.1.

**5.2.3 Mesenchymal Stem Cell Injection:** Two weeks after SRT, rats in the IO and IV groups (Table 1) were injected with the GFP-expressing adipose-derived MSCs that were isolated in Chapter 4. Rats were anesthetized to a surgical plane of anesthesia with isoflurane / oxygen by facemask. The left hind limb was clipped of hair and scrubbed with 4% betadine and 70% ethanol. A cell suspension of  $4 \times 10^6$  (IO MSC Group) or  $2 \times 10^6$  (IV MSC Group) MSCs in a 10% heparin solution was injected over a period of two minutes into the distal left femur or tail vein respectively. Heparin was used to prevent a thromboembolism following IV injection that has been observed in previous studies in our laboratory.

**5.2.4 Imaging:** Animals were monitored by weekly radiography and bioluminescence imaging of the left femur to assess tumor viability and radiographic changes using the same anesthesia, animal positioning and imaging parameters previously described in Chapter 2.2.5 and 2.2.6.

**5.2.5 Osteocalcin ELISA:** Osteocalcin (OC), a biomarker for bone formation, is a specific product of osteoblasts (157). It promotes the binding of osteocalcin to mineral and accumulates in the bone matrix. Osteocalcin levels in the bloodstream are considered to correlate with newly synthesized bone and have been shown to increase when using MSCs to induce bone growth (157). Osteocalcin was measured weekly from the serum. Approximately 200 ul of blood was collected (Weeks 0, 2, 4, 5-9) under anesthesia from the tail vein and stored at -20°C. Sera was isolated from whole blood using BD Microtainer serum separation tubes (Franklin Lakes, NJ), diluted 1:10 and subject to the Rat Osteocalcin ELISA (USCN Life Science Inc, Wuhan, China) per the manufacturer's instructions (ng/ml).

**5.2.6 Urine Collection and PYD ELISA:** Urine was collected weekly (Weeks 0-10) and PYD and creatinine levels were measured by the ELISA assay as previously described in 3.2.6.

**5.2.7 Euthanasia:** The euthanasia protocol was modified in this specific aim to provide a more complete fixation of the rat femur that was required for the use of the novel fluorescent as described below. Two days prior to euthanasia, rats were injected intraperitoneally with 30mg/kg Alizarin red to aid in identifying bone deposition in histological analysis. On the day of euthanasia, rats were then anesthetized under deep anesthesia by isoflurane. The animal was placed on the operating table with its back down and restrained. An incision with sharp scissors was made through the abdomen the length of the diaphragm to open up the thoracic cavity. While holding the heart steady with forceps, a 22G needle, attached to a perfusion pump, was inserted into the left ventricle. An incision was made in the atrium with sharp

scissors to allow blood and fluid egress during perfusion. Approximately 200 mL of 0.9% saline solution was perfused through the animal via the ventricular needle perfusion pump at a flow rate of 20ml/min. Once the blood cleared the body the saline solution was replaced with a 4% paraformaldehyde solution. Two hundred milliliters were perfused through the animal to ensure complete fixing of the tissues. The left femur was disarticulated at the coxofemoral and knee joints, the skin and partial soft tissues removed and the femur placed in 10% formalin. The femurs were imaged with microCT as described in 5.2.8. After microCT, the leg was then sent to Dr. David Rowe's laboratory at the University of Connecticut for fluorescent histology and analysis.

**5.2.8 MicroCT:** Femurs were subject to microCT analysis. Due to the variable location and size of the tumor in each femur, bone volume was normalized to three standardized volumes of interest within the tumor in each bone (Appendix D). Volume was calculated by averaging bone volume in these three sections each treatment group (IV and IO) and comparing them with the control group (SRT only) to evaluate any differences in bone volume that could be attributable to administered MSCs. Further details of this analysis is available in Appendix D.

**5.2.9 Histology:** Femurs were sent to Dr. David Rowe's laboratory at the University of Connecticut Health Center for cryosectioning and fluorescence imaging. This laboratory developed the novel fluorescent histology techniques used in these experiments (158). Untreated contralateral normal femurs (n=3) were used as a control standard for reference to compare against the SRT only, IO and IV MSC treatment groups. Femurs were sectioned at the mid-diaphysis and the distal half, which contained the implanted tumor cells, was

processed for sectioning. The samples were soaked overnight in 30% sucrose/PBS solution and embedded in Neg-50 frozen section medium (Richard-Allan Scientific, #6502).

Longitudinal full-length 5  $\mu\text{m}$  cryosections (Leica CM3050S Cryostat, Germany) of the femur were taken using a disposable steel blade (Fisher Scientific, # 3051835) and non-autofluorescent adhesive film (Section Lab, Co., Ltd, Toyota-gun, Hiroshima, Japan 7250301) to capture the cut section. Three sections, each selected from one of the three tissue depths, were chosen for microscopic examination. They were transferred to a single glass slide (Gold Seal #3051) using a 2% chitosan (Sigma #C3646) solution in 0.25% acetic acid to adhere the film side to the glass surface and allowed to air dry for 48 hrs at 4°C frost free refrigerator. Subsequently the four quadrants of the tissue slice were spotted with 1 $\mu\text{l}$  suspension of a 6 $\mu\text{m}$  fluorescent beads (Molecular Probes #I-14785m green; #I-14787 red) and allowed to dry for 30 min. The slide was soaked for 10 min in PBS, stained in a 30 mg/ml calcein blue solution (Sigma, #M1255-1G) for 30 min and cover slipped with 50% glycerin in PBS prior to microscopy for the endogenous fluorescent signals (bone mineral, mineralization lines and GFP when present).

Femur sections were transferred to a single glass slide (Gold Seal #3051) using a 2% chitosan (Sigma #C3646) solution in 0.25% acetic acid to adhere the film side to the glass surface and allowed to air dry for 48 hrs at 4°C frost free refrigerator. Subsequently the four quadrants of the tissue slice were spotted with 1 $\mu\text{l}$  suspension of a 6 $\mu\text{m}$  fluorescent beads (Molecular Probes #I-14785m green; #I-14787 red) and allowed to dry for 30 min. The slide was soaked for 10 min in PBS, stained in a 30 mg/ml calcein blue solution (Sigma, #M1255-1G) for 30 min and cover slipped with 50% glycerin in PBS prior to microscopy for the

endogenous fluorescent signals (bone mineral, mineralization lines and GFP when present).

After endogenous fluorescent signals were captured, the slide was removed from the microscope and the coverslip removed by brief soaking in PBS. Osteoclasts were identified using the fluorescent ELF-97 phosphatase substrate (E6589, Invitrogen, (159)). After imaging, the slides were processed to identify cells expressing alkaline phosphatase (AP) activity using neutral AP staining conditions and the fluorescent substrate fast red (Sigma, #F8764-5G) (160). Finally, hematoxylin staining was performed on the same slides after all the fluorescent staining and imaging steps were completed to generate a chromogenic image familiar to the bone biologist.

The fluorescent signals within the bone sections were recorded by a Zeiss Mirax Midi scanning fluorescence microscope (Carl Zeiss, Thornwood, NY) equipped with a 9 chamber filter cassette. The bone mineral that was stained with calcein blue was detected with a DAPI filter (Chroma, #49000ET) while the AC mineralization lines utilized a TRITC filter (Chroma 49005ET). The osteoclasts that were stained with ELF-97 using a yellow filter optimized for tetracycline (Chroma Technology Custom HQ409sp, 425dcxr, HQ555/30, set lot C-104285), while the sections stained for AP activity with the fast red substrate used a TRITC filter (Chroma 49005ET). This step does not conflict with the filter's prior use to image the AC stain because the acidic condition of the TRAP protocol removes the fluorescent mineralization lines. All of the fluorescent images were recorded with a high-resolution monochromic digital camera (Zeiss AxioCam HRm) and pseudocolored. After all the fluorescent imaging was completed, the hematoxylin stained slides were imaged using the

Zeiss AxioCam MRc 5 color camera. The Mirax software creates an image stack for each filter setting. The stack of images for each staining set is merged as a flat file for a visual quality assessment before all files from each fluorescent imaging step are exported as a multilayered jpg file for image analysis.

**5.2.10 Statistics:** Data in the PYD and OC ELISA tests were logarithmically transformed and expressed as mean  $\pm$ SD. Difference between the mean PYD and OC values were evaluated between treatment groups at week 0, week 2 (SRT treatment), week 4 (MSC injection), week 8 and week 12 (Sacrifice) using a repeated measures ANOVA. Statistical significance for comparison of means between time points was calculated using the pair-wise T-test. Mean tumor necrosis, microCT, bone volume and quantitative histological analysis for each group is expressed as mean  $\pm$ SD and were evaluated for statistical significance using a one-way ANOVA. Statistical significance for comparison of means of each group was calculated using Tukey HSD and Bonferroni post-hoc analysis. The differences were considered significant at P values less than 0.05. The IBM SPSS software was used for all statistical analysis.

## 5.3 Results

**5.3.1 Tumor Development (Weeks 0-2):** In all groups, the tumor lesions showed clear radiographic progression of the tumor at weeks 1 and 2 (Figure 29). Luciferase imaging was observed in all animals after OSA cell inoculation up to SRT treatment (Week 2). Significant

increases ( $p < 0.05$ ) in PYD over baseline levels were observed up to SRT treatment (Figure 30). Tumors development was observed in 100% of rats.

**5.3.2 Response to SRT (Weeks 2-4):** After SRT, tumor lesions became stable radiographically in all groups as compared to untreated rats in Aim 1 (Figure 29). Luciferase levels were completely inhibited and PYD levels significantly decreased ( $p < 0.05$ ) after SRT to baseline levels (Figure 30).

**5.3.3 Response to MSCs (Weeks 4-12):** Radiographic evidence of new bone formation in the IV or IO or SRT only groups was not observed throughout the duration of the experiment (Figure 29). Luciferase recurrence was observed in a limited number of animals at the end of the experiment as follows: SRT Only ( $n=1$ , 12.5%, Week 6), IO ( $n = 2$ , 25%, Week 5, 6) and IV ( $n = 3$ , 37.5%, Week 6, 7, 8). There were no differences in PYD levels between the IO and IV MSC groups and the SRT only control group after MSC injections at week 4 or at the end of the experiment (Figure 30,  $p < 0.19$ ). Osteocalcin levels in the IO and IV groups remained consistent with the SRT only animals after MSC injections. No differences in osteocalcin levels were observed throughout the experiment overall or between groups, even after MSC injection at week 4 (Figure 31). Osteocalcin values averaged approximately 14 ng/mL, which is comparable to normal levels (17 ng/mL) previously observed in rats of similar age (16).

#### 5.3.4 Histology

**Alkaline Phosphatase is decreased in rats treated with SRT.** Alkaline Phosphatase (AP) is a marker of osteoblast-mediated bone formation. In Figure 34, AP is indicated by red staining and cell nuclei are indicated by the blue staining (DAPI) in the histological section of each group. Staining reveals decreased AP expression in the SRT only, IV and IO groups compared to the control femur and indicates limited or no osteoblast activity bone growth in these groups. Quantitative image analysis (Figure 38 & Table 4) further indicates approximately 50-fold decrease in AP activity in all SRT treated groups compared with the control femur.

**Calcium formation is decreased in rats treated with SRT.** Alizarin staining has been widely used as a marker of new bone formation as it stains calcium. In this study, rats were injected with alizarin two days before sacrifice. Using a fluorescent microscope, alizarin staining was visualized by the red color as shown in Figure 35. Levels in each treatment group are greatly decreased as compared to the normal bone indicating there is no new calcium formation present in these animals. Quantitative image analysis (Figure 38 & Table 4) further indicates a five-fold decrease in Alizarin activity in all SRT treated groups compared with the control femur.

**GFP imaging in rat femurs:** GFP expressing MSCs were injected IV or IO at week 4 into the distal femur of these rats. GFP expression in harvested tissues at sacrifice were evaluated to identify donor MSCs as well as any direct MSC mediated bone formation in the femurs. As shown in Figure 34, expression of GFP was not observed in the IO or IV MSC groups

compared to the SRT only group. These results indicate that there were no viable GFP MSCs present in the femurs or they had lost their ability to express GFP.

**Osteoclast activity is decreased in rats treated with SRT.** TRAP staining is used as a marker of osteoclast activity (161). Using a fluorescent microscope, TRAP staining was visualized as shown in Figure 36. Osteoclast activity was decreased in all SRT treated groups as compared to the normal bone indicating there is little or no active bone resorption present. Quantitative image analysis (Figure 38 & Table 4) further indicates approximately 50-fold decrease in TRAP activity in all SRT treated groups compared with the control femur.

**Percent tumor necrosis.** Mean percent tumor necrosis at the end of the experiment in each group was as follows in each group: 96% SRT Only, 82% IO and 50% IV (Figure 33). The mean overall percent tumor necrosis was 76% (Range: SRT only, 90-99%, IO, 55-99% IV, 10-95%). There was a significant increase in percent tumor necrosis in the SRT only group (95%) compared to the IV group (50%) ( $p < 0.040$ ). Histology revealed large areas of necrosis and sclerosis indicated by areas of cells lacking nuclei (Figure 37). Areas indicative of viable tumor consist of areas of randomly oriented confluent nuclei, which are consistent with osteoid development. Although viable tumor was found, they do not appear to be progressing in size. This is likely due to radiation damage that did not necessarily kill the cells but prevented them from replicating.

**Micro CT reveals no increase in bone volume between groups:** After sacrifice at week 10 and before histology, microCT was performed on the femurs to determine differences in bone

volume between groups. Bone volume was normalized by selecting three equal regions of interest around the tumor and calculating the mean bone volume within those regions. Detailed methods describing the normalization can be found in Appendix D. As shown in Figure 32, no differences in volume were observed between the SRT only, IO and IV groups. These results indicate there was no increase in bone volume following the administration of IV or IO MSCs.

## 5.4 Figures

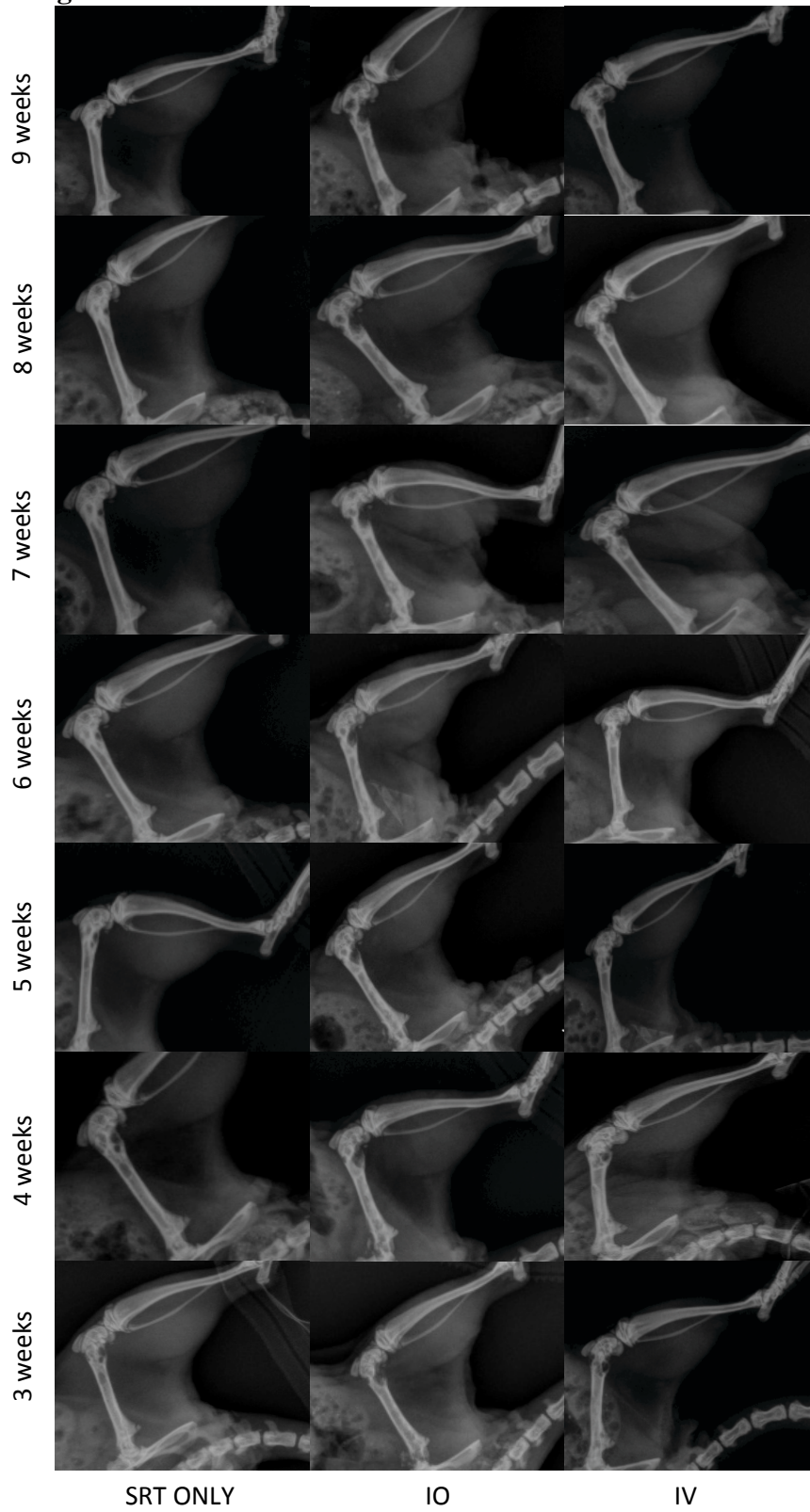
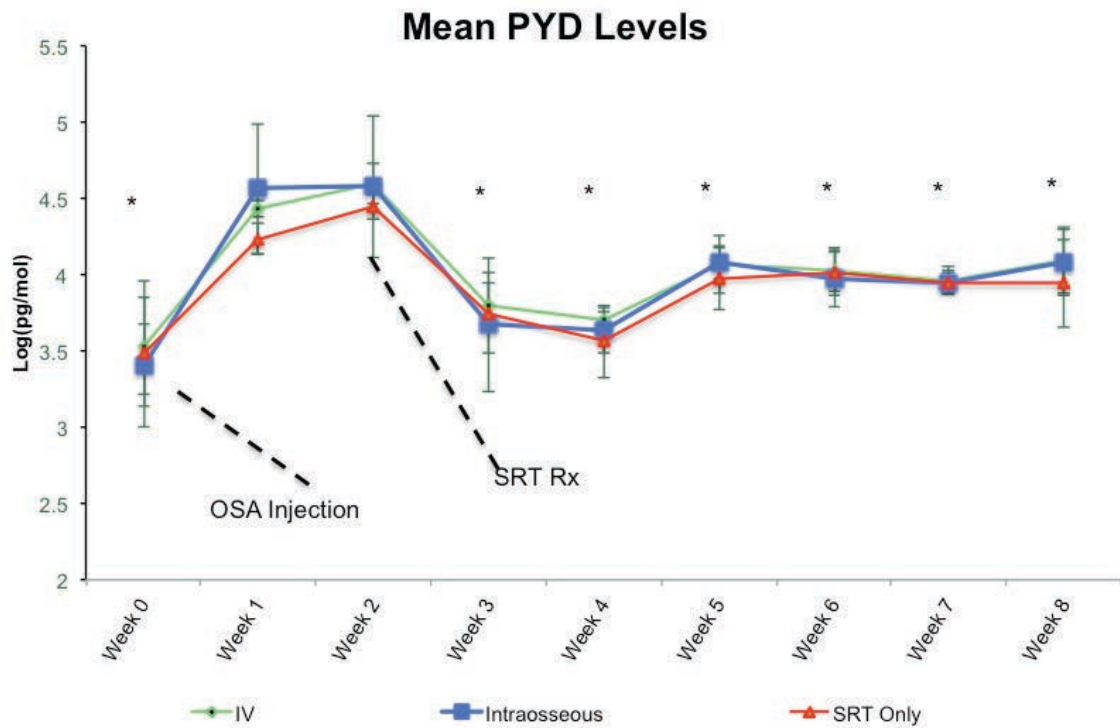
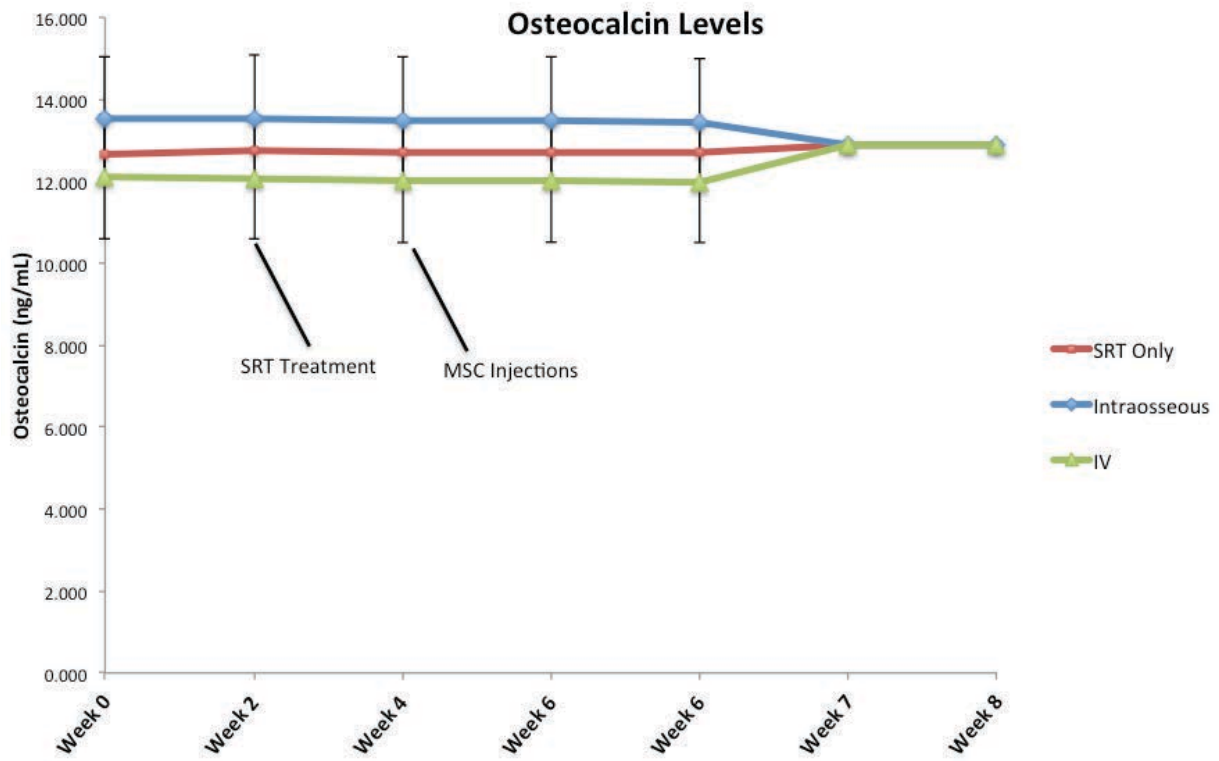


Figure 29: Representative radiographs in the SRT only, IO and IV groups.



**Figure 30: Mean PYD levels between groups. Data was log transformed to allow for easy interpretation. PYD levels significantly increased ( $p < 0.05$ ) after tumor induction (Weeks 1 & 2) and then significantly decreased within 1 week after SRT administration (Week 3) ( $p < 0.05$ ) and remained at these levels for the duration of the experiment (Weeks 4-8). Injection of MSCs showed no increase in PYD levels throughout the remainder of the experiment.**



**Figure 31: Osteocalcin levels between groups. There were no statistical differences between groups even after MSC injection**

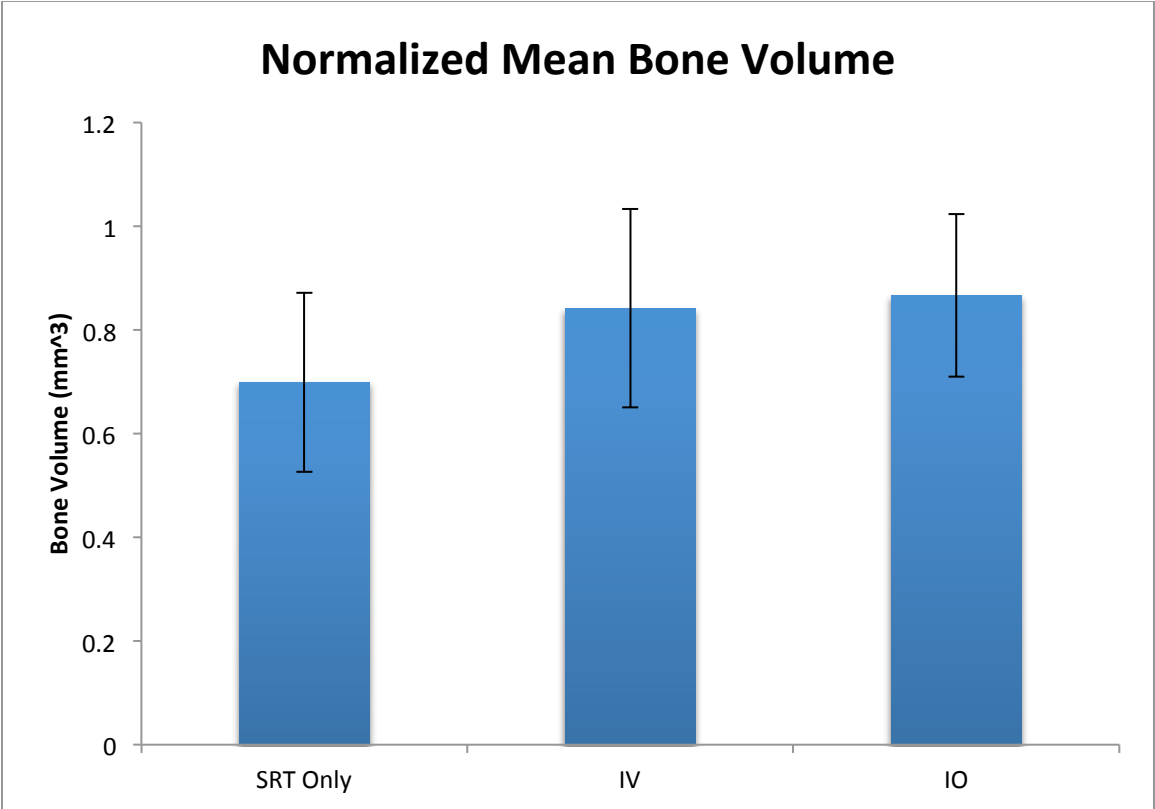


**Figure 32: Normalized bone volume between groups as measured by microCT. No differences in bone volume were observed between SRT Only (Mean: 0.69 +/- 0.17), IV (Mean: 0.84 +/- 0.19) or IO (Mean: 0.86 +/- 0.15).**

## Percent Tumor Necrosis

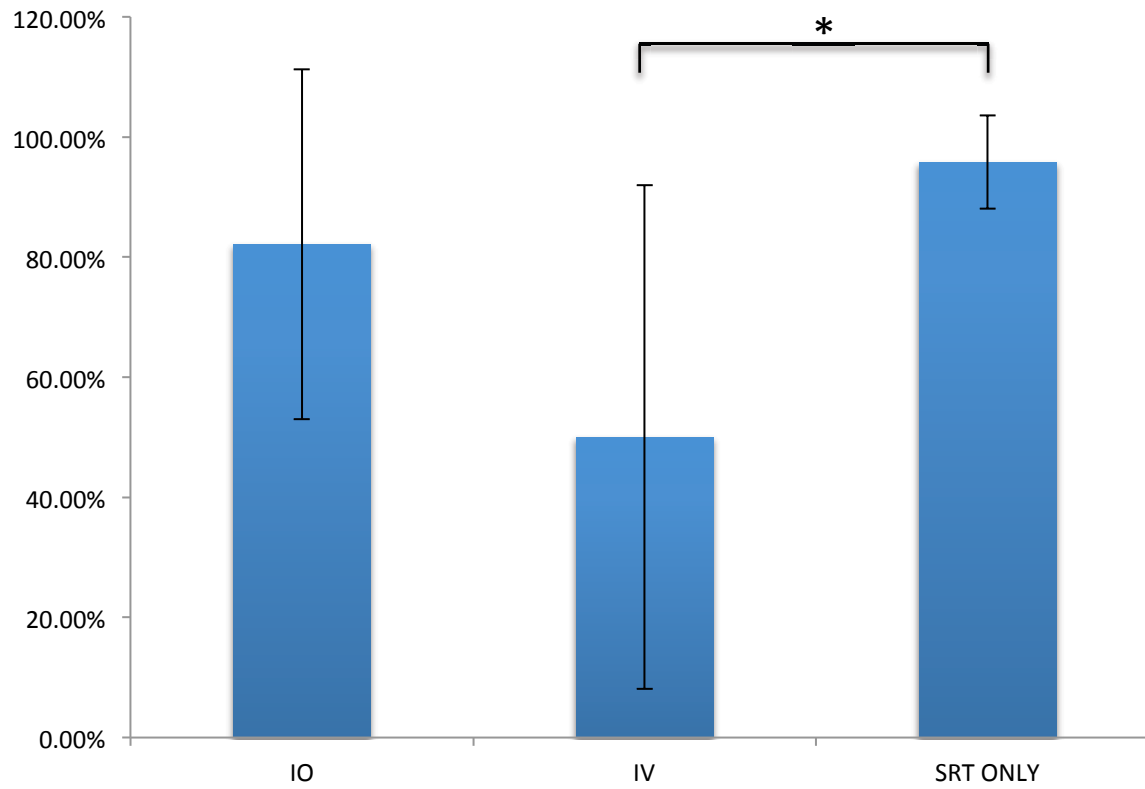


**Figure 33: Percent tumor necrosis between groups. The IV group has significantly less tumor necrosis than the SRT only group ( $p < 0.05$ ).**

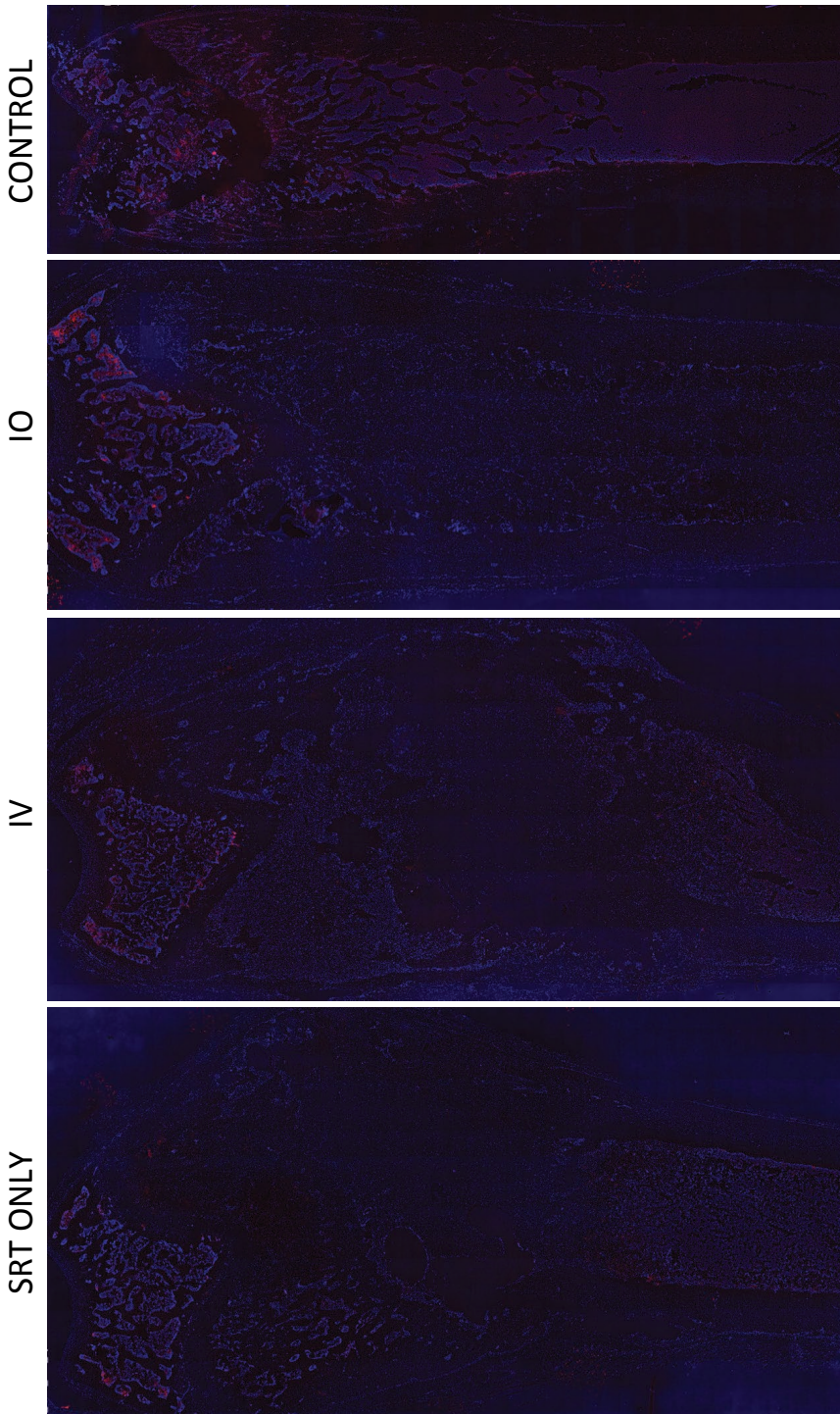
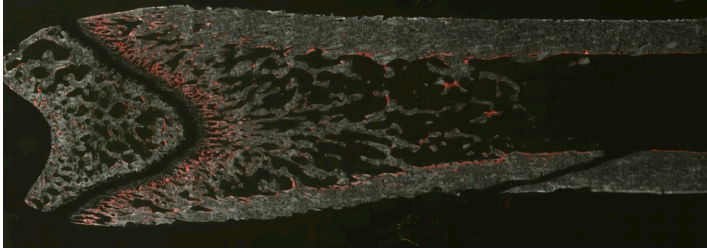
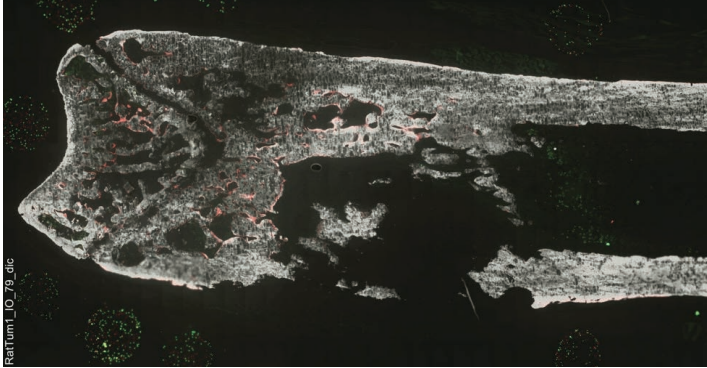


**Figure 34: Fluorescent staining of cell nuclei, AP and GFP of histological sections in each group. Cell nuclei are indicated by blue (DAPI Staining), AK by red and GFP by green coloring. AK expression is decreased in all SRT treated groups indicating there are no active osteoblasts even after MSC implantation. Furthermore, no GFP expression is observed indicating there are no MSCs present in these treatment groups.**

CONTROL



IO



IV



SRT ONLY



**Figure 35: Representative alizarin staining of histological sections in each group. The red coloring indicates the presence of alizarin or calcium formation. Alizarin expression is greatly decreased in the treated animals when compared to the normal bone. These observations indicate little, if any, calcium formation is present in any of the treatment groups.**

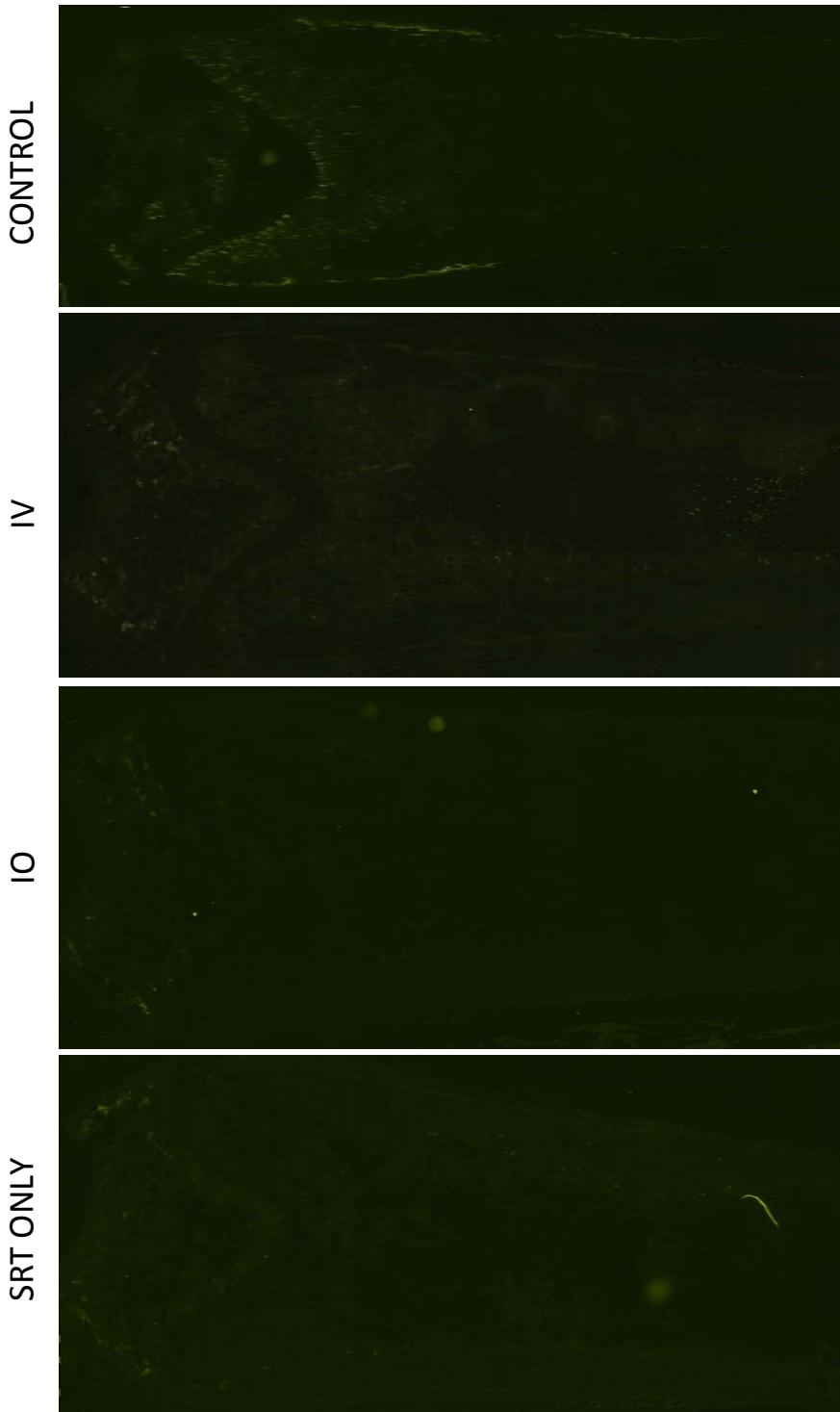


**Figure 36: Representative fluorescent TRAP staining of osteoclasts in each group. Yellow coloring indicates viable osteoclast activity. Visually, only small amounts of TRAP expression is observed in any of the SRT treated groups as compared to the normal bone indicating there is very little osteoclast activity**

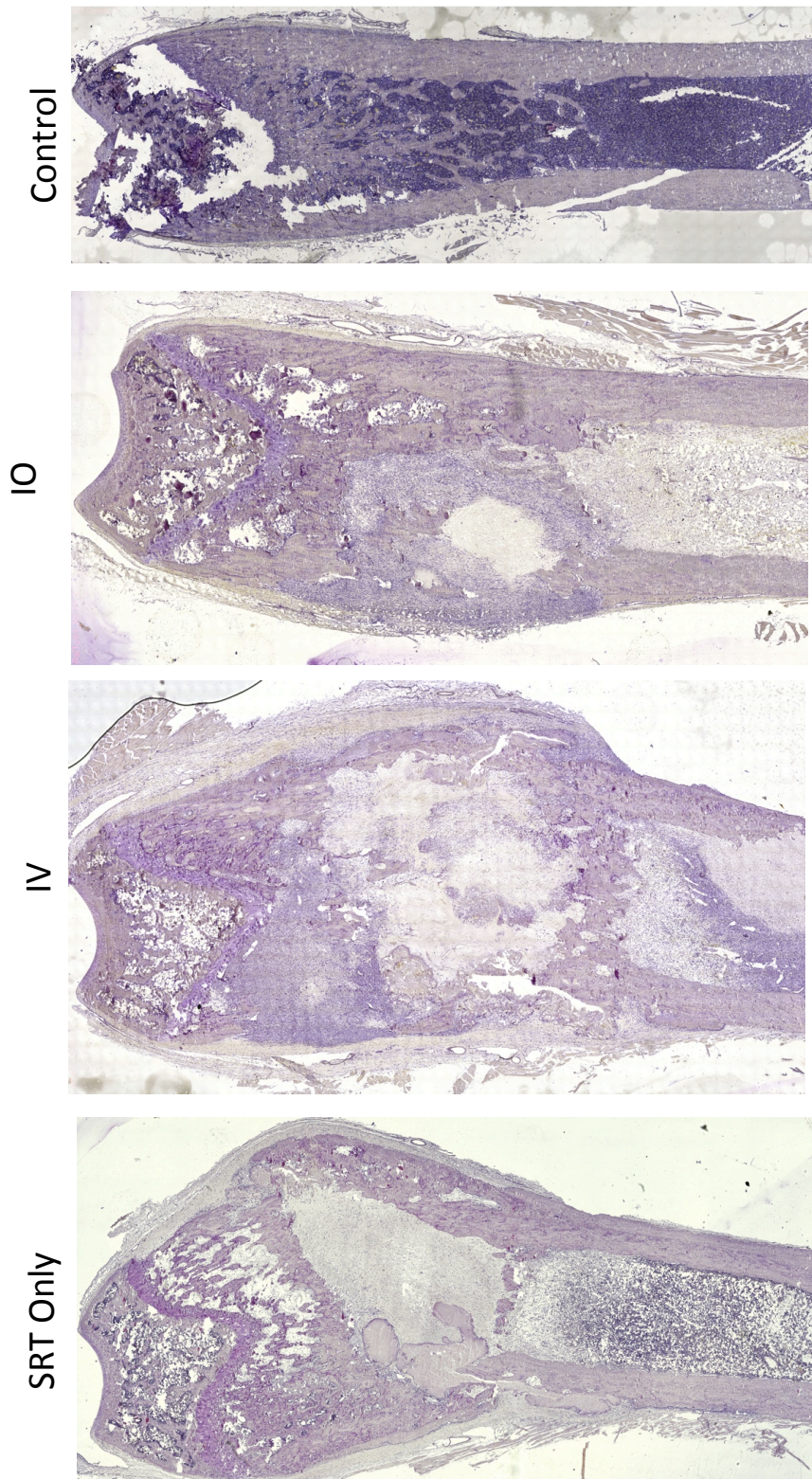


**Figure 37: Representative histological (Hematoxylin staining) of each group to document percent tumor necrosis. Histology indicates large areas of tumor necrosis, marrow necrosis and osteosclerosis as compared to the normal bone.**

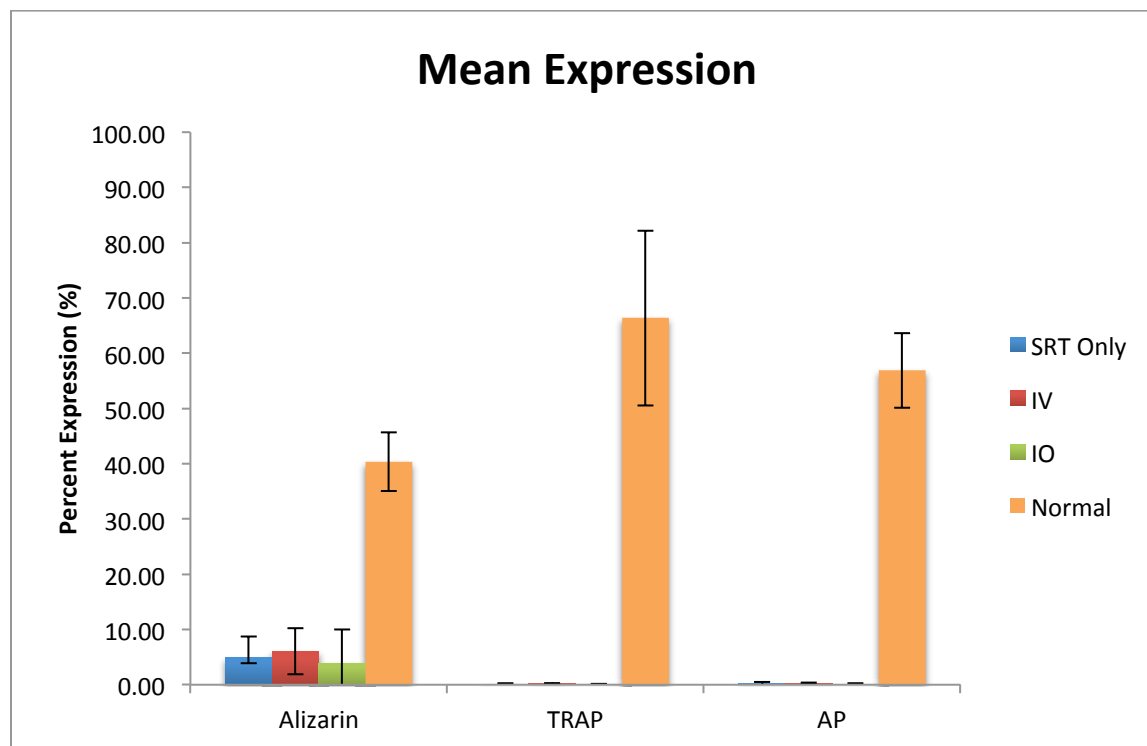


Figure 38: Percent expression of Alizarin, TRAP and Alkaline Phosphatase (AP) in the tumor area. No differences between the IV, IO and SRT only groups were observed.

Table 4: Percent expression of Alizarin, TRAP and Alkaline Phosphatase (AP) in the tumor area.

Group	Alizarin %	TRAP %	Alkaline Phosphatase %
SRT Only	4.89±3.29	0.12 ± 0.16	1.13 ± 0.28
IV	6.04±4.16	0.21 ± 0.11	0.17 ± 0.18
IO	3.92±3.80	0.07 ± 0.07	0.21 ± 0.28
Normal	40.38± 5.32	66.38± 15.84	56.88 ± 6.75

## 5.4 Discussion

Mesenchymal stem cells are multipotent adult stem that have been shown to home to damaged tissues, promote angiogenesis and regenerate bone (71, 89, 90). The ability of MSCs to promote these regenerative capabilities indicates that they may be useful in a variety of tissue engineering and regenerative therapies. In relevance to this thesis, studies have shown MSC's can migrate directly to radiation-injured bone and can promote osteogenesis (100-102). Although these studies show MSCs can migrate to injured bone and increase markers of bone formation, there are currently no *in vivo* studies assessing MSC bone generation after the use of SRT for the treatment of OSA. In this present study, we used SRT to ablate OSA in the orthotopic rat model previously described herein and evaluated the ability of allogeneic adipose derived MSCs to regenerate bone after SRT.

Currently, studies assessing the use of MSCs for tissue recovery after radiation are limited and utilize low doses of radiation to non-tumor bearing animals. One such study in mice consisted of administering total body irradiation (3.5 Gy total) and then intravenously injecting MSCs 24 hours after treatment. Animals treated with radiation had a high homing rate of MSCs to the bone marrow and muscle. Untreated animals showed little or no MSC engraftment to these tissues. This study suggests the potential of systemically injected MSCs to migrate to radiation-injured tissues (162). In another study using a femoral defect model, rat allografts received a single radiation dose of 60 Gy, treated with MSCs and transplanted back into the heterotopic location (102). Femur segments receiving MSCs showed increased alkaline phosphatase and osteocalcin activity compared to control femurs indicating the possibility that MSCs can rescue bone after irradiation.

In our model, we injected GFP expressing MSCs intraosseously (IO) into the medullary canal of the tumor-bearing limb or intravenously (IV) into the tail vein two weeks after SRT. We hypothesized that the IO MSCs would directly engraft in the femur while the IV MSCs would migrate to the femur and result in increased bone growth. Injecting MSCs immediately after SRT could potentially lead to tumor promotion, as the tumor cells may still be viable. We sacrificed the animals six weeks after MSC implantation to allow for adequate time for MSC engraftment and new bone generation. Unlike models previously discussed which showed increased markers of bone formation after irradiation, we showed no increases in osteocalcin or alkaline phosphatase in either the IO or IV MSC treated groups. Other studies showed homing of MSCs to the irradiated bone; however, our MSCs failed to show engraftment via GFP histological analysis. We also measured bone volume with microCT, PYD and osteoclasts levels (TRAP staining), which indicated no increases in bone volume or bone resorption after MSC injection.

It is well recognized that radiation can cause detrimental alterations not only to the physical bone properties, but also to the osteogenic progenitor cells, blood vessels and inflammatory responses, which are critical for normal bone growth and repair as well as MSC homing and engraftment (71, 81). Previous rodent models demonstrating the homing and osteogenic potential of MSCs after radiation are limited to low dose treatments (between 1 and 5 Gy) (100, 162). In our model, we administered a much larger dose of 3 fractions of 12 Gy (BED = 159 Gy). The large dose in our studies may have more adversely affected the inflammatory and cellular responses involved in MSC homing as well as bone repair. Low dose radiation has been shown to initially increase inflammatory markers and then subside within several days. This short inflammatory period may allow MSCs to home to the site of inflammation and promote

regenerative processes in low dose radiation models. However, in larger dose per fraction protocols as administered in this study, inflammatory markers have been shown to persist at high levels for up to 26 weeks (76). It has been shown that less than 12.5% of MSCs injected systematically actually reach bones irradiated with one fraction of 26.5 Gy (162). Furthermore, another study in bone after irradiation using a single dose of 30 Gy revealed decreased MSC viability from 70% at 2 hours to less than 40% a week after IO MSC injection (163). Although the inflammatory processes may allow for the homing of MSCs, the excessive production of inflammatory mediators may have had deleterious affect on the viability of MSCs. Our high dose radiation model also showed large areas of sclerosis, necrosis, as well as necrotic bone marrow resulting in an environment where normal dynamic bone remodeling is not occurring. Vascular ischemia, fibrosis and injury of irradiated tissue induced by large doses of irradiation in this study could be hindering the ability of MSCs to survive in this environment to the lack of vital nutrients and oxygen from the blood (164). Further studies are needed to assess the viability of MSCs after high dose radiation immediately following implantation as well as several weeks afterward.

Although GFP expressing cells can help track the migration and engraftment of MSCs, we evaluated bone volume, TRAP, alizarin, and alkaline phosphatase expression and to further confirm the lack of bone repair with MSCs. Again, no differences were observed between any of the groups. There were significant decreases between a normal control bone and the expression of TRAP, Alizarin and alkaline phosphatase in the SRT only, IO and IV groups. These significant decreases observed in these markers of bone formation indicate that the large dose of radiation is inhibiting all normal and reparative processes regardless of whether the animals

received MSCs. The normal tissue tolerance of bone is approximately 20 Gy. The BED in this study far exceeds this threshold thus further confirming the lack of bone repair in the MSC groups and clearly shows the adverse effects (osteosclerosis, marrow necrosis, lacking Alizarin and AP expression) to bone in a high dose model as compared to lower dose models in which alkaline phosphatase and alizarin levels were elevated after MSC injection (89, 90).

The secondary aim of this study was to determine whether allogeneic MSCs administered by either IO or IV enhanced tumor progression or recurrence after treatment with SRT. Several studies have shown that MSCs can home to existing tumors and promote tumor growth at local and distant metastatic sites (101, 152). Therefore, if SRT did not effectively achieve local tumor control, then the use of MSCs could potentially promote the growth and progression of OSA. Percent tumor necrosis and luciferase expression were used as an indirect measure of the tumor viability and compared between groups. The SRT only group had the highest percent tumor necrosis of 95.8 percent with one recurrence in luciferase expression, which was comparable to similar studies in Chapter 3. There were no differences between the SRT only and the IO group. Interestingly, there was a significant difference in tumor necrosis between the SRT only and the IV group. Luciferase expression also recurred in three animals in the IV group. Although the data suggests the IV group had a higher percentage of viable tumors, the high variability of tumor necrosis and limited number of animals make it difficult to make an accurate conclusion as to whether this finding is directly attributed to the MSCs. Furthermore, the lack of GFP expressing cells in the tumor regions indicates the MSCs were not present at the time of sacrifice. However, it is possible that MSCs may have secreted other tumor promoting factors (e.g. chemokines, cytokines and growth factors) at an earlier time point that consequently

resulted in decreased tumor necrosis in the IV group (153). Further investigation is needed to elucidate this possibility. It is also feasible that the irradiated environment hindered MSCs survival thus blocking their ability to secrete tumor-promoting factors and hindering their ability to promote tumor growth. Evaluation of distant lesions after MSC injection by gross observation revealed no metastases in the lungs or adjacent bones. Previous studies have shown MSCs can increase progression of distant OSA metastases using a highly metastatic OSA cell line (152). The use of a highly metastatic cell line may better evaluate role of MSCs in local and distant tumor progression when using SRT as a primary means of local tumor control.

A limitation of this study is that SRT was administered to the entire femur rather than just the tumor lesion. Irradiating the entire bone was required due to the small size of the rat femur and the limitations of the linear accelerator. In clinical canine OSA cases, the tumor lesion is irradiated with acceptable margins to the normal bone. The remaining bone is spared from irradiation, thus leaving a source of osteogenic progenitor cells, marrow and vascularity immediately adjoining the irradiated bone. It is unlikely that local tumor control can be achieved at total radiation doses in the 20-25 Gy range to permit sparing of the normal bone immediately surrounding the tumor. For successful MSC engraftment and osteogenic differentiation, a healthy vascular supply, physical microenvironment, growth factors and cytokines are required. The adverse effects of high dose radiation administered to the entire bone in this study are consequently causing bone marrow necrosis as observed in the histology. These effects are likely limiting the viability of systematically injected and IO MSCs to promote new bone growth (165). A study previously discussed administered radiation doses as high as 60 Gy and showed increases in bone formation markers; however, this was a femoral defect model where only 5mm

of the implanted femur had been irradiated and submerged with MSCs (102). Limiting the radiation field with SRT to the tumor with acceptable margins rather than the entire bone may provide a better environment for MSC engraftment. This would also increase the recruitment of host osteoprogenitor cells from the surrounding normal bone as well as vascular ingrowth that would result in new bone formation at the site of irradiation. Optimizing SRT to ablate the tumor region or using SRT in a partial section of normal bone in a larger rabbit or sheep animal model would help to further evaluate this hypothesis.

Another limitation is that this study used undifferentiated MSCs and it's unclear what percentage of these cells could potentially differentiate into osteoblasts. There are a number of studies that suggest that priming MSCs towards a specific lineage (e.g. osteoblasts or chondrocytes) before implantation may promote more bone growth than MSCs in their native state (166, 167). Thus, priming MSCs before implantation in this SRT model may promote bone growth over undifferentiated MSCs. A recent study showed that chondrogenic priming of MSCs resulted in more bone repair and regeneration than osteogenic priming (168). Unlike osteoblasts, which induce bone growth through intramembranous ossification, chondrocytes can induce bone growth through endochondral ossification. This process carried is out in a low oxygen and avascular environment similar to that of a bone after radiation therapy. Therefore, chondrogenically primed MSCs could be advantageous in irradiated bone over osteogenically primed or undifferentiated MSCs due to their ability to promote bone formation in areas of low oxygen and vasculature (169).

With consideration for future studies evaluating the potential role of MSCs for bone regeneration in SRT treated tumor affected bone, SRT will first have to be optimized to target the tumor lesion itself while sparing as much normal bone as possible. Leaving the remaining normal bone relatively unaffected from the radiation will then allow the evaluation of bone promoting strategies after SRT. The administration of MSCs may then be able to home to the affected bone and induce bone growth. Repeated administration of MSCs may also help further enhance this effect. Predifferentiating MSCs, particularly down the chondrogenic lineage, could potentially promote more bone formation in irradiated areas. Furthermore, genetically modifying MSCs to express bone promoting genes or in combinations with growth factors, parathyroid hormone and bone promoting biomaterials may further deem efficacious. The addition of bisphosphonates, which inhibit tumor associated bone resorption as well as drugs that can reduce the dose needed to achieve tumor control could further benefit bone formation strategies. These future directions can then be translated into clinical canine cases and ultimately into humans.

In summary, we evaluated the ability of MSCs to regenerate bone growth after SRT as well as the possibility that MSCs will promote tumor growth. Our results indicate that there was no new bone formation in the IV or IO MSC treatment groups when compared to the control group (SRT only). Lack of new bone formation is most likely due to the effects of high dose radiation creating an unfavorable environment for survival and differentiation of administered allogeneic MSCs.

## **Chapter 6: Summary of Findings and Future Directions**

Chapter 2 was devoted to the development an orthotopic rat model of canine osteosarcoma. We hypothesized that canine OSA cells injected into the tibias and femurs of rats would engraft and exhibit predictable progression. As expected, tumors engrafted in both locations, predictably progressed and exhibited similar characteristics to clinical cases. These data supported our hypothesis and described the first rat model of orthotopically located canine OSA that can be used for the evaluation of clinically relevant therapeutics for the treatments for this devastating disease.

Chapter 3 described the development of techniques to deliver SRT to a femur as well as its effectiveness in achieving acceptable percent tumor necrosis in the OSA model described in Chapter 2. We hypothesized that SRT could be successfully administered to a rat and would result in an increase of percent tumor necrosis. Different total dose and fractionation protocols were administered to OSA lesions in rats and tumor necrosis as well as acute effects was evaluated. Administration of SRT was feasible and three fractions of 12 Gy was determined to be the optimal protocol to achieve greater than 80% tumor necrosis while minimizing the acute radiation effects. These data supported our hypothesis and described the first use of SRT in a rat model. Furthermore, it resulted in a viable dosing and fractionation protocol that achieved increased tumor necrosis that could be clinically relevant to clinical cases of OSA.

In Chapter 4, mesenchymal stem cells were isolated from the bone marrow and adipose tissue from GFP expressing rats. We hypothesized that these MSCs would exhibit multipotency when subjected to differentiation media as well as GFP expression. Cells were confirmed to

differentiate into adipocytes, chondrocytes and osteoblasts as well as to express GFP thus confirming our hypothesis. The establishment of this GFP expressing MSC cell line allowed for the visualization of these MSCs in histological analysis when evaluating the bone forming potential of MSCs.

Chapter 5 evaluated the ability of intravenously or systemically injected MSCs to regenerate bone after SRT of OSA in the rat model described herein. We hypothesized that MSCs would induce new bone growth and no new bone growth would be observed in animals that did not receive MSCs. The results indicated that MSCs did not regenerate new bone growth most likely due to the adverse effects of high dose radiation on the entire bone. Although the results did not support our hypothesis, this experiment described the first use of MSCs for bone generation following SRT in an OSA model. These results provided a great deal of information including potential modification of SRT protocols in future experiments, which could permit MSCs to promote bone generation following SRT.

With consideration for future studies evaluating the potential role of MSCs for bone regeneration in SRT treated tumor affected bone, SRT will first have to be optimized to target the tumor lesion itself while sparing as much normal bone as possible. Leaving the remaining normal bone relatively unaffected from the radiation can allow for the recovery of MSCs in the untreated areas of bone. This will also help preserve vasculature, host cells (osteoblasts, osteoclasts, progenitor cells, etc) and structural integrity of the existing bone. The preservation of the unaffected bone may allow MSCs to encounter a better environment and subsequently induce bone growth. Repeated administration (e.g. daily or weekly injections) of MSCs may also help

further enhance this effect. As previously discussed, predifferentiating or sorting MSCs that express osteogenic markers, particularly down the chondrogenic lineage, could potentially promote more bone formation in irradiated areas. The chondrogenic lineage could lead to endochondral bone growth, which is a vital process in bone healing. Furthermore, genetically modifying MSCs to express bone promoting genes or in combinations with growth factors, parathyroid hormone and bone promoting biomaterials may further deem efficacious. The addition of bisphosphonates, which inhibit tumor associated bone resorption as well as drugs that can reduce the dose needed to achieve tumor control could further benefit bone formation strategies. Any use of MSCs alone or in combination any of the methods described above in a tumor environment would need to be thoroughly evaluated for safety to ensure the treatment is not promoting tumor growth or recurrence. A positive outcome in these future experiments could potentially be translated into new bone healing therapies for canine OSA and humans.

## References

1. Liptak JM, Dernell WS, Ehrhart N, Withrow SJ. Canine appendicular osteosarcoma: Diagnosis and palliative treatment. *Comp Cont Educ Pract.* 2004 Mar;26(3):172-+.
2. Mueller F, Fuchs B, Kaser-Hotz B. Comparative biology of human and canine osteosarcoma. *Anticancer Res.* 2007 Jan-Feb;27(1A):155-64.
3. Priester WA, Mantel N. Occurrence of tumors in domestic animals. Data from 12 United States and Canadian colleges of veterinary medicine. *J Natl Cancer Inst.* 1971 Dec;47(6):1333-44.
4. Withrow SJ. Limb Sparing Trials and Canine Osteosarcoma. *Genes, Dogs and Cancer: 3rd Annual Canine Cancer.* 2003.
5. Dernell WS, Straw, R.C., Withrow, S.J. *Tumors of the skeletal system: WB Saunders Co;* 2001.
6. Levine RA, Fleischli MA. Inactivation of p53 and retinoblastoma family pathways in canine osteosarcoma cell lines. *Vet Pathol.* 2000 Jan;37(1):54-61.
7. van Leeuwen IS, Cornelisse CJ, Misdorp W, Goedegebuure SA, Kirpensteijn J, Rutteman GR. P53 gene mutations in osteosarcomas in the dog. *Cancer Lett.* 1997 Jan 1;111(1-2):173-8.
8. Gillette SM, Gillette EL, Powers BE, Withrow SJ. Radiation-induced osteosarcoma in dogs after external beam or intraoperative radiation therapy. *Cancer research.* 1990 Jan 1;50(1):54-7.
9. McEntee MC, Page RL, Theon A, Erb HN, Thrall DE. Malignant tumor formation in dogs previously irradiated for acanthomatous epulis. *Veterinary radiology & ultrasound : the official journal of the American College of Veterinary Radiology and the International Veterinary Radiology Association.* 2004 Jul-Aug;45(4):357-61.
10. Sinibaldi K, Rosen H, Liu SK, DeAngelis M. Tumors associated with metallic implants in animals. *Clin Orthop Relat Res.* 1976 Jul-Aug(118):257-66.

11. Ottaviani G, Jaffe N. The epidemiology of osteosarcoma. *Cancer Treat Res.* 2009;152:3-13.
12. Khanna C, Wan X, Bose S, Cassaday R, Olomu O, Mendoza A, et al. The membrane-cytoskeleton linker ezrin is necessary for osteosarcoma metastasis. *Nat Med.* 2004 Feb;10(2):182-6.
13. Berg J. Canine osteosarcoma: amputation and chemotherapy. *Vet Clin North Am Small Anim Pract.* 1996 Jan;26(1):111-21.
14. Boston SE, Duerr F, Bacon N, Larue S, Ehrhart EJ, Withrow S. Intraoperative radiation for limb sparing of the distal aspect of the radius without transcarpal plating in five dogs. *Vet Surg.* 2007 Jun;36(4):314-23.
15. Jankowski MK, Steyn PF, Lana SE, Dernell WS, Blom CM, Uhrig JL, et al. Nuclear scanning with 99mTc-HDP for the initial evaluation of osseous metastasis in canine osteosarcoma. *Vet Comp Oncol.* 2003 Sep;1(3):152-8.
16. Hillers KR, Dernell WS, Lafferty MH, Withrow SJ, Lana SE. Incidence and prognostic importance of lymph node metastases in dogs with appendicular osteosarcoma: 228 cases (1986-2003). *Journal of the American Veterinary Medical Association.* 2005 Apr 15;226(8):1364-7.
17. Martin JW, Zielenska M, Stein GS, van Wijnen AJ, Squire JA. The Role of RUNX2 in Osteosarcoma Oncogenesis. *Sarcoma.* 2011;2011:282745.
18. Society AC. What are the key statistics about osteosarcoma? 2010; Available from: <http://www.cancer.org/Cancer/Osteosarcoma/DetailedGuide/osteosarcoma-key-statistics>.
19. Kansara M, Thomas DM. Molecular pathogenesis of osteosarcoma. *DNA Cell Biol.* 2007 Jan;26(1):1-18.
20. Kurzman ID, MacEwen EG, Rosenthal RC, Fox LE, Keller ET, Helfand SC, et al. Adjuvant therapy for osteosarcoma in dogs: results of randomized clinical trials using combined liposome-encapsulated muramyl tripeptide and cisplatin. *Clin Cancer Res.* 1995 Dec;1(12):1595-601.
21. Green EM, Adams WM, Forrest LJ. Four fraction palliative radiotherapy for osteosarcoma in 24 dogs. *J Am Anim Hosp Assoc.* 2002 Sep-Oct;38(5):445-51.

22. Knapp-Hoch HM, Fidel JL, Sellon RK, Gavin PR. An expedited palliative radiation protocol for lytic or proliferative lesions of appendicular bone in dogs. *Journal of the American Animal Hospital Association*. 2009 Jan-Feb;45(1):24-32.
23. Park C, Papiez L, Zhang S, Story M, Timmerman RD. Universal survival curve and single fraction equivalent dose: useful tools in understanding potency of ablative radiotherapy. *Int J Radiat Oncol Biol Phys*. 2008 Mar 1;70(3):847-52.
24. Fan TM, de LLP, O'Dell-Anderson K, Lacoste HI, Charney SC. Single-agent pamidronate for palliative therapy of canine appendicular osteosarcoma bone pain. *Journal of veterinary internal medicine / American College of Veterinary Internal Medicine*. [Research Support, Non-U.S. Gov't]. 2007 May-Jun;21(3):431-9.
25. Fan TM, de LLP, Garrett LD, Lacoste HI. The bone biologic effects of zoledronate in healthy dogs and dogs with malignant osteolysis. *Journal of veterinary internal medicine / American College of Veterinary Internal Medicine*. [Comparative Study]. 2008 Mar-Apr;22(2):380-7.
26. Fan TM, Charney SC, de LLP, Garrett LD, Griffon DJ, Gordon-Evans WJ, et al. Double-blind placebo-controlled trial of adjuvant pamidronate with palliative radiotherapy and intravenous doxorubicin for canine appendicular osteosarcoma bone pain. *Journal of veterinary internal medicine / American College of Veterinary Internal Medicine*. 2009 Jan-Feb;23(1):152-60.
27. Ramirez O, 3rd, Dodge RK, Page RL, Price GS, Hauck ML, LaDue TA, et al. Palliative radiotherapy of appendicular osteosarcoma in 95 dogs. *Vet Radiol Ultrasound*. 1999 Sep-Oct;40(5):517-22.
28. Spodnick GJ, Berg J, Rand WM, Schelling SH, Couto G, Harvey HJ, et al. Prognosis for dogs with appendicular osteosarcoma treated by amputation alone: 162 cases (1978-1988). *Journal of the American Veterinary Medical Association*. 1992 Apr 1;200(7):995-9.
29. Mauldin GN, Matus RE, Withrow SJ, Patnaik AK. Canine osteosarcoma. Treatment by amputation versus amputation and adjuvant chemotherapy using doxorubicin and cisplatin. *Journal of veterinary internal medicine / American College of Veterinary Internal Medicine*. 1988 Oct-Dec;2(4):177-80.
30. Kirpensteijn J, van dBR, Endenburg N. Adaptation of dogs to the amputation of a limb and their owners' satisfaction with the procedure. *Vet Rec*. 1999 Jan 30;144(5):115-8.

31. LaRue SM, Withrow SJ, Powers BE, Wrigley RH, Gillette EL, Schwarz PD, et al. Limb-sparing treatment for osteosarcoma in dogs. *Journal of the American Veterinary Medical Association*. [Research Support, U.S. Gov't, P.H.S.]. 1989 Dec 15;195(12):1734-44.
32. Straw RC, Withrow SJ. Limb-sparing surgery versus amputation for dogs with bone tumors. *Vet Clin North Am Small Anim Pract*. 1996 Jan;26(1):135-43.
33. Liptak JM, Dernell WS, Ehrhart N, Lafferty MH, Monteith GJ, Withrow SJ. Cortical allograft and endoprosthesis for limb-sparing surgery in dogs with distal radial osteosarcoma: a prospective clinical comparison of two different limb-sparing techniques. *Veterinary surgery : VS : the official journal of the American College of Veterinary Surgeons*. 2006 Aug;35(6):518-33.
34. Liptak JM, Pluhar GE, Dernell WS, Withrow SJ. Limb-sparing surgery in a dog with osteosarcoma of the proximal femur. *Veterinary surgery : VS : the official journal of the American College of Veterinary Surgeons*. [Case Reports]. 2005 Jan-Feb;34(1):71-7.
35. Morello E, Buracco P, Martano M, Peirone B, Capurro C, Valazza A, et al. Bone allografts and adjuvant cisplatin for the treatment of canine appendicular osteosarcoma in 18 dogs. *J Small Anim Pract*. 2001 Feb;42(2):61-6.
36. Lascelles BD, Dernell WS, Correa MT, Lafferty M, Devitt CM, Kuntz CA, et al. Improved survival associated with postoperative wound infection in dogs treated with limb-salvage surgery for osteosarcoma. *Ann Surg Oncol*. [Research Support, N.I.H., Extramural]. 2005 Dec;12(12):1073-83.
37. Jeys LM, Grimer RJ, Carter SR, Tillman RM, Abudu A. Post operative infection and increased survival in osteosarcoma patients: are they associated? *Ann Surg Oncol*. 2007 Oct;14(10):2887-95.
38. Saam DE, Liptak JM, Stalker MJ, Chun R. Predictors of outcome in dogs treated with adjuvant carboplatin for appendicular osteosarcoma: 65 cases (1996-2006). *J Am Vet Med Assoc*. 2011 Jan 15;238(2):195-206.
39. Knox RJ, Friedlos F, Lydall DA, Roberts JJ. Mechanism of cytotoxicity of anticancer platinum drugs: evidence that cis-diamminedichloroplatinum(II) and cis-diammine-(1,1-cyclobutanedicarboxylato)platinum(II) differ only in the kinetics of their interaction with DNA. *Cancer Res*. 1986 Apr;46(4 Pt 2):1972-9.

40. W. Culp FO-P, C. Aldridge, S. Withrow, M. Lafferty, Ehrhart aN, editors. Retrospective evaluation of dogs living greater than 1 year after diagnosis with osteosarcoma. Annual VCS Conference; 2009.
41. Fidler IJ, Schroit AJ. Recognition and destruction of neoplastic cells by activated macrophages: discrimination of altered self. *Biochim Biophys Acta*. 1988 Nov 15;948(2):151-73.
42. MacEwen EG, Kurzman ID, Rosenthal RC, Smith BW, Manley PA, Roush JK, et al. Therapy for osteosarcoma in dogs with intravenous injection of liposome-encapsulated muramyl tripeptide. *J Natl Cancer Inst*. 1989 Jun 21;81(12):935-8.
43. Beck JC, Wara WM, Bovill EG, Jr., Phillips TL. The role of radiation therapy in the treatment of osteosarcoma. *Radiology*. 1976 Jul;120(1):163-5.
44. Oertel S, Blattmann C, Rieken S, Jensen A, Combs SE, Huber PE, et al. Radiotherapy in the treatment of primary osteosarcoma--a single center experience. *Tumori*. 2010 Jul-Aug;96(4):582-8.
45. Weichselbaum RR, Epstein J, Little JB, Kornblith P. Inherent cellular radiosensitivity of human tumors of varying clinical curability. *AJR Am J Roentgenol*. 1976 Dec;127(6):1027-32.
46. DeLaney TF, Park L, Goldberg SI, Hug EB, Liebsch NJ, Munzenrider JE, et al. Radiotherapy for local control of osteosarcoma. *Int J Radiat Oncol Biol Phys*. 2005 Feb 1;61(2):492-8.
47. Walter CU, Dernell WS, LaRue SM, Lana SE, Lafferty MH, LaDue TA, et al. Curative-intent radiation therapy as a treatment modality for appendicular and axial osteosarcoma: a preliminary retrospective evaluation of 14 dogs with the disease. *Vet Comp Oncol*. 2005 Mar;3(1):1-7.
48. Liptak JM, Dernell WS, Lascelles BD, Larue SM, Jameson VJ, Powers BE, et al. Intraoperative extracorporeal irradiation for limb sparing in 13 dogs. *Veterinary surgery : VS : the official journal of the American College of Veterinary Surgeons*. [Evaluation Studies]. 2004 Sep-Oct;33(5):446-56.
49. Willett CG, Czito BG, Tyler DS. Intraoperative radiation therapy. *J Clin Oncol*. 2007 Mar 10;25(8):971-7.

50. Dincbas FO, Koca S, Mandel NM, Hiz M, Dervisoglu S, Secmezacar H, et al. The role of preoperative radiotherapy in nonmetastatic high-grade osteosarcoma of the extremities for limb-sparing surgery. *International journal of radiation oncology, biology, physics*. 2005 Jul 1;62(3):820-8.
51. Caceres E, Zaharia M. Massive preoperative radiation therapy in the treatment of osteogenic sarcoma. *Cancer*. 1972 Sep;30(3):634-8.
52. Machak GN, Tkachev SI, Solovyev YN, Sinyukov PA, Ivanov SM, Kochergina NV, et al. Neoadjuvant chemotherapy and local radiotherapy for high-grade osteosarcoma of the extremities. *Mayo Clin Proc. [Research Support, Non-U.S. Gov't]*. 2003 Feb;78(2):147-55.
53. Caceres E, Zaharia M, Valdivia S, Misad O, de IFJ, Tejada F, et al. Local control of osteogenic sarcoma by radiation and chemotherapy. *International journal of radiation oncology, biology, physics*. 1984 Jan;10(1):35-9.
54. Paul Okenieff SS, Yuhchyaw Chen. *Intraoperative Irradiation: Techniques and Results*. . Totowa: Human Press; 1999.
55. Hall EJ. *Radiobiology for the Radiologist* 5th ed: Lippincott Williams & Wilkins; 2000.
56. Soisson ET, Tome WA, Richards GM, Mehta MP. Comparison of linac based fractionated stereotactic radiotherapy and tomotherapy treatment plans for skull-base tumors. *Radiother Oncol*. 2006 Mar;78(3):313-21.
57. Fitzpatrick CL, Farese JP, Milner RJ, Salute ME, Rajon DA, Morris CG, et al. Intrinsic radiosensitivity and repair of sublethal radiation-induced damage in canine osteosarcoma cell lines. *Am J Vet Res*. 2008 Sep;69(9):1197-202.
58. Levine AM, Coleman C, Horasek S. Stereotactic radiosurgery for the treatment of primary sarcomas and sarcoma metastases of the spine. *Neurosurgery*. 2009 Feb;64(2 Suppl):A54-9.
59. Kepka L, DeLaney TF, Suit HD, Goldberg SI. Results of radiation therapy for unresected soft-tissue sarcomas. *Int J Radiat Oncol Biol Phys*. 2005 Nov 1;63(3):852-9.

60. Farese JP, Milner R, Thompson MS, Lester N, Cooke K, Fox L, et al. Stereotactic radiosurgery for treatment of osteosarcomas involving the distal portions of the limbs in dogs. *J Am Vet Med Assoc.* 2004 Nov 15;225(10):1567-72, 48.
61. Douple EB, Richmond RC, O'Hara JA, Coughlin CT. Carboplatin as a potentiator of radiation therapy. *Cancer Treatment Reviews.* 1985;12(Supplement 1):111-24.
62. Yang LX, Douple EB, O'Hara JA, Wang HJ. Production of DNA double-strand breaks by interactions between carboplatin and radiation: a potential mechanism for radiopotentialiation. *Radiat Res.* 1995 Sep;143(3):309-15.
63. Ryan SD. Stereotactic Radiosurgery for Treatment of Extremity Osteosarcoma. In: Meeting IMC, editor. Boston, MA2009.
64. Karsenty G, Wagner EF. Reaching a genetic and molecular understanding of skeletal development. *Dev Cell.* 2002 Apr;2(4):389-406.
65. Caetano-Lopes J, Canhao H, Fonseca JE. Osteoblasts and bone formation. *Acta Reumatol Port.* 2007 Apr-Jun;32(2):103-10.
66. Hoehn ENMK. *Human Anatomy & Physiology*: Benjamin-Cummings Pub Co; 2008.
67. Street J, Bao M, deGuzman L, Bunting S, Peale FV, Jr., Ferrara N, et al. Vascular endothelial growth factor stimulates bone repair by promoting angiogenesis and bone turnover. *Proc Natl Acad Sci U S A.* 2002 Jul 23;99(15):9656-61.
68. Schindeler A, McDonald MM, Bokko P, Little DG. Bone remodeling during fracture repair: The cellular picture. *Semin Cell Dev Biol.* 2008 Oct;19(5):459-66.
69. Bolander ME. Regulation of fracture repair by growth factors. *Proc Soc Exp Biol Med.* 1992 Jun;200(2):165-70.
70. Hopewell JW. Radiation-therapy effects on bone density. *Med Pediatr Oncol.* 2003 Sep;41(3):208-11.
71. Cao X, Wu X, Frassica D, Yu B, Pang L, Xian L, et al. Irradiation induces bone injury by damaging bone marrow microenvironment for stem cells. *Proc Natl Acad Sci U S A.* 2011 Jan 10.

72. Soejima T, Hirota S, Tsujino K, Yoden E, Fujii O, Ichimiya Y, et al. Total body irradiation followed by bone marrow transplantation: comparison of once-daily and twice-daily fractionation regimens. *Radiat Med.* 2007 Oct;25(8):402-6.
73. Dudziak ME, Saadeh PB, Mehrara BJ, Steinbrech DS, Greenwald JA, Gittes GK, et al. The effects of ionizing radiation on osteoblast-like cells in vitro. *Plast Reconstr Surg.* 2000 Oct;106(5):1049-61.
74. Takahashi S, Sugimoto M, Kotoura Y, Yamamuro T, Oka M, Shibamoto Y, et al. Incorporation of cortical bone autografts following intraoperative extracorporeal irradiation in rabbits. *International journal of radiation oncology, biology, physics.* [Comparative Study]. 1991 Oct;21(5):1221-30.
75. Jegoux F, Malard O, Goyenvalle E, Aguado E, Daculsi G. Radiation effects on bone healing and reconstruction: interpretation of the literature. *Oral Surg Oral Med Oral Pathol Oral Radiol Endod.* 2010 Feb;109(2):173-84.
76. Denham JW, Hauer-Jensen M. The radiotherapeutic injury--a complex 'wound'. *Radiother Oncol.* 2002 May;63(2):129-45.
77. Boston SE, Bacon NJ, Culp WT, Bhandal J, Bruce C, Cavanaugh RP, et al. Outcome after repair of a sarcoma-related pathologic fracture in dogs: a veterinary society of surgical oncology retrospective study. *Veterinary surgery : VS.* 2011 Jun;40(4):431-7.
78. Bottcher P, Krastel D, Hierholzer J, Westphalen K, Florian S, Hildebrandt G, et al. Percutaneous cementoplasty in the palliative, multimodal treatment of primary bone tumors of the distal aspect of the radius in four dogs. *Veterinary surgery : VS.* [Case Reports]. 2009 Oct;38(7):888-901.
79. Krempien R, Huber PE, Harms W, Treiber M, Wannemacher M, Krempien B. Combination of early bisphosphonate administration and irradiation leads to improved remineralization and restabilization of osteolytic bone metastases in an animal tumor model. *Cancer.* [Research Support, Non-U.S. Gov't]. 2003 Sep 15;98(6):1318-24.
80. Yamamoto M, Takahashi Y, Tabata Y. Controlled release by biodegradable hydrogels enhances the ectopic bone formation of bone morphogenetic protein. *Biomaterials.* 2003 Nov;24(24):4375-83.

81. Ehrhart NP, Hong L, Morgan AL, Eurell JA, Jamison RD. Effect of transforming growth factor-beta1 on bone regeneration in critical-sized bone defects after irradiation of host tissues. *Am J Vet Res.* 2005 Jun;66(6):1039-45.
82. Springer IN, Niehoff P, Acil Y, Marget M, Lange A, Warnke PH, et al. BMP-2 and bFGF in an irradiated bone model. *J Craniomaxillofac Surg.* [Research Support, Non-U.S. Gov't]. 2008 Jun;36(4):210-7.
83. Bentzen SM, Thames HD, Overgaard M. Latent-time estimation for late cutaneous and subcutaneous radiation reactions in a single-follow-up clinical study. *Radiother Oncol.* 1989 Jul;15(3):267-74.
84. Bentzen SM. Preventing or reducing late side effects of radiation therapy: radiobiology meets molecular pathology. *Nat Rev Cancer.* 2006 Sep;6(9):702-13.
85. Powers BE GE, McChesney SL, LeCouteur RA, and Withrow SJ. Bone necrosis and tumor induction following experimental intraoperative irradiation. *Int J Radiat Oncol Biol Phys.* 1989;17:559-67.
86. Milano MT, Constine LS, Okunieff P. Normal tissue toxicity after small field hypofractionated stereotactic body radiation. *Radiat Oncol.* 2008;3:36.
87. Kolf CM, Cho E, Tuan RS. Mesenchymal stromal cells. Biology of adult mesenchymal stem cells: regulation of niche, self-renewal and differentiation. *Arthritis Res Ther.* 2007;9(1):204.
88. Bianco P, Robey PG, Simmons PJ. Mesenchymal stem cells: revisiting history, concepts, and assays. *Cell Stem Cell.* 2008 Apr 10;2(4):313-9.
89. Breitbart EA, Meade S, Azad V, Yeh S, Al-Zube L, Lee YS, et al. Mesenchymal stem cells accelerate bone allograft incorporation in the presence of diabetes mellitus. *J Orthop Res.* 2010 Jul;28(7):942-9.
90. Granero-Molto F, Weis JA, Miga MI, Landis B, Myers TJ, O'Rear L, et al. Regenerative effects of transplanted mesenchymal stem cells in fracture healing. *Stem Cells.* 2009 Aug;27(8):1887-98.

91. Nather A, David V, Teng JW, Lee CW, Pereira BP. Effect of autologous mesenchymal stem cells on biological healing of allografts in critical-sized tibial defects simulated in adult rabbits. *Ann Acad Med Singapore*. 2010 Aug;39(8):599-606.
92. Enneking WF, Campanacci DA. Retrieved human allografts : a clinicopathological study. *J Bone Joint Surg Am*. 2001 Jul;83-A(7):971-86.
93. Cheung WH, Chin WC, Wei FY, Li G, Leung KS. Applications of Exogenous Mesenchymal Stem Cells and Low Intensity Pulsed Ultrasound Enhance Fracture Healing in Rat Model. *Ultrasound Med Biol*. 2012 Oct 10.
94. Scotti C, Tonnarelli B, Papadimitropoulos A, Scherberich A, Schaeren S, Schauerte A, et al. Recapitulation of endochondral bone formation using human adult mesenchymal stem cells as a paradigm for developmental engineering. *Proc Natl Acad Sci U S A*. 2010 Apr 20;107(16):7251-6.
95. Albrektsson T, Johansson C. Osteoinduction, osteoconduction and osseointegration. *Eur Spine J*. 2001 Oct;10 Suppl 2:S96-101.
96. Phinney DG, Prockop DJ. Concise review: mesenchymal stem/multipotent stromal cells: the state of transdifferentiation and modes of tissue repair--current views. *Stem Cells*. 2007 Nov;25(11):2896-902.
97. Jones E, Yang X. Mesenchymal stem cells and bone regeneration: current status. *Injury*. 2011 Jun;42(6):562-8.
98. Moore ST, Katz JM, Zhukauskas RM, Hernandez RM, Lewis CS, Supronowicz PR, et al. Osteoconductivity and osteoinductivity of Puros(R) DBM putty. *J Biomater Appl*. 2011 Aug;26(2):151-71.
99. Lind M, Overgaard S, Nguyen T, Ongpipattanakul B, Bunger C, Soballe K. Transforming growth factor-beta stimulates bone ongrowth. Hydroxyapatite-coated implants studied in dogs. *Acta Orthop Scand*. 1996 Dec;67(6):611-6.
100. Mouiseddine M, Francois S, Semont A, Sache A, Allenet B, Mathieu N, et al. Human mesenchymal stem cells home specifically to radiation-injured tissues in a non-obese diabetes/severe combined immunodeficiency mouse model. *Br J Radiol*. 2007 Sep;80 Spec No 1:S49-55.

101. Klopp AH, Spaeth EL, Dembinski JL, Woodward WA, Munshi A, Meyn RE, et al. Tumor irradiation increases the recruitment of circulating mesenchymal stem cells into the tumor microenvironment. *Cancer Res.* 2007 Dec 15;67(24):11687-95.
102. Tohma Y, Ohgushi H, Morishita T, Dohi Y, Tadokoro M, Tanaka Y, et al. Bone marrow-derived mesenchymal cells can rescue osteogenic capacity of devitalized autologous bone. *J Tissue Eng Regen Med.* [Research Support, Non-U.S. Gov't]. 2008 Jan;2(1):61-8.
103. Mauch P, Constine L, Greenberger J, Knospe W, Sullivan J, Liesveld JL, et al. Hematopoietic stem cell compartment: acute and late effects of radiation therapy and chemotherapy. *Int J Radiat Oncol Biol Phys.* 1995 Mar 30;31(5):1319-39.
104. Greenberger JS, Epperly M. Bone marrow-derived stem cells and radiation response. *Semin Radiat Oncol.* 2009 Apr;19(2):133-9.
105. Hung SC, Deng WP, Yang WK, Liu RS, Lee CC, Su TC, et al. Mesenchymal stem cell targeting of microscopic tumors and tumor stroma development monitored by noninvasive in vivo positron emission tomography imaging. *Clin Cancer Res.* 2005 Nov 1;11(21):7749-56.
106. Bian ZY, Fan QM, Li G, Xu WT, Tang TT. Human mesenchymal stem cells promote growth of osteosarcoma: involvement of interleukin-6 in the interaction between human mesenchymal stem cells and Saos-2. *Cancer Sci.* 2010 Dec;101(12):2554-60.
107. Killion JJ, Radinsky R, Fidler IJ. Orthotopic models are necessary to predict therapy of transplantable tumors in mice. *Cancer Metastasis Rev.* 1998;17(3):279-84.
108. Nieves MA, Vahle J, Ackermann M, Howard M, Dietz AB, Carpenter SL, et al. Production and characterization of canine osteosarcoma cell lines that induce transplantable tumors in nude mice. *Am J Vet Res.* [Research Support, Non-U.S. Gov't]. 1998 Mar;59(3):359-62.
109. Yu Z, Sun H, Fan Q, Long H, Yang T, Ma B. Establishment of reproducible osteosarcoma rat model using orthotopic implantation technique. *Oncology reports.* [Research Support, Non-U.S. Gov't]. 2009 May;21(5):1175-80.
110. Coomer AR, Farese JP, Milner R, Taylor D, Salute ME, Rajon DA, et al. Development of an intramuscular xenograft model of canine osteosarcoma in mice for evaluation of the effects of radiation therapy. *Am J Vet Res.* [Research Support, Non-U.S. Gov't]. 2009 Jan;70(1):127-33.

111. Fan F, Wood KV. Bioluminescent assays for high-throughput screening. *Assay Drug Dev Technol.* 2007 Feb;5(1):127-36.
112. Weilbaecher KN, Guise TA, McCauley LK. Cancer to bone: a fatal attraction. *Nat Rev Cancer.* 2011 Jun;11(6):411-25.
113. Allen MJ. Biochemical markers of bone metabolism in animals: uses and limitations. *Vet Clin Pathol.* [Review]. 2003;32(3):101-13.
114. Lucas PW, Fan TM, Garrett LD, Griffon DJ, Wypij JM. A comparison of five different bone resorption markers in osteosarcoma-bearing dogs, normal dogs, and dogs with orthopedic diseases. *Journal of veterinary internal medicine / American College of Veterinary Internal Medicine.* [Comparative Study]. 2008 Jul-Aug;22(4):1008-13.
115. Lacoste H, Fan TM, de Lorimier LP, Charney SC. Urine N-telopeptide excretion in dogs with appendicular osteosarcoma. *J Vet Intern Med.* 2006 Mar-Apr;20(2):335-41.
116. Wada N, Ishii S, Ikeda T, Kitajima M. Inhibition of bone metastasis from breast cancer with pamidronate resulting in reduction of urinary pyridinoline and deoxypyridinoline in a rat model. *Breast Cancer.* 2004;11(3):282-7.
117. O'Donoghue LE, Rivest JP, Duval DL. Polymerase chain reaction-based species verification and microsatellite analysis for canine cell line validation. *J Vet Diagn Invest.* 2011 Jul;23(4):780-5.
118. de Almeida PE, van Rappard JR, Wu JC. In vivo bioluminescence for tracking cell fate and function. *Am J Physiol Heart Circ Physiol.* 2011 Sep;301(3):H663-71.
119. Luker KE, Luker GD. Applications of bioluminescence imaging to antiviral research and therapy: multiple luciferase enzymes and quantitation. *Antiviral Res.* 2008 Jun;78(3):179-87.
120. Ferrari S, Zolezzi C, Pratelli L, Fasano MC, Bacci G. Urinary excretion of pyridinium cross-links and serum osteocalcin levels in patients with primary high-grade osteosarcoma. *Calcif Tissue Int.* 2003 Jul;73(1):1-4.
121. Taylor JM, Withers HR, Mason KA, Davis CA. Repopulation of mouse jejunal crypt cells. *Radiother Oncol.* 1991 Mar;20(3):181-90.

122. DeLaney TF, Park L, Goldberg SI, Hug EB, Liebsch NJ, Munzenrider JE, et al. Radiotherapy for local control of osteosarcoma. *International journal of radiation oncology, biology, physics*. 2005 Feb 1;61(2):492-8.
123. Ladue T, Klein MK. Toxicity criteria of the veterinary radiation therapy oncology group. *Veterinary radiology & ultrasound : the official journal of the American College of Veterinary Radiology and the International Veterinary Radiology Association*. 2001 Sep-Oct;42(5):475-6.
124. Powers BE, Withrow SJ, Thrall DE, Straw RC, LaRue SM, Page RL, et al. Percent tumor necrosis as a predictor of treatment response in canine osteosarcoma. *Cancer*. 1991 Jan 1;67(1):126-34.
125. Mueller F, Poirier V, Melzer K, Nitzl D, Roos M, Kaser-Hotz B. Palliative radiotherapy with electrons of appendicular osteosarcoma in 54 dogs. *In Vivo*. 2005 Jul-Aug;19(4):713-6.
126. Moriyama EH, Niedre MJ, Jarvi MT, Mocanu JD, Moriyama Y, Subarsky P, et al. The influence of hypoxia on bioluminescence in luciferase-transfected gliosarcoma tumor cells in vitro. *Photochem Photobiol Sci*. 2008 Jun;7(6):675-80.
127. Bruehlmeier M, Kaser-Hotz B, Achermann R, Bley CR, Wergin M, Schubiger PA, et al. Measurement of tumor hypoxia in spontaneous canine sarcomas. *Vet Radiol Ultrasound*. 2005 Jul-Aug;46(4):348-54.
128. Ayala AG, Raymond AK, Jaffe N. The pathologist's role in the diagnosis and treatment of osteosarcoma in children. *Hum Pathol*. 1984 Mar;15(3):258-66.
129. Baksh D, Song L, Tuan RS. Adult mesenchymal stem cells: characterization, differentiation, and application in cell and gene therapy. *J Cell Mol Med*. [Review]. 2004 Jul-Sep;8(3):301-16.
130. Reger RL, Tucker AH, Wolfe MR. Differentiation and characterization of human MSCs. *Methods Mol Biol*. 2008;449:93-107.
131. Bosnakovski D, Mizuno M, Kim G, Takagi S, Okumura M, Fujinaga T. Chondrogenic differentiation of bovine bone marrow mesenchymal stem cells (MSCs) in different hydrogels: influence of collagen type II extracellular matrix on MSC chondrogenesis. *Biotechnol Bioeng*. 2006 Apr 20;93(6):1152-63.

132. Datta N, Pham QP, Sharma U, Sikavitsas VI, Jansen JA, Mikos AG. In vitro generated extracellular matrix and fluid shear stress synergistically enhance 3D osteoblastic differentiation. *Proc Natl Acad Sci U S A*. 2006 Feb 21;103(8):2488-93.
133. Lennon DP, Caplan AI. Isolation of rat marrow-derived mesenchymal stem cells. *Exp Hematol*. 2006 Nov;34(11):1606-7.
134. Dominici M, Le Blanc K, Mueller I, Slaper-Cortenbach I, Marini F, Krause D, et al. Minimal criteria for defining multipotent mesenchymal stromal cells. The International Society for Cellular Therapy position statement. *Cytotherapy*. 2006;8(4):315-7.
135. Baum CM, Weissman IL, Tsukamoto AS, Buckle AM, Peault B. Isolation of a candidate human hematopoietic stem-cell population. *Proc Natl Acad Sci U S A*. 1992 Apr 1;89(7):2804-8.
136. P M, S H, R M, M G, W SK. Adult mesenchymal stem cells and cell surface characterization - a systematic review of the literature. *Open Orthop J*. 2011;5(Suppl 2):253-60.
137. Gronthos S, Franklin DM, Leddy HA, Robey PG, Storms RW, Gimble JM. Surface protein characterization of human adipose tissue-derived stromal cells. *J Cell Physiol*. 2001 Oct;189(1):54-63.
138. Arufe MC, De la Fuente A, Fuentes-Boquete I, De Toro FJ, Blanco FJ. Differentiation of synovial CD-105(+) human mesenchymal stem cells into chondrocyte-like cells through spheroid formation. *J Cell Biochem*. 2009 Sep 1;108(1):145-55.
139. Kern S, Eichler H, Stoeve J, Kluter H, Bieback K. Comparative analysis of mesenchymal stem cells from bone marrow, umbilical cord blood, or adipose tissue. *Stem Cells*. 2006 May;24(5):1294-301.
140. Wang X, Li F, Niyibizi C. Progenitors systemically transplanted into neonatal mice localize to areas of active bone formation in vivo: implications of cell therapy for skeletal diseases. *Stem cells*. 2006 Aug;24(8):1869-78.
141. Bunnell BA, Flaatt M, Gagliardi C, Patel B, Ripoll C. Adipose-derived stem cells: isolation, expansion and differentiation. *Methods*. 2008 Jun;45(2):115-20.

142. Arrigoni E, Lopa S, de GL, Stanco D, Brini AT. Isolation, characterization and osteogenic differentiation of adipose-derived stem cells: from small to large animal models. *Cell Tissue Res.* [Research Support, Non-U.S. Gov't]. 2009 Dec;338(3):401-11.
143. Inoue H, Ohsawa I, Murakami T, Kimura A, Hakamata Y, Sato Y, et al. Development of new inbred transgenic strains of rats with LacZ or GFP. *Biochem Biophys Res Commun.* [Research Support, Non-U.S. Gov't]. 2005 Apr 1;329(1):288-95.
144. Schorpp M, Jager R, Schellander K, Schenkel J, Wagner EF, Weiher H, et al. The human ubiquitin C promoter directs high ubiquitous expression of transgenes in mice. *Nucleic Acids Res.* 1996 May 1;24(9):1787-8.
145. Salasznyk RM, Williams WA, Boskey A, Batorsky A, Plopper GE. Adhesion to Vitronectin and Collagen I Promotes Osteogenic Differentiation of Human Mesenchymal Stem Cells. *J Biomed Biotechnol.* 2004;2004(1):24-34.
146. Phinney DG, Kopen G, Isaacson RL, Prockop DJ. Plastic adherent stromal cells from the bone marrow of commonly used strains of inbred mice: variations in yield, growth, and differentiation. *J Cell Biochem.* 1999 Mar 15;72(4):570-85.
147. Baddoo M, Hill K, Wilkinson R, Gaupp D, Hughes C, Kopen GC, et al. Characterization of mesenchymal stem cells isolated from murine bone marrow by negative selection. *J Cell Biochem.* 2003 Aug 15;89(6):1235-49.
148. Hao W, Pang L, Jiang M, Lv R, Xiong Z, Hu YY. Skeletal repair in rabbits using a novel biomimetic composite based on adipose-derived stem cells encapsulated in collagen I gel with PLGA-beta-TCP scaffold. *Journal of orthopaedic research : official publication of the Orthopaedic Research Society.* [Research Support, Non-U.S. Gov't]. 2010 Feb;28(2):252-7.
149. Tobita M, Orbay H, Mizuno H. Adipose-derived stem cells: current findings and future perspectives. *Discov Med.* 2011 Feb;11(57):160-70.
150. Yoon E, Dhar S, Chun DE, Gharibjanian NA, Evans GR. In vivo osteogenic potential of human adipose-derived stem cells/poly lactide-co-glycolic acid constructs for bone regeneration in a rat critical-sized calvarial defect model. *Tissue Eng.* [Research Support, Non-U.S. Gov't]. 2007 Mar;13(3):619-27.

151. Di BC, Farlie P, Penington AJ. Bone regeneration in a rabbit critical-sized skull defect using autologous adipose-derived cells. *Tissue Eng Part A*. [Research Support, Non-U.S. Gov't]. 2008 Apr;14(4):483-90.
152. Xu WT, Bian ZY, Fan QM, Li G, Tang TT. Human mesenchymal stem cells (hMSCs) target osteosarcoma and promote its growth and pulmonary metastasis. *Cancer Lett*. 2009 Aug 18;281(1):32-41.
153. Relf M, LeJeune S, Scott PA, Fox S, Smith K, Leek R, et al. Expression of the angiogenic factors vascular endothelial cell growth factor, acidic and basic fibroblast growth factor, tumor growth factor beta-1, platelet-derived endothelial cell growth factor, placenta growth factor, and pleiotrophin in human primary breast cancer and its relation to angiogenesis. *Cancer Res*. 1997 Mar 1;57(5):963-9.
154. Hoyte DA. Alizarin as an indicator of bone growth. *J Anat*. 1960 Jul;94:432-42.
155. Wenstrup RJ, Fowlkes JL, Witte DP, Florer JB. Discordant expression of osteoblast markers in MC3T3-E1 cells that synthesize a high turnover matrix. *J Biol Chem*. 1996 Apr 26;271(17):10271-6.
156. Golub EE, Harrison G, Taylor AG, Camper S, Shapiro IM. The role of alkaline phosphatase in cartilage mineralization. *Bone Miner*. 1992 May;17(2):273-8.
157. Hauschka PV, Lian JB, Cole DE, Gundberg CM. Osteocalcin and matrix Gla protein: vitamin K-dependent proteins in bone. *Physiol Rev*. 1989 Jul;69(3):990-1047.
158. Jiang X, Kalajzic Z, Maye P, Braut A, Bellizzi J, Mina M, et al. Histological analysis of GFP expression in murine bone. *J Histochem Cytochem*. 2005 May;53(5):593-602.
159. Filgueira L. Fluorescence-based staining for tartrate-resistant acidic phosphatase (TRAP) in osteoclasts combined with other fluorescent dyes and protocols. *J Histochem Cytochem*. 2004 Mar;52(3):411-4.
160. Cox WG, Singer VL. A high-resolution, fluorescence-based method for localization of endogenous alkaline phosphatase activity. *J Histochem Cytochem*. 1999 Nov;47(11):1443-56.

161. Hayman AR, Bune AJ, Bradley JR, Rashbass J, Cox TM. Osteoclastic tartrate-resistant acid phosphatase (Acp 5): its localization to dendritic cells and diverse murine tissues. *J Histochem Cytochem.* 2000 Feb;48(2):219-28.
162. François S, Bensidhoum M, Mouiseddine M, Mazurier C, Allenet B, Semont A, et al. Local Irradiation Not Only Induces Homing of Human Mesenchymal Stem Cells at Exposed Sites but Promotes Their Widespread Engraftment to Multiple Organs: A Study of Their Quantitative Distribution After Irradiation Damage. *STEM CELLS.* 2006;24(4):1020-9.
163. Phulpin B, Dolivet G, Marie PY, Poussier S, Huger S, Bravetti P, et al. Feasibility of treating irradiated bone with intramedullary delivered autologous mesenchymal stem cells. *J Biomed Biotechnol.* 2011;2011:560257.
164. Stone HB, Coleman CN, Anscher MS, McBride WH. Effects of radiation on normal tissue: consequences and mechanisms. *Lancet Oncol.* 2003 Sep;4(9):529-36.
165. Eifel PJ, Donaldson SS, Thomas PR. Response of growing bone to irradiation: a proposed late effects scoring system. *Int J Radiat Oncol Biol Phys.* 1995 Mar 30;31(5):1301-7.
166. Grayson WL, Bhumiratana S, Grace Chao PH, Hung CT, Vunjak-Novakovic G. Spatial regulation of human mesenchymal stem cell differentiation in engineered osteochondral constructs: effects of pre-differentiation, soluble factors and medium perfusion. *Osteoarthritis Cartilage.* 2010 May;18(5):714-23.
167. Delorme B, Ringe J, Pontikoglou C, Gaillard J, Langonne A, Sensebe L, et al. Specific lineage-priming of bone marrow mesenchymal stem cells provides the molecular framework for their plasticity. *Stem Cells.* 2009 May;27(5):1142-51.
168. Farrell E, Both SK, Odorfer KI, Koevoet W, Kops N, O'Brien FJ, et al. In-vivo generation of bone via endochondral ossification by in-vitro chondrogenic priming of adult human and rat mesenchymal stem cells. *BMC Musculoskelet Disord.* 2011;12:31.
169. Robins JC, Akeno N, Mukherjee A, Dalal RR, Aronow BJ, Koopman P, et al. Hypoxia induces chondrocyte-specific gene expression in mesenchymal cells in association with transcriptional activation of Sox9. *Bone.* 2005 Sep;37(3):313-22.

## Appendix A: Specific Aim 1 Detailed Protocols and Data

### 7.1 Cell culture of Abram's OSA CELLS

#### 1.0 Purpose:

To grow and propagate the Abram's osteosarcoma cell line in culture

#### 2.0 Scope:

Applies to the osteosarcoma rat model

#### 3.0 Responsibility:

3.1 It is the responsibility of the ACC MS Lab Director(s), study director or qualified personnel to ensure that personnel performing the allograft isolation procedure have received adequate training to perform the procedure.

#### 4.0 Reference Documents: N/A

#### 5.0 Definitions: N/A

#### 6.0 Safety Precautions:

6.1 Place sharps in appropriate medical waste containers after procedure and wear PPE for a BSL2 Lab

#### 7.0 Procedure:

##### 7.1 Materials

- 7.1.1 Pipettes
- 7.1.2 70% Ethanol
- 7.1.3 150 cm Cell culture flask
- 7.1.4 Sterile Gloves, mask, cap, and scrubs

##### Equipment

- 7.1.5 Culture hood, Incubator 5% CO<sub>2</sub>
- 7.1.6 Microscope

##### 7.2 Reagents

- 7.2.1 DMEM + 10% FBS Growth Media
- 7.2.2 Trypsin

##### 7.3 Working Reagent Preparation N/A

##### 7.4 (Test) Procedure

#### 2.2.12

- 7.4.1 Sterilize the hood, Warm media to 37 degrees for 15 minutes

- 7.4.2 Thaw the vial of OSA cells in 37 degrees for 5 minutes
- 7.4.3 Carefully pipette out the thawed OSA cells and place them into the cell culture flask
- 7.4.4 Add 15mL of media to the flask and place in the incubator overnight
- 7.4.5 During the next day, check the cells for adherence to the plate and monitor daily until cells become confluent
- 7.4.6 Split the cells by aspirating the existing media and adding 2 mLs of Trypsin to the place
- 7.4.7 Incubate for ~5 minutes until cells are detached and add ~8 mLs of culture media to the flask.
- 7.4.8 Distribute in 1 mL increments to additional flasks and add 14 mLs of media to each flask for a total volume of 15 mLs
- 7.4.9 Incubate until confluent and repeat 7.4.6 to continue cell culture

7.7 Reporting Results N/A

8.0 Attachments: N/A

## 7.2 Osteosarcoma Cell Injections into nude rats

### 1.0 Purpose:

To inoculate nude rats with the Abram's OSA cell line

### 2.0 Scope:

Applies to the the osteosarcoma rat model

### 3.0 Responsibility:

3.1 It is the responsibility of the ACC MS Lab Director(s), study director or qualified personnel to ensure that personnel performing the allograft isolation procedure have received adequate training to perform the procedure.

### 4.0 Reference Documents: N/A

### 5.0 Definitions: N/A

### 6.0 Safety Precautions:

6.1 Place sharps in appropriate medical waste containers after procedure and wear PPE for a BSL2 Lab

### 7.0 Procedure:

#### 7.1 Materials

- 7.1.1 24 G Needles
- 7.1.2 70% Ethanol & Betadine
- 7.1.3 Cultured Abram's OSA cells
- 7.1.4 5% Isofluroane
- 7.1.5 Sterile Gloves, mask, cap, and scrubs
- 7.1.6 Nude Rats

#### Equipment

- 4.1.1 Heating pad
- 4.1.2 Surgical Table

#### 4.2 Reagents

- 4.2.1 N/A

#### 4.3 Working Reagent Preparation N/A

#### 4.4 (Test) Procedure

### 2.2.13

- 4.4.1 Sterilize the surgical table
- 4.4.2 Prepare enough cells as outlined in the OSA culture SOP to inject  $1e^6$  Cells per rat in 50ul of media
- 4.4.3 Anesthetize the rat using 5% isoflurane induction chamber

- 4.4.4 Place the rat on the surgical table and clean the limb to be injected three times with ethanol and betadine
- 4.4.5 Insert a 22G needle into the femur at level of the trochantic fossa and advance distally within the medullary canal with a rotating motion to the distal metaphysis and then withdraw. This needle cannot be used for injection because it is clogged with a bone plug.
- 4.4.6 Insert a second 22G needle into the femur at level of the trochantic fossa and advance distally to the desired inoculation area. Attach a 10mL syringe filled with the OSA cells to the 22G needle inserted into the animal. Inject the cells very slowly to prevent embolism.
- 4.4.7 Once cells have been injected, remove the needle slowly and discard.
- 4.4.8 Return the rat to its cage and observe until it has recovered.
- 4.4.9 Repeat with the remaining rats

7.7 Reporting Results N/A

5.0 Attachments: N/A

## 7.3 PYD ELISA

### 1.0 Purpose:

To analyze the urine concentrations from rats

### 2.0 Scope:

Applies to the osteosarcoma rat model

### 3.0 Responsibility:

3.1 It is the responsibility of the ACC MS Lab Director(s), study director or qualified personnel to ensure that personnel performing the allograft isolation procedure have received adequate training to perform the procedure.

### 4.0 Reference Documents: N/A

### 5.0 Definitions: N/A

### 6.0 Safety Precautions:

6.1 Place sharps in appropriate medical waste containers after procedure and wear PPE for a BSL2 Lab

### 7.0 Procedure:

#### 7.1 Materials

- 7.1.1 Urine Samples
- 7.1.2 Quidel PYD Urine ELISA Kit
- 7.1.3 Pipettes, Tips, Multi-Channel Pipetter

#### Equipment

- 4.1.1 Plate Reader

#### 5.1 Reagents

- 5.1.1 PBS, ddH<sub>2</sub>O

#### 5.2 Working Reagent Preparation N/A

#### 5.3 (Test) Procedure

- 5.3.1 Dilute Standards and Controls 1:10 with Assay Buffer
- 5.3.2 Dilute urine samples 1:50 in assay buffer.
- 5.3.3 Remove coated strips from the pouch and place in the provided holding tray.
- 5.3.4 Label wells to identify samples
- 5.3.5 Add 50 µL diluted Standard, Control or sample to each well within 30 minutes.
- 5.3.6 Prepare Enzyme Conjugate within 2 hours of use by reconstituting the vial of Enzyme Conjugate with 7 mL of the assay buffer and keep cold until ready for use.
- 5.3.7 Add 100 µL of reconstituted Enzyme Conjugate to each well and cover with the cover strip.
- 5.3.8 Incubate for 3 hours at 2–8°C in the dark.

- 5.3.9 Prepare Working Substrate Solution within 1 hour of use by adding the Substrate Tablet into each required bottle. Allow 30–60 minutes for tablet(s) to dissolve. Vortex vigorously to mix.
  - 5.3.10 Prepare required amount of 1X wash buffer by diluting 10X wash buffer with ddH<sub>2</sub>O. Add 250  $\mu$ L of the wash buffer to each well and manually invert/empty strips to remove buffer. Repeat two more times for a total of three washes. Vigorously blot the strips dry on paper towels after the last wash. While strips are inverted, carefully wipe bottom of strips with a lint-free paper towel to ensure that the bottom of the strips are clean.
  - 5.3.11 Add 150  $\mu$ L of the working substrate solution to each well and incubate for 60 minutes.
  - 5.3.12 Add 100  $\mu$ L of stop solution to each well.
  - 5.3.13 Read the optical density at 405 nm within 15 minutes of adding the stop solution.
  - 5.3.14 The computer will calculate the concentrations and output them to an excel sheet.
- 7.7 Reporting Results N/A

6.0 Attachments: N/A

7.4 Orthotopic Radiographs Supplementary Data

2 Weeks Post-OSA



4 Weeks Post-OSA



1 Week Post-OSA



3 Weeks Post-OSA



128

2 Weeks Post-OSA



4 Weeks Post-OSA



1 Week Post-OSA



3 Weeks Post-OSA



129

1 Week Post-OSA



130

2 Weeks Post-OSA



3 Weeks Post-OSA



4 Weeks Post-OSA



131

1 Week Post-OSA



2 Weeks Post-OSA



168

3 Weeks Post-OSA



4 Weeks Post-OSA



1 Week Post-OSA



2 Weeks Post-OSA



132

3 Weeks Post-OSA

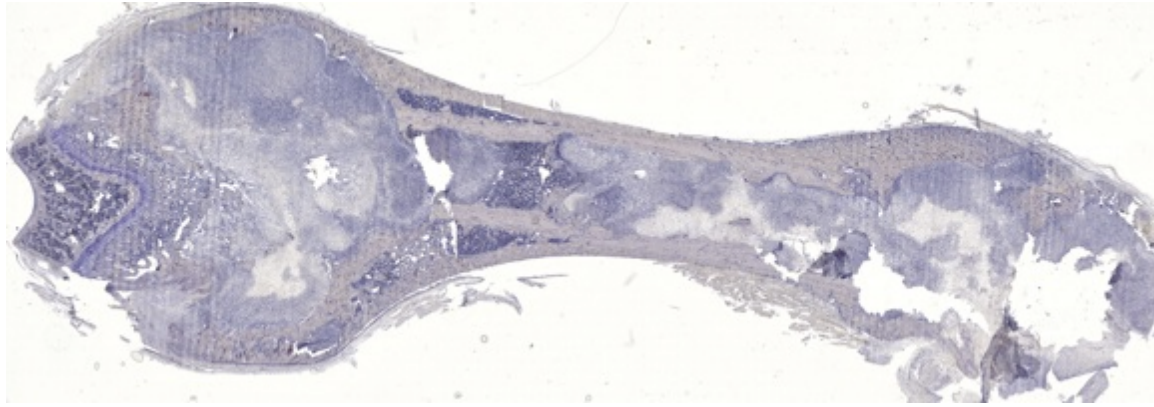


4 Weeks Post-OSA

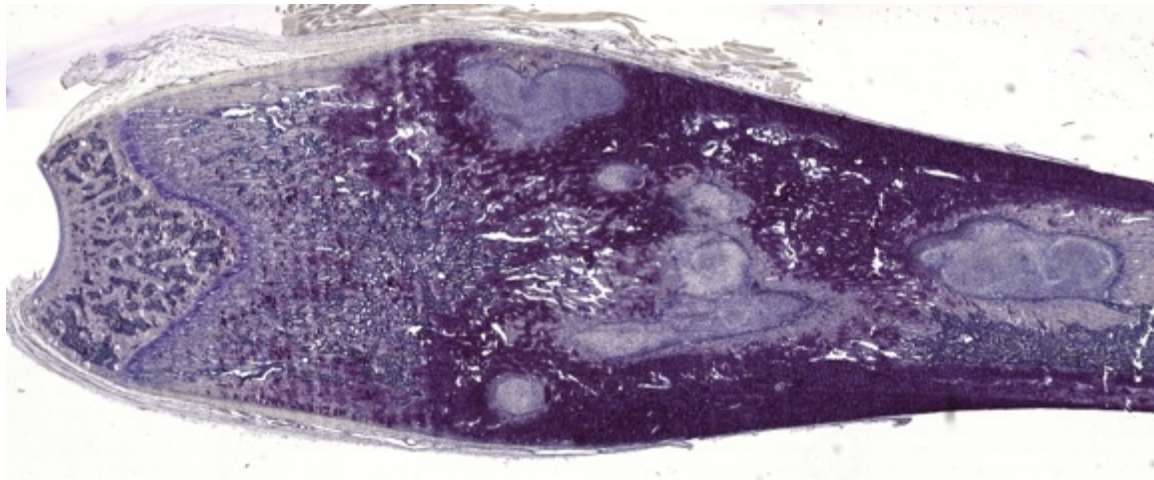


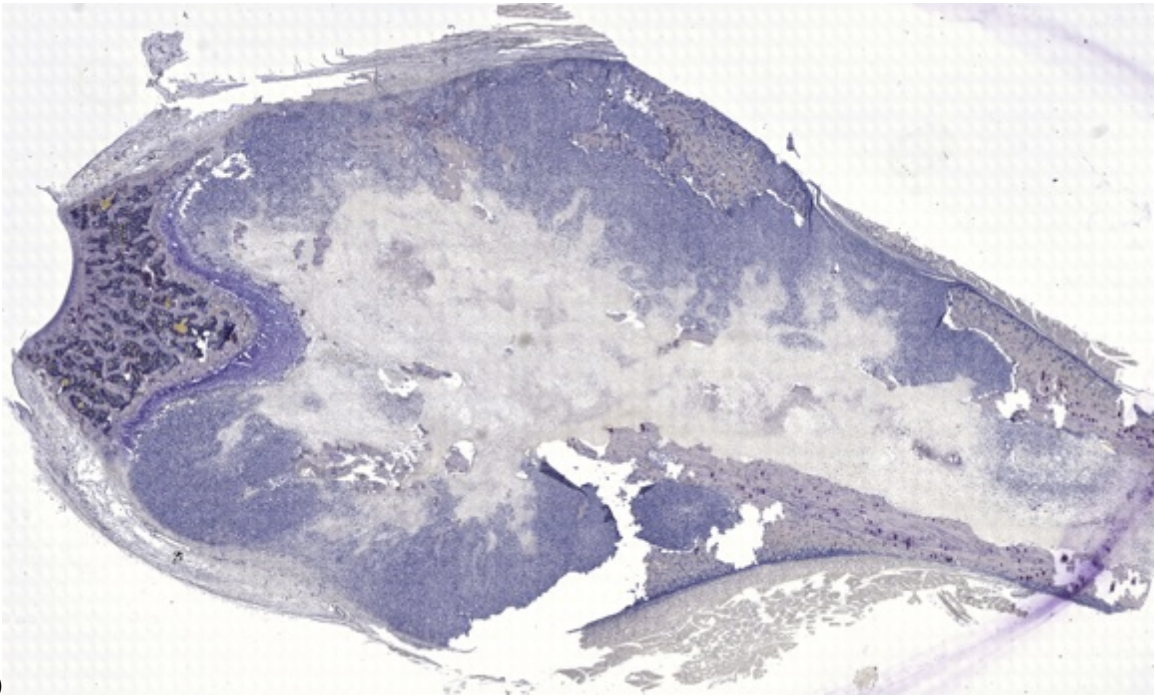
## 7.5 Orthotopic Supplemental Histology

128



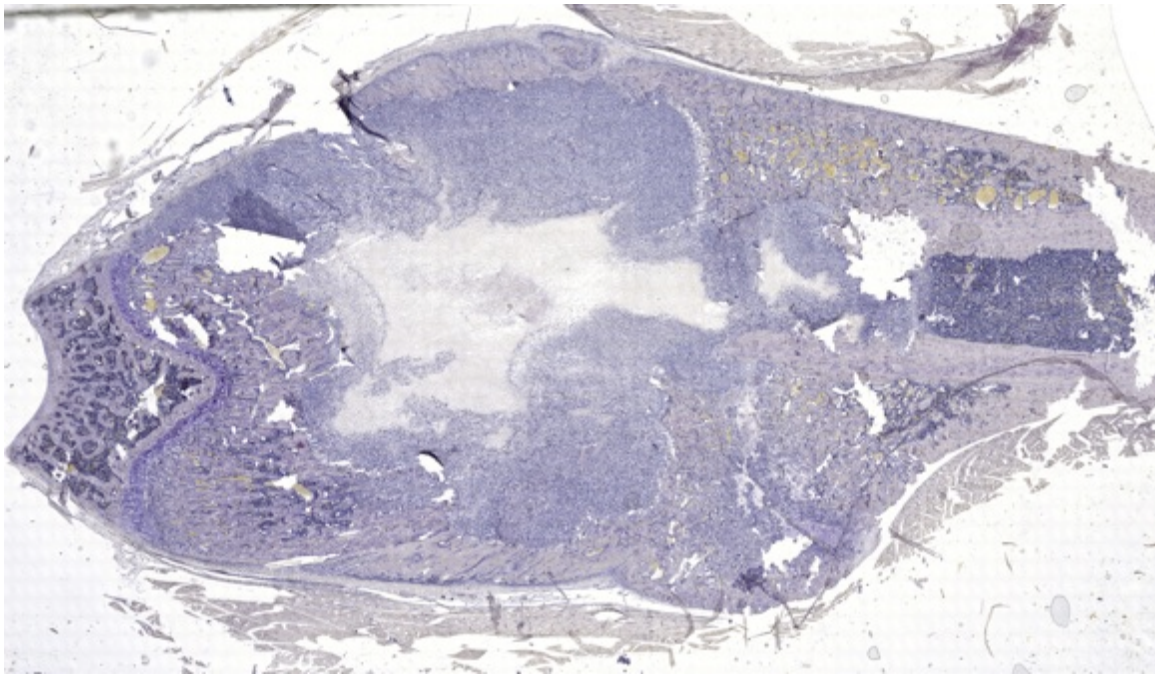
129



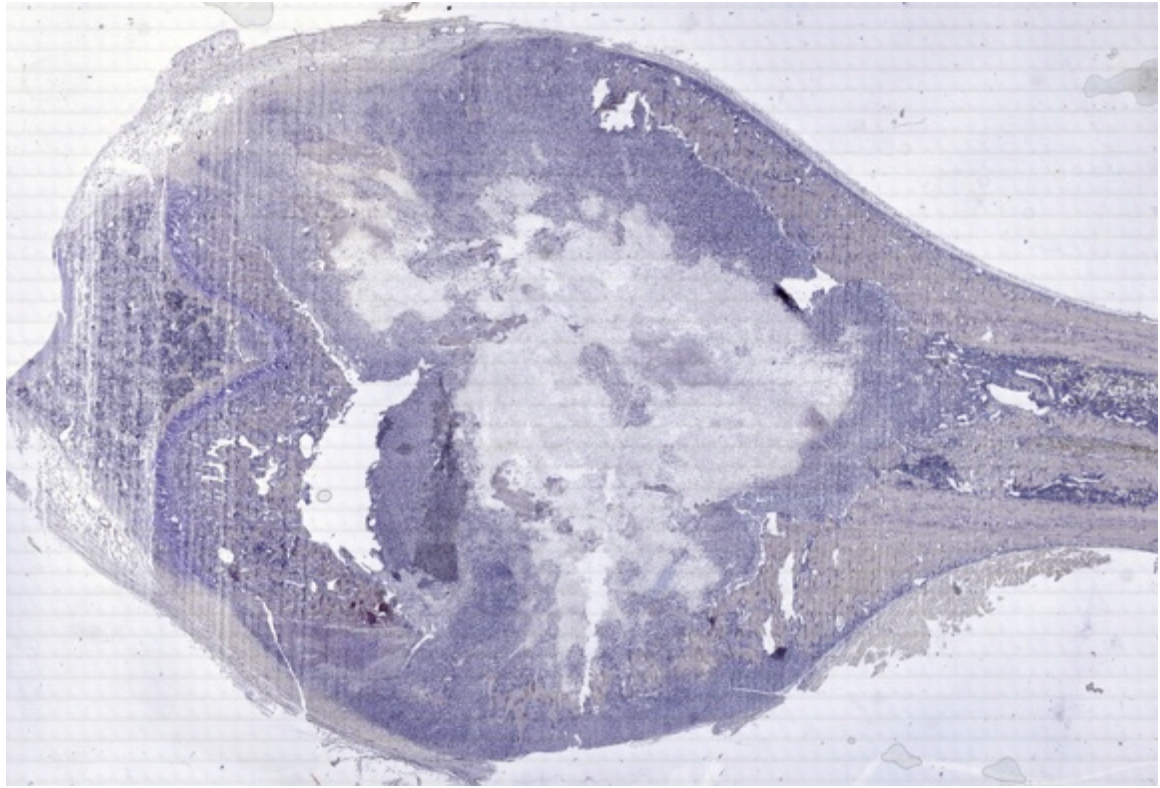


130

131

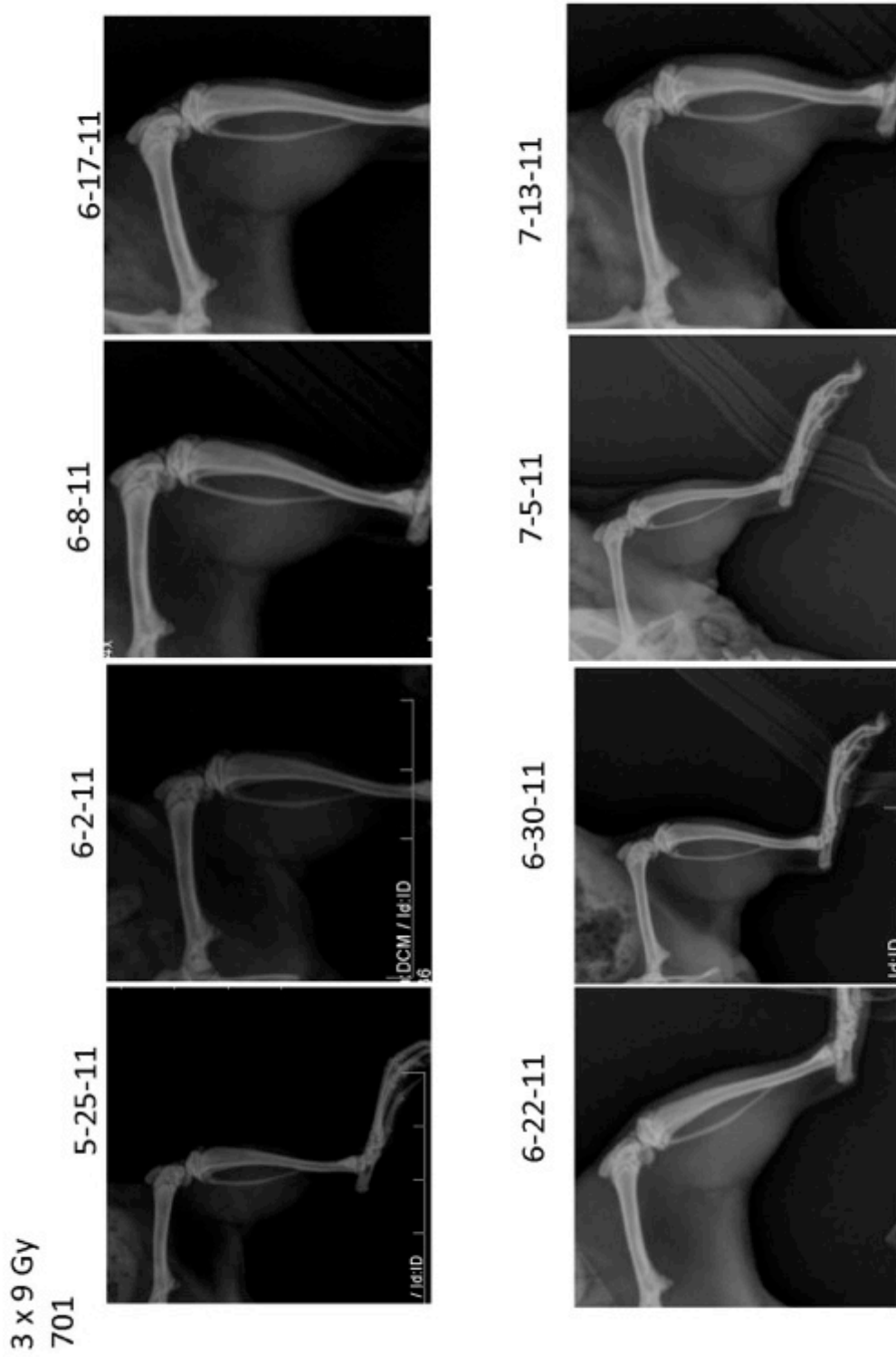


132



## Appendix B: Specific Aim 2 Protocols and Data

### 8.1 SRT Supplementary Radiographs



3 x 9 Gy  
704

5-25-11



6-2-11



6-8-11



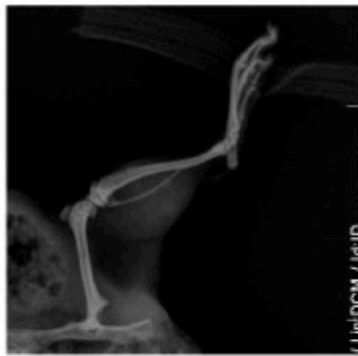
6-17-11



6-22-11



6-30-11



7-5-11

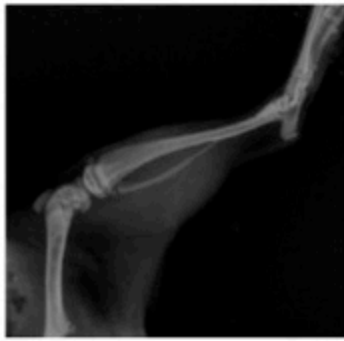


7-13-11



3 x 10 Gy  
705

5-25-11



6-2-11



6-8-11



6-17-11



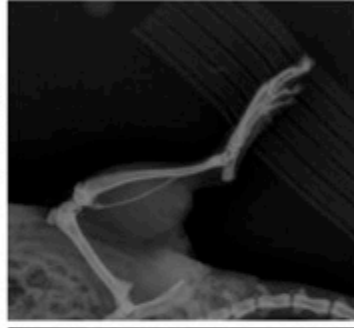
6-22-11



6-30-11



7-5-11



7-13-11



3 x 10 Gy  
706

5-25-11



6-2-11



6-8-11



6-17-11



6-22-11



6-30-11



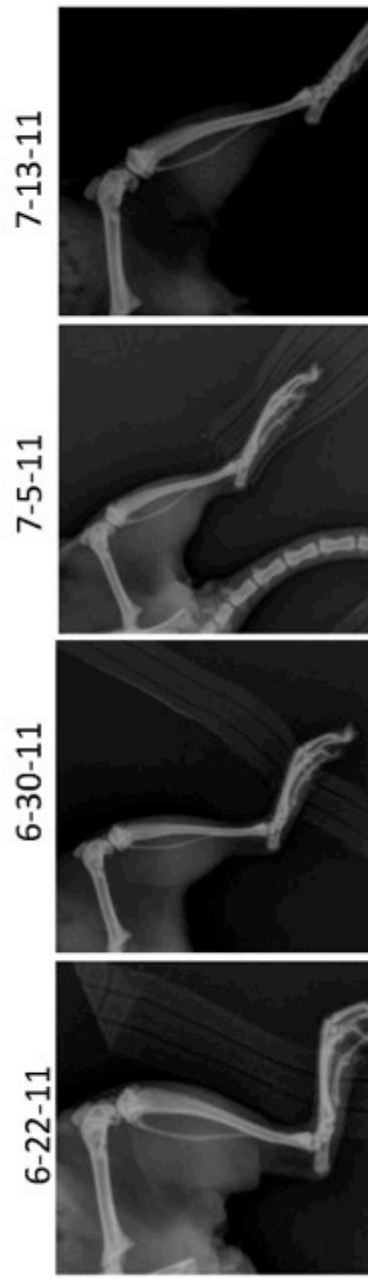
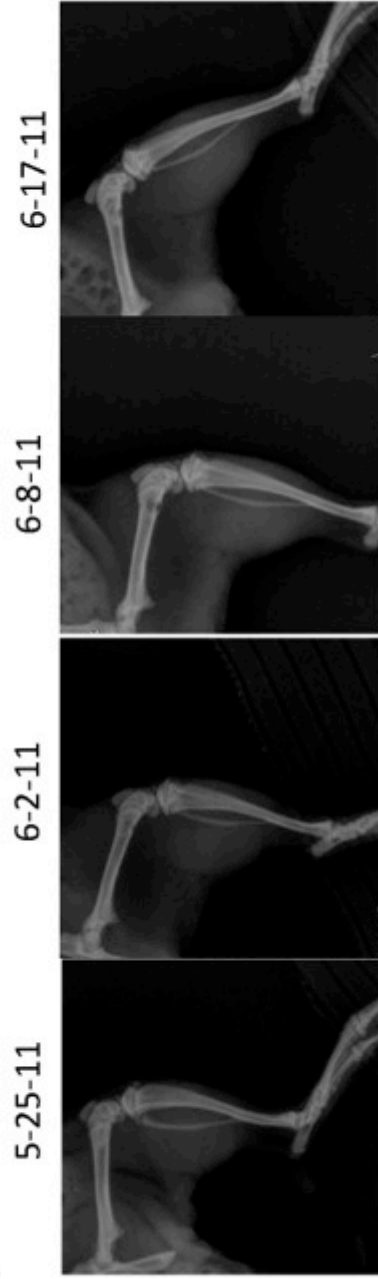
7-5-11



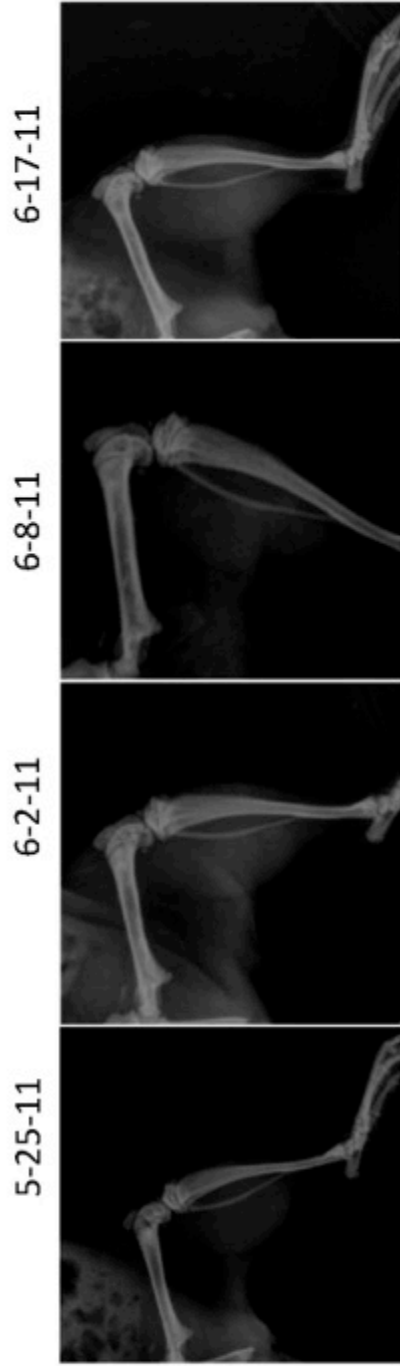
7-13-11



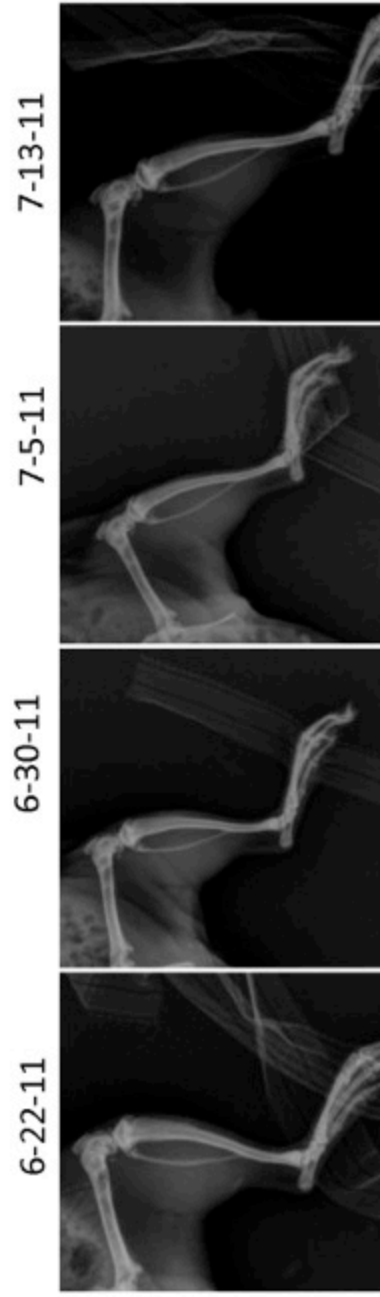
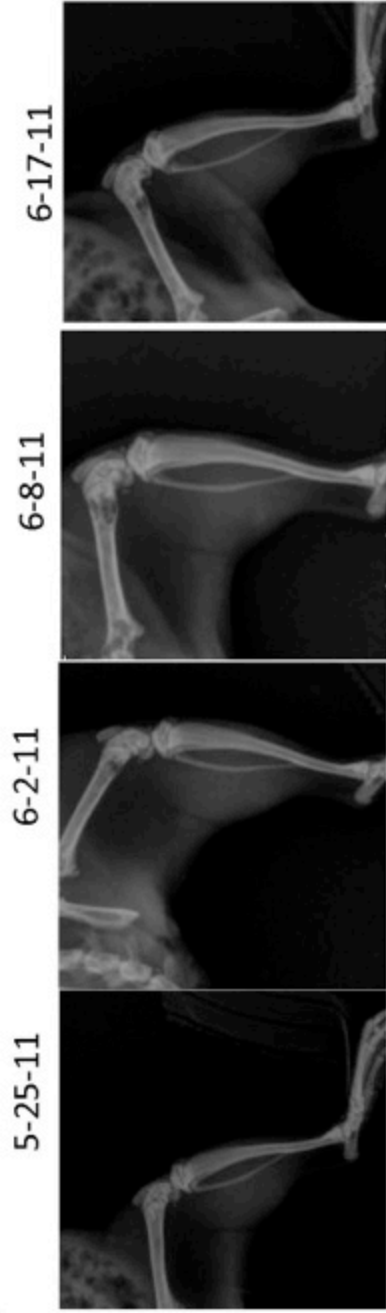
3 x 11 Gy  
707



3 x 11 Gy  
708



3 x 12 Gy  
709



3 x 12 Gy  
710

5-25-11



6-2-11



6-8-11



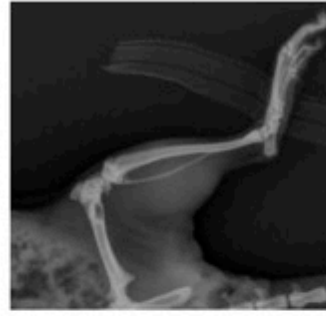
6-17-11



6-22-11



6-30-11



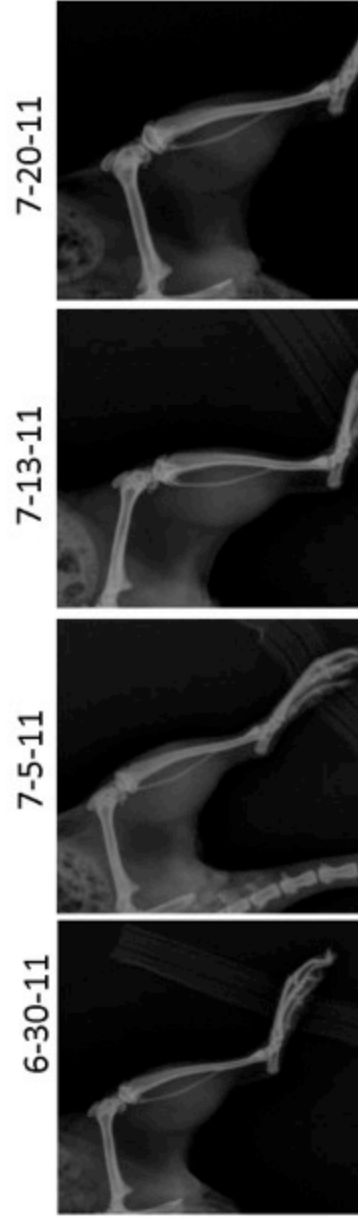
7-5-11



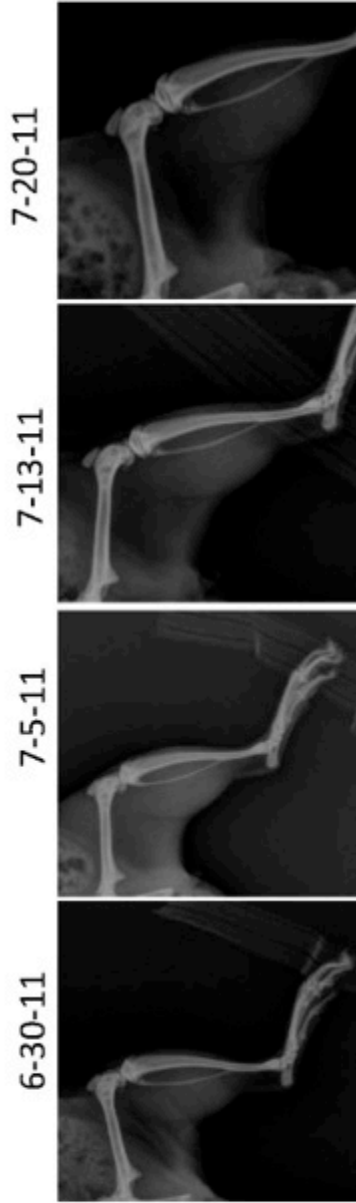
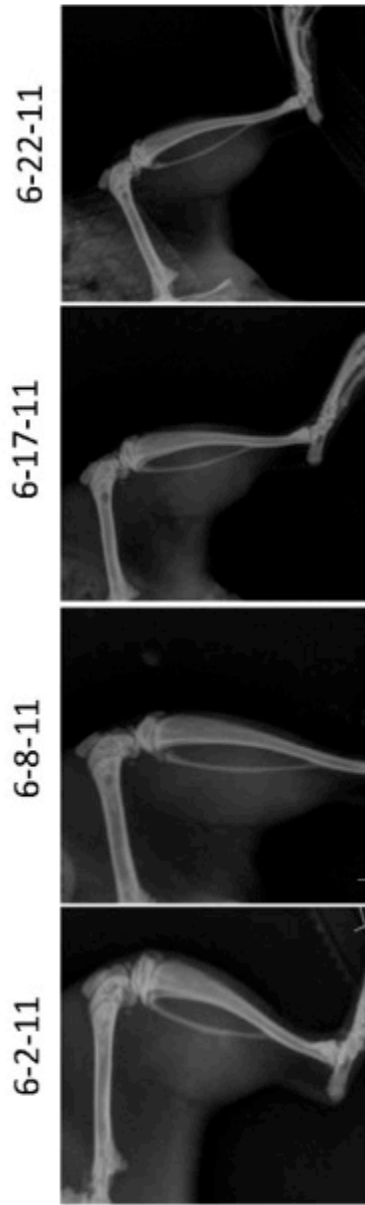
7-13-11



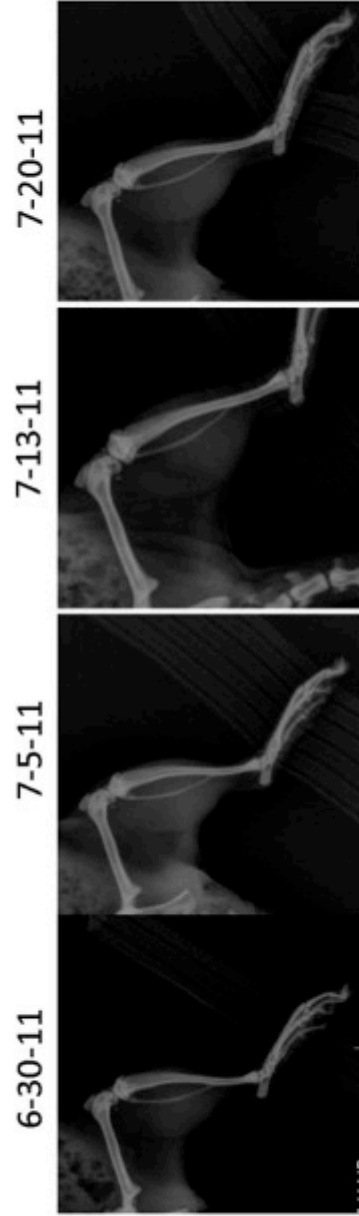
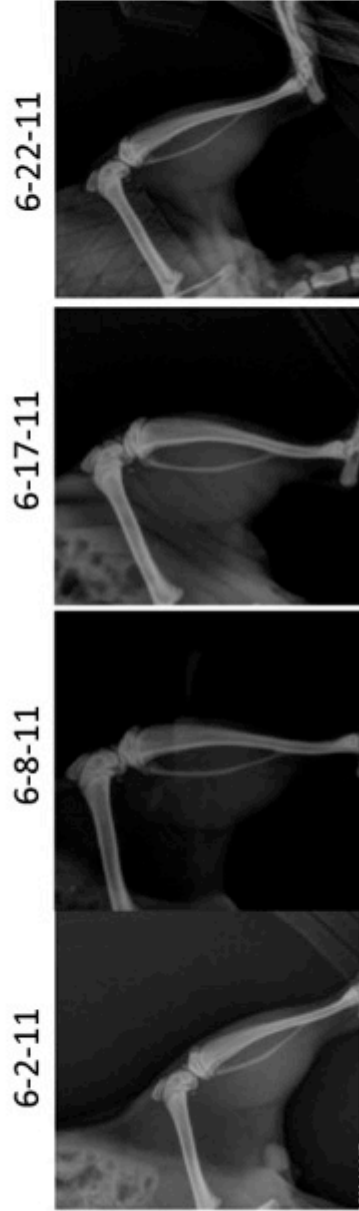
3 x 9 Gy  
712



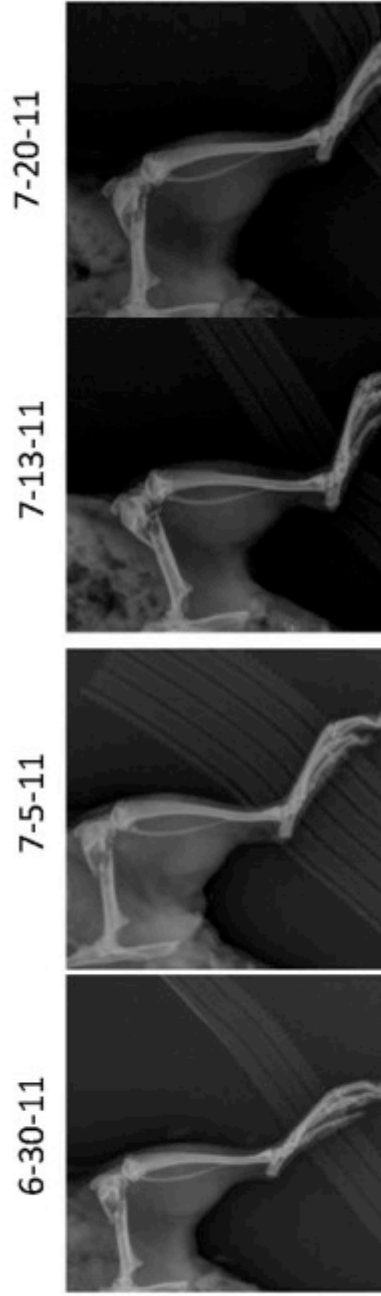
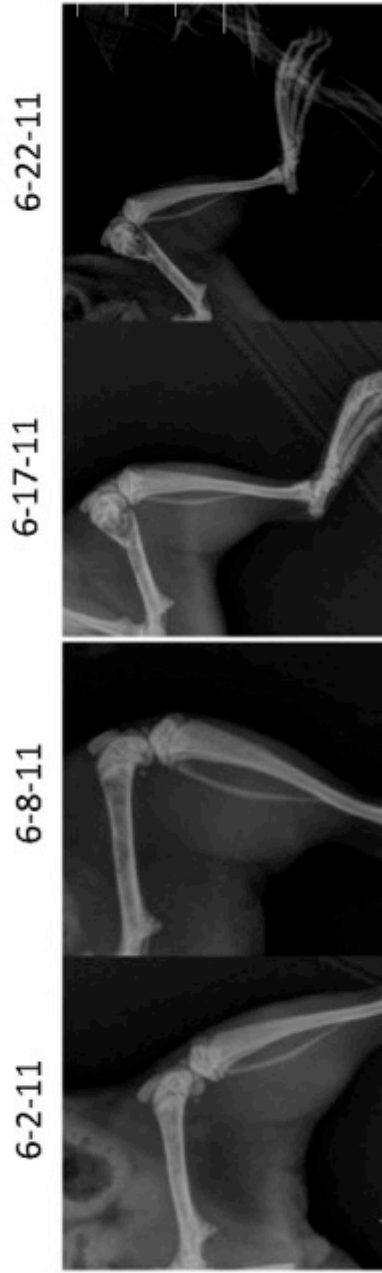
3 x 9 Gy  
713



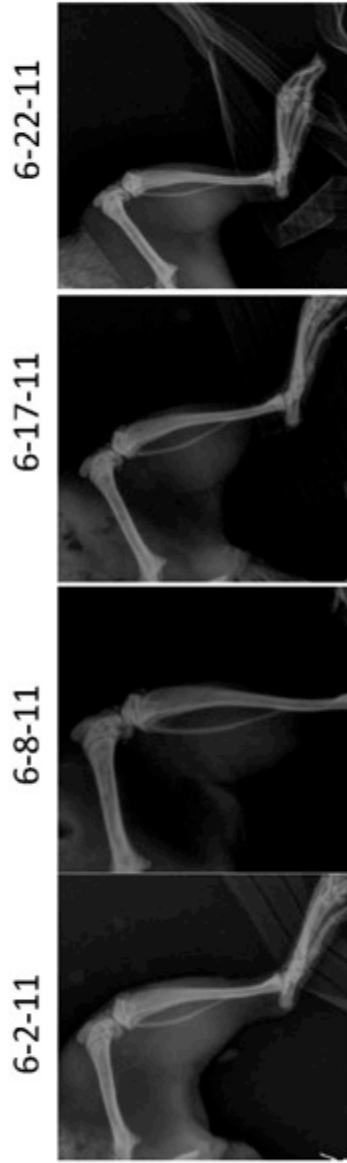
3 x 10 Gy  
714



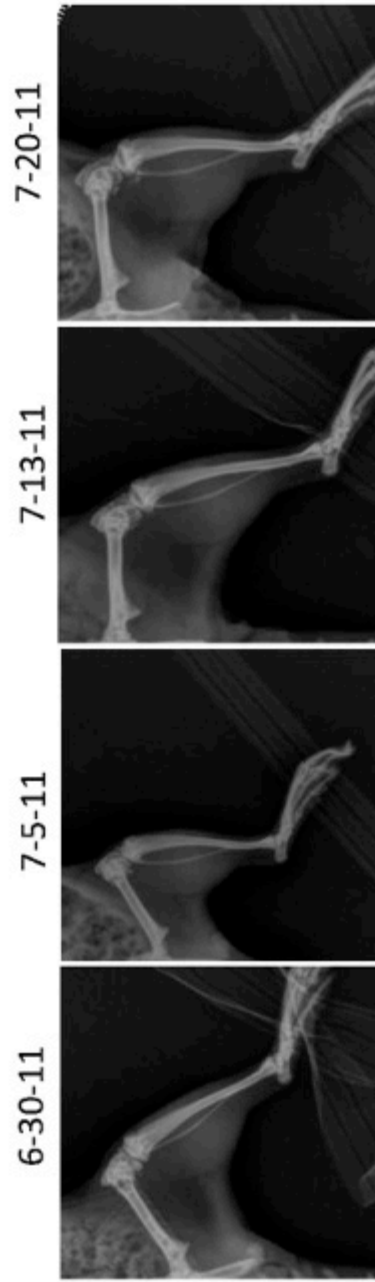
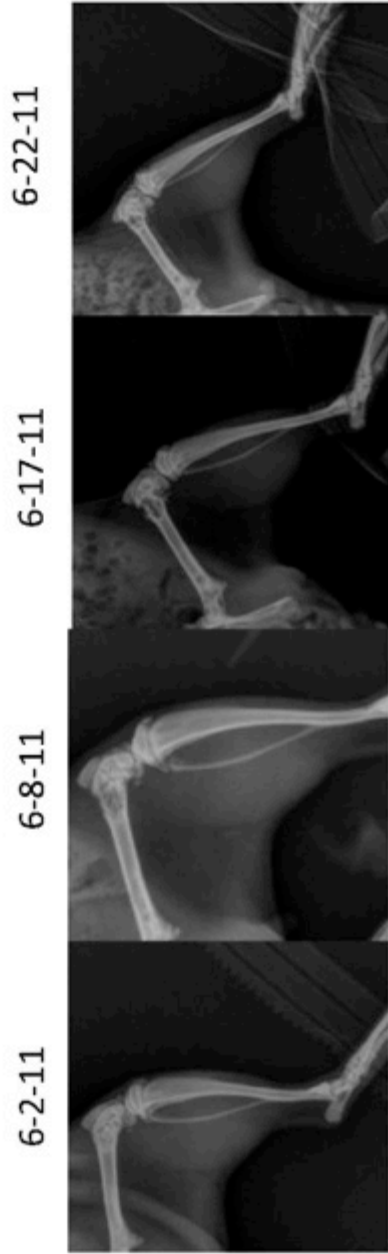
3 x 10 Gy  
716



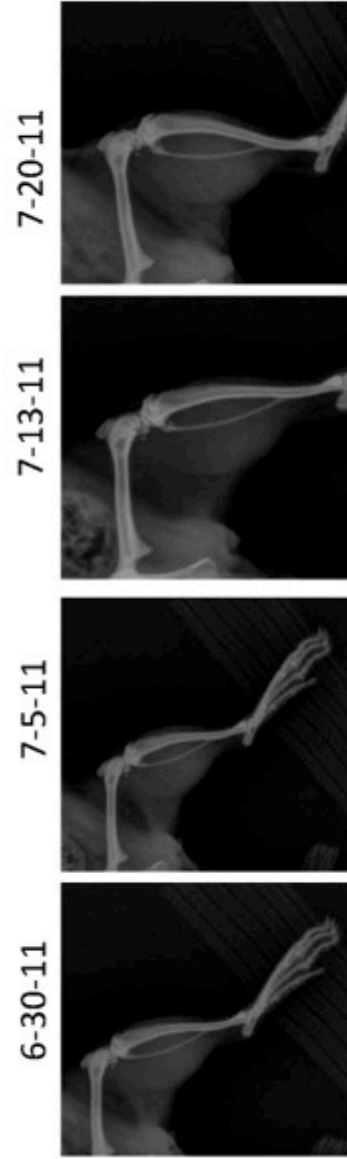
3 x 11 Gy  
717



3 x 11 Gy  
718



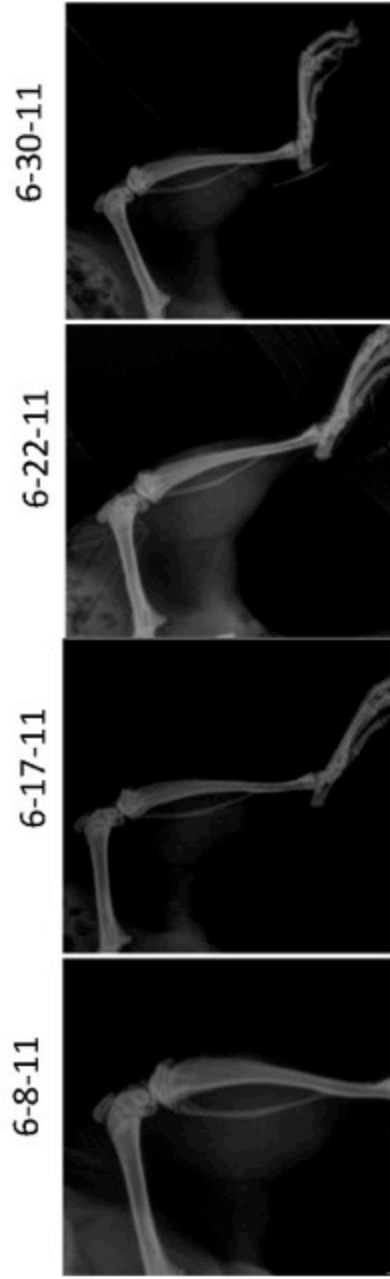
3 x 12 Gy  
720



3 x 9 Gy  
721



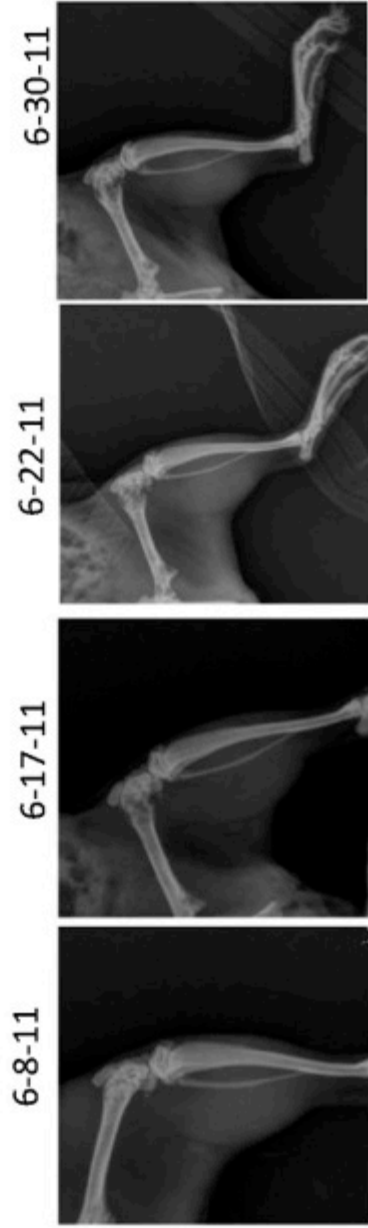
3 x 9 Gy  
722



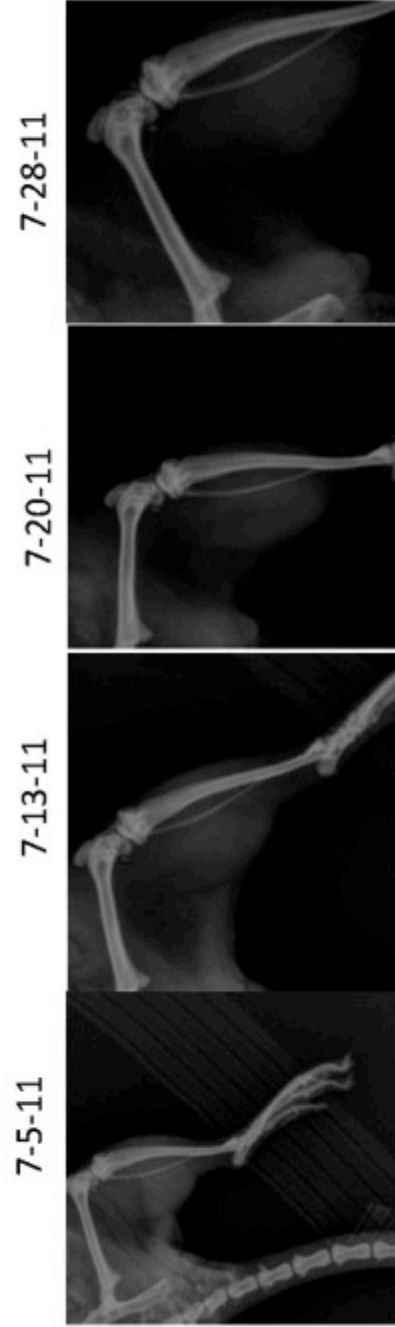
3 x 10 Gy  
723



3 x 10 Gy  
724



725



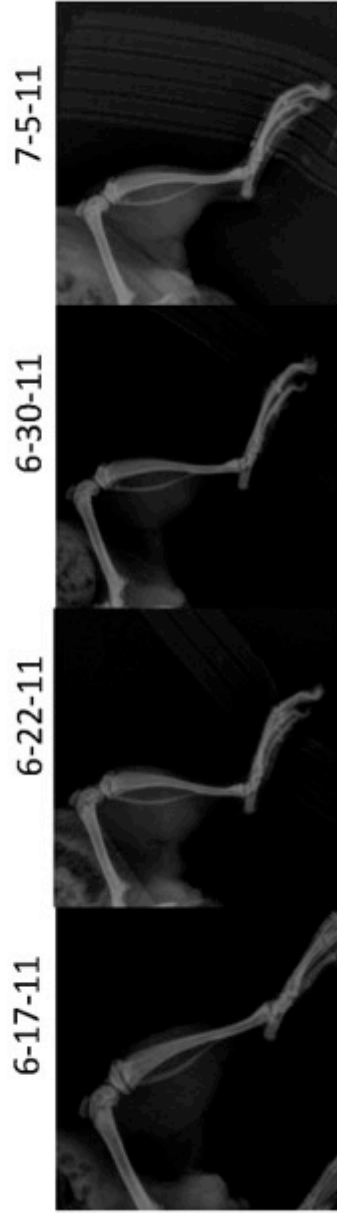
3 x 11 Gy  
747



3 x 12 Gy  
776



3 x 12 Gy  
777

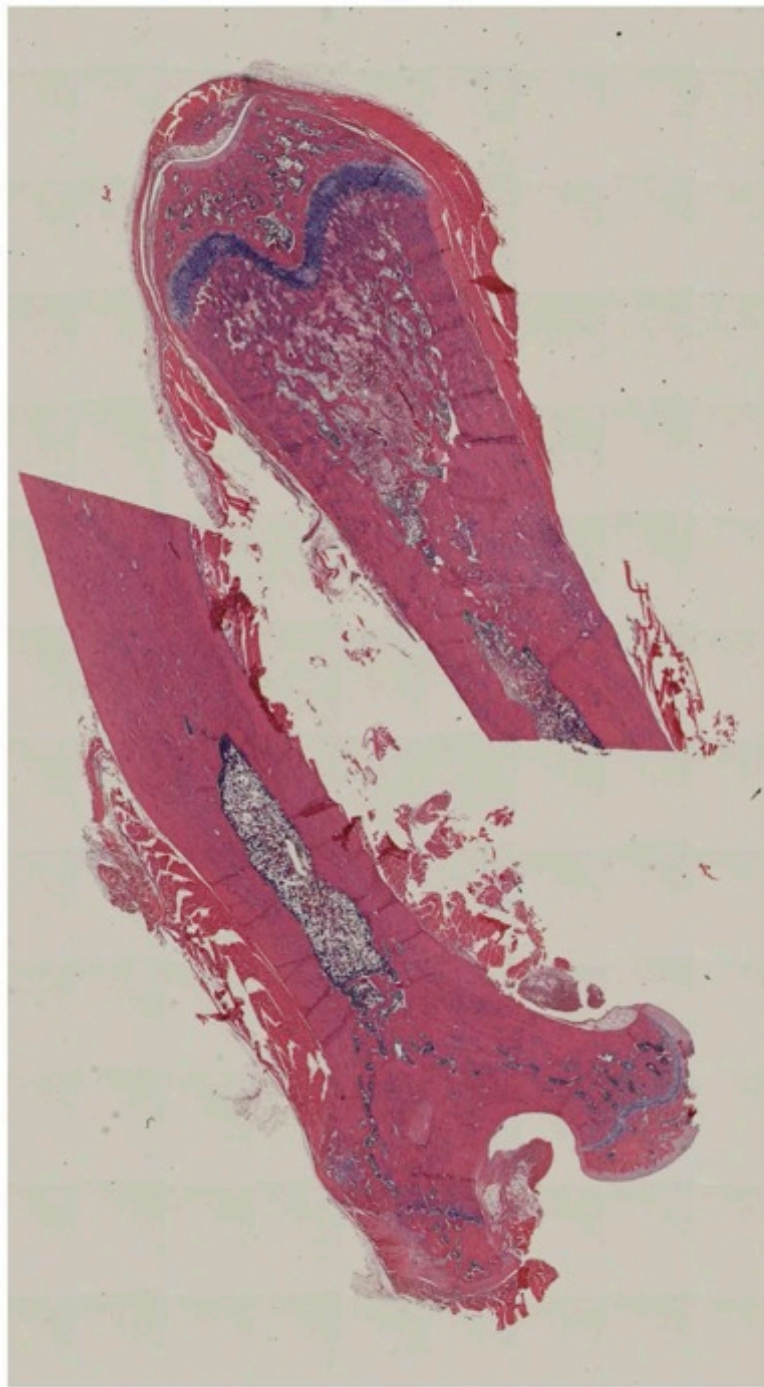


8.2 SRT Supplementary Histology

701 – 3x9 Gy



705 – 3x10 Gy



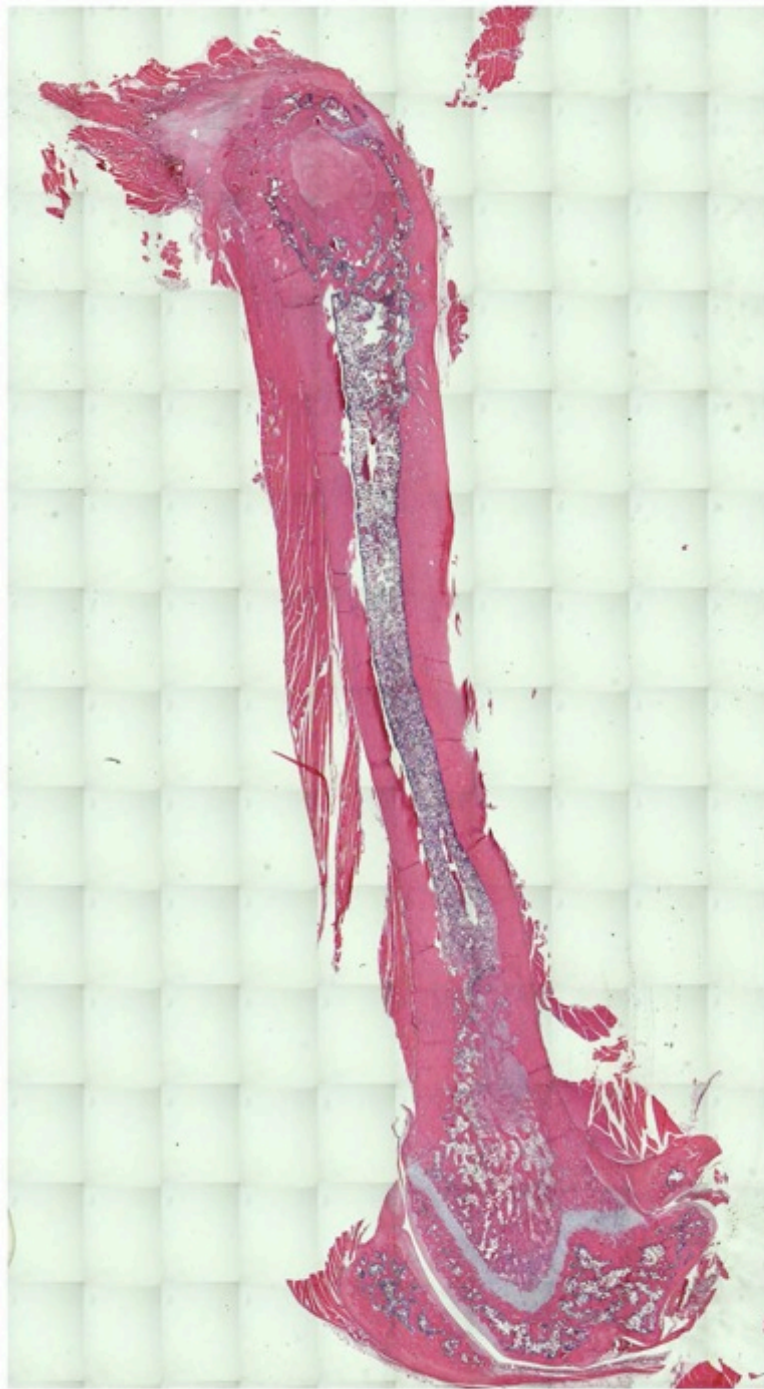
704 -3x9 Gy



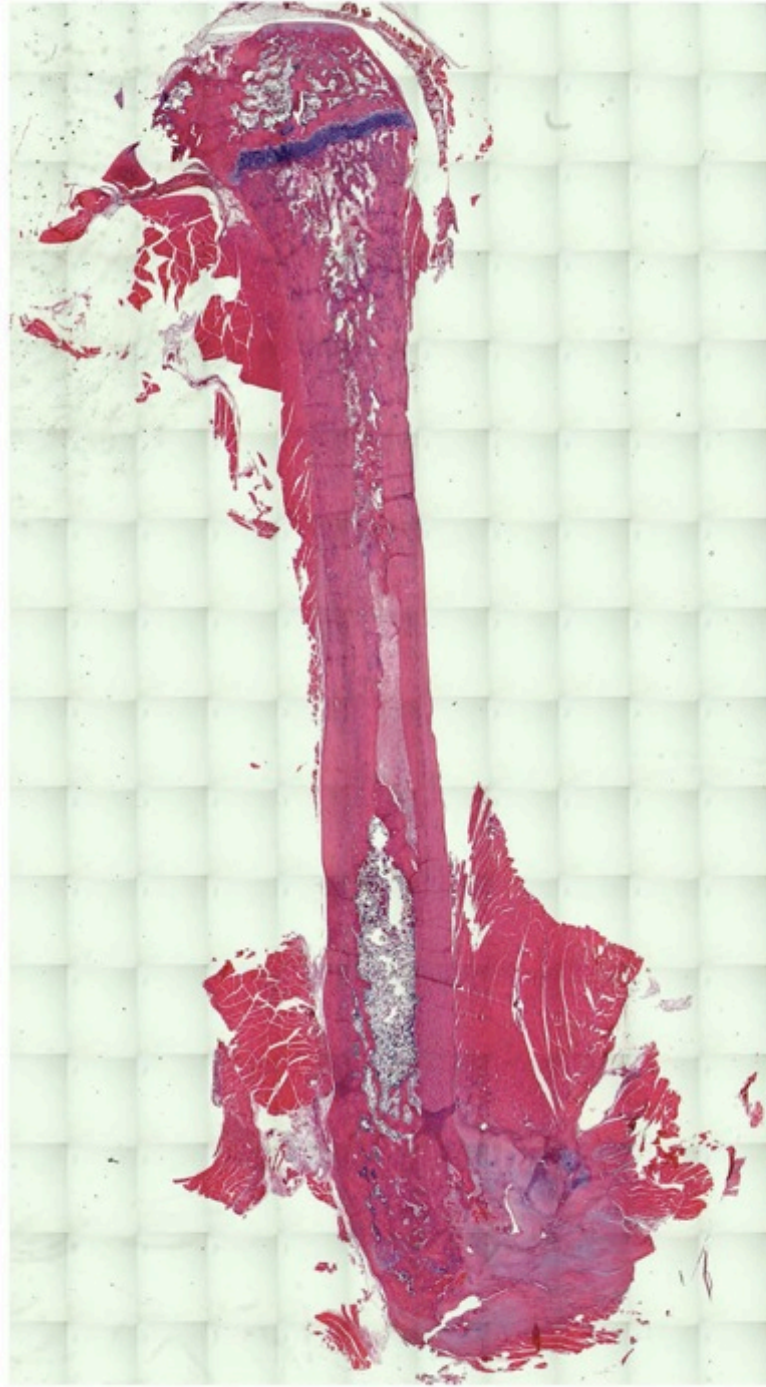
706 – 3x10 Gy



707 – 3x11 Gy



708 – 3x11 Gy



709 – 3x12 Gy



710 3x12 Gy



712 – No Tumor



713 – 3x9 Gy



714 – No tumor



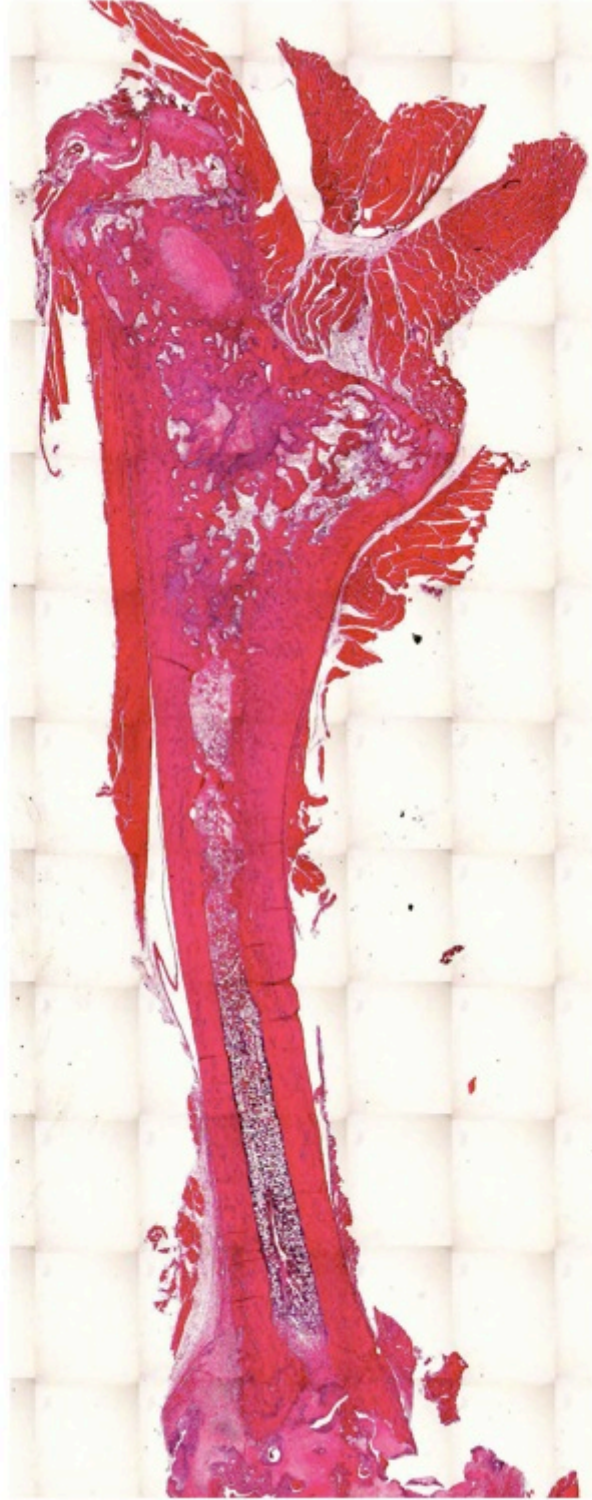
716 – 3x10 Gy



717 - 3x11 Gy



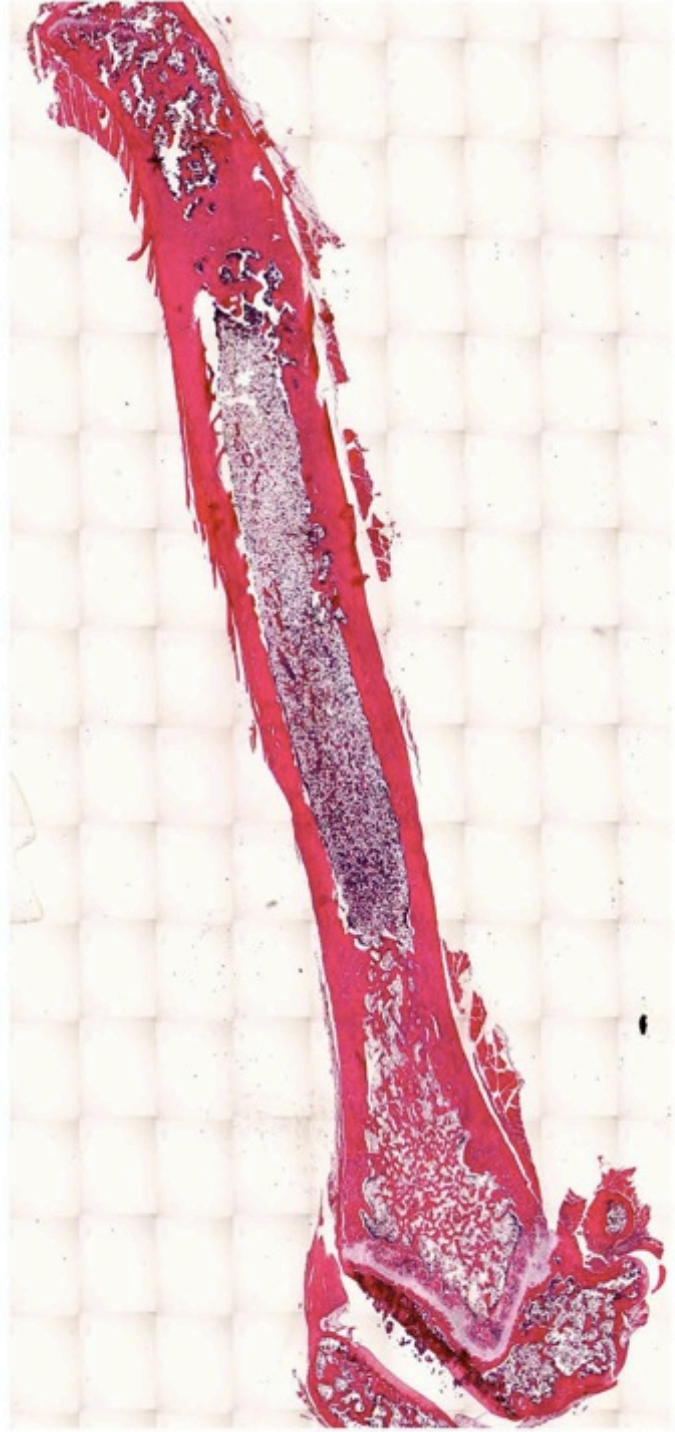
718 – 3x11 Gy



720 - 3x12 Gy



721 – 3x9 Gy



723 – 3x10 Gy



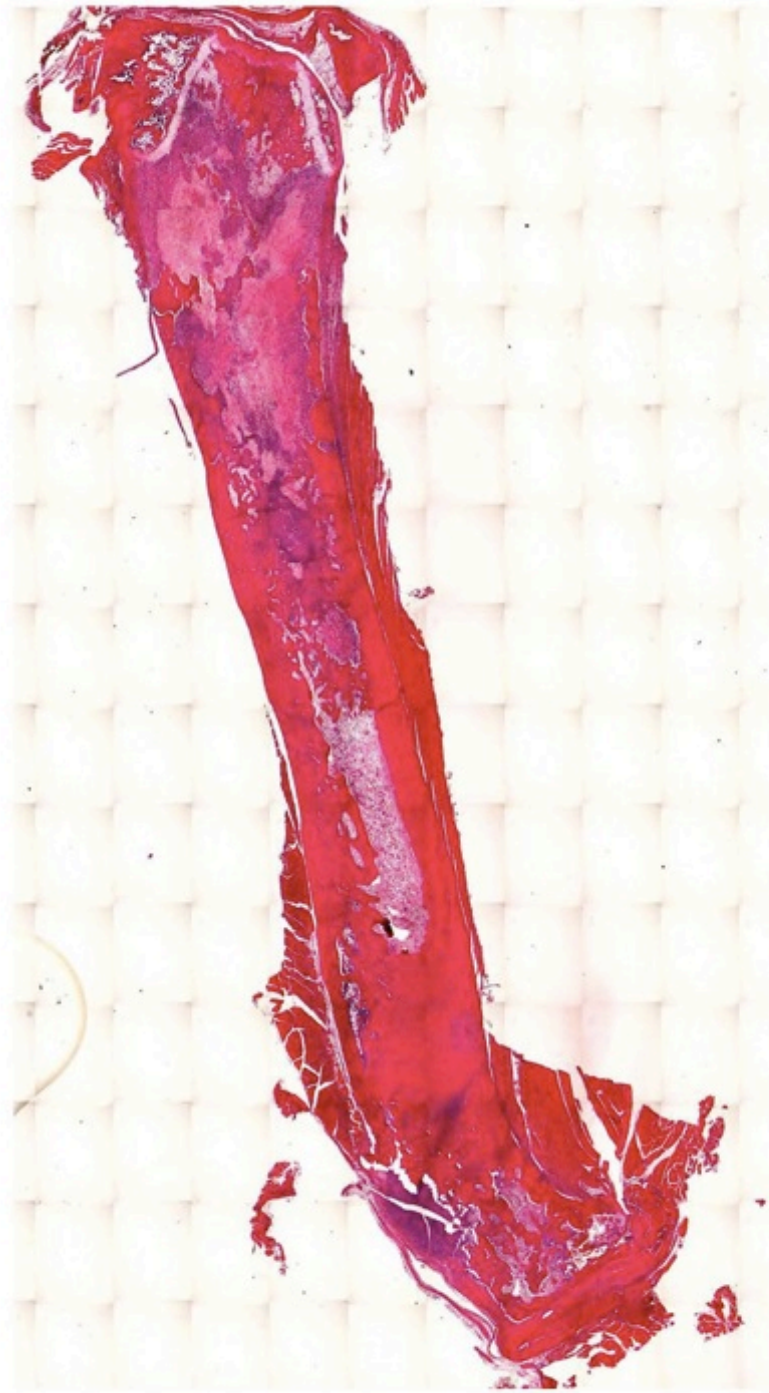
724 – 3x10 Gy



725 – No tumor



747 - 3x11 Gy



No Tumor - 776



## Appendix C: Specific Aim 3 Detailed Protocols and Data

### 9.1 Isolation of bone marrow rat mesenchymal stem cells that express GFP

#### 1.0 Purpose:

To isolate bone marrow mesenchymal stem cells from rats

#### 2.0 Scope:

Applies to the MSC injections in the osteosarcoma rat model

#### 3.0 Responsibility:

3.1 It is the responsibility of the ACC MS Lab Director(s), study director or qualified personnel to ensure that personnel performing the allograft isolation procedure have received adequate training to perform the procedure.

#### 4.0 Reference Documents: N/A

#### 5.0 Definitions: N/A

#### 6.0 Safety Precautions:

6.1 Place sharps in appropriate medical waste containers after procedure and wear PPE for a BSL2 Lab

#### 7.0 Procedure:

##### 7.1 Materials

- 7.1.1 At least four GFP expressing rats
- 7.1.2 Pipettes, centrifuge, syringes
- 7.1.3 70% Ethanol, PBS, collagenase
- 7.1.4 150 cm Cell culture flask
- 7.1.5 Sterile Gloves, mask, cap, and scrubs

##### Equipment

- 7.1.6 Culture hood, Incubator 5% CO<sub>2</sub>
- 7.1.7 Microscope
- 7.1.8 Surgical table
- 7.1.9 Surgical scissors and a scalpel
- 7.1.10 Isoflurane induction chamber

##### 7.2 Reagents

- 7.2.1 DMEM + 15% FBS Growth Media
- 7.2.2 Trypsin

##### 7.3 Working Reagent Preparation N/A

**2.2.14**

7.4 (Test) Procedure

- 7.4.1 Sterilize the hood, Warm media to 37 degrees for 15 minutes
- 7.4.2 Anesthetize rats and euthanize via cardiac puncture
- 7.4.3 Use the scissors to cut away skin around each leg being sure to be sterile and use ethanol to sterilize the skin before cutting.
- 7.4.4 Once skin is removed, disarticulate the femurs and place them in a cell culuture plate in growth media
- 7.4.5 Remove the distal and proximal ends of each femur and flush the inner marrow cavity with growth media using a 16-gauge needle attached to a syringe into a collection tube.
- 7.4.6 Once all marrow has been aspirated from all femurs, disperse the cells using 18 and 20 gauge needles.
- 7.4.7 Centrifuge dispersed cells at 1000 RPM for 5 minutes
- 7.4.8 Remove the supernatant and then resuspend the cell pellet with growth media
- 7.4.9 Add the cells to the culture flask and place in the incubator overnight
- 7.4.10 During the next day, check the cells for adherence to the plate and monitor daily until cells become confluent
- 7.4.11 Split the cells by aspirating the existing media and adding 2 mLs of Trypsin to the plate
- 7.4.12 Incubate for ~5 minutes until cells are detached and add ~8 mLs of culture media to the flask.
- 7.4.13 Distribute in 1 mL increments to additional flasks and add 14 Mls of media to each flask for a total volume of 15 Mls
- 7.4.14 Incubate until confluent and repeat 7.4.10 to continue cell culture

7.7 Reporting Results N/A

8.0 Attachments: N/A

## 9.2 Isolation of adipose rat mesenchymal stem cells that express GFP

### Purpose:

To isolate adipose mesenchymal stem cells from rats

### 1.0 Scope:

Applies to the MSC injections in the osteosarcoma rat model

### 2.0 Responsibility:

2.1 It is the responsibility of the ACC MS Lab Director(s), study director or qualified personnel to ensure that personnel performing the allograft isolation procedure have received adequate training to perform the procedure.

### 4.0 Reference Documents: N/A

### 5.0 Definitions: N/A

### 6.0 Safety Precautions:

6.1 Place sharps in appropriate medical waste containers after procedure and wear PPE for a BSL2 Lab

### 7.0 Procedure:

#### 7.1 Materials

- 7.1.1 Two GFP expressing rats
- 7.1.2 Pipettes, centrifuge, syringes
- 7.1.3 70% Ethanol, PBS, collagenase
- 7.1.4 150 cm Cell culture flask
- 7.1.5 Sterile Gloves, mask, cap, and scrubs

#### Equipment

- 7.1.6 Culture hood, Incubator 5% CO<sub>2</sub>
- 7.1.7 Microscope
- 7.1.8 Surgical table
- 7.1.9 Surgical scissors and a scalpel
- 7.1.10 Isoflurane induction chamber

#### 7.2 Reagents

- 7.2.1 DMEM + 15% FBS Growth Media
- 7.2.2 Trypsin

#### 7.3 Working Reagent Preparation N/A

#### 7.4 (Test) Procedure

### 2.2.15

- 7.4.1 Sterilize the hood, Warm media to 37 degrees for 15 minutes

- 7.4.2 Anesthetize rats and euthanize via cardiac puncture
- 7.4.3 Use the scissors to make an incision in the abdominal area and remove excess skin to avoid contamination
- 7.4.4 Use the scalpel to remove the Epididymal fat pad and place it a tube with PBS
- 7.4.5 Once all fat is collected from both mice, add an equal volume of collagenase to the PBS and place in the incubator until the solution become homogenous
- 7.4.6 Centrifuge the collagenase solution at 1,200 RPM for 5 minutes
- 7.4.7 Remove the supernatant and then resuspend the cell pellet with growth media
- 7.4.8 Add the cells to the culture flask and place in the incubator overnight
- 7.4.9 During the next day, check the cells for adherence to the plate and monitor daily until cells become confluent
- 7.4.10 Split the cells by aspirating the existing media and adding 2 mLs of Trypsin to the plate
- 7.4.11 Incubate for ~5 minutes until cells are detached and add ~8 mLs of culture media to the flask.
- 7.4.12 Distribute in 1 mL increments to additional flasks and add 14 Mls of media to each flask for a total volume of 15 Mls
- 7.4.13 Incubate until confluent and repeat 7.4.10 to continue cell culture

7.7 Reporting Results N/A

8.0 Attachments: N/A

## 9.3 Cell culture of bone and adipose rat mesenchymal Stem cells

### 1.0 Purpose:

To grow and propagate the adipose or bone marrow derived mesenchymal stem cells in culture

### 2.0 Scope:

Applies to the MSC injections in the osteosarcoma rat model

### 3.0 Responsibility:

3.1 It is the responsibility of the ACC MS Lab Director(s), study director or qualified personnel to ensure that personnel performing the allograft isolation procedure have received adequate training to perform the procedure.

### 4.0 Reference Documents: N/A

### 5.0 Definitions: N/A

### 6.0 Safety Precautions:

6.1 Place sharps in appropriate medical waste containers after procedure and wear PPE for a BSL2 Lab

### 7.0 Procedure:

#### 7.1 Materials

- 7.1.1 Pipettes
- 7.1.2 70% Ethanol
- 7.1.3 150 cm Cell culture flask
- 7.1.4 Sterile Gloves, mask, cap, and scrubs

#### Equipment

- 7.1.5 Culture hood, Incubator 5% CO<sub>2</sub>
- 7.1.6 Microscope

#### 7.2 Reagents

- 7.2.1 DMEM + 10% FBS Growth Media
- 7.2.2 Trypsin

#### 7.3 Working Reagent Preparation N/A

#### 7.4 (Test) Procedure

### 2.2.16

- 7.4.1 Sterilize the hood, Warm media to 37 degrees for 15 minutes
- 7.4.2 Thaw the vial of MSCs in 37 degrees for 5 minutes
- 7.4.3 Carefully pipette out the thawed OSA cells and place them into the cell culture flask
- 7.4.4 Add 15mL of media to the flask and place in the incubator overnight

- 7.4.5 During the next day, check the cells for adherence to the plate and monitor daily until cells become confluent
- 7.4.6 Split the cells by aspirating the existing media and adding 2 mLs of Trypsin to the plate
- 7.4.7 Incubate for ~5 minutes until cells are detached and add ~8 mLs of culture media to the flask.
- 7.4.8 Distribute in 1 mL increments to additional flasks and add 14 MLs of media to each flask for a total volume of 15 MLs
- 7.4.9 Incubate until confluent and repeat 7.4.6 to continue cell culture

7.7 Reporting Results N/A

8.0 Attachments: N/A

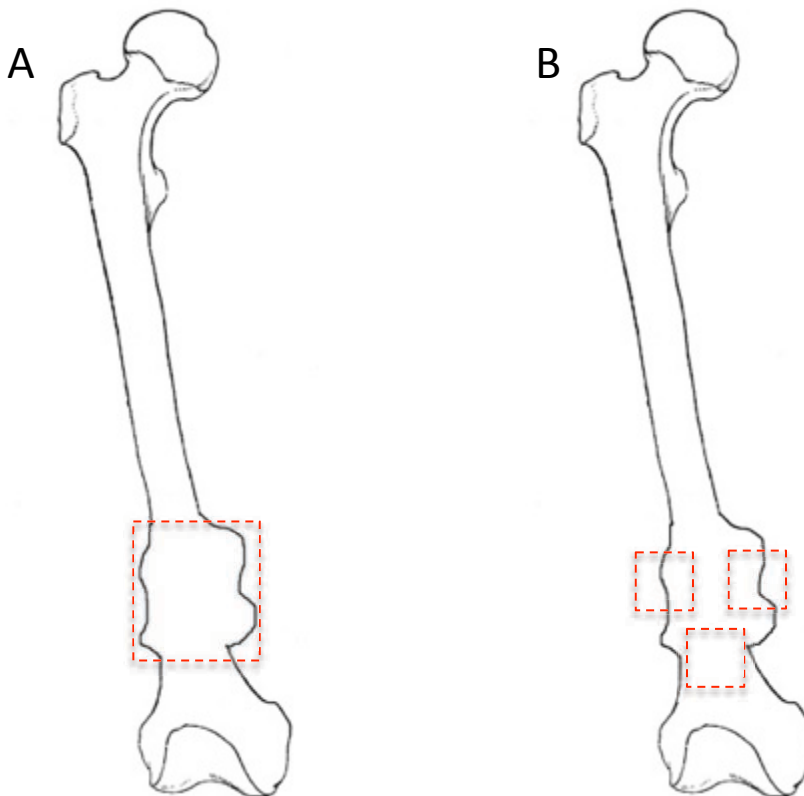
## Appendix D: Specific Aim 4 Supplementary Protocols and Data

### 10.1 Calculation of Bone Volume via microCT

Rat femurs were scanned with a Scanco uCT40 (Brüttisellen, Switzerland) at a 10-micron resolution. Bone volume was then determined as follows with the Scanco Image Analysis Software:

- 1) Total bone volume of each femur was determined using the femur as the volume of interest (VOI)
- 2) Normalized VOI based using the smallest tumor as the reference VOI and calculated for each femur (Figure 1A)
- 3) Normalized VOI based on three region of equal areas of volume (100 X 100 X 200 slices) around the tumor as shown in Figure 1B). The same regions were used to calculate bone volume in each femur.

Volumes were then compiled for each group, outputted to an excel file and evaluated for statistical significance using SPSS software.



## 10.2 Osteocalcin ELISA

### 4.0 Purpose:

To analyze the serum osteocalcin in rats

### 5.0 Scope:

Applies to the osteosarcoma rat model

### 6.0 Responsibility:

6.1 It is the responsibility of the ACC MS Lab Director(s), study director or qualified personnel to ensure that personnel performing the allograft isolation procedure have received adequate training to perform the procedure.

### 8.0 Reference Documents: N/A

### 9.0 Definitions: N/A

### 10.0 Safety Precautions:

10.1 Place sharps in appropriate medical waste containers after procedure and wear PPE for a BSL2 Lab

### 11.0 Procedure:

#### 11.1 Materials

11.1.1 Serum Samples

11.1.2 Biomedical Technologies Rat Osteocalcin ELISA (BT-490)

11.1.3 Pipettes, Tips, Multi-Channel Pipetter

#### Equipment

4.1.2 Plate Reader

#### 6.1 Reagents

6.1.1 PBS, ddH<sub>2</sub>O

#### 6.2 Working Reagent Preparation N/A

#### 6.3 (Test) Procedure

6.3.1 Remove ELISA plate from re-sealable bag.

6.3.2 Dilute the stock standard (100ng/ml) in polypropylene tubes with sample buffer to give six or seven standards in the range of 0.25 to 20ng/ml. (0.33, 1.0, 2.5, 5.0, 10 and 20ng/ml)

6.3.3 Dilute the serum samples 1:10 in the sample buffer.

6.3.4 Pipet 25ul of sample buffer (Blank), Standards, Controls and Unknowns into labeled wells followed by 100ul of osteocalcin antiserum in each well.

6.3.5 Seal the plate with the provided cover slip.

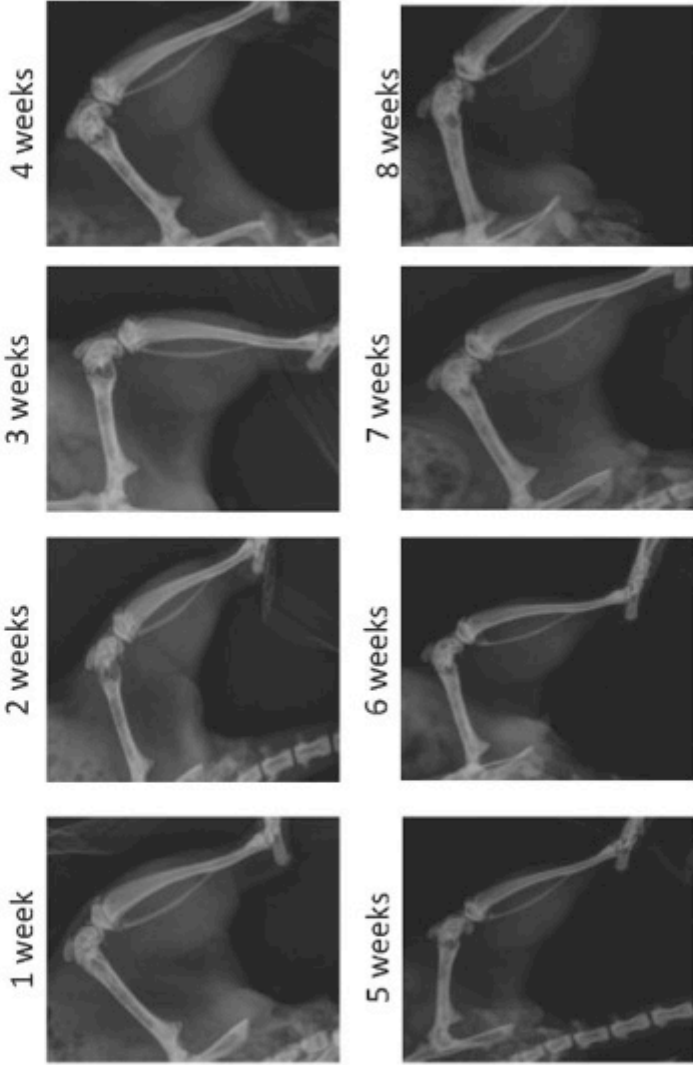
6.3.6 Incubate at 37°C for 2.5 hours.

- 6.3.7 Aspirate wells completely and wash the plate 3 to 5 times with 300 ul per well with the provided Phosphate-Saline wash buffer.
- 6.3.8 Add 100ul of the diluted Donkey anti-Goat IgG Peroxidase to each well.
- 6.3.9 Incubate at room temperature for 1 hour.
- 6.3.10 Mix one volume of TMB solution with one volume of Hydrogen Peroxide solution (provided).
- 6.3.11 Wash the plate as in step 6.3.7.
- 6.3.12 Immediately add 100ul of substrate mix to all wells and incubate in the dark at room temperature for 30 minutes.
- 6.3.13 Add 100ul of Stop Solution to each well and swirl.
- 6.3.14 Measure absorbance at 450nm within 15 minutes.
- 6.3.15 The computer will calculate the concentrations and output them to an excel sheet.
- 7.7 Reporting Results N/A

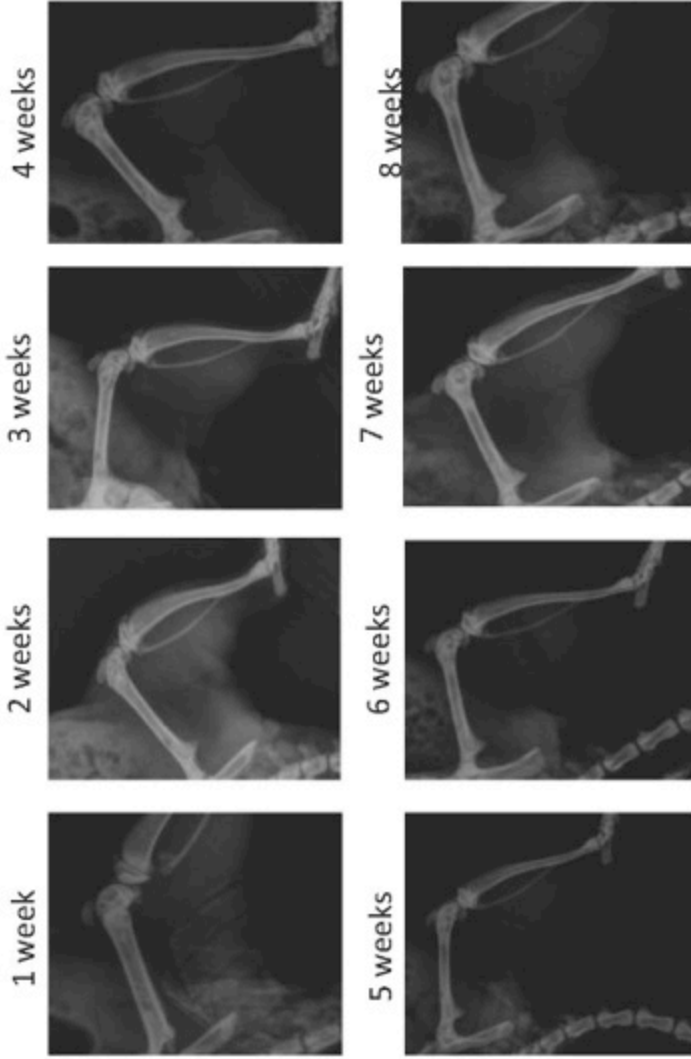
7.0 Attachments: N/A

10.3 Radiographs

77 - IV

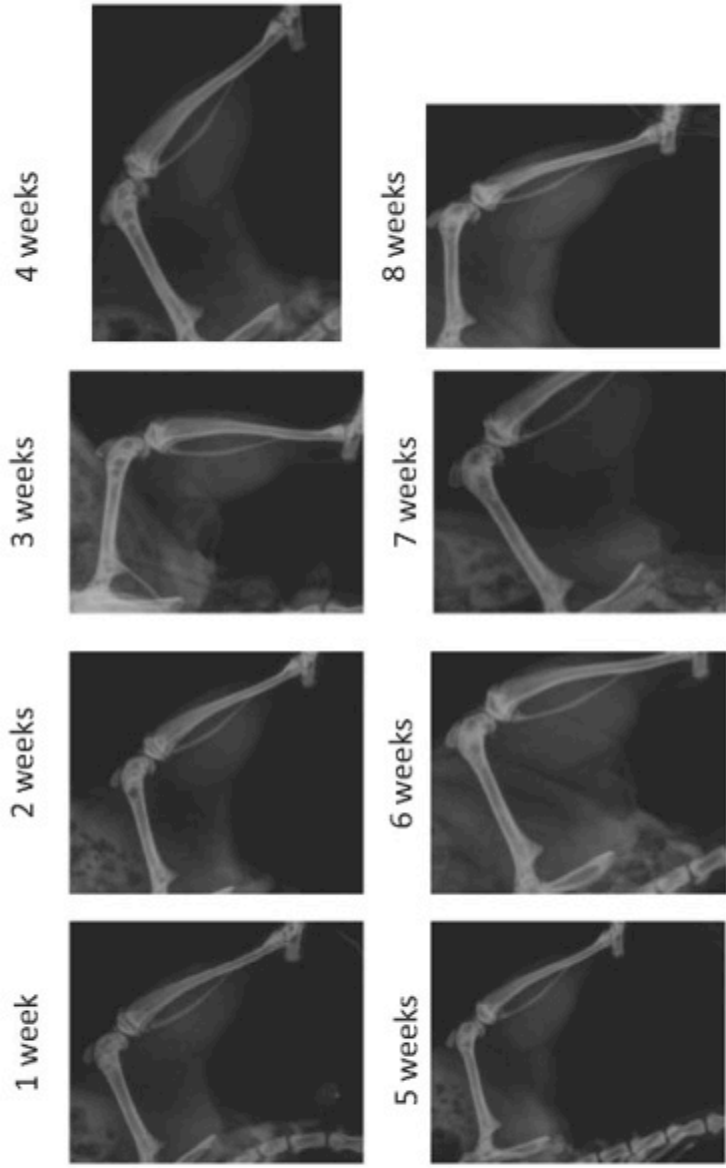


78 - IV

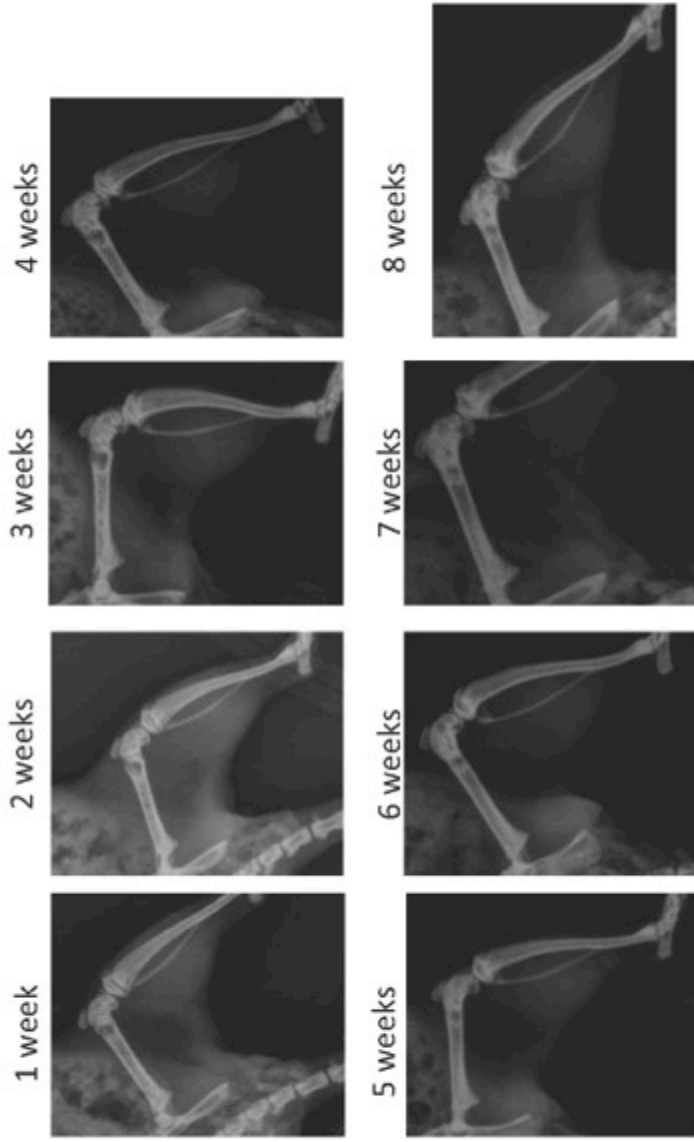


# MSC Experiment Radiographs

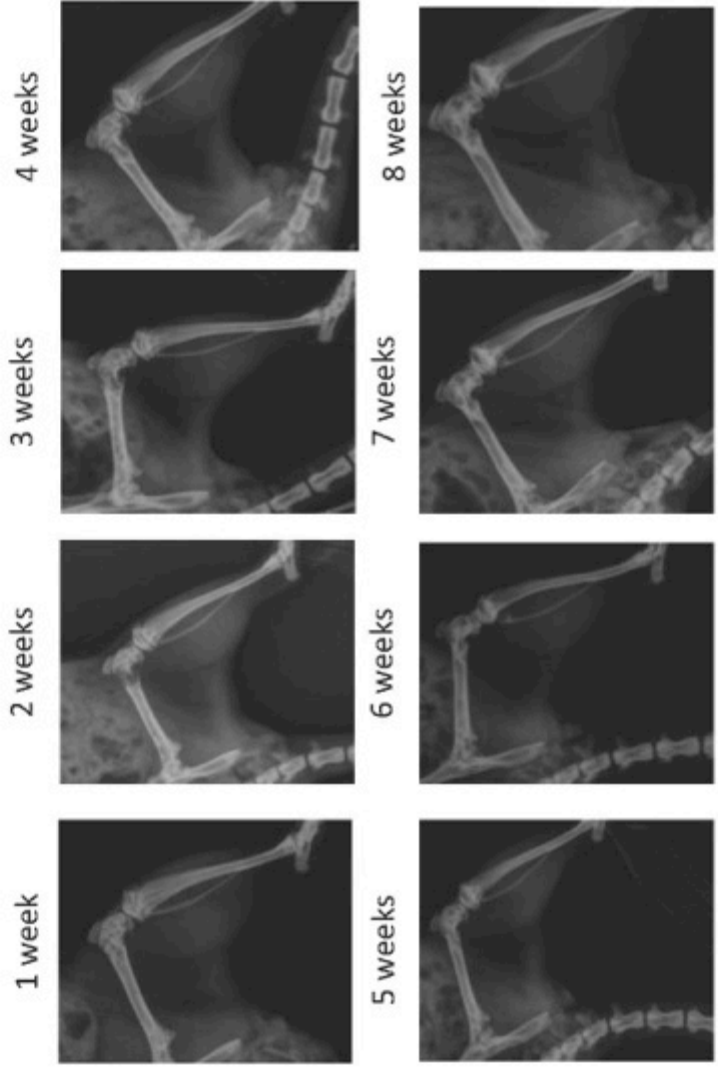
## 79 - Intraosseous



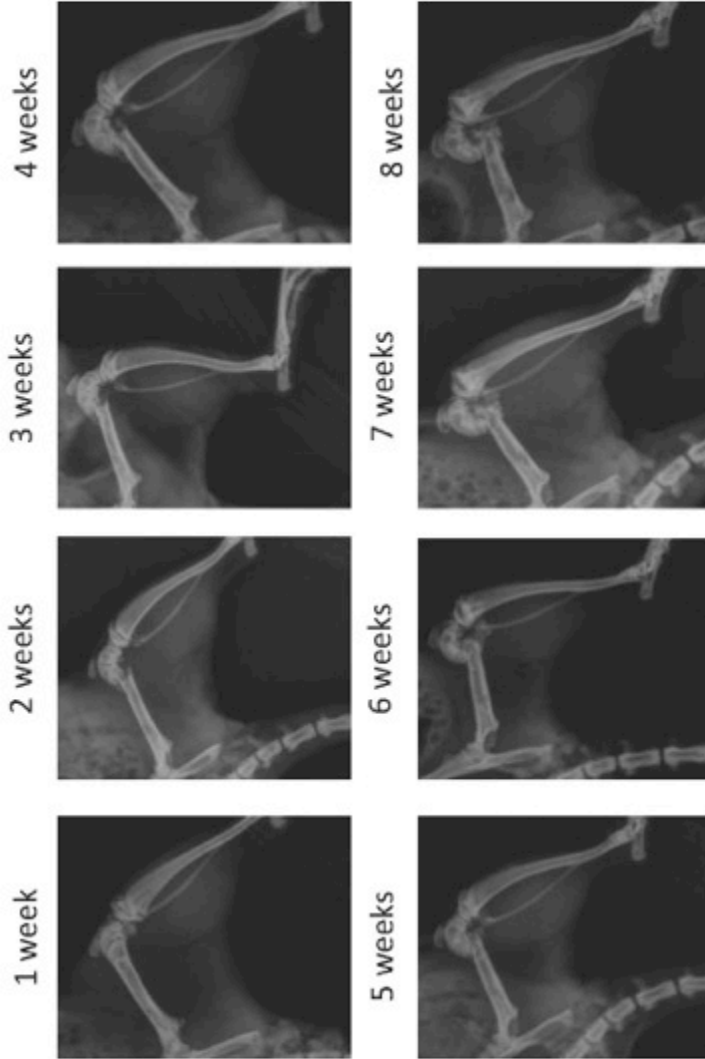
80 - Intraosseous



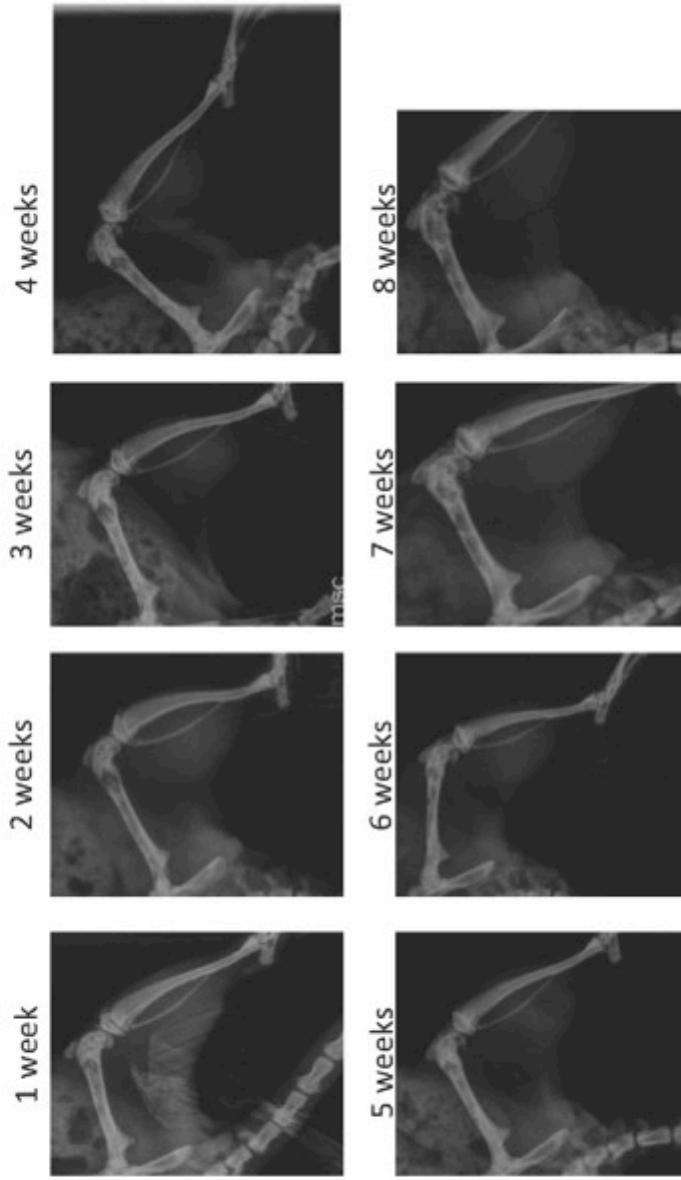
81 - IV



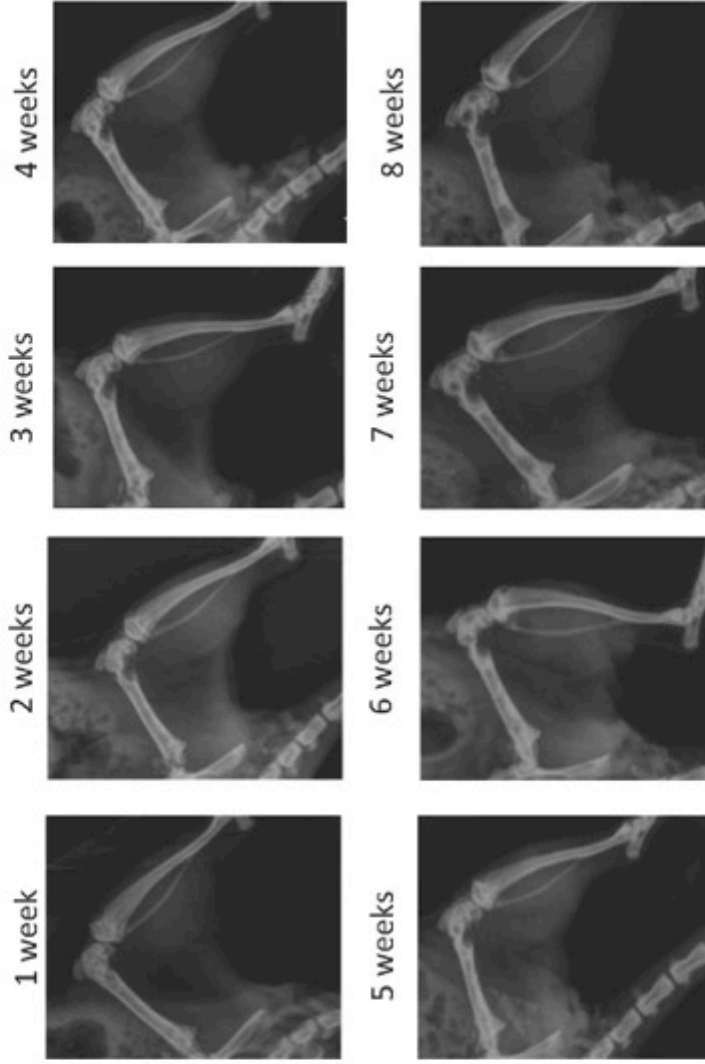
82 - IV



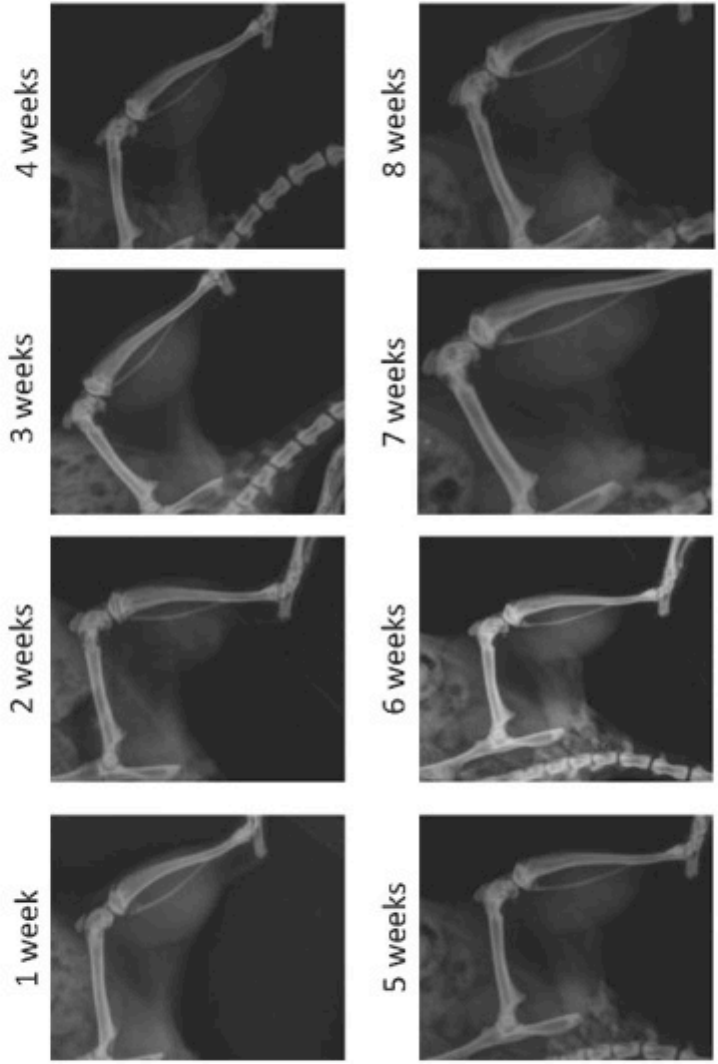
83 - IV



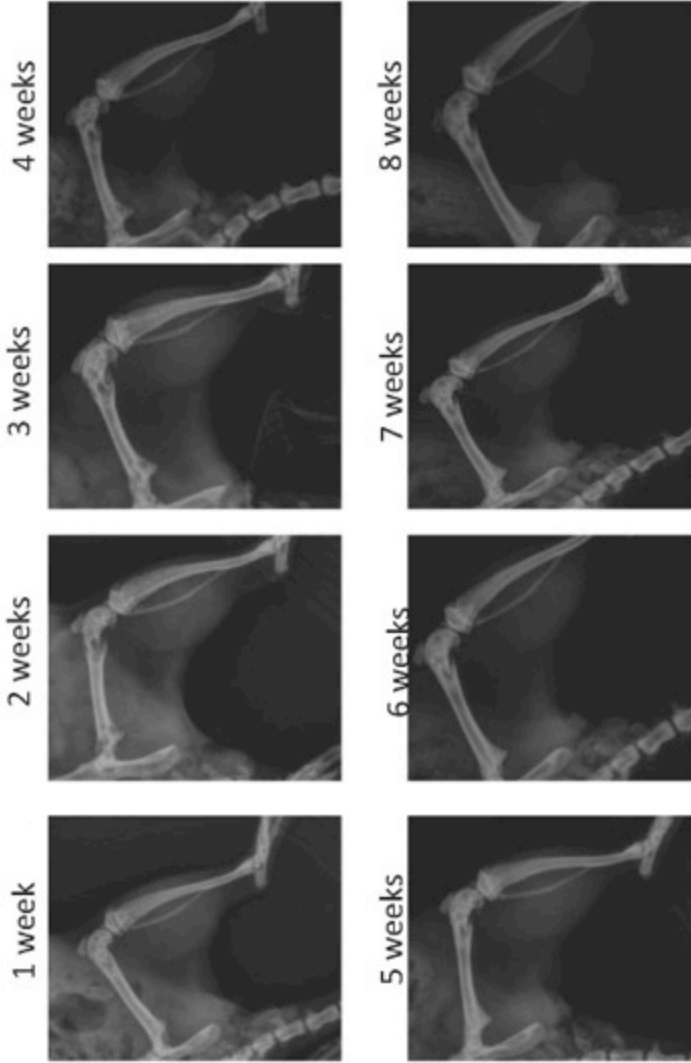
84 - IV



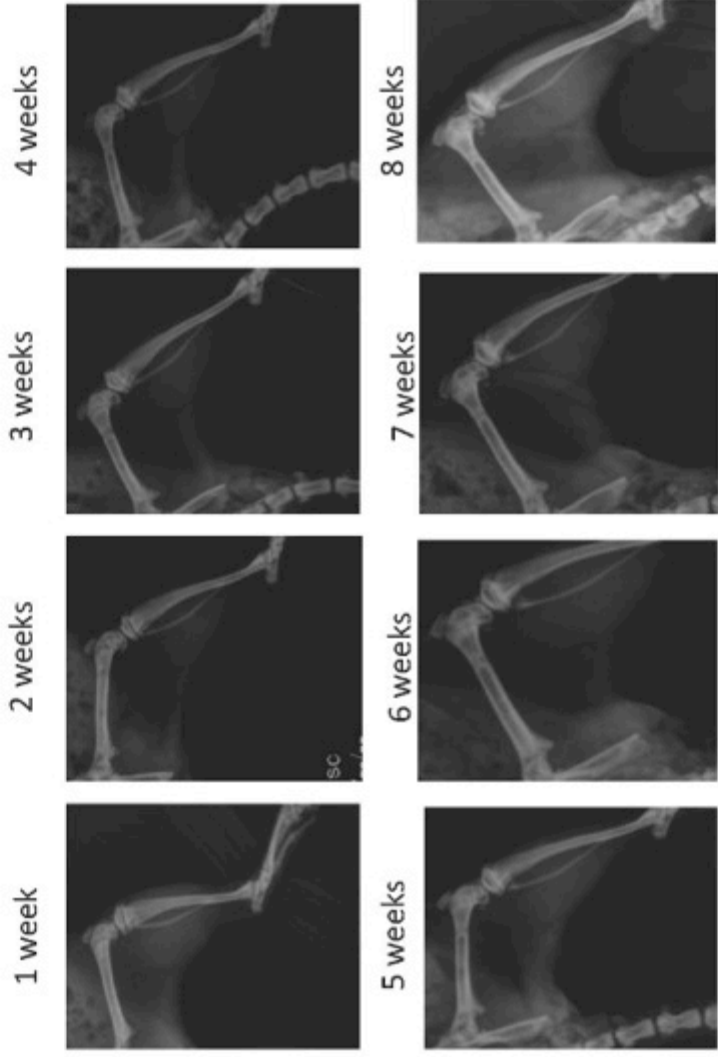
85 - IV



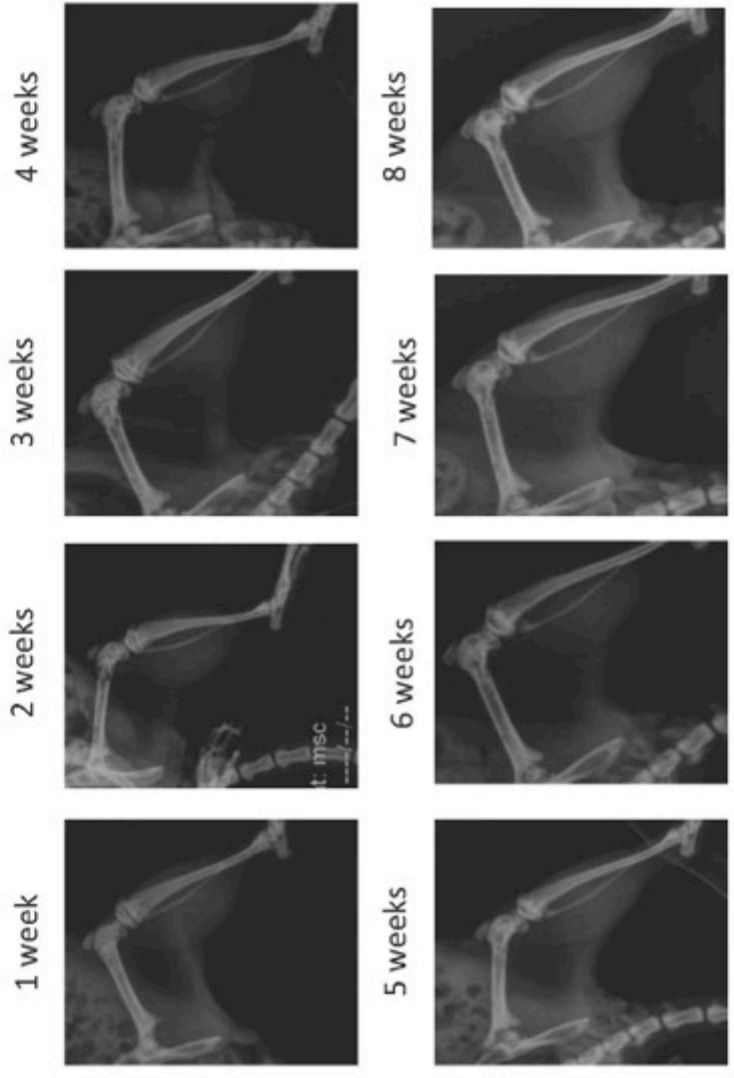
86 - IV



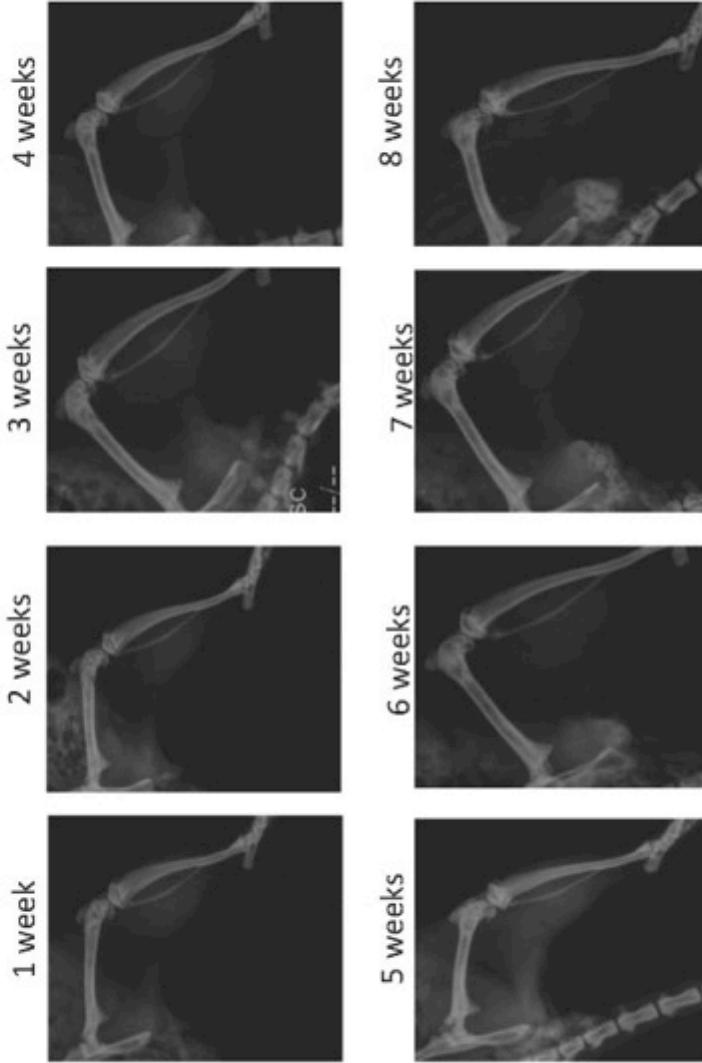
87 - Intraosseous



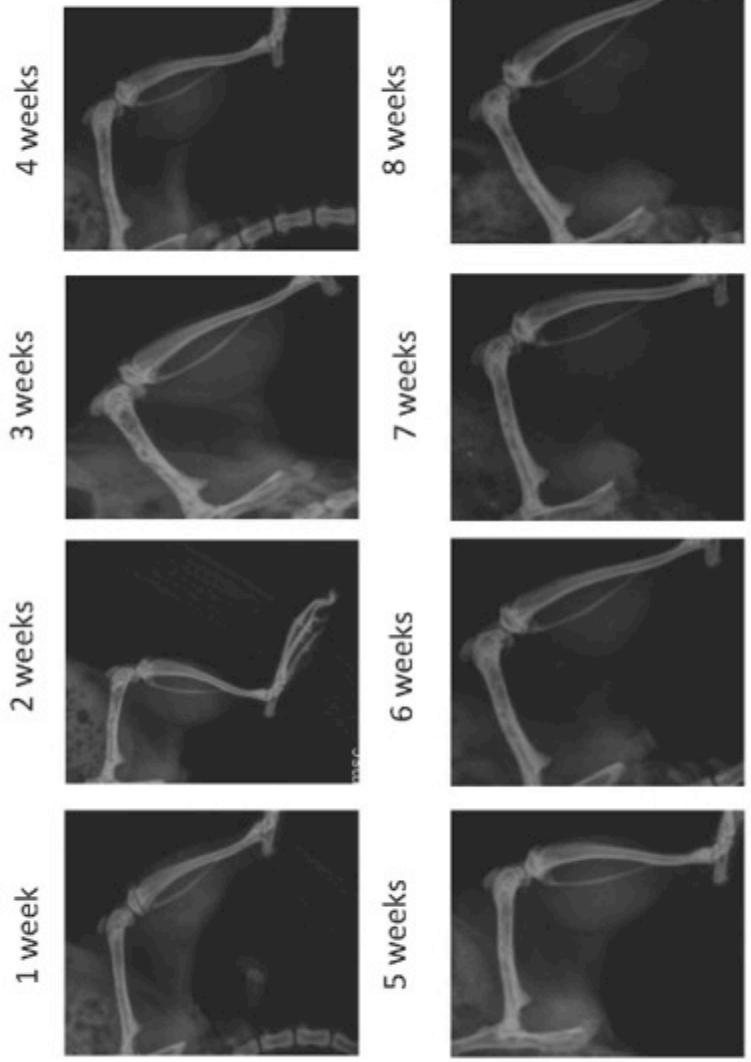
88 - Intraosseous



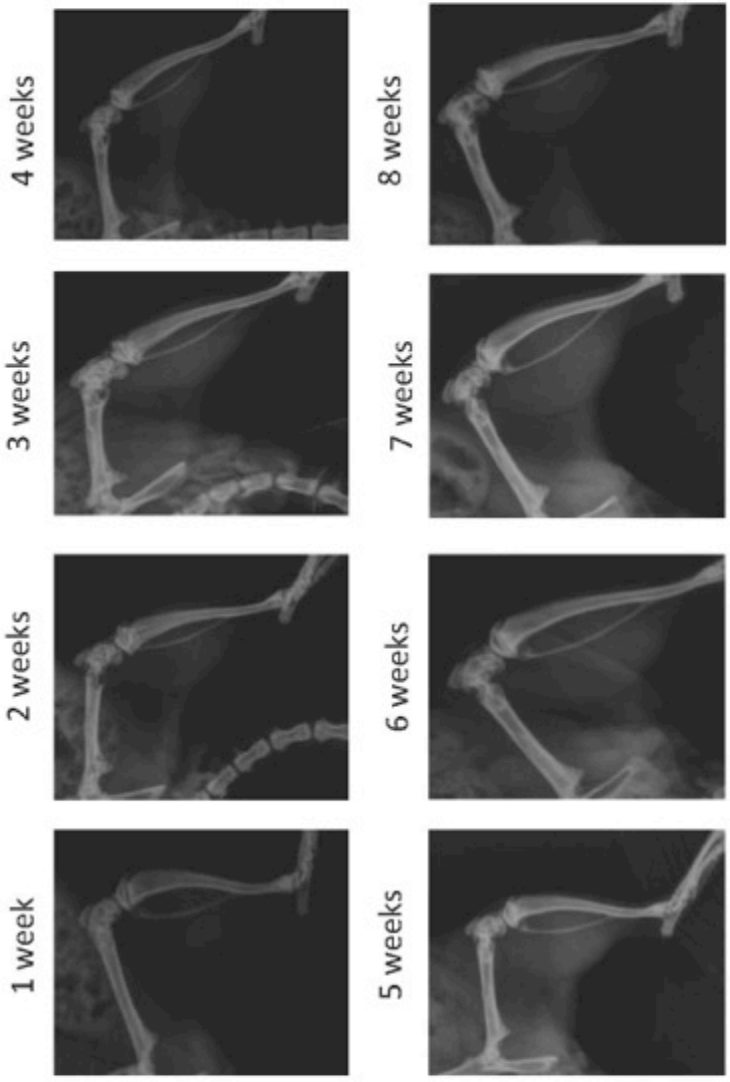
90 - Intraosseous



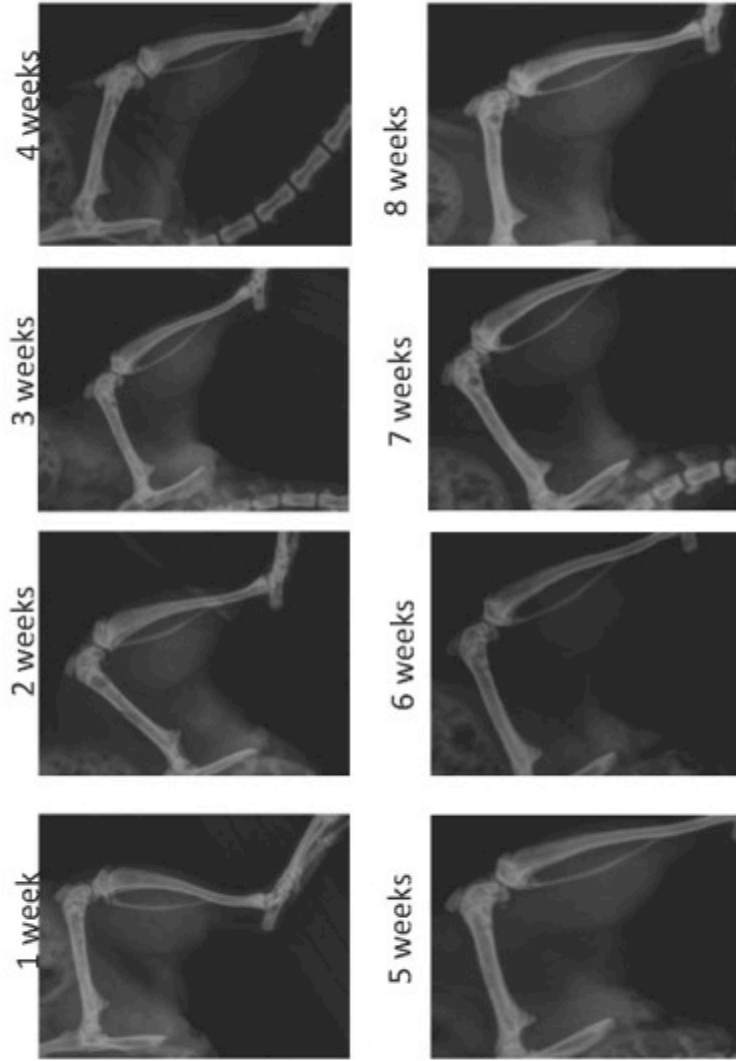
91 - Intraosseous



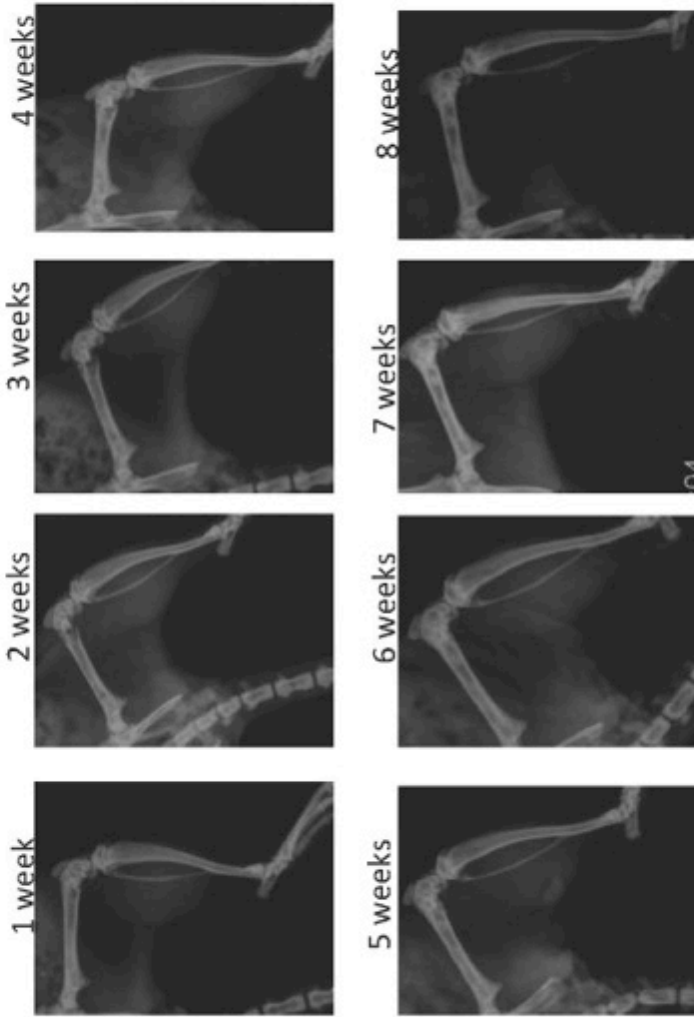
92 - Intraosseous



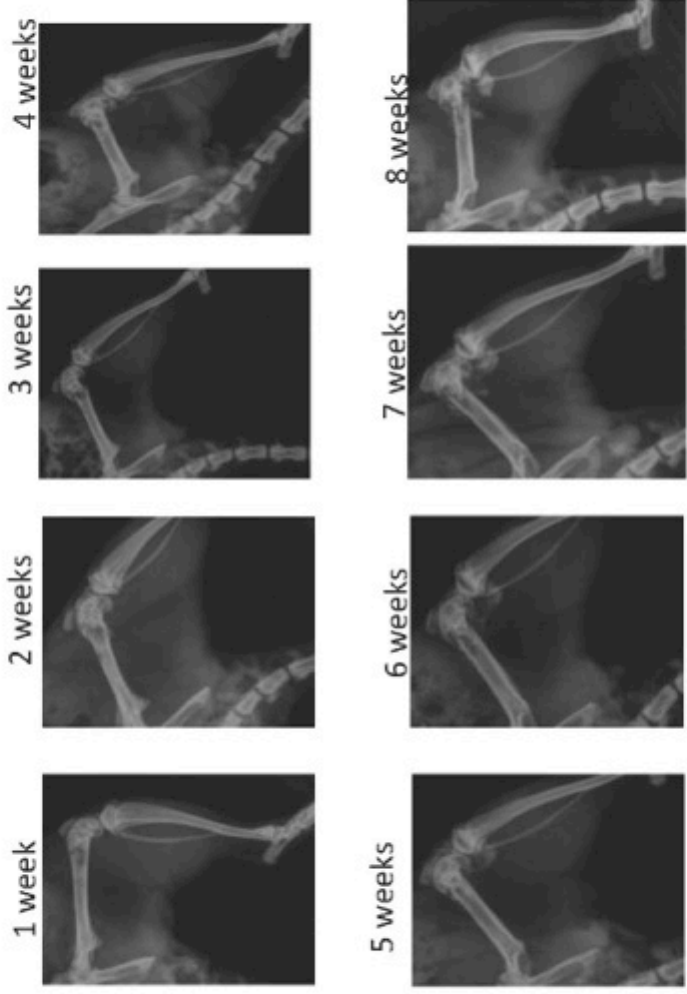
94 – SRT Only



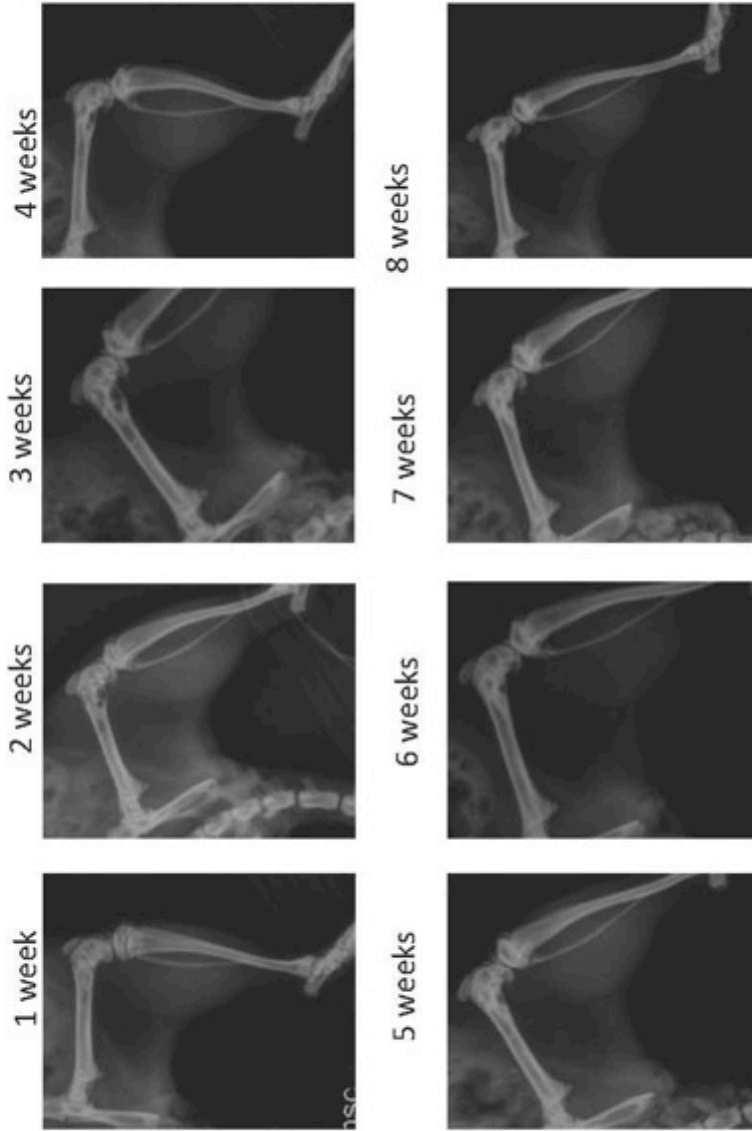
95 – SRT Only



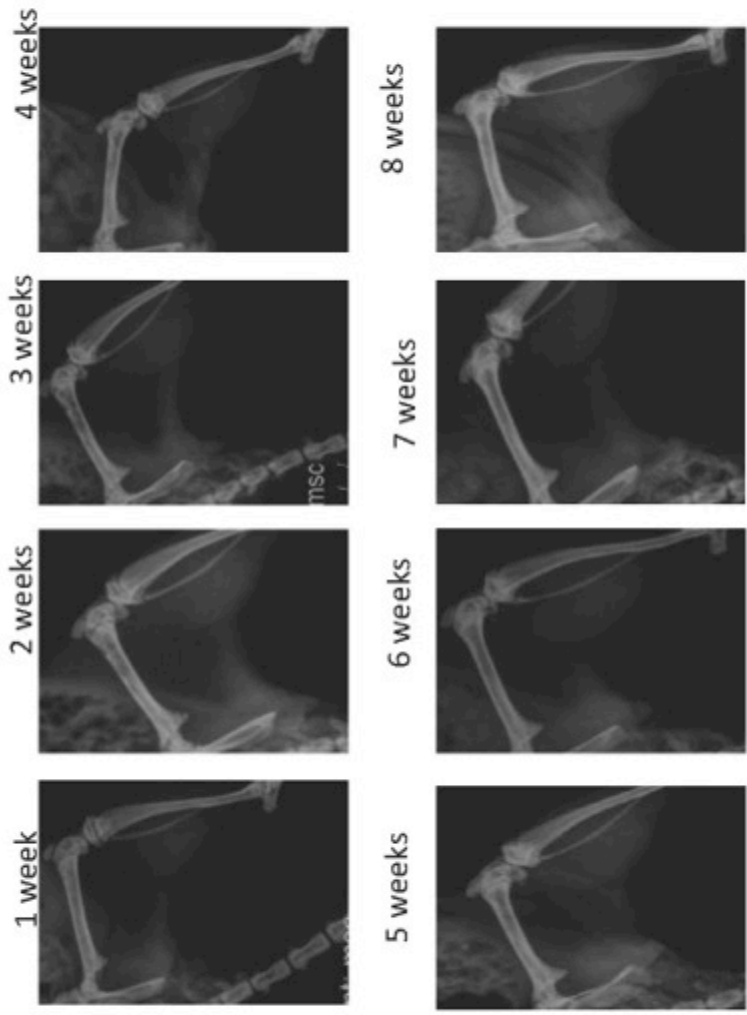
96 – SRT Only



97 – SRT Only



98 – SRT Only



99 – SRT Only

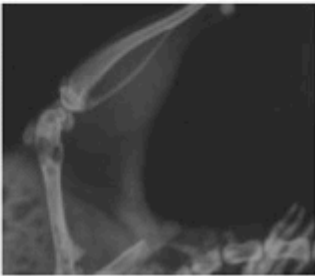
1 week



2 weeks



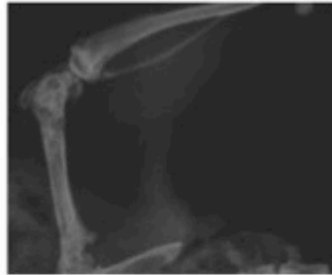
3 weeks



4 weeks



5 weeks



6 weeks



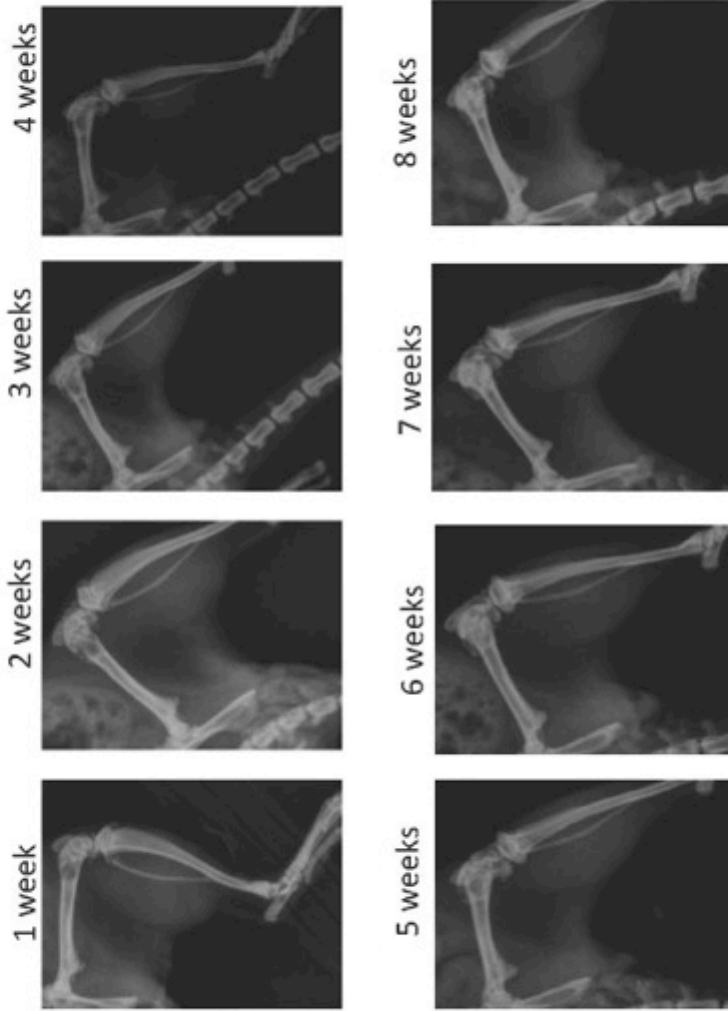
7 weeks



8 weeks

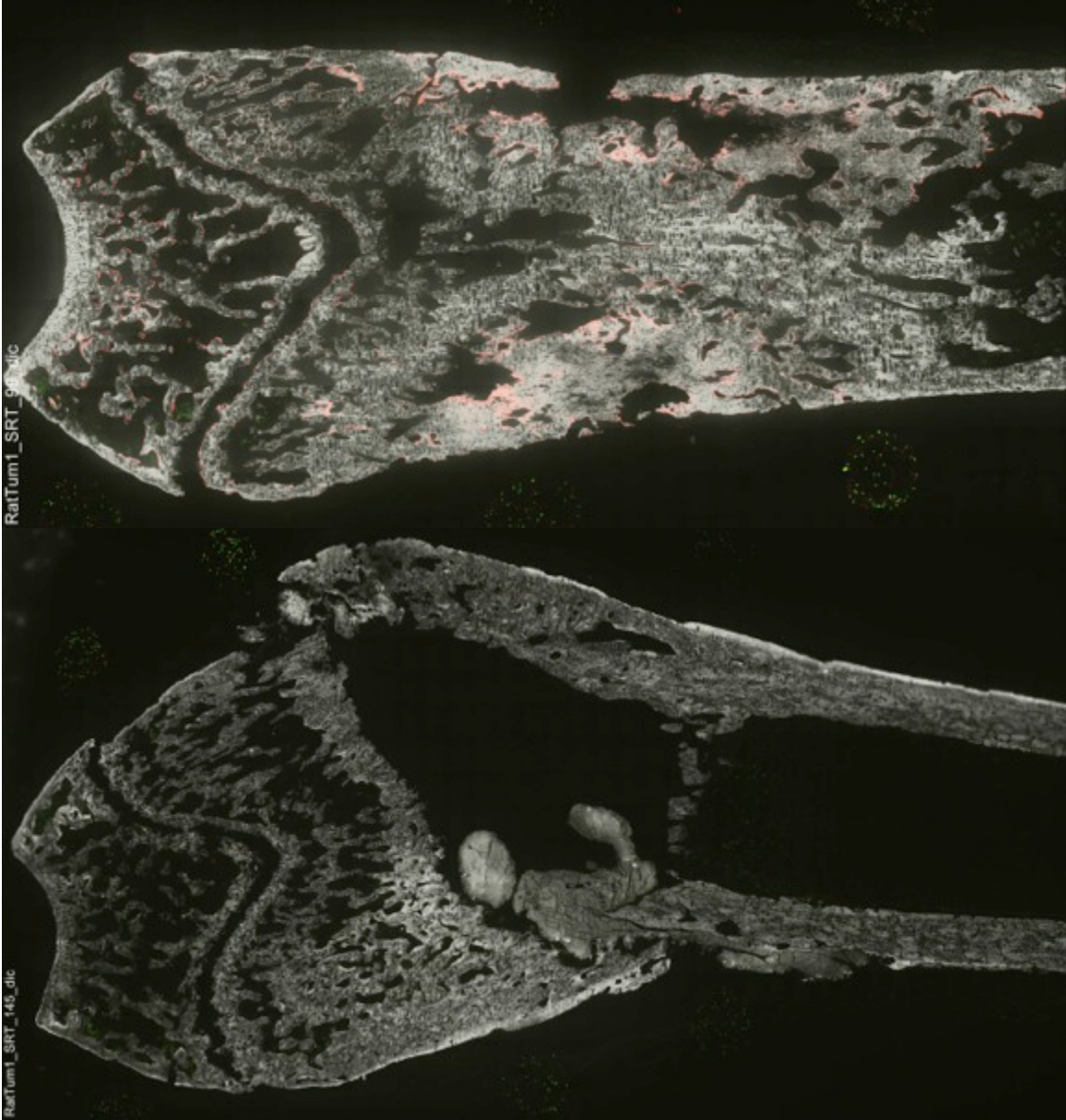


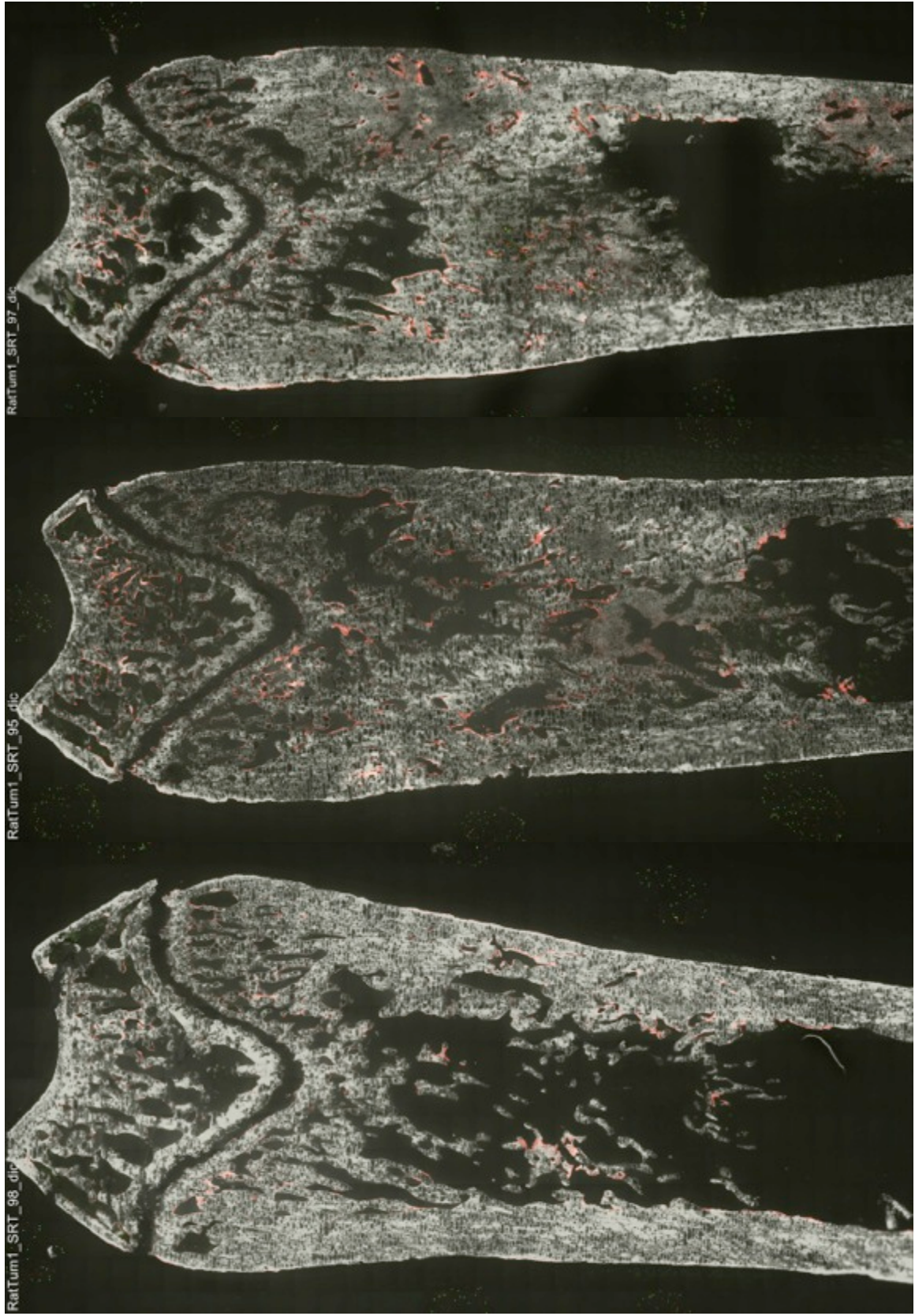
145 – SRT Only

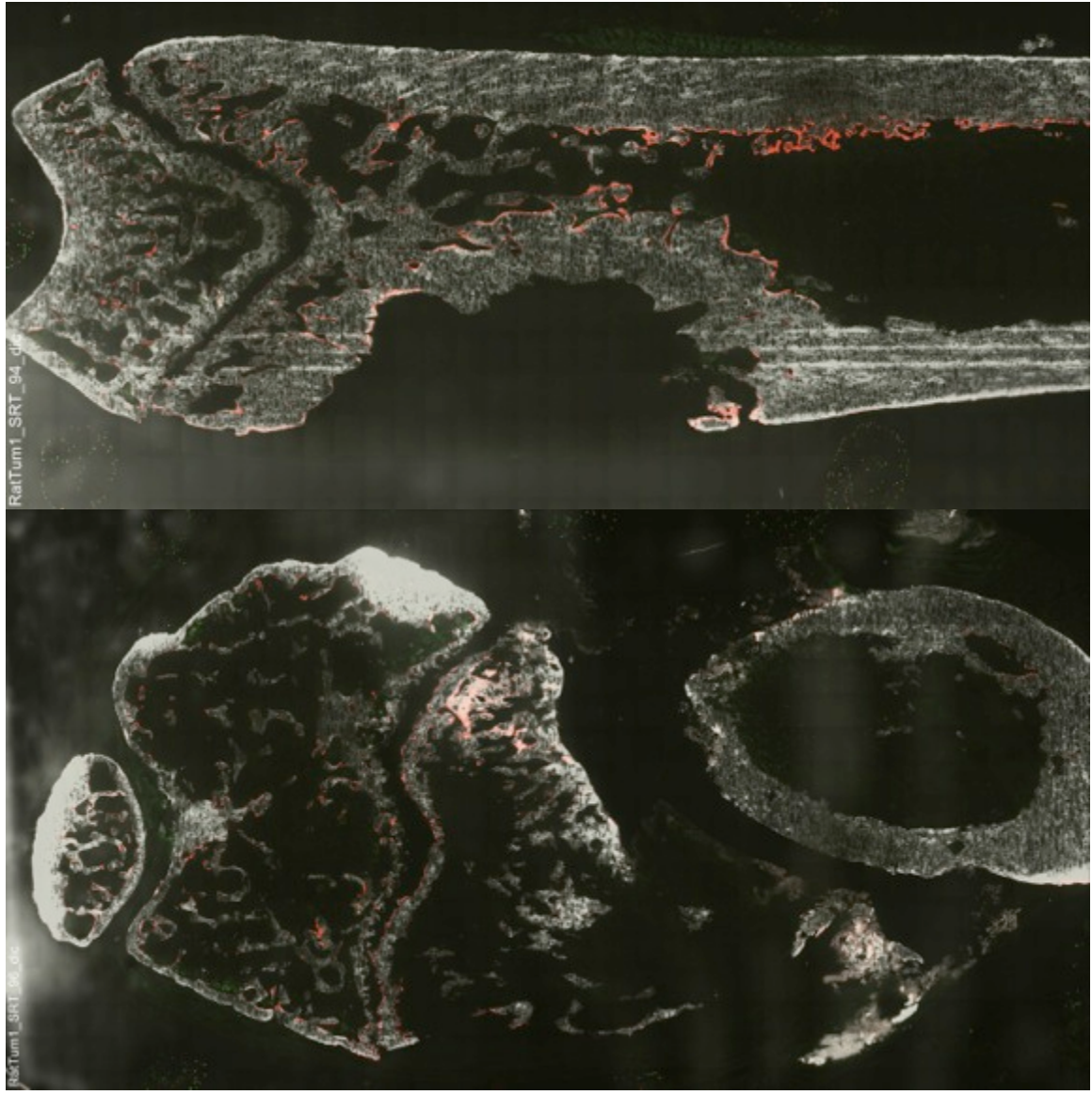


10.4 Histology

Alizarin Staining



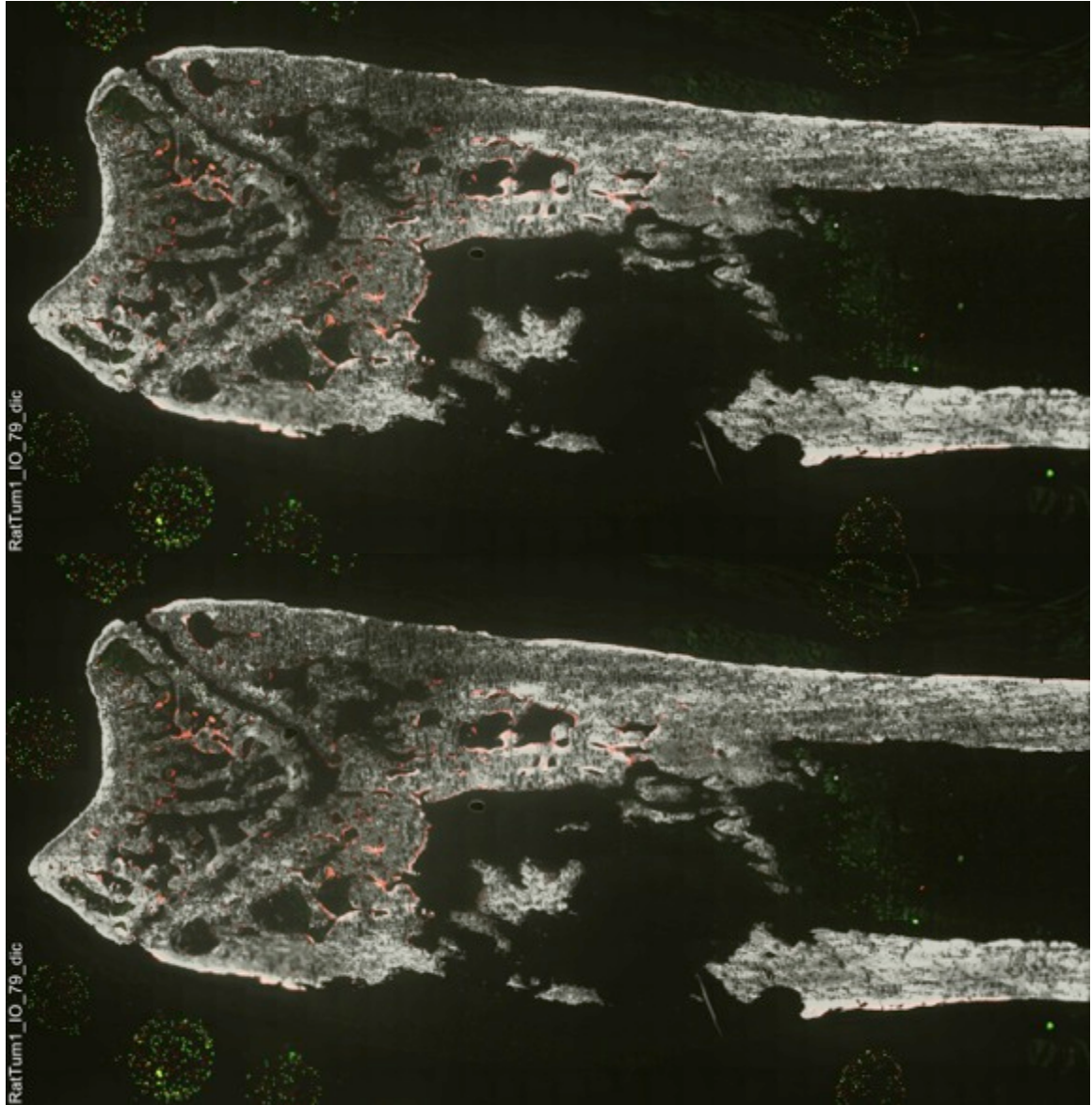




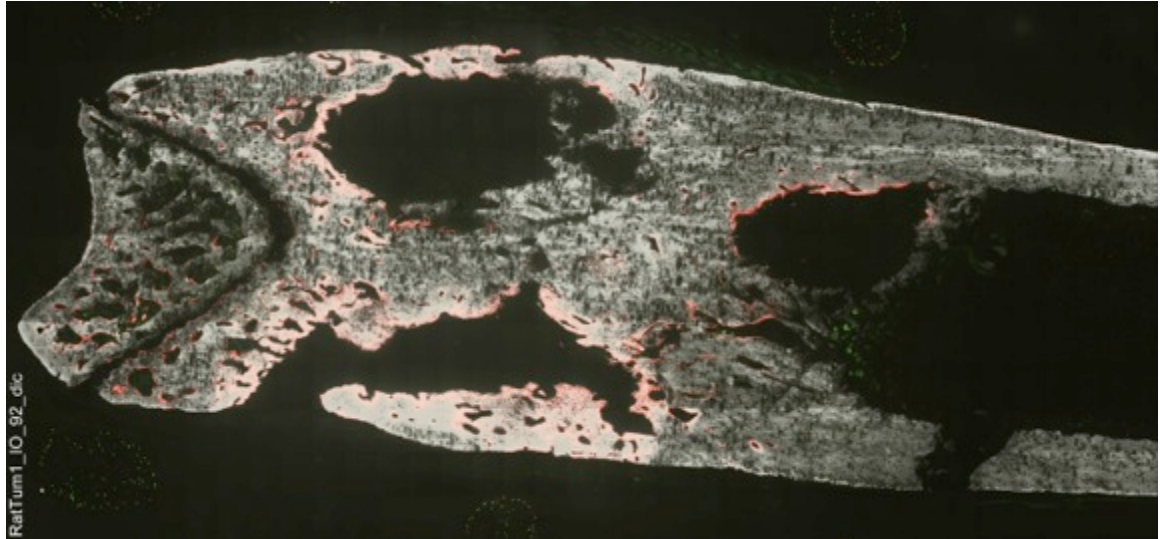




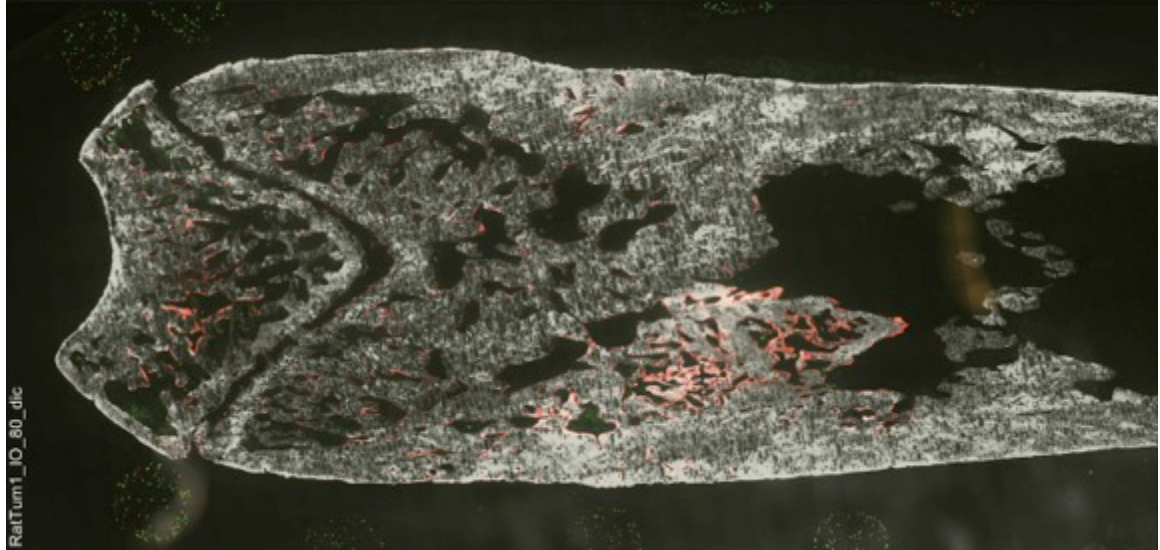






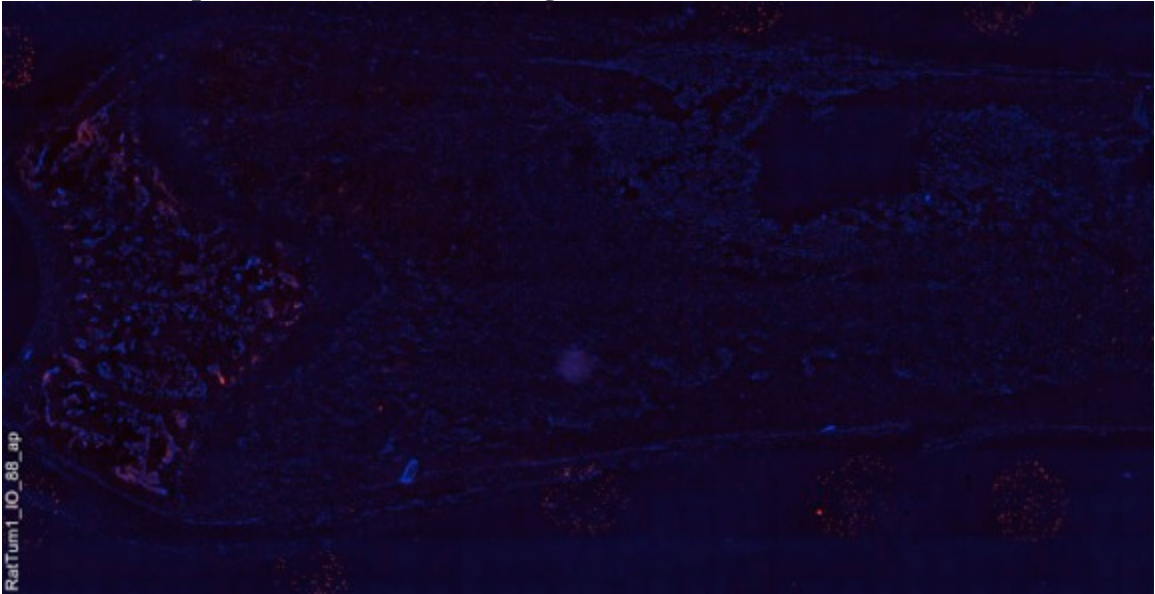


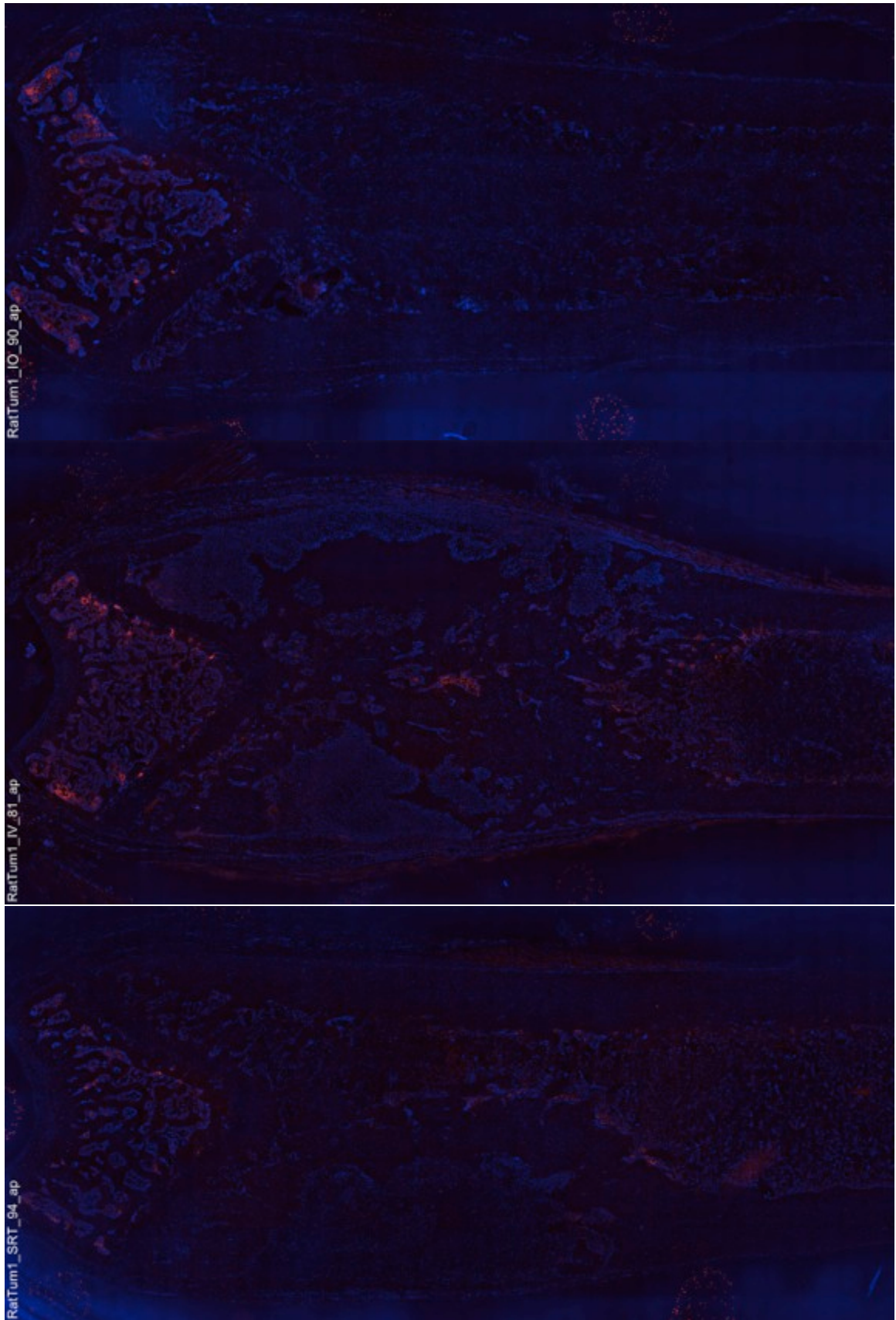
RaiTum1\_IO\_92\_dic

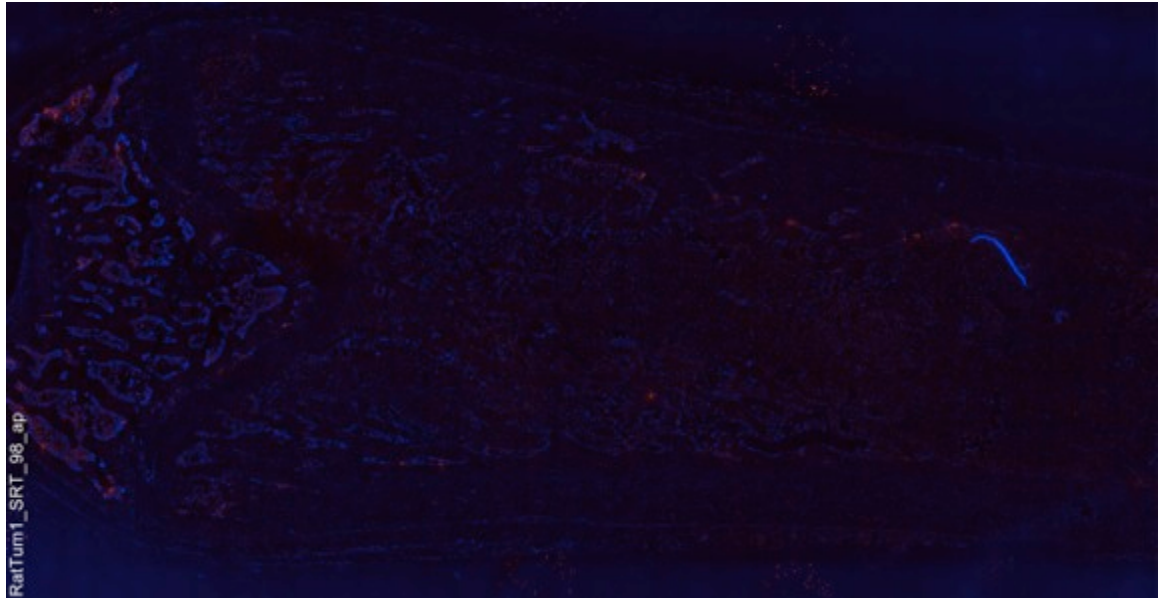
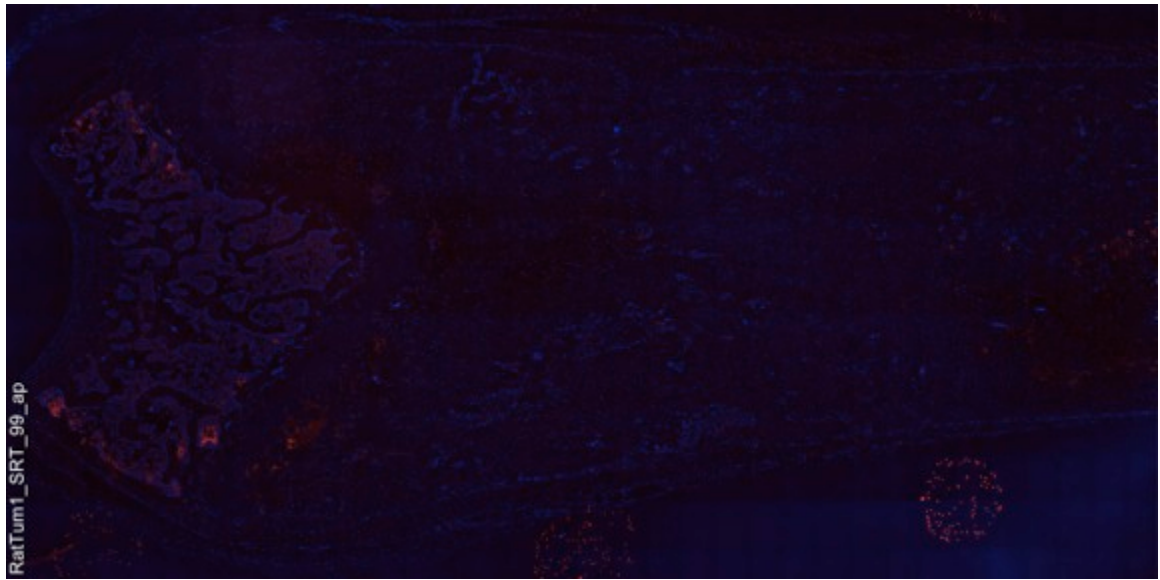


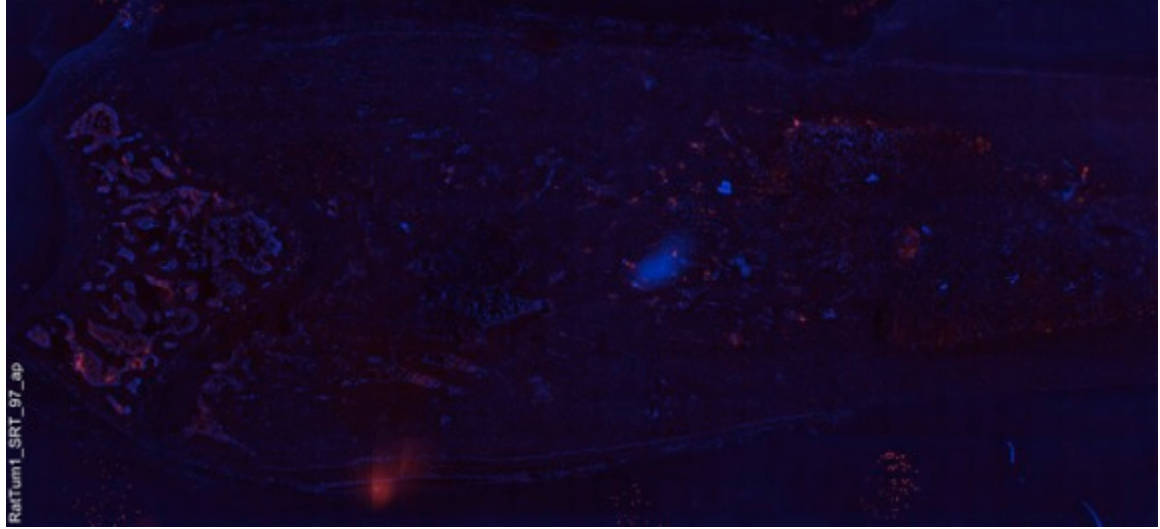
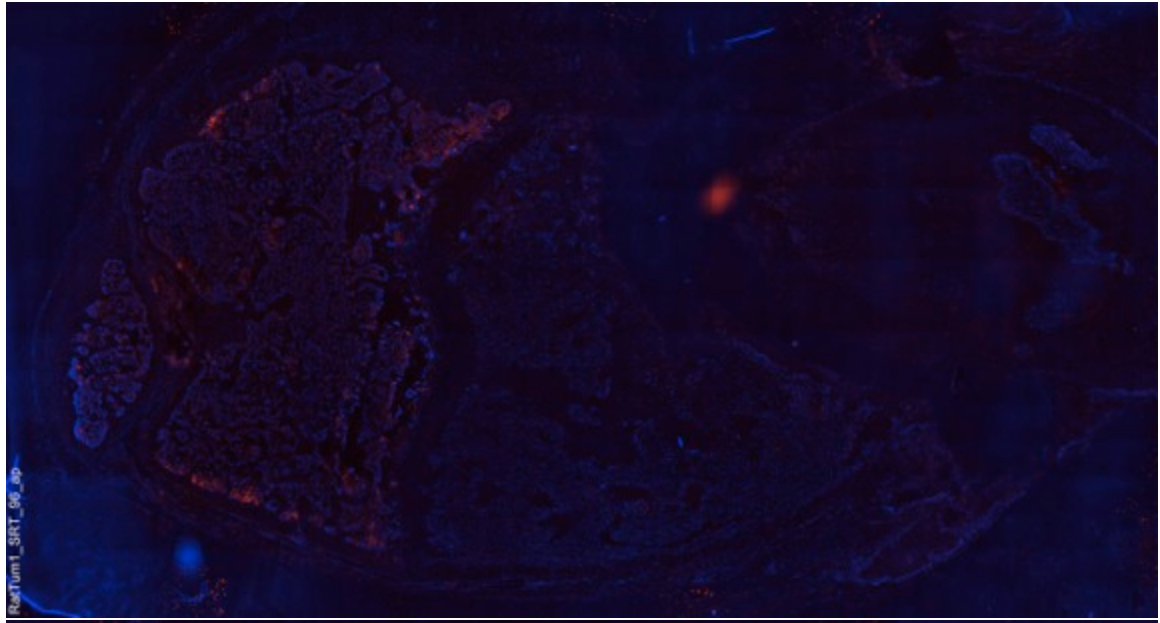
RaiTum1\_IO\_80\_dic

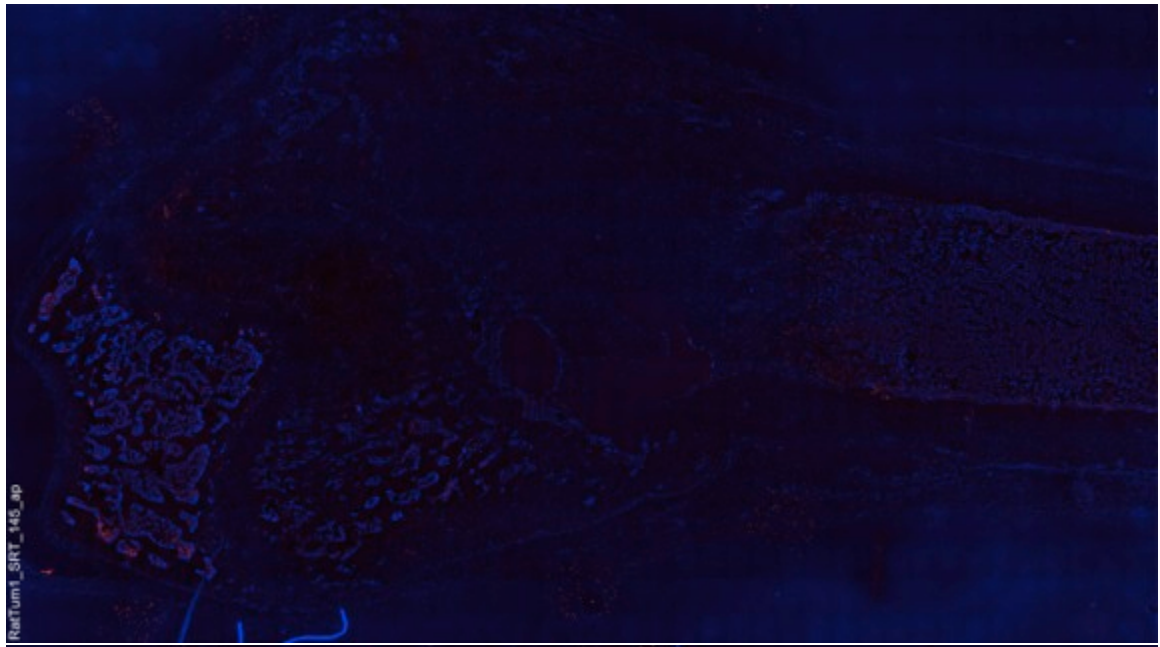
**Alkaline Phosphatase and DAPI staining**

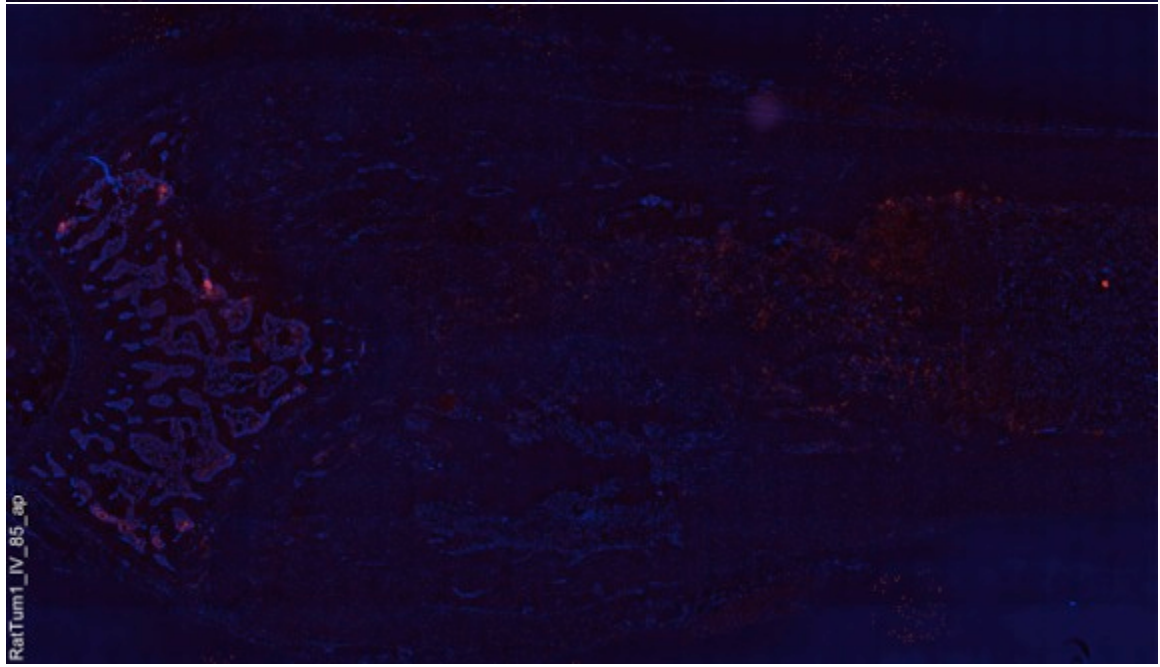
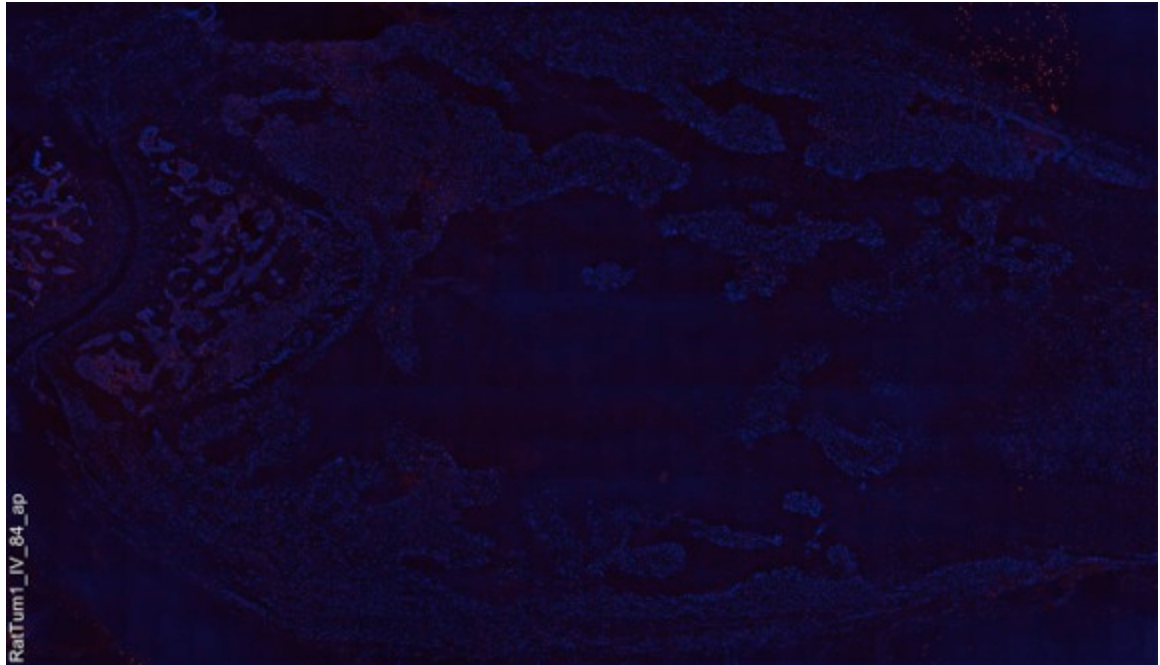


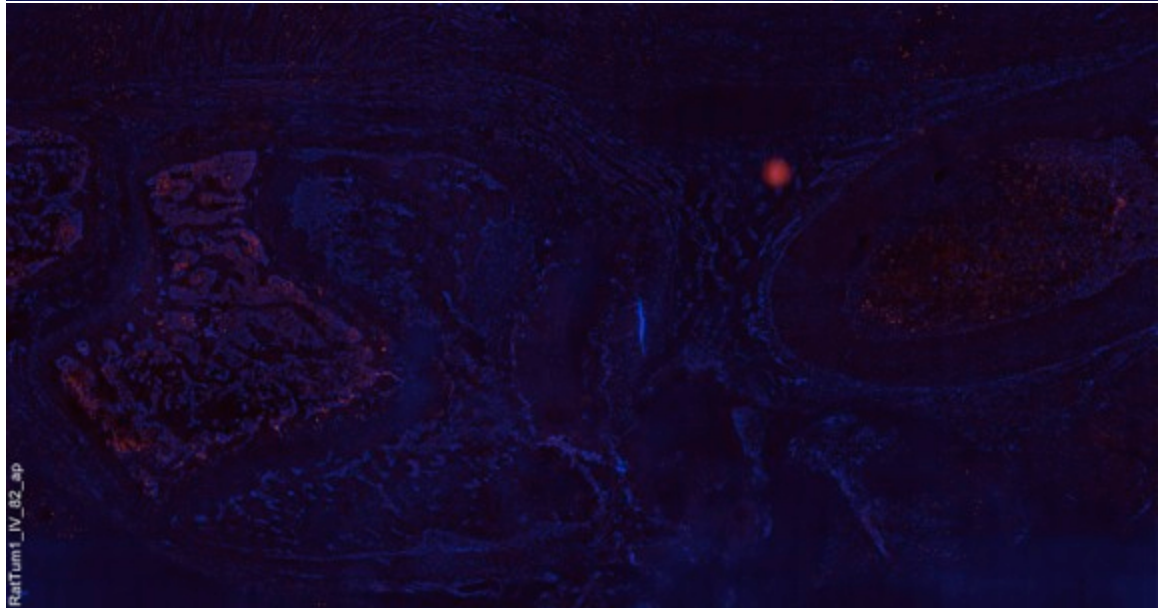


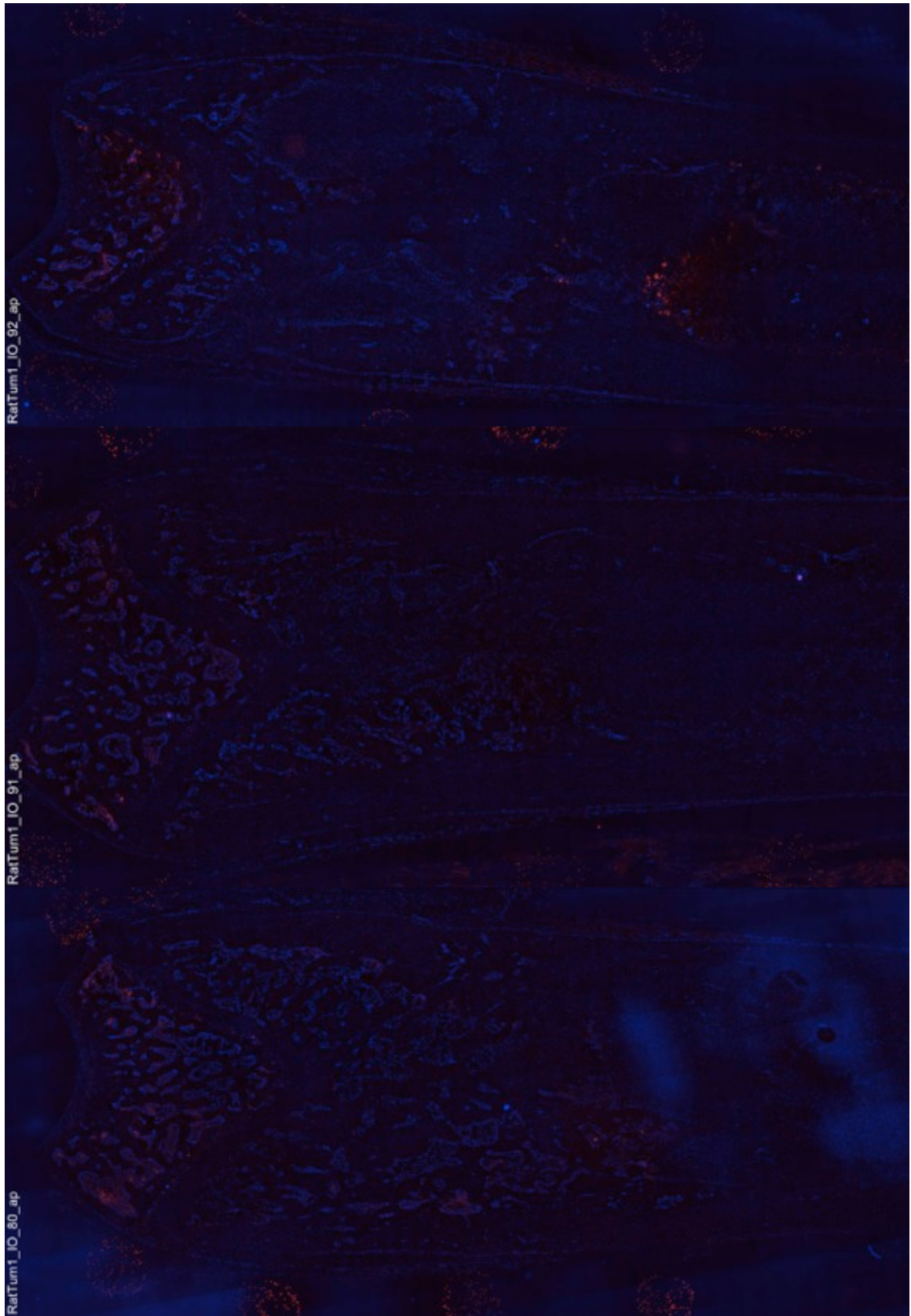


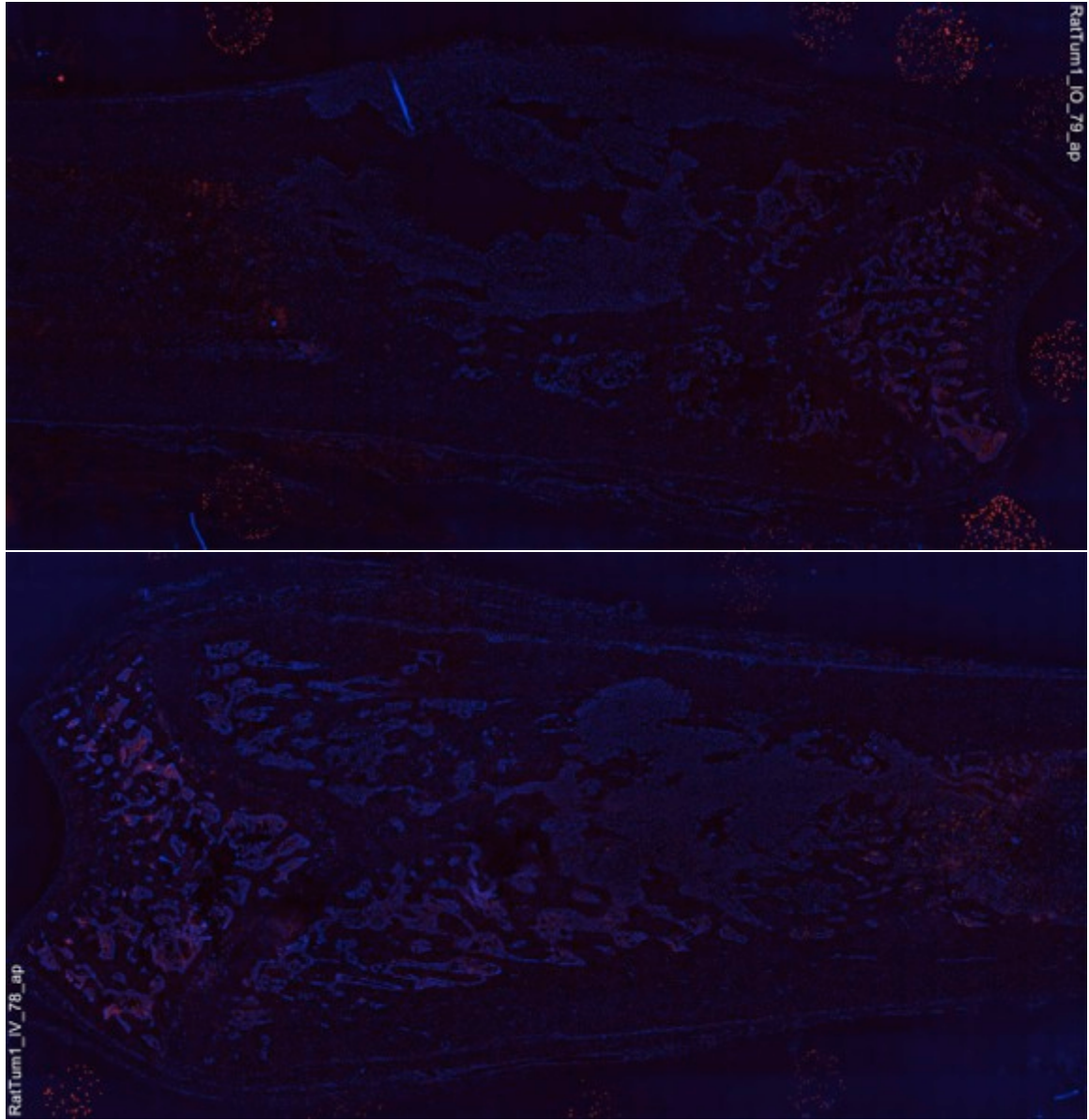


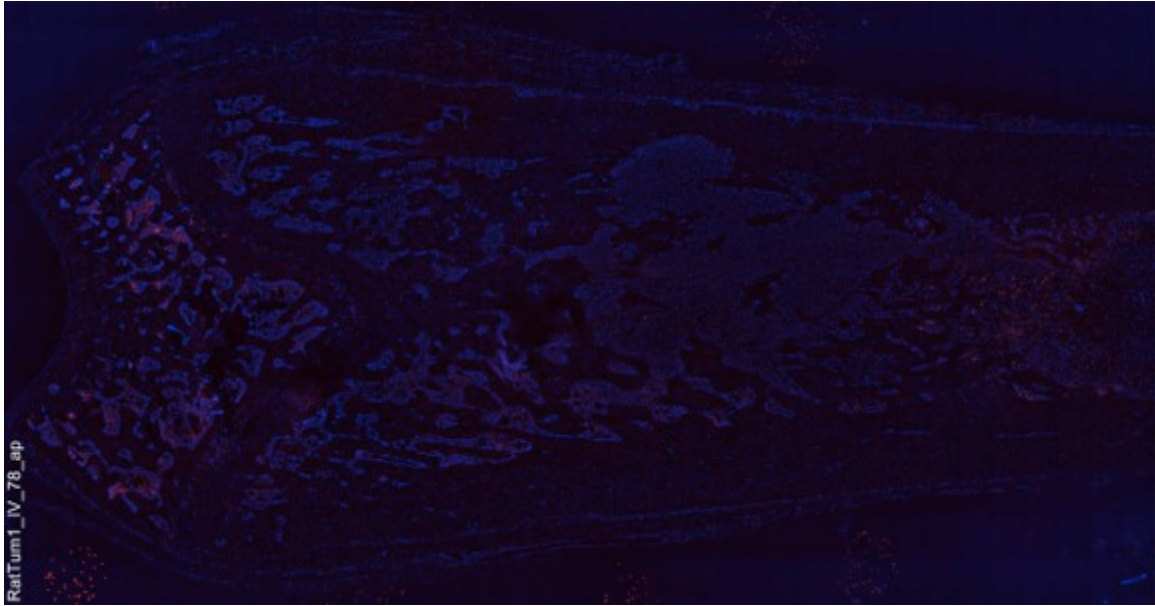




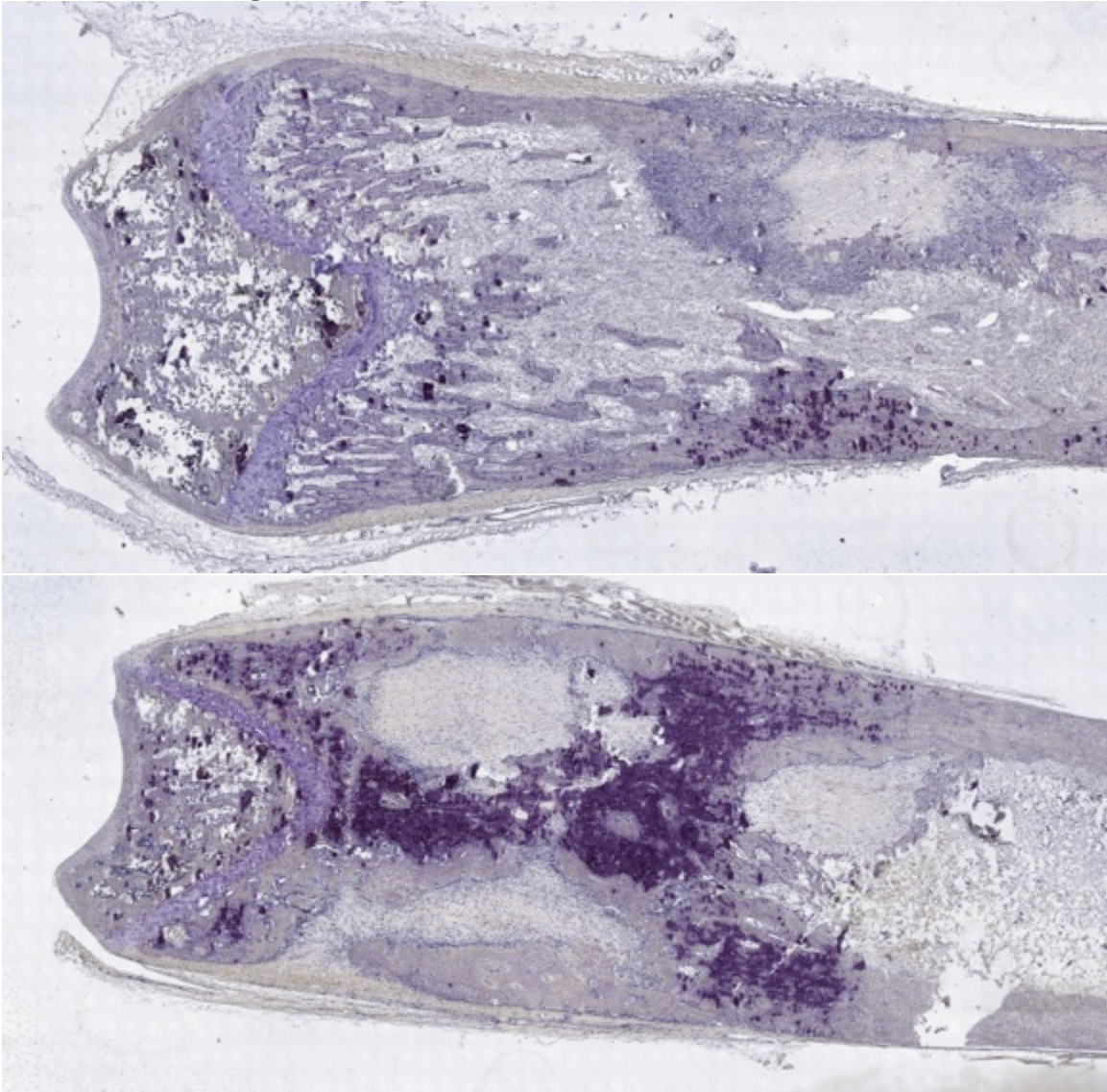


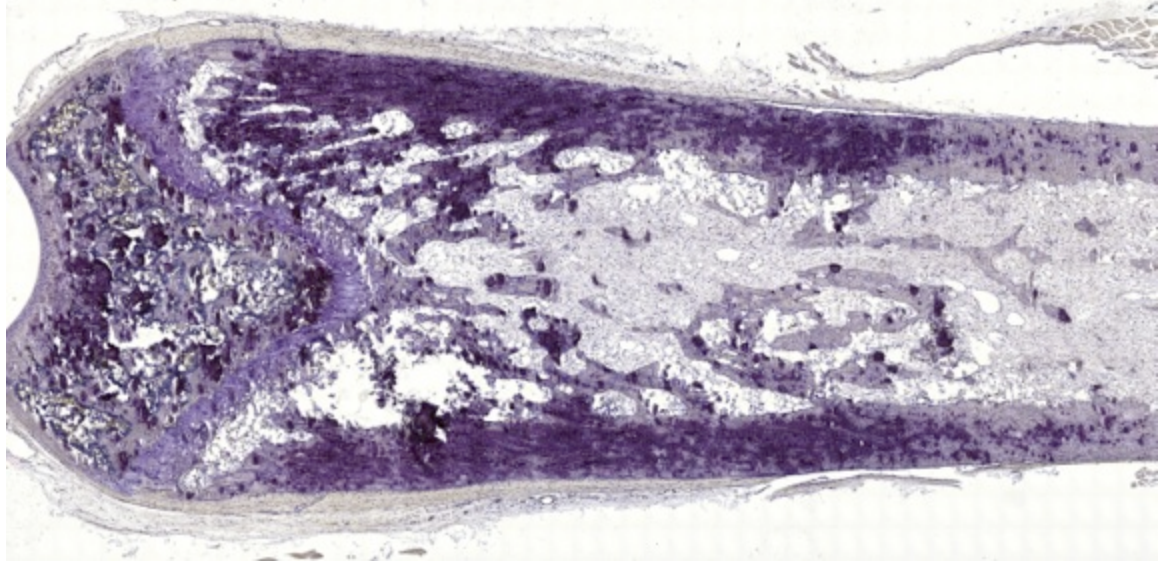
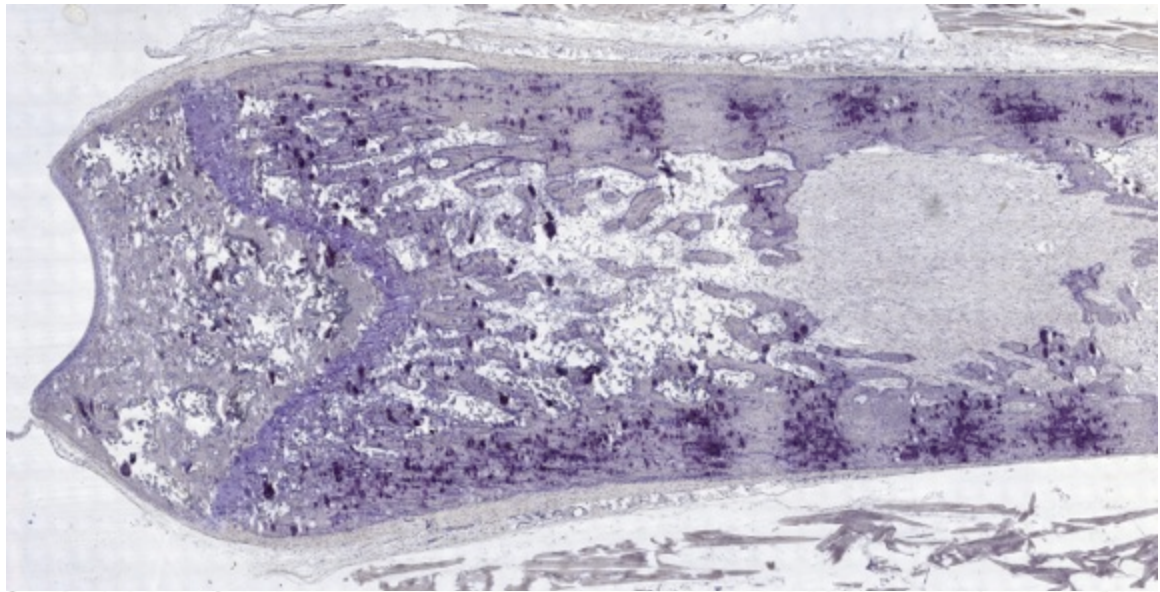


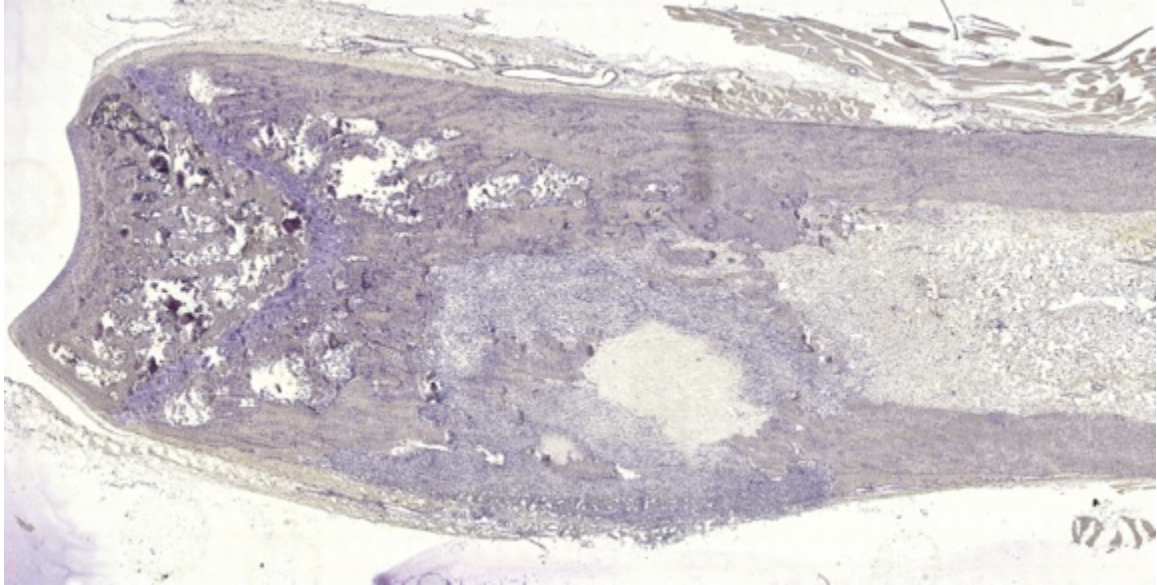
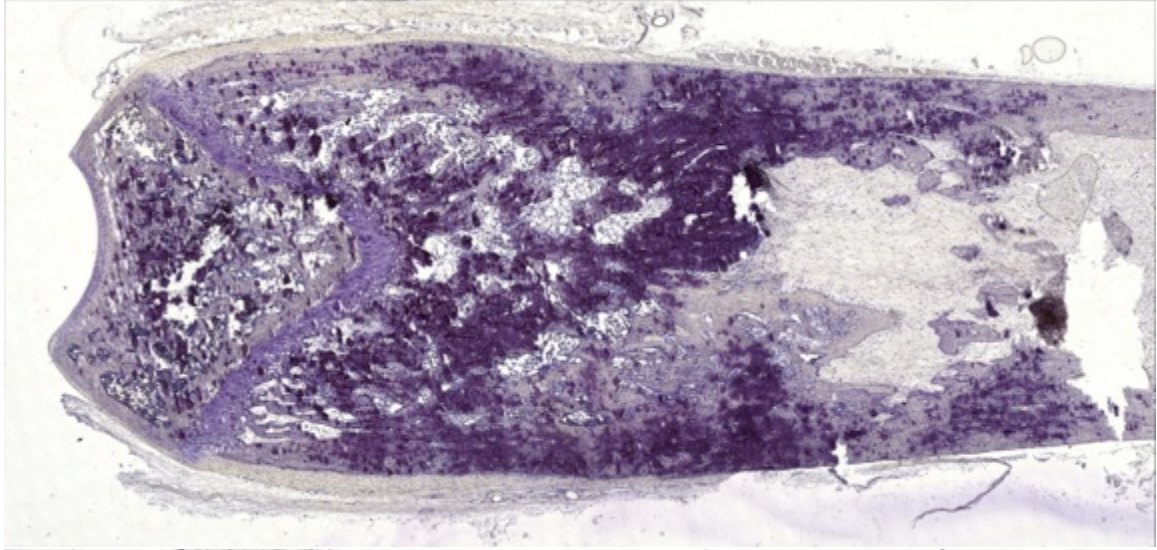


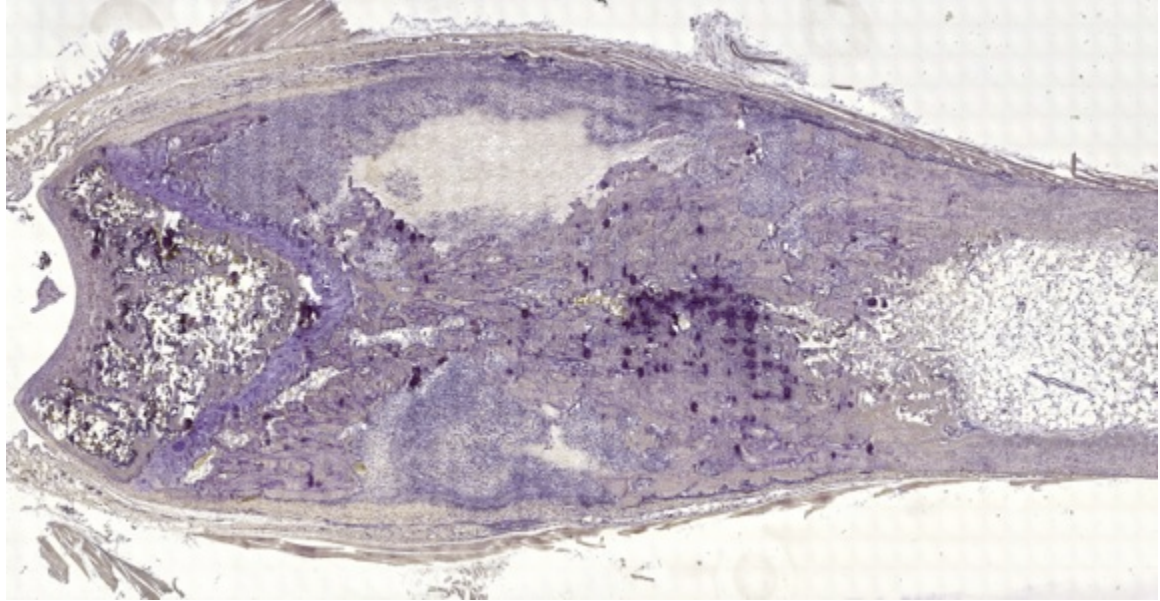
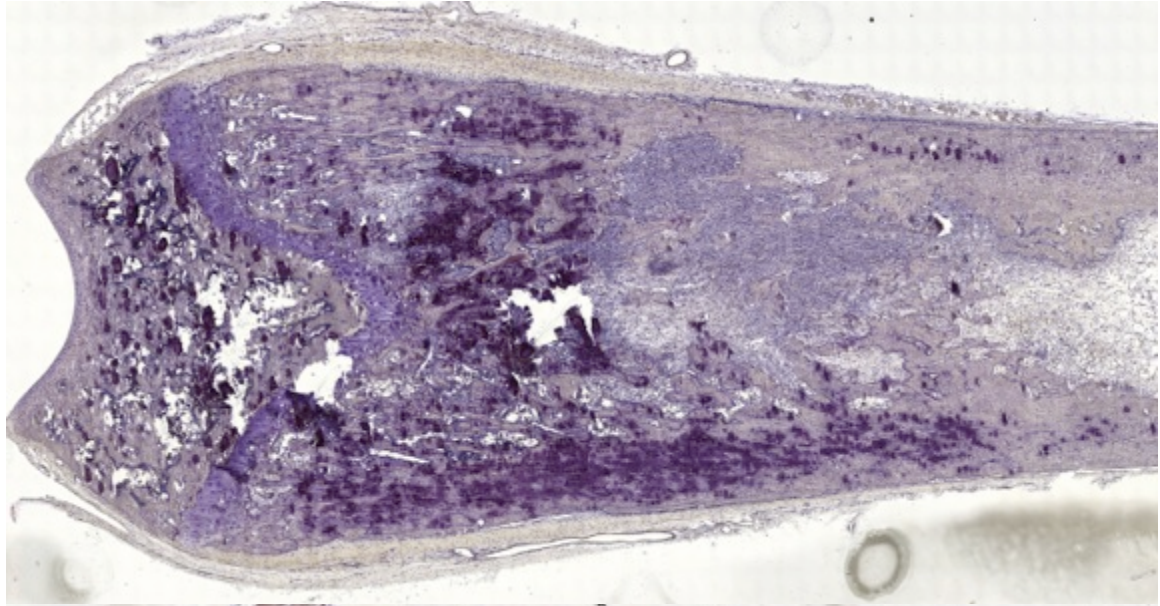


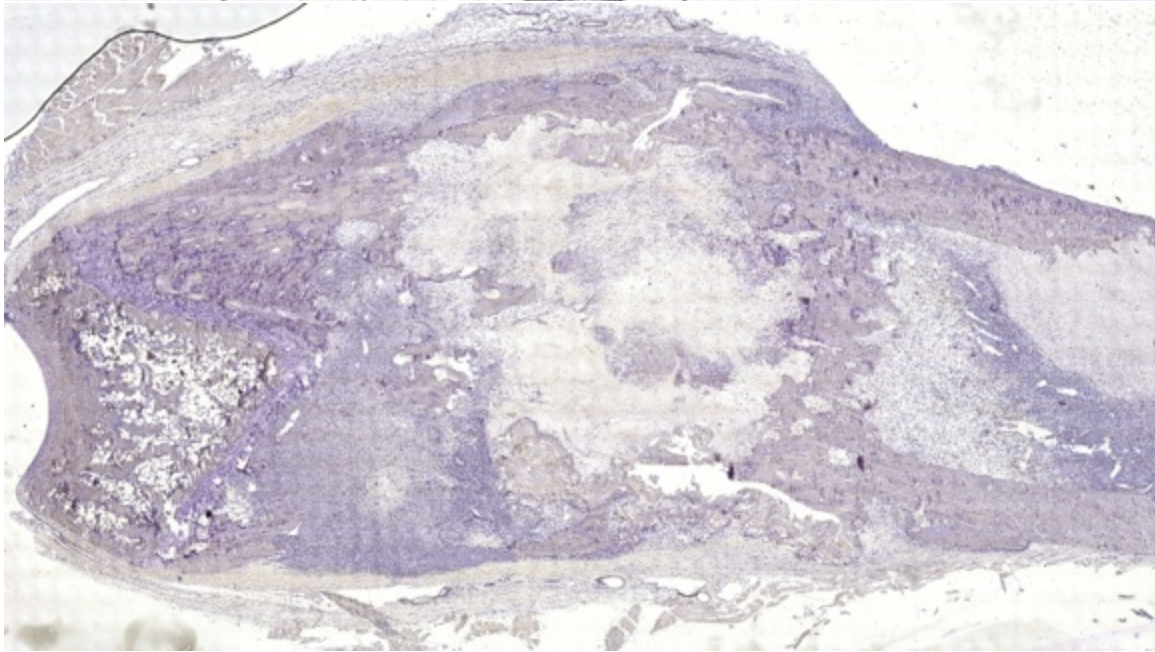
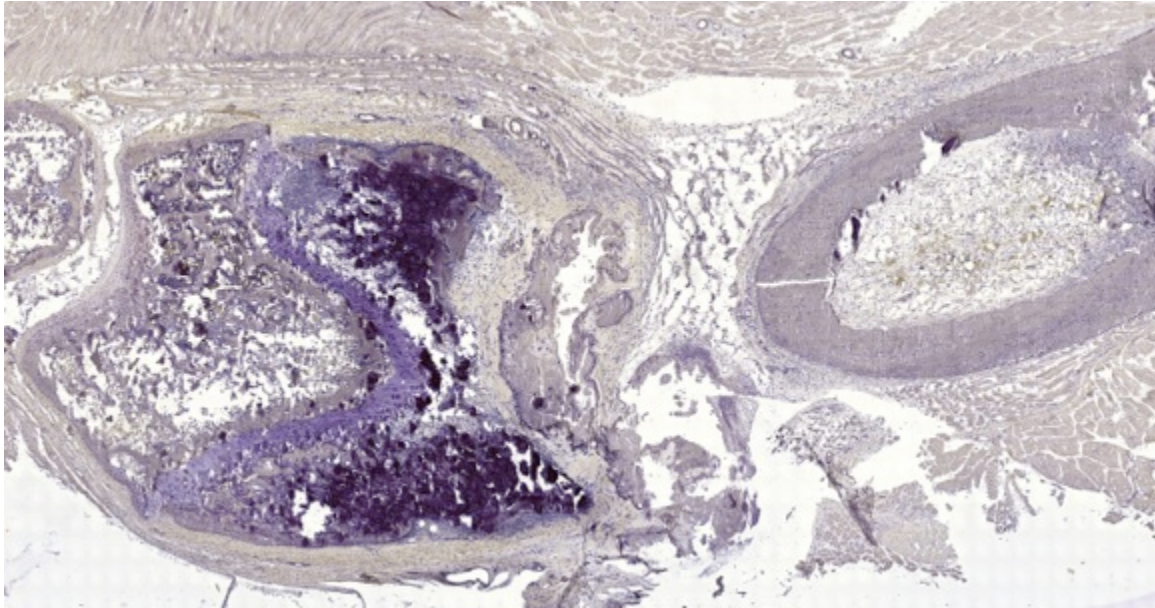
**Hematoxin Staining**

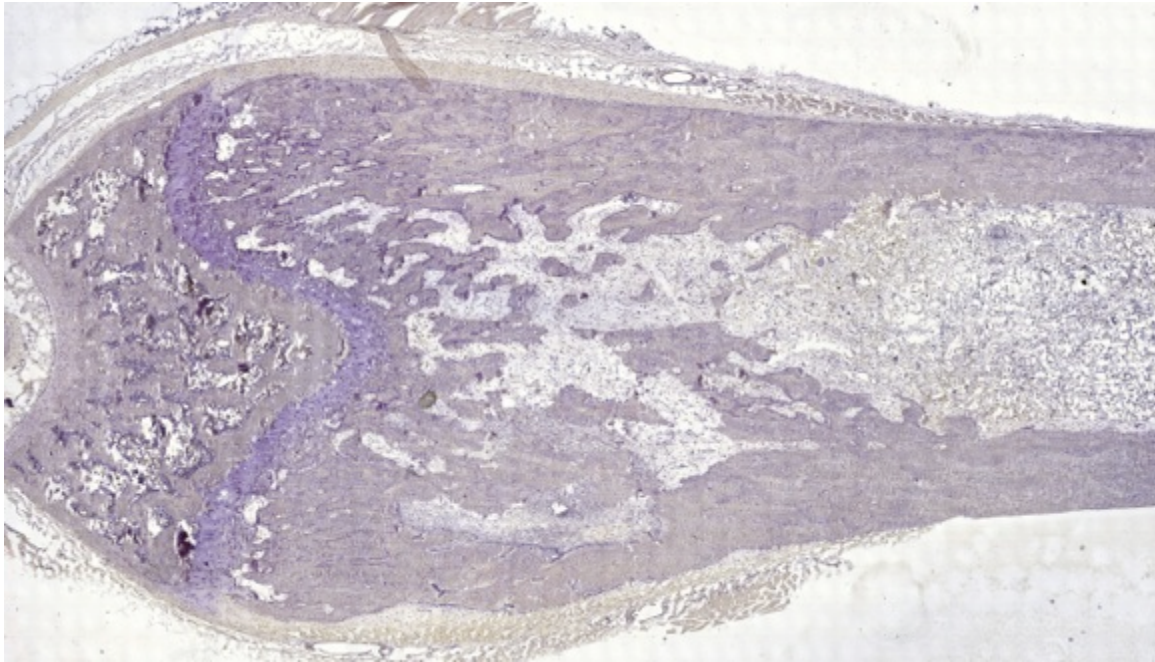
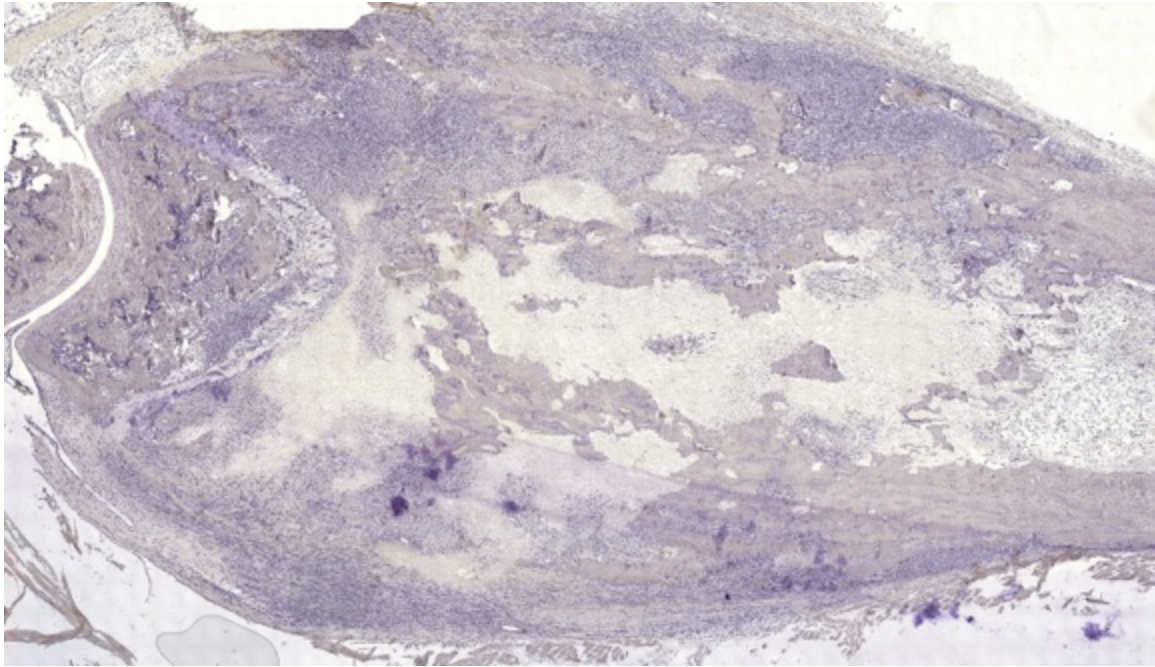


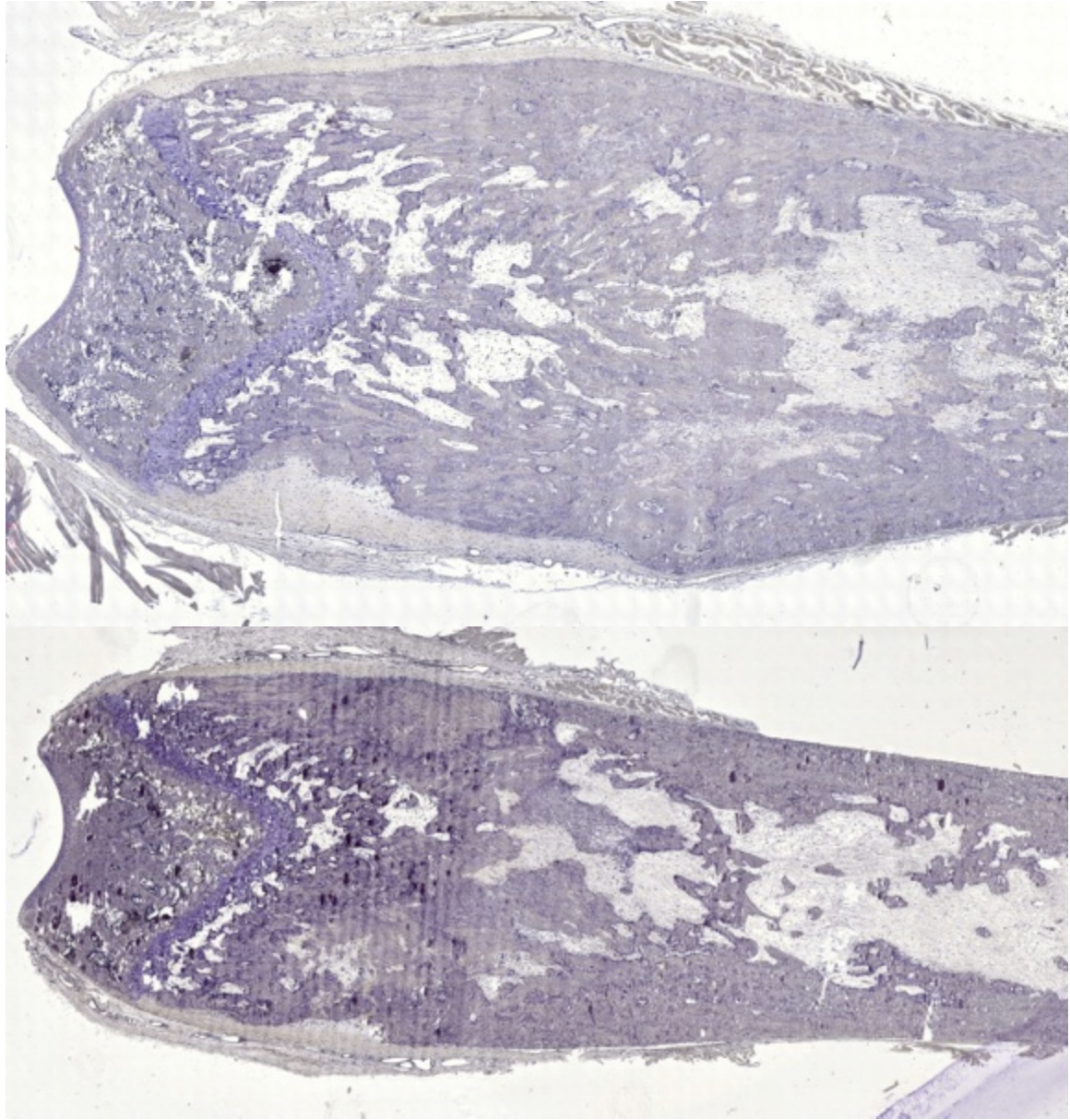


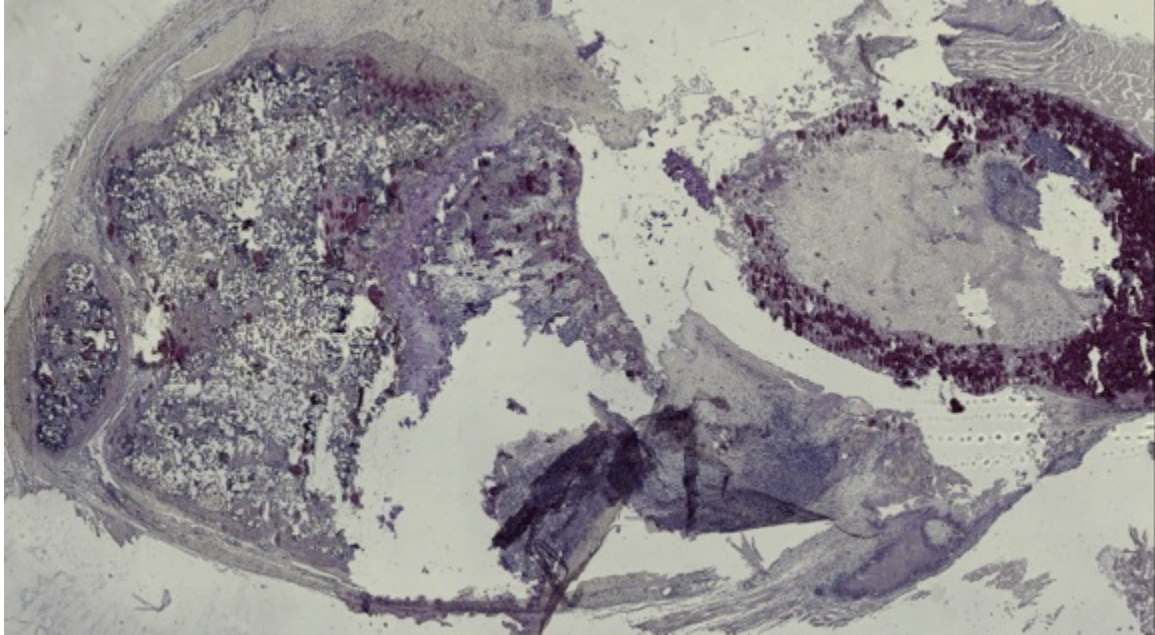
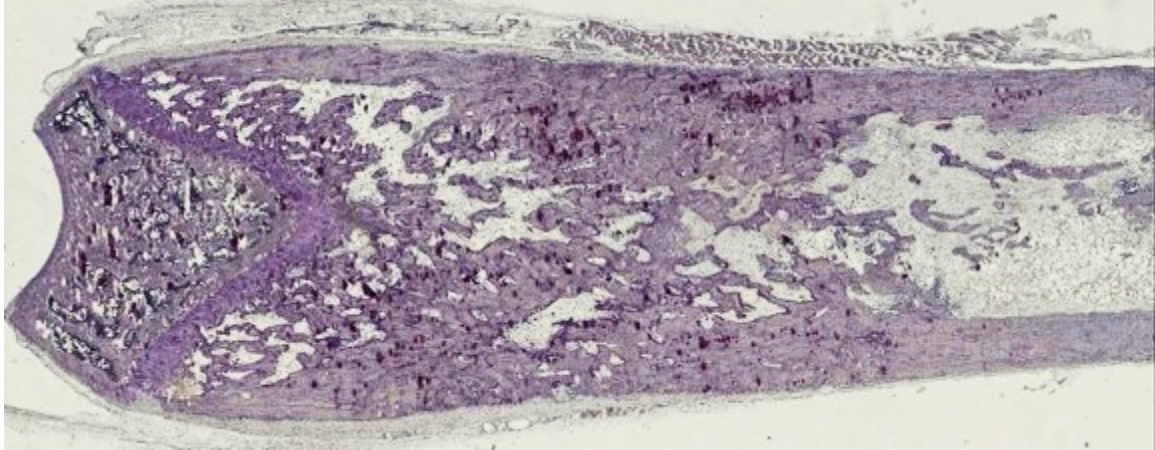


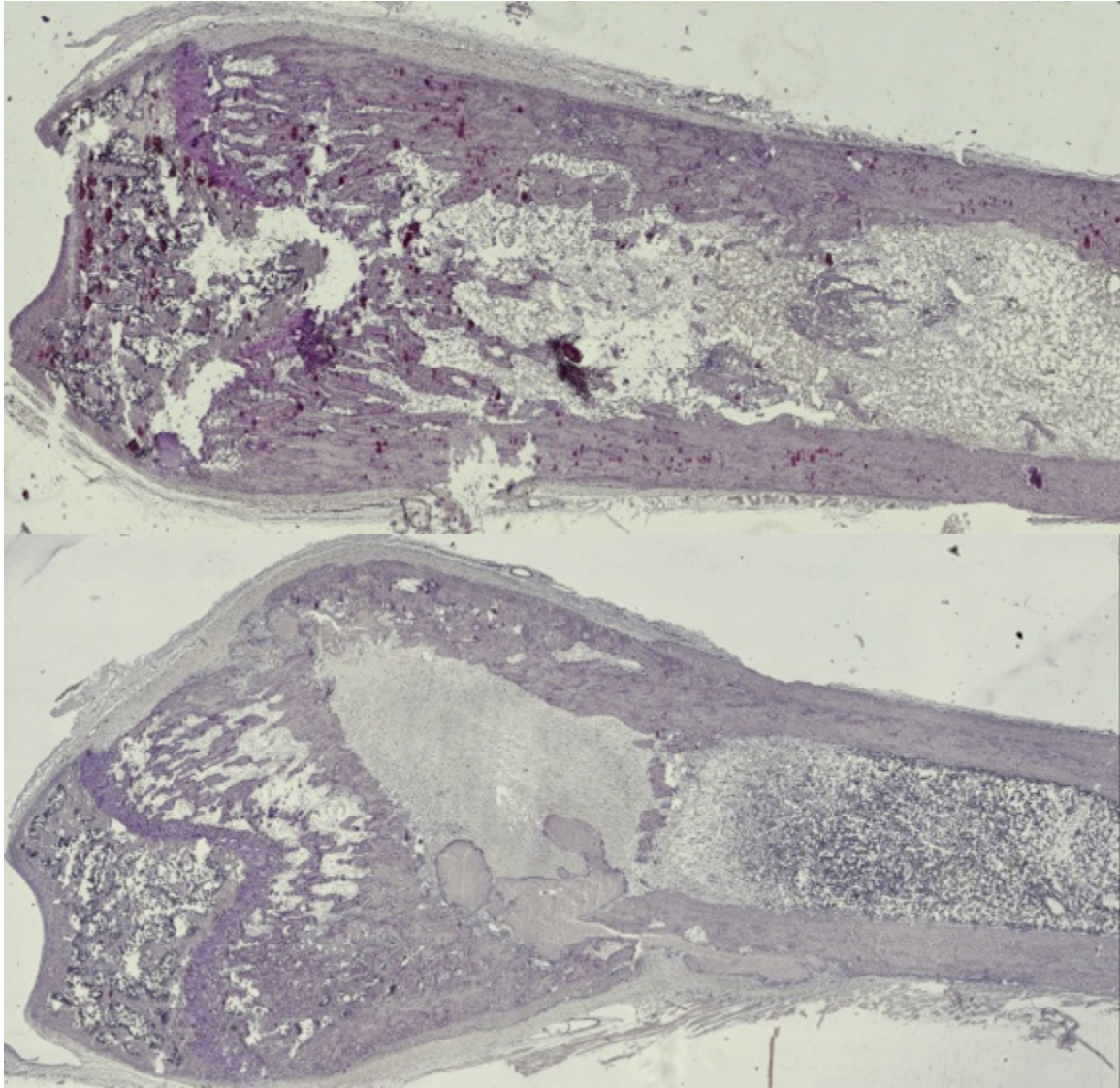


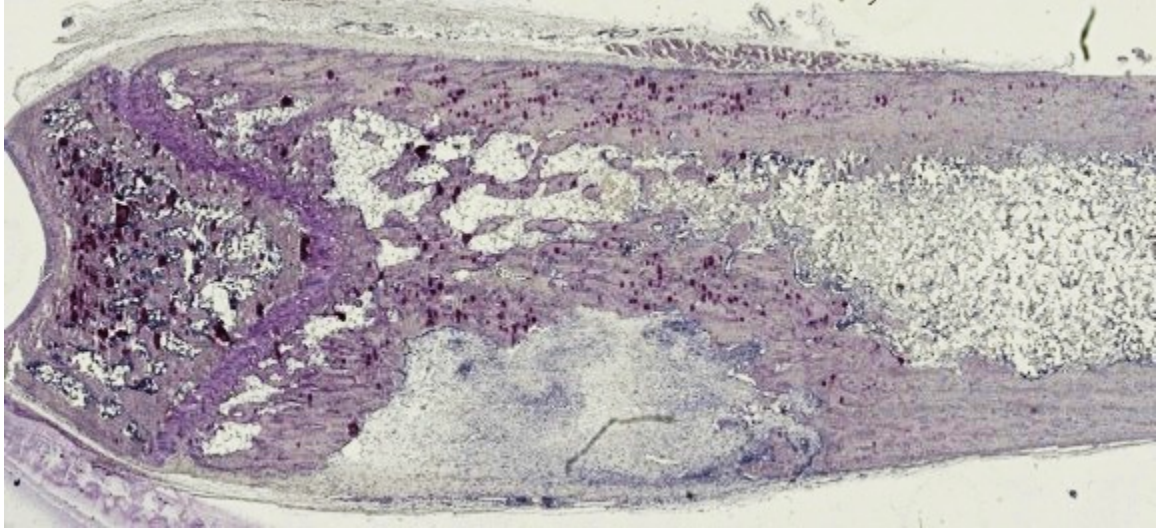
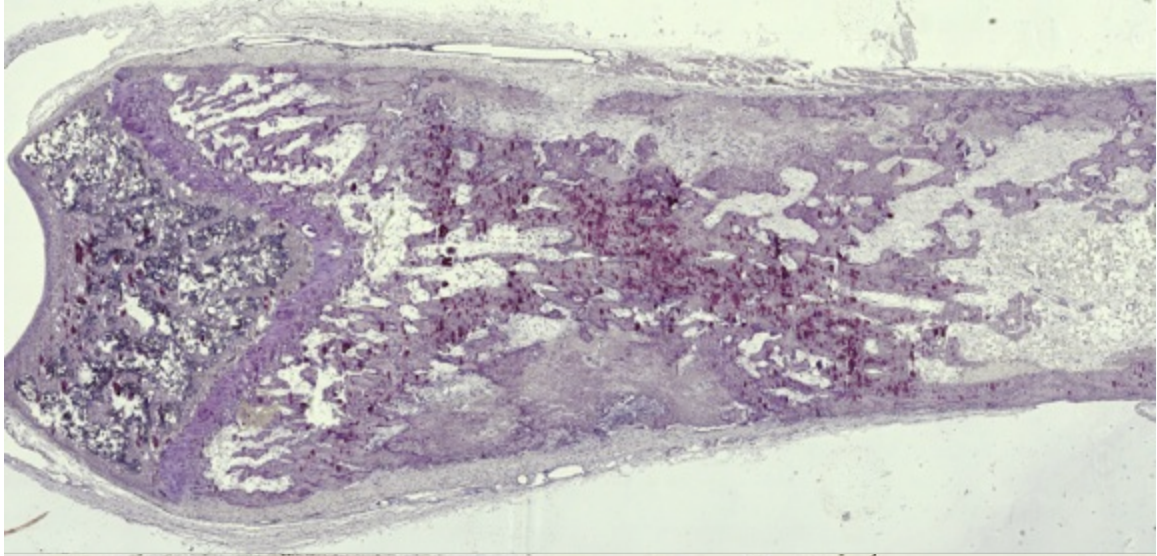












## 10.5 Supplemental Power Analysis

### Introduction

The design of a statistical study must be carefully planned prior to execution to ensure that the desired effect can be observed using a particular sample size. A power analysis is usually conducted to determine the sample size required to reject the null hypothesis if in fact the null hypothesis is false. An insufficient power analysis can result in two common types of statistical errors. The first is a Type 1 error, which occurs when the null hypothesis is rejected when it is actually true (False Positive). The second is a Type 2 error, where the alternative hypothesis is rejected when it is actually true (False Negative). Determining an adequately powered experiment can minimize these errors from occurring.

Before conducting a power analysis, certain parameters must first be determined about the experiment. First, a hypothesis must be devised that aims to detect differences in two or more populations. The investigator must determine the effect size (ES), or the desired effect that is expected in the hypothesis. For example, “Does the addition of chemotherapy in cancer patients receiving radiation therapy increase survival?” A 1% increase in survival may not be clinically relevant; however, a 25% increase may indicate a response to treatment. It is important to note that smaller treatment effects require larger sample sizes while larger treatment effects can reduce the sample size. Effect size is usually derived from previously published data or pilot experiments. The equation for effect size is depicted in Equation 1 (1). It consists of the difference in means ( $\mu_1 - \mu_2$ ) divided by the pooled standard deviation between the means. Next, power (1- $\beta$ ) and significance ( $\alpha$ ) levels must be determined. The power is the probability of concluding that a particular treatment is effective, when the treatment is actually effective. Most

commonly, a power level of 80% is used in experimental design. The significance level, often chosen to be  $\alpha = 0.05$ , is the probability of concluding the treatment is effective when it is actually not effective. The power level can be increased and the alpha level can be decreased, but changing these parameters can result in large increases in the sample size, which may not be feasible. Once these parameters have been established, a power analysis can be conducted to determine the sample size by using the following equations:

$$ES = \text{Effect Size} = (u_1 - u_2) / s_{\text{pooled}} \quad (1)$$

$$s_{\text{pooled}} = \sqrt{.5(s_1^2 + s_2^2)}$$

**Equation 2:** Effect size equation where  $U_1$  and  $U_2$  are means and  $s$  is standard deviation.  $S_1$  and  $S_2$  are the standard deviation of each mean.

$$\text{Sample size} = n = (Z_{1-\alpha} + Z_{1-\beta})^2 (s_1 + s_2)^2 / (u_1 - u_2)^2 \quad (1)$$

**Equation 3:** Power equation for determining sample size. Values for  $Z_\alpha$  and  $Z_{1-\beta}$  can be found in Table 2 in the Appendix for specific power and significance levels. For the calculations described herein,  $Z_{1-\beta} = 0.823$  (80%) and  $Z_\alpha = 1.960$  (5%).

A power analysis is usually calculated prior to conducting the experiment; however, a *post-hoc* analysis may be conducted after an experiment has ended to determine if the study was adequately powered. This can be useful in a variety of situations particularly when sample size cannot necessarily be controlled (e.g. when using wild animals). In a *post-hoc* analysis, the sample and effect sizes are obtained from the data collected. The equation for power as follows:

$$\text{Power} = \delta = ES \frac{\sqrt{n}}{2} \quad (1)$$

**Equation 4: Power equation using ES = effect size and n = sample size. The resultant  $\delta$  (power) can be found in Table 2 in the appendix to determine power.**

The following is a *post-hoc* power analysis on the experiments examining the bone regeneration and tumor promoting potential of mesenchymal stem cells (MSCs) after stereotactic radiotherapy (SRT) for the treatment of osteosarcoma (OSA). The primary aim was to determine if MSCs increased bone volume, PYD, osteocalcin, alizarin, alkaline phosphatase (ALP), and TRAP levels. Increases in these were expected after the administration of (MSCs). The secondary aim was to determine if MSCs induced tumor growth by decreasing tumor necrosis. Effect sizes for each experiment were determined using data from the experiments. The power was then calculated using the equations above and verified with the G\*Power computer application (2). Once power was determined, a new power analysis was performed using the newly defined effect sizes to determine the sample size required for a new and more adequately powered study.

## Post-hoc Power Analysis

### Normalized Mean Bone Volume

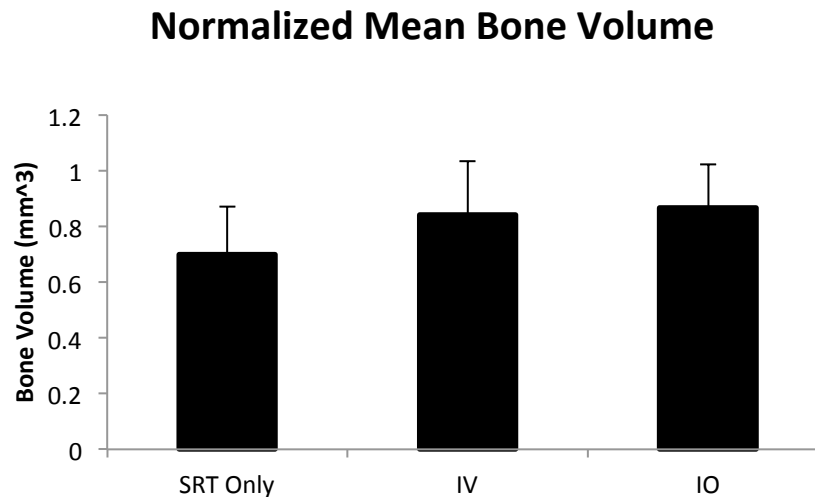


**Figure 39: Normalized mean bone volume from MSC experiments (n=8 per group, n=24 total).**

The graph in Figure 1 represents the normalized mean bone volume between the control group (SRT Only, Mean: 0.69 +/-0.17 mm<sup>3</sup>) and the animals that received MSCs through Intravenous (IV, Mean: 0.84 +/- 0.19 mm<sup>3</sup>) or Intraosseous (IO, Mean: 0.86 +/-0.16 mm<sup>3</sup>) injection. MSCs were expected to increase bone volume; however, there were no differences observed between groups. Means were used to calculate the effect sizes and power as follows:

IV versus SRT Only:

$$\text{Effect size} = |(.69 - .84)| / 0.18 = 0.83$$

Using the above effect size and Equation 3, the power was calculated as follows:

$$\delta = \text{power} = \text{ES} \sqrt{(n/2)} = 2.10 \sqrt{(8/2)} = 1.66$$

The reference value for  $\delta = 1.66$  in Table 2 in the Appendix resulted in a power of approximately 47.50%.

IO versus SRT Only:

$$\text{Effect size} = |(.69 - .86)| / 0.19 = 1.02$$

Using the above effect size and Equation 3, the power was calculated as follows:

$$\delta = \text{power} = \text{ES} \sqrt{(n/2)} = 2.10 \sqrt{(8/2)} = 2.05$$

The reference value for  $\delta = 4.20$  in Table 2 in the Appendix resulted in a power of approximately 62.30%.

## Osteocalcin

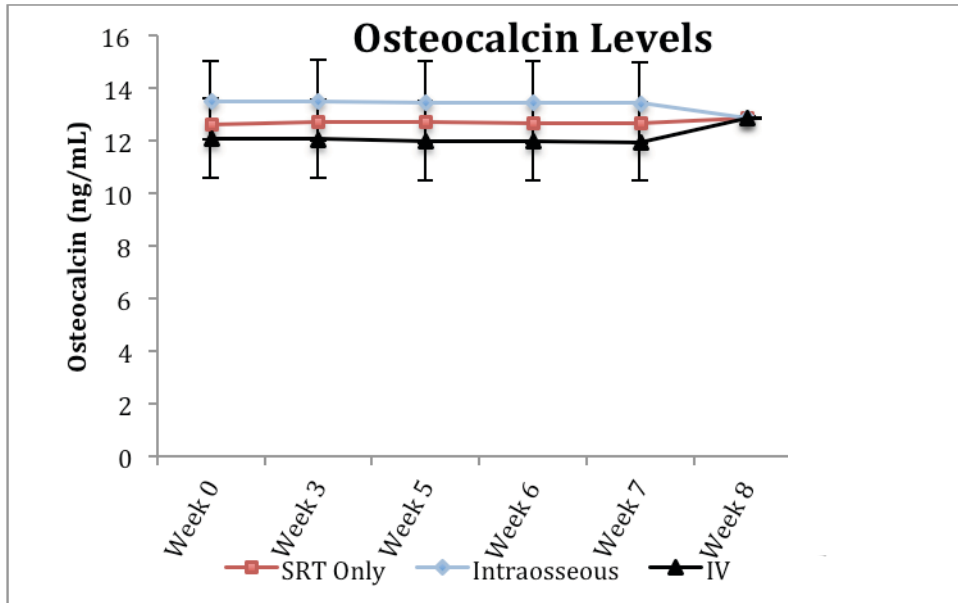


Figure 40: Mean osteocalcin levels between each group. (n=8 per group, n=24 total).

The graph in Figure 2 depicts mean osteocalcin levels between the baseline control group (SRT Only, Mean: 12.75 +/- 0.02 ng/ml) and the animals that received MSCs through Intravenous (IV, Mean: 12.27 +/- 0.7 ng/ml) or Intraosseous (IO, Mean: 13.31 +/- 0.74 ng/ml) injection. In this study, the goal was to determine if administering MSCs at week 4 would increase osteocalcin levels. There were no differences between baseline (SRT only) and the IO or IV groups. The means were used to calculate the effect sizes and power as follows:

IV versus SRT Only:

$$\text{Effect size} = |(12.75 - 12.27)| / 0.97 = 0.83$$

Using the above effect size and Equation 3, the power was calculated as follows:

$$\delta = \text{power} = \text{ES} \sqrt{(n/2)} = 0.83 \sqrt{(8/2)} = 1.66$$

The reference value for  $\delta = 1.66$  in Table 2 in the Appendix resulted in a power of approximately 36.00%.

IO versus SRT Only:

$$\text{Effect size} = |(13.31 - 12.75)| / 0.52 = 1.06$$

Using the above effect size and Equation 3, the power was calculated as follows:

$$\delta = \text{power} = \text{ES} \sqrt{(n/2)} = 1.06 \sqrt{(8/2)} = 1.76$$

The reference value for  $\delta = 1.66$  in Table 2 in the Appendix resulted in a power of approximately 40.00%.

## PYD Levels

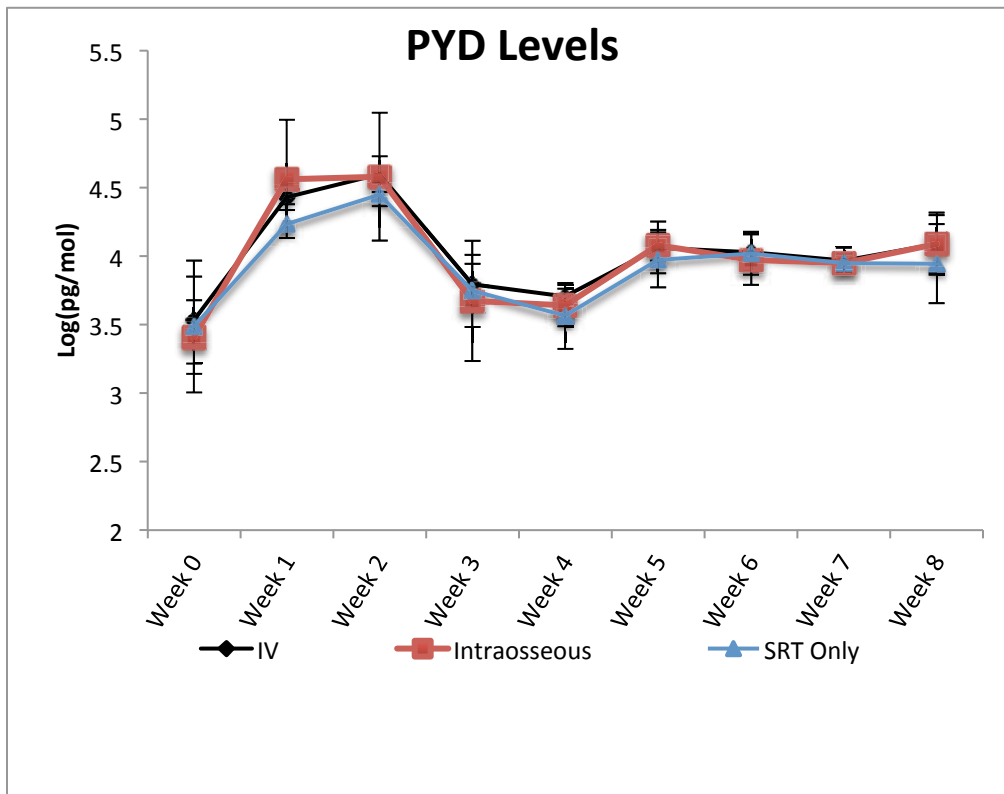


Figure 41: Mean PYD levels between each group. (n=8 per group, n=24 total).

The graph in Figure 3 depicts changes in PYD levels throughout the duration of the experiment to assess the effects of MSC administration on PYD levels. In this study, the goal was to determine if administering MSCs at week 4 would increase PYD levels. There were no statistical differences between the MSC groups and the SRT Only group. To determine effect sizes and power, the SRT only mean (4.02 +/- 0.08) was compared to the IV (3.99 +/- 0.15) and IO (3.92 +/- 0.12) means using Equation 1 as follows:

IV versus SRT Only:

$$\text{Effect size} = |(4.02 - 3.99)| / 0.12 = 0.25$$

Using the above effect size and Equation 3, the power was calculated as follows:

$$\delta = \text{power} = \text{ES} \sqrt{(n/2)} = 0.25 \sqrt{(8/2)} = 0.50$$

The reference value for  $\delta = 0.50$  in Table 2 in the Appendix resulted in a power of approximately 12.00%.

#### IO versus SRT Only

$$\text{Effect size} = |(4.02 - 3.92)| / 0.10 = 1.00$$

Using the above effect size and Equation 3, the power was calculated as follows:

$$\delta = \text{power} = \text{ES} \sqrt{(n/2)} = 1 \sqrt{(8/2)} = 2$$

The reference value for  $\delta = 2.00$  in Table 2 in the Appendix resulted in a power of approximately 50.00%.

## Bone Marker Expression

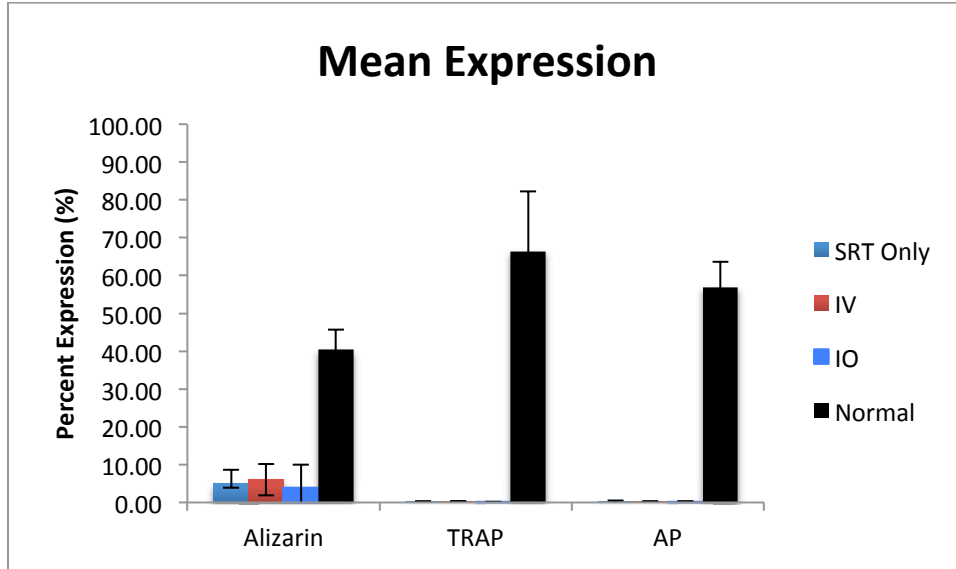


Figure 42: Mean Alizarin, TRAP and ALP levels between groups (n=8 per group).

The graph in Figure 4 depicts Alizarin, TRAP and Alkaline Phosphatase expression in each group as compared to the SRT only group. MSCs were expected to increase these levels above the SRT only group. No statistically significant changes were observed. The means in the SRT only and MSC groups are as follows:

Alizarin IO: 3.92 +/- 3.80 %

Alizarin IV: 6.04 +/- 4.16

Alizarin SRT: 4.89 +/- 3.29 %

TRAP IO: 0.07 +/- 0.07 %

TRAP IV: .21 +/- 0.11

TRAP SRT: 0.12 +/- 0.16%

Alkaline Phosphatase IO: 0.21 +/- 0.28 %

Alkaline Phosphatase IV: 0.17 +/- 0.18 %

Alkaline Phosphatase SRT: 1.13 +/- 0.28%

Using these figures, effect sizes were calculated using Equation 1 as follows for the IV versus SRT Only groups:

$$\text{ALP Effect size} = |(1.31 - 0.17)| / 0.67 = 1.69$$

$$\text{TRAP Effect size} = |(0.12 - 0.21)| / 0.13 = 0.65$$

$$\text{Alizarin Effect Size} = |(4.89 - 6.04)| / 3.75 = 0.30$$

Using the above effect sizes and Equation 3, power was calculated for the IV versus SRT only groups:

$$(\text{ALP}) \delta = \text{power} = \text{ES} \sqrt{(n/2)} = 1.69 \sqrt{(8/2)} = 1.76$$

$$(\text{TRAP}) \delta = \text{power} = \text{ES} \sqrt{(n/2)} = 0.65 \sqrt{(8/2)} = 3.38$$

$$(\text{Alizarin}) \delta = \text{power} = \text{ES} \sqrt{(n/2)} = 0.30 \sqrt{(8/2)} = 0.60$$

The reference values for  $\delta$  were found in Table 2 in the Appendix and resulted in power values of approximately 14.40% (Alizarin), 34.56% (TRAP), and 94.10% (ALP) for the IV versus SRT groups.

For the IO versus SRT Only groups, effect sizes and power were calculated as follows:

$$\text{ALP Effect size} = |(1.31 - 0.21)| / .28 = 3.92$$

$$\text{TRAP Effect size} = |(0.12 - 0.07)| / 0.12 = 0.40$$

$$\text{Alizarin Effect Size} = |(4.89 - 3.92)| / 0.28 = 0.35$$

Using the above effect sizes and Equation 3, the power was calculated:

$$(\text{ALP}) \delta = \text{power} = \text{ES} \sqrt{(n/2)} = 3.92 \sqrt{(8/2)} = 7.85$$

$$\text{(TRAP)} \delta = \text{power} = \text{ES} \sqrt{(n/2)} = 0.40 \sqrt{(8/2)} = 0.80$$

$$\text{(Alizarin)} \delta = \text{power} = \text{ES} \sqrt{(n/2)} = 0.35 \sqrt{(8/2)} = 0.71$$

The reference values for  $\delta$  in Table 2 in the Appendix and resulted in powers values of approximately 16.80% (Alizarin), 19.11% (TRAP), and 99% (ALP) for the IO versus SRT Group.

## Tumor Necrosis

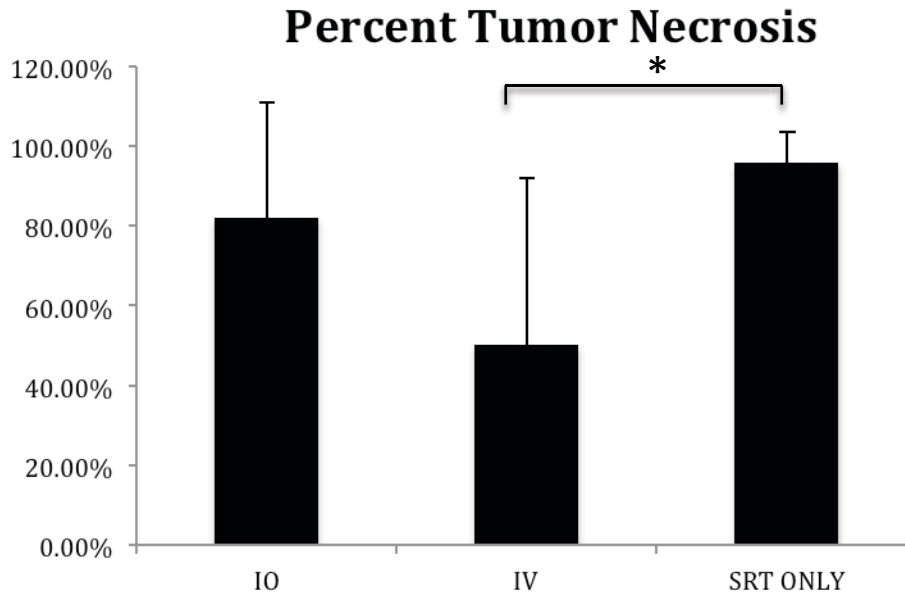


Figure 43: Mean percent tumor necrosis between each group (n=8 per group, n=24 total).

The graph in Figure 5 depicts percent tumor necrosis between the control group and the animals that received MSCs through IV or IO injection. This analysis was evaluated to detect decreases in tumor necrosis with the addition of MSCs as compared to the SRT only group. The data show that there was a statistically significant decrease between the IV (50 +/- 41%) and the SRT only group (96 +/- 7%). To that end, a *post-hoc* power analysis was calculated to determine if the sample size was large enough to observe the 48% decrease in tumor necrosis. Then, another *post-hoc* analysis was used to determine the power of observing the IO effect. Using these figures, the effect size was calculated using Equation 1 for the SRT versus IV groups:

$$\text{Effect size} = |(0.96 - 0.50)| / 0.29 = 1.56$$

Using the above effect size and Equation 3, the power was calculated as follows:

$$\delta = \text{power} = ES \sqrt{(n/2)} = 1.56\sqrt{(8/2)} = 3.12$$

The reference value for  $\delta = 3.12$  in Table 2 in the Appendix indicated a power of approximately 90.0%.

For the IO versus SRT Only:

$$\text{Effect size} = |(0.96 - 0.81)| / 0.29 = 0.711$$

Using the above effect size and Equation 3, the power was calculated as follows:

$$\delta = \text{power} = ES \sqrt{(n/2)} = 1.56\sqrt{(8/2)} = 1.42$$

The reference value for  $\delta = 3.12$  in Table 2 in the Appendix results in a power of approximately 38.50% for the IO versus SRT only groups.

## Bioluminescence

Table 5: Luciferase expression at Week 8

	Yes	No
SRT Only	1	7
IV	3	5
IO	2	6

Bioluminescent imaging was used to evaluate tumor viability between the SRT Only (1/8 = 12.50%) and the IV (3/8 = 37.5%) and (2/8 = 25.00%) groups at the conclusion of the experiment based on a yes or no criteria (Week 8). The binomial proportion *post-hoc* power analysis was evaluated as follows:

$$\text{Power for proportions: } Z_{\text{power}} = \text{Effect} / \sqrt{(0.5/n)} - 1.64$$

Equation 5: Power for proportions

IV versus SRT (25.0% increase):

$$Z_{\text{power}} = 0.25 / \sqrt{(0.5/8)} - 1.64 = - 0.64$$

Power as referenced in Table 4 in the Appendix: 27.00%

IO versus SRT (12.50% increase):

$$Z_{\text{power}} = 0.125 / \sqrt{(0.5/8)} - 1.64 = - 1.14$$

Power as referenced in Table 4 in the Appendix: 15.41%

## **Power Analysis And Experimental Redesign**

The analysis performed thus far revealed that most of the experiments were underpowered; however, it is important to note that in planning the study, effect size and power were calculated solely on the bone volume analysis prior to conducting these experiments. To that end, the experiments can be redesigned with more relevant effect sizes as well as other modifications that result in an adequately powered study that can observe clinically relevant changes. This section describes determining new effect sizes for each experiment based on data previously collected or from published literature. The sample size was then calculated based on the new effect sizes and a power of 80%. The overall experimental design was then modified to account for these changes in terms of the most clinically relevant experiments and the feasibility of performing the study.

## Bone Volume Power Analysis

The bone volume experiment was originally powered to detect a 20% increase in bone volume. This was based off a previous study that showed a mean bone volume increase of 2.1 +/- 0.25 mm<sup>3</sup> with MSCs compared to the control group with a mean bone volume of 1.70 +/-0.10 mm<sup>3</sup>. Using these figures, a ~20% increase in bone volume with MSCs was the desired effect size. No differences were seen in this experiment, but it's important to realize that the previously published study did not administer radiation, which has been shown to cause adverse effects to bone. It's quite feasible that the amount of bone formation at the conclusion of these experiments may have increased, but to a lesser extent than 20 percent. Therefore, the power calculations below were modified to determine the sample size of observing a 5% or 10% increase in bone formation. Equation 3 was used to calculate sample sizes assuming 80% power:

For 10% increase:

$$\begin{aligned} & (Z_{1-\alpha} + Z_{1-\beta})^2 (s_1+s_2)^2 / (u^1-u^2) = \\ & (1.96+0.842)^2 (0.1225)/(1.7-1.9)^2 = \\ & \quad \quad \quad 12 \text{ animals per group} \end{aligned}$$

For 5% increase:

$$\begin{aligned} & (Z_{1-\alpha} + Z_{1-\beta})^2 (s_1+s_2)^2 / (u^1-u^2) = \\ & (1.96+0.842)^2 (0.1225)/(1.7-1.8)^2 = \\ & \quad \quad \quad 46 \text{ animals per group} \end{aligned}$$

The results from this power analysis showed that to observe a 10% or 5% increase in bone volume, the experiment would require 12 to 46 animals per group, respectively.

## Bone Markers Power Analysis

The *post-hoc* power analysis of the bone formation markers determined that the experiment was underpowered. The ideal outcome would result in TRAP, Alizarin and ALP to return to normal levels after treatment with MSCs. To achieve these levels, a ~10 fold increase in Alizarin, ~550 fold increase in TRAP and ~50 fold increase in ALP expression would be needed as shown by the control group in Figure 4. Due to the detrimental radiation induced effects to the bone, this scenario is highly unlikely. The previous experiment provided baseline expression levels after SRT, but these do not help determine a desired effect size from MSCs. Therefore, a previously published study that examined ALP expression in irradiated bone after MSC administration was used to determine the effect size. The authors observed a 4-fold increase in ALP levels in the irradiated group that received MSCs over the irradiated group that did not receive MSCs (3). However, this study used a much lower total radiation dose and only a small section of femur was exposed to radiation. As a result, the same 4-fold increase may not be observed in our studies. In this power analysis, a smaller 2-fold increase in ALP expression was assumed to be the desired effect size. The sample size was then calculated as follows:

$$\begin{aligned} & (Z_{1-a} + Z_{1-b})^2 (s_1 + s_2)^2 / (u^1 - u^2) = \\ & (1.96 + 0.842)^2 (0.28) / (1.13 - 2.26)^2 = \\ & \quad \quad \quad 4 \text{ animals per group} \end{aligned}$$

Next, the effect sizes for TRAP and Alizarin were determined. To date, no studies have examined Alizarin or TRAP after radiation with or without MSCs in the manner in which these experiments were evaluated. Therefore, TRAP and Alizarin were also assumed to have the same small effect size (2-fold). Sample sizes were then calculated as follows:

TRAP:

$$\begin{aligned} & (Z_{1-a} + Z_{1-b})^2 (s_1 + s_2)^2 / (u^1 - u^2) = \\ & (1.96 + 0.842)^2 (0.11) / (0.24 - 0.12)^2 = \\ & \quad 12 \text{ animals per group} \end{aligned}$$

Alizarin:

$$\begin{aligned} & (Z_{1-a} + Z_{1-b})^2 (s_1 + s_2)^2 / (u^1 - u^2) = \\ & (1.96 + 0.842)^2 (4.02) / (4.89 - 9.78)^2 = \\ & \quad 7 \text{ animals per group} \end{aligned}$$

## Osteocalcin Power Analysis

The power analysis for the osteocalcin study concluded there was insufficient power to detect any differences between groups after MSC administration. It's important to note that the means were approximately the same between groups at each time point thus it's difficult to determine an effect size for a new experiment from these data. To redesign this experiment in hopes of observing an effect, a previously published study was used to determine a new effect size. Currently, there are no available studies that have measured serum osteocalcin levels in rats after MSC administration. Only one study exists that examined serum osteocalcin levels after administration of a bone growth-inducing agent. This study used parathyroid hormone (PTH) to increase bone mineral density (4). Although not particularly relevant to MSCs, it provided a basis for osteocalcin levels that might be observed if stimulated by a bone growth-inducing treatment such as MSCs. This study showed that stimulation with PTH resulted in a 60% increase in osteocalcin levels. In our studies, we would not expect to observe the same increase in osteocalcin due to the large dose of radiation administered. Therefore, following MSC injection, smaller effect sizes of 10% and 30% were assumed as the desired increase in osteocalcin over baseline levels (SRT Only). Using these assumed effect sizes, sample size was calculated as follows:

For 10% increase:

$$\begin{aligned} & (Z_{1-\alpha} + Z_{1-\beta})^2 (s_1 + s_2)^2 / (u^1 - u^2) = \\ & (1.96 + 0.842)^2 (1.69) / (12.75 - 14.50)^2 = \\ & \quad \quad \quad 2 \text{ animals per group} \end{aligned}$$

For 30% increase:

$$(Z_{1-a} + Z_{1-b})^2 (s_1 + s_2)^2 / (u^1 - u^2) =$$
$$(1.96 + 0.842)^2 (1.69) / (12.75 - 16.57)^2 =$$

2 animals per group

## PYD Power Analysis

The PYD power analysis was insignificantly powered to detect the small differences (almost identical means) between groups after MSC administration. To redesign this experiment, the effect size was determined by using the post-SRT mean (Week 4, 3.63 +/- 0.15) as baseline and the pre-SRT mean (Week 2, 4.0 +/- 0.46) as the desired effect. Using this effect size, it is assumed that the administration of MSCs would result in an increase in PYD to pre-SRT levels. Using these figures the power was calculated as follows:

50% increase in MSC groups versus SRT:

$$\begin{aligned} & (Z_{1-\alpha} + Z_{1-\beta})^2 (s_1 + s_2)^2 / (u^1 - u^2) = \\ & (1.96 + 0.842)^2 (0.36) / (4.00 - 3.63)^2 = \\ & \quad \quad \quad 12 \text{ animals per group} \end{aligned}$$

## Tumor Necrosis Power Analysis

The tumor necrosis study determined there was sufficient power to detect a 48% decrease in tumor necrosis in the IV group as compared to the SRT only group. Studies have shown that tumor necrosis above 80% results in durable tumor control (5). However, tumor necrosis levels below 80% often result in poor tumor control (5). This is of particularly importance to the IO group, which had a higher mean percent of tumor necrosis (81% +/- 29 %) than the IV group but with a large standard deviation. Therefore, being able to detect decreases in tumor necrosis below 80% would be of clinical relevance and help determine if the IO MSCs are decreasing necrosis to levels that could indicate a lack of tumor control. To determine the power of such an experiment, the following equation was used to determine the sample size to observe a decrease of 17 +/- 29% in tumor necrosis (79% total) from the SRT only group (96 +/- 7%).

$$\begin{aligned} & (Z_{1-a} + Z_{1-b})^2 (s_1 + s_2)^2 / (u^1 - u^2) = \\ & (1.960 + 0.842)^2 (0.089) / (.96 - .79)^2 = \\ & \quad 20 \text{ animals per group} \end{aligned}$$

These results indicated that increasing the animal numbers to 20 per group would give adequate power to observe a 17% decrease in necrosis.

## **Bioluminescence Power Analysis**

The bioluminescence experiment was underpowered in both the IO and IV comparisons to the SRT Only group. In order to achieve the power required to observe the changes in the IV (12.5% effect) and IO groups (25.00% effect) from the SRT Only, new sample sizes were calculated using Equation 4 solved for n:

$$\text{Sample size for proportions: } n = 0.5 * (0.84 - 1.64)^2 / \text{Effect Size}^2$$

IV versus SRT Only:

$$= 0.5 * (0.84 + 1.64)^2 / 0.25^2$$

50 animals per group

IO versus SRT Only:

$$= 0.5 * (0.84 + 1.64)^2 / 0.125$$

196 animals per group

The results indicate that 50 animals per group would be needed to detect the IV change (25%) and 196 animals per group would be needed to observe the IO change (12.5%).

## **Conclusions**

### **Bone Growth Studies**

The power analysis performed using the newly defined effect sizes in the bone growth studies yielded a total of 46 animals per group if the desired effect was to observe a 5% increase in bone volume. Forty-six animals per group (138 total for 3 groups) is a very large sample size to accurately treat with SRT. It can take up to three hours just to plan and deliver the first fraction of radiation for each rat. This does not include the extra time required to deliver the second and third fractions; therefore, it is not feasible to accurately administer SRT to this large sample size. Increasing the effect level for bone growth to 10% reduces the sample size to a more feasible 12 animals per group. Even though the primary aim of the previous study was to evaluate bone volume after MSCs administration, it may not be the best tool to evaluate MSC activity. Histology revealed that SRT caused detrimental effects to the normal parts of the bone; therefore, the potential bone volume changes induced by MSCs may not be visible at the conclusion of this short experiment. If the experiment were to be extended, it may be more likely to observe an increase in bone volume if the MSCs were inducing bone growth. It's more plausible that at the earlier time points, as evaluated by this experiment, that the molecular levels of bone markers (ALP, TRAP and Alizarin) as well as osteocalcin and PYD would be increased before any new bone volume could be detected by microCT. Thus bone marker expression may be a better indicator of early bone formation with MSCs. Using previously published data and the baseline levels observed in this study, it was determined that a 2-fold increase in ALP at the end of the experiment would be sufficient to determine an effect mediated by MSCs. This would require a sample size of 12 animals per group. No data were available to determine an effect size for Alizarin and TRAP and were assumed to have the same effect (2-fold increase) size as ALP.

It would be beneficial to perform a pilot study to examine baseline TRAP and Alizarin levels after MSC injection in a normal bone using the novel histology techniques performed in these studies. This would help provide a better understanding of Alizarin, TRAP and ALP expression that might be observed with MSCs and could determine a more appropriate effect size. In the osteocalcin experiment, the sample size yielded 4 animals per group; however, it's important to note the small variability and the desired effect (well above the standard deviation of baseline) resulted in a small sample size. The desired effect in the osteocalcin assay was based off a previously published study that observed significant increases after PTH. A limitation of our study was that the detection capabilities of the osteocalcin ELISA were only in the ng/ml range, whereas in the PTH study an improved assay was used capable of detecting levels in the pg/ml range. Thus, it may be beneficial to run a small pilot experiment with the remaining urine samples in the previous experiment with a more sensitive assay to better determine a more accurate effect size. The changes in osteocalcin may be much smaller than our assay was capable of detecting, yet could still be an important indicator of early bone formation. In the PYD analysis, decreased levels after SRT served as a baseline for the MSC experiments. The effect size was determined by the PYD levels immediately before SRT as the potential increase induced by MSCs. The power analysis indicated that 12 animals per group would be required to adequately power this assay. Therefore, in the bone generation experiments, a sample size of 12 animals per group would be sufficient to observe the desired effects in the bone markers along with a 10% increase in bone volume.

## **Tumor Promotion Studies**

In the tumor necrosis power analysis, it was determined that in order to observe an effect of 79% or less tumor necrosis that 20 animals per group would be required to achieve adequate power. The increased sample size in this analysis was mediated by the large variability in the percent necrosis in the MSC groups. Reducing this variability would in turn decrease the sample size while still achieving the desired power level. A limitation of the tumor necrosis evaluation that may be contributing to the large variability is that the samples were stained with hematoxylin. Usually, tumor necrosis quantification is evaluated from samples stained with both hematoxylin and eosin (H&E). The hematoxylin staining allows for the visualization of the nuclei in cells while the eosin staining allows for the visualization of various cellular components. The lack of eosin staining created difficulty differentiating between tumor necrosis and overall bone necrosis/sclerosis and likely contributed to the variability in the tumor necrosis analysis. Staining the samples with both hematoxylin and eosin may provide a more accurate analysis of the percent tumor necrosis and may subsequently decrease the variability. Decreasing this variability by 10% would decrease the animal numbers to just 10 per group. Bioluminescence expression was also used to detect viable OSA cells at the end of the experiment; however, the power analysis indicated a very large sample size would be needed to observe a 10-25% change in expression. A limitation of bioluminescence is that it has been shown to be unreliable in this particular OSA animal model most likely due to the large baseline tumor necrosis that can hinder luciferin from sufficiently reaching the viable cells. For this reason, bioluminescence was not an accurate indicator of endpoint tumor control. Histology is the gold standard for assessing tumor control and requires substantially fewer animals (5). Even though bioluminescence was not adequately powered, it can still be used to track initial tumor

engraftment and endpoint expression. Most importantly, bioluminescence allows for the detection of metastasis that might not otherwise be detectable by gross observation. Considering that metastasis to the lungs are the primary cause of death in OSA patients, it is still an important outcome measure.

Taking together the power analysis described herein and the potential limitations of the various experiments, a new study would include 20 animals per group. This would provide the power to observe the desired increases in bone markers, osteocalcin and PYD levels which would most likely be observed at the early time points evaluated in this experiment. This study would also be powered to observe tumor necrosis below 80%. This threshold has been shown to be a reliable indicator of tumor control in the clinical setting. Levels below 80% have been shown to result in tumor control in only ~27% of patients whereas levels above 80% result in control in more than 77% of patients (5). Thus, this would provide clinically relevant information as to the safety of MSCs through both the IV and IO routes. Although, 20 animals per group provide adequate power for these analyses, it would be ideal to reduce this number. As previously stated, reducing the variability in the tumor necrosis analysis by properly staining the samples could reduce the sample size and while maintaining the desired power.

In addition to modifying parameters of the current experimental design, other modifications may help to better evaluate the bone forming potential of MSCs. For instance, due to the limitations of the SRT machine at the time of this experiment, the entire bone was irradiated which has been shown to adversely affect the vasculature and osteoprogenitor cells. Recent findings have shown that it's now possible to irradiate half of the femur with SRT. The

advantage of sparing the existing bone, as done in the clinical setting, leaves the other half of the bone less affected by radiation and subsequently spares the vasculature and osteoprogenitor cells. Sparing these cells may help the existing bone to heal and allow for a more inhabitable environment for the MSCs. To that end, extending the experiment may also be beneficial as it could allow more time for the bone to heal and the MSCs to induce bone growth. Repeat administration of MSCs could potentially increase their effectiveness. Later time points would also allow for better detection of increased bone markers as well as new bone formation. Another benefit of extending the experiment is for better for analysis of the tumor promotion studies. If MSCs were promoting tumor growth, then extending the study would allow more time for the tumors to increase in size and may reduce the variability in tumor necrosis as observed in the previous study. Taking together these modification as well as the newly defined effects and sample sizes, MSCs can be more adequately evaluated for their bone regeneration capabilities and safety.

## Supplement References

1. Cohen J. Statistical Power Analysis for the Behavioral Sciences. 1988.
2. Aßfalg A, Bell R, Brandt M, Hauke R, Lindemann O, Mayr S, et al. G\*Power. 3.1.6 ed2009.
3. Tohma Y, Ohgushi H, Morishita T, Dohi Y, Tadokoro M, Tanaka Y, et al. Bone marrow-derived mesenchymal cells can rescue osteogenic capacity of devitalized autologous bone. *J Tissue Eng Regen Med.* [Research Support, Non-U.S. Gov't]. 2008 Jan;2(1):61-8.
4. Mitlak BH, Williams DC, Bryant HU, Paul DC, Neer RM. Intermittent administration of bovine PTH-(1-34) increases serum 1,25-dihydroxyvitamin D concentrations and spinal bone density in senile (23 month) rats. *J Bone Miner Res.* 1992 May;7(5):479-84.
5. Powers BE, Withrow SJ, Thrall DE, Straw RC, LaRue SM, Page RL, et al. Percent tumor necrosis as a predictor of treatment response in canine osteosarcoma. *Cancer.* 1991 Jan 1;67(1):126-34.

## Supplement Appendix

**Table 6: Power as a function of  $\delta$  and significance level (a) (1)**

$\delta$	One-tailed $\alpha$			
	.10	.05	.02	.01
1.00	.26	.17	.09	.06
1.10	.29	.20	.11	.07
1.20	.33	.22	.13	.08
1.30	.37	.26	.15	.10
1.40	.40	.29	.18	.12
1.50	.44	.32	.20	.14
1.60	.48	.36	.23	.17
1.70	.52	.40	.27	.19
1.80	.56	.44	.30	.22
1.90	.60	.48	.34	.25
2.00	.64	.52	.37	.28
2.10	.68	.56	.41	.32
2.20	.71	.60	.45	.35
2.30	.74	.63	.49	.39
2.40	.78	.67	.53	.43
2.50	.80	.71	.57	.47
2.60	.83	.74	.61	.51
2.70	.85	.77	.65	.55
2.80	.88	.80	.68	.59
2.90	.90	.83	.72	.63
3.00	.91	.95	.75	.66
3.10	.93	.87	.78	.70
3.20	.94	.89	.81	.73
3.30	.95	.91	.84	.77
3.40	.96	.93	.86	.80
3.50	.97	.94	.88	.82
3.60	.98	.95	.90	.85
3.70	.98	.96	.92	.87
3.80	.98	.97	.93	.89
3.90	.99	.97	.94	.91
4.00	.99	.98	.95	.92
4.10	.99	.98	.96	.94
4.20	-	.99	.97	.95
4.30	-	.99	.98	.96
4.40	-	.99	.98	.97
4.50	-	.99	.99	.97
4.60	-	-	.99	.98
4.70	-	-	.99	.98
4.80	-	-	.99	.99
4.90	-	-	-	.99
5.00	-	-	-	.99

Table 7: t-table for determining  $\alpha$  and  $1-\beta$  [Howell, 2012 #236]

<b>t Table</b>											
cum. prob	$t_{.50}$	$t_{.75}$	$t_{.80}$	$t_{.85}$	$t_{.90}$	$t_{.95}$	$t_{.975}$	$t_{.99}$	$t_{.995}$	$t_{.999}$	$t_{.9995}$
one-tail	<b>0.50</b>	<b>0.25</b>	<b>0.20</b>	<b>0.15</b>	<b>0.10</b>	<b>0.05</b>	<b>0.025</b>	<b>0.01</b>	<b>0.005</b>	<b>0.001</b>	<b>0.0005</b>
two-tails	<b>1.00</b>	<b>0.50</b>	<b>0.40</b>	<b>0.30</b>	<b>0.20</b>	<b>0.10</b>	<b>0.05</b>	<b>0.02</b>	<b>0.01</b>	<b>0.002</b>	<b>0.001</b>
df											
1	0.000	1.000	1.376	1.963	3.078	6.314	12.71	31.82	63.66	318.31	636.62
2	0.000	0.816	1.061	1.386	1.886	2.920	4.303	6.965	9.925	22.327	31.599
3	0.000	0.765	0.978	1.250	1.638	2.353	3.182	4.541	5.841	10.215	12.924
4	0.000	0.741	0.941	1.190	1.533	2.132	2.776	3.747	4.604	7.173	8.610
5	0.000	0.727	0.920	1.156	1.476	2.015	2.571	3.365	4.032	5.893	6.869
6	0.000	0.718	0.906	1.134	1.440	1.943	2.447	3.143	3.707	5.208	5.959
7	0.000	0.711	0.896	1.119	1.415	1.895	2.365	2.998	3.499	4.785	5.408
8	0.000	0.706	0.889	1.108	1.397	1.860	2.306	2.896	3.355	4.501	5.041
9	0.000	0.703	0.883	1.100	1.383	1.833	2.262	2.821	3.250	4.297	4.781
10	0.000	0.700	0.879	1.093	1.372	1.812	2.228	2.764	3.169	4.144	4.587
11	0.000	0.697	0.876	1.088	1.363	1.796	2.201	2.718	3.106	4.025	4.437
12	0.000	0.695	0.873	1.083	1.356	1.782	2.179	2.681	3.055	3.930	4.318
13	0.000	0.694	0.870	1.079	1.350	1.771	2.160	2.650	3.012	3.852	4.221
14	0.000	0.692	0.868	1.076	1.345	1.761	2.145	2.624	2.977	3.787	4.140
15	0.000	0.691	0.866	1.074	1.341	1.753	2.131	2.602	2.947	3.733	4.073
16	0.000	0.690	0.865	1.071	1.337	1.746	2.120	2.583	2.921	3.686	4.015
17	0.000	0.689	0.863	1.069	1.333	1.740	2.110	2.567	2.898	3.646	3.965
18	0.000	0.688	0.862	1.067	1.330	1.734	2.101	2.552	2.878	3.610	3.922
19	0.000	0.688	0.861	1.066	1.328	1.729	2.093	2.539	2.861	3.579	3.883
20	0.000	0.687	0.860	1.064	1.325	1.725	2.086	2.528	2.845	3.552	3.850
21	0.000	0.686	0.859	1.063	1.323	1.721	2.080	2.518	2.831	3.527	3.819
22	0.000	0.686	0.858	1.061	1.321	1.717	2.074	2.508	2.819	3.505	3.792
23	0.000	0.685	0.858	1.060	1.319	1.714	2.069	2.500	2.807	3.485	3.768
24	0.000	0.685	0.857	1.059	1.318	1.711	2.064	2.492	2.797	3.467	3.745
25	0.000	0.684	0.856	1.058	1.316	1.708	2.060	2.485	2.787	3.450	3.725
26	0.000	0.684	0.856	1.058	1.315	1.706	2.056	2.479	2.779	3.435	3.707
27	0.000	0.684	0.855	1.057	1.314	1.703	2.052	2.473	2.771	3.421	3.690
28	0.000	0.683	0.855	1.056	1.313	1.701	2.048	2.467	2.763	3.408	3.674
29	0.000	0.683	0.854	1.055	1.311	1.699	2.045	2.462	2.756	3.396	3.659
30	0.000	0.683	0.854	1.055	1.310	1.697	2.042	2.457	2.750	3.385	3.646
40	0.000	0.681	0.851	1.050	1.303	1.684	2.021	2.423	2.704	3.307	3.551
60	0.000	0.679	0.848	1.045	1.296	1.671	2.000	2.390	2.660	3.232	3.460
80	0.000	0.678	0.846	1.043	1.292	1.664	1.990	2.374	2.639	3.195	3.416
100	0.000	0.677	0.845	1.042	1.290	1.660	1.984	2.364	2.626	3.174	3.390
1000	0.000	0.675	0.842	1.037	1.282	1.646	1.962	2.330	2.581	3.098	3.300
<b>Z</b>	0.000	0.674	0.842	1.036	1.282	1.645	1.960	2.326	2.576	3.090	3.291
	0%	50%	60%	70%	80%	90%	95%	98%	99%	99.8%	99.9%
	<b>Confidence Level</b>										

Table 8: Negative Z table

<i>z</i>	.00	.01	.02	.03	.04	.05	.06	.07	.08	.09
-3.4	.0003	.0003	.0003	.0003	.0003	.0003	.0003	.0003	.0003	.0002
-3.3	.0005	.0005	.0005	.0004	.0004	.0004	.0004	.0004	.0004	.0003
-3.2	.0007	.0007	.0006	.0006	.0006	.0006	.0006	.0005	.0005	.0005
-3.1	.0010	.0009	.0009	.0009	.0008	.0008	.0008	.0008	.0007	.0007
-3.0	.0013	.0013	.0013	.0012	.0012	.0011	.0011	.0011	.0010	.0010
-2.9	.0019	.0018	.0018	.0017	.0016	.0016	.0015	.0015	.0014	.0014
-2.8	.0026	.0025	.0024	.0023	.0023	.0022	.0021	.0021	.0020	.0019
-2.7	.0035	.0034	.0033	.0032	.0031	.0030	.0029	.0028	.0027	.0026
-2.6	.0047	.0045	.0044	.0043	.0041	.0040	.0039	.0038	.0037	.0036
-2.5	.0062	.0060	.0059	.0057	.0055	.0054	.0052	.0051	.0049	.0048
-2.4	.0082	.0080	.0078	.0075	.0073	.0071	.0069	.0068	.0066	.0064
-2.3	.0107	.0104	.0102	.0099	.0096	.0094	.0091	.0089	.0087	.0084
-2.2	.0139	.0136	.0132	.0129	.0125	.0122	.0119	.0116	.0113	.0110
-2.1	.0179	.0174	.0170	.0166	.0162	.0158	.0154	.0150	.0146	.0143
-2.0	.0228	.0222	.0217	.0212	.0207	.0202	.0197	.0192	.0188	.0183
-1.9	.0287	.0281	.0274	.0268	.0262	.0256	.0250	.0244	.0239	.0233
-1.8	.0359	.0351	.0344	.0336	.0329	.0322	.0314	.0307	.0301	.0294
-1.7	.0446	.0436	.0427	.0418	.0409	.0401	.0392	.0384	.0375	.0367
-1.6	.0548	.0537	.0526	.0516	.0505	.0495	.0485	.0475	.0465	.0455
-1.5	.0668	.0655	.0643	.0630	.0618	.0606	.0594	.0582	.0571	.0559
-1.4	.0808	.0793	.0778	.0764	.0749	.0735	.0721	.0708	.0694	.0681
-1.3	.0968	.0951	.0934	.0918	.0901	.0885	.0869	.0853	.0838	.0823
-1.2	.1151	.1131	.1112	.1093	.1075	.1056	.1038	.1020	.1003	.0985
-1.1	.1357	.1335	.1314	.1292	.1271	.1251	.1230	.1210	.1190	.1170
-1.0	.1587	.1562	.1539	.1515	.1492	.1469	.1446	.1423	.1401	.1379
-0.9	.1841	.1814	.1788	.1762	.1736	.1711	.1685	.1660	.1635	.1611
-0.8	.2119	.2090	.2061	.2033	.2005	.1977	.1949	.1922	.1894	.1867
-0.7	.2420	.2389	.2358	.2327	.2296	.2266	.2236	.2206	.2177	.2148
-0.6	.2743	.2709	.2676	.2643	.2611	.2578	.2546	.2514	.2483	.2451
-0.5	.3085	.3050	.3015	.2981	.2946	.2912	.2877	.2843	.2810	.2776
-0.4	.3446	.3409	.3372	.3336	.3300	.3264	.3228	.3192	.3156	.3121
-0.3	.3821	.3783	.3745	.3707	.3669	.3632	.3594	.3557	.3520	.3483
-0.2	.4207	.4168	.4129	.4090	.4052	.4013	.3974	.3936	.3897	.3859
-0.1	.4602	.4562	.4522	.4483	.4443	.4404	.4364	.4325	.4286	.4247
-0.0	.5000	.4960	.4920	.4880	.4840	.4801	.4761	.4721	.4681	.4641

## List of Abbreviations

BMP	Bone Morphogenetic Protein
BMP-2	Bone Morphogenetic Protein-2
CBCT	Cone Beam Computed Tomography
CTx	C-telopeptide
DAPI	4',6-diamidino-2-phenylindole
DMEM	Dulbecco's Modified Eagle Medium
DMSO	Dimethyl sulfoxide
DPD	Deoxy pyridinoline
eGFP	Enhanced Green Fluorescent Protein
GDF	Growth Differentiation Factors
GFP	Green Fluorescent Protein
Gy	Gray
HBSS	Hank's Balanced Salt Solution
H & E	Hematoxylin and Eosin Staining
IACUC	Institutional Animal Care and Use Committee
IO	Intraosseous
IORT	Intraoperative irradiation therapy
IV	Intravenous
MEM	Minimum Essential Media
microCT	Micro-computed Tomography
MSC	Mesenchymal Stem Cell
MTPE	Liposome-Encapsulated Muramyl Tripeptide
NTx	N-telopeptide
OC	Osteocalcin
OSA	Osteosarcoma
PBS	Phosphate Buffered Saline
PPAR $\gamma$	Peroxisome Proliferator-Activated Receptor Gamma
PYD	Pyridinoline
RPMI	Roswell Park Memorial Institute medium
SD	Standard Deviation
SRT	Stereotactic Radiotherapy
TGF-b	Transforming Growth Factor Beta
TRAP	Tartrate resistant acid phosphatase
microCT	Micro-computed Tomography
VRTOG	Veterinary Radiation Therapy Oncology Group
XRT	Finely Fractionated Radiotherapy